Proceedings of the International Workshop on e^+e^- collisions from ϕ to ψ (PHIPSI15)

Hefei, September 23～26, 2015

International Advisory Committee

R. Baldini (INFN, Frascati)
K. T. Chao (PKU, Beijing)
G. Colangelo (University of Bern)
H. Czyz (University of Katowice)
M. Davier (LAL, Orsay)
A. Denig (University of Mainz)
S. Eidelman (Budker Institute, Novosibirsk)
P. Gauzzi (Universita' La Sapienza, Roma)
F. A. Harris (University of Hawaii)
G. Isidori (INFN, Frascati)
J. H. Kuehn (KIT, Karlsruhe)
A. Lusiani (Scuola Normale Superiore, Pisa)
J. P. Ma (ITP, Beijing)
M. Passera (INFN, Padova)
B. L. Roberts (University of Boston)
X. Y. Shen (IHEP, Beijing)
E. Solodov (Budker Institute, Novosibirsk)
E. Tomasi-Gustafsson (IRFU, Saclay)
L. Trentadue (University of Parma)
A. Vainshtein (University of Minnesota)
G. Venanzoni (INFN, Frascati)
Z. P. Zheng (IHEP, Beijing)

Local Organizing Committee (USTC, Hefei)

X. L. Wang
Q. Wang
H. P. Peng
W. B. Yan
J. B. Liu
Y. W. Liu
L. Yan
H. J. Xu
M. H. Liu
Z. B. Tang
Y. F. Zhang
H. Zeng
J. Dong
X. R. Zhou
Y. Liang
C. Z. Yuan (co-chair, IHEP, Beijing)
G. S. Huang (co-chair)
Z. G. Zhao (chair)

FOREWORD

ZHAO Zhengguo
(for the PHIPSI15 Local Organizing Committee)
University of Science and Technology of China, Hefei 230026, China

The "International Workshop on e^+e^- collisions from ϕ to ψ" (PHIPSI15), was held at University of Science and Technology of China (USTC), Hefei, China, from Wednesday, September 23 to Saturday, September 26, 2015. This is the 10th workshop in a series, which started in Karlsruhe in 1996 and continued in Novosibirsk (1999), SLAC (2001), Pisa (2003), Novosibirsk (2006), Frascati (2008), Beijing (2009), Novosibirsk (2011) and Rome (2013), carrying now the name "from ϕ to ψ" first used at the Novosibirsk workshop in 1999. The aim of the workshop is to discuss in detail the state of art of various problems in hadronic physics at low energy e^+e^- colliders and the potential of existing and future facilities.

The subjects of the Workshop include: (1) R-measurements; (2) Radiative corrections; (3) Form factors and OZI rule violation; (4) Spectroscopy (light and heavy); (5) Muon $g-2$, experimental measurements and theoretical calculations; (6) Flavor physics; (7) Proton radius puzzle; (8) Gamma-gamma physics; (9) Tau lepton physics; (10) Machines and detectors.

We thank all the participants and the international advisory committee for making a very successful Workshop.

The Workshop was sponsored by the Chinese Center for Advanced Science and Technology (CCAST), the National Natural Science Foundation of China (NSFC), the Ministry of Science and Technology of China, the Chinese Academy of Sciences (CAS), and the University of Science and Technology of China (USTC).

中国科学技术大学学报

第 46 卷　第 7 期(总第 279 期)　2016 年 7 月

目　　次

[期刊基本参数]　CN34-1054/N * 1965 * m * A4 * 102 * zh/en * P * ¥30.00 * 1200 * 12 * 2016-07

责任编辑　贺　伟　　**英文编辑**　崔海建　Federick Firstbrook

JOURNAL OF UNIVERSITY OF SCIENCE AND TECHNOLOGY OF CHINA

Vol. 46 No. 7(Serial No. 279) Jul. 2016

CONTENTS

Article ID:0253-2778(2016)07-0533-08

Theoretical review of XYZ

LIU Xiang[1,2]

(1. *School of Physical Science and Technology, Lanzhou University, Lanzhou* 730000, *China*;
2. *Research Center for Hadron and CSR Physics, Lanzhou University & Institute of Modern Physics of CAS, Lanzhou* 730000, *China*)

Abstract: In the past 12 years, dozens of charmonium-like states have been reported in experiment. Facing so abundant novel phenomena, theorists have been hard at work to reveal the underlying mechanism relevant to these XYZ states. A concise review of the observed XYZ states is first given. Then, an introduction is presented to the theoretical progress made by our group in the study of XYZ states, which includes ① the hadronic molecular state explanations to $Y(3940)$, $Y(4140)$ and $Y(4274)$; ② the non-resonant explanation to $Y(4260)$ and $Y(4360)$; ③ the P-wave charmonium assignment to $Y(3915)$, $Z(3930)$ and $X(4350)$; ④ the initial single pion emission mechanism and the observation of $Z_c(3900)$.

Key words: charmonium-like states; non-perturbative QCD; phenomenological model

CLC number: O572.3 **Document code**: A doi:10.3969/j.issn.0253-2778.2016.07.001

Citation: LIU Xiang. Theoretical review of XYZ [J]. Journal of University of Science and Technology of China, 2016,46(7):533-540,586.

XYZ 类粲偶素的理论回顾

刘 翔[1,2]

(1. 兰州大学物理科学与技术学院,甘肃兰州 730000;
2. 兰州大学与中国科学院近代物理研究所共建强子与CSR物理研究中心,甘肃兰州 730000)

摘要:在过去的12年中,实验上发现了大量的类粲偶素.面对如此多新奇的态,理论学家们致力于去解释这些 XYZ 粒子内在的动力学机制.本文首先简短地回顾已发现的 XYZ 态,然后主要介绍我们组在 XYZ 类粲偶素理论研究中的一些工作,其中主要包括:① 将 $Y(3940)$, $Y(4140)$ 和 $Y(4274)$ 解释为强子分子态;② $Y(4260)$ 和 $Y(4360)$的非共振态解释;③ 将 $Y(3915)$, $Z(3930)$ 和 $X(4350)$这3个态解释为 P 波粲偶素;④ 初态单 π 发射机制和对 $Z_c(3900)$的研究.

关键词:类粲偶素;非微扰QCD;唯象模型

0 Introduction

Due to big experimental advances in the observation of charmonium-like XYZ states, theoretical study of XYZ has became a hot research field full of challenges and opportunities. Studying charmonium-like XYZ states will be helpful to deepen our understanding of non-perturbative

Received: 2015-11-30; **Revised**: 2016-04-20

Foundation item: Supported by National Natural Science Foundation of China (11222547, 11175073, 11035006).

Biography: LIU Xiang, male, born in 1978, PhD/Prof. Research field: particle physics. E-mail: xiangliu@lzu.edu.cn

QCD.

In the following, I mainly focus on the XYZ states produced by B meson decays, the $\gamma\gamma$ fusion, e^+e^- annihilation, and the hadronic decays of $Y(4260)$. Combing the progress made by our group, I will illustrate the present research status.

1 The observed XYZ states

Since the first charmonium-like state $X(3871)$ was reported by BaBar in B meson decay $B\to KJ/\psi\pi^+\pi^-$[1], more and more charmonium-like states have been observed in the the past 12 years. According to the difference in production mechanisms, the observed XYZ states can be categorized into five groups: B meson decay, e^+e^- annihilation via initial state radiation, double charmonium production process, $\gamma\gamma$ fusion, and hadronic decays of $Y(4260)$.

In Tab. 1, I summarize these observed charmonium-like states, where the XYZ states listed in the first, the second, the third, the fourth and the fifth columns correspond to B meson decay, e^+e^- annihilation via initial state radiation, double charmonium production process, $\gamma\gamma$ fusion, and hadronic decays of $Y(4260)$, respectively, which provides an ideal platform to explore XYZ states experimentally.

Tab. 1 The observed charmonium-like states

A	B	C	D	E
$X(3872)$	$Y(4260)$	$X(3940)$	$X(3915)$	$Z_c(3900)$
$Y(3930)$	$Y(4008)$	$X(4160)$	$X(4350)$	$Z_c(4020)$
$Z^+(4430)$	$Y(4360)$		$Z(3930)$	$Z_c(4025)$
$Z(4051)$	$Y(4630)$			$Z_c(3885)$
$Z(4248)$	$Y(4660)$			
$Y(4140)$				
$Y(4274)$				
$Z_c^+(4200)$				
$Z^+(4240)$				

For readers' connivence, I also show the production and decay information relevant to these XYZ states in Eq. (1)~(5).

$$B\to\begin{cases}X(3872)K\to\underline{J/\psi\pi^+\pi^-}K\\ Y(3940)K\to\underline{J/\psi\omega}K\\ Z^+(4430)K\to\underline{\psi'\pi^+}K\\ Z^+(4051)K\\ Z^+(4248)K\end{cases}\to\underline{\chi_{c1}\pi^+}K\quad\begin{cases}Y(4140)K\\ Y(4274)K\end{cases}\to\underline{J/\psi\phi}K \tag{1}$$

$$e^+e^-\to\begin{cases}Y(4260)\to\underline{J/\psi\pi^+\pi^-}\\ Y(4008)\\ Y(4360)\\ Y(4660)\end{cases}\to\underline{\psi'\pi^+\pi^-}\quad\begin{cases}\\ \\ \\ Y(4630)\to\underline{\Lambda_c\bar{\Lambda}_c}\end{cases} \tag{2}$$

$$e^+e^-\to\begin{cases}X(3940)J/\psi\to\underline{D^*\bar{D}}J/\psi\\ X(4160)J/\psi\to\underline{D^{*+}D^{*-}}J/\psi\end{cases} \tag{3}$$

$$\gamma\gamma\to\begin{cases}X(3915)\to\underline{D\bar{D}}\\ X(4350)\to\underline{J/\psi\phi}\\ Z(3930)\to\underline{J/\psi\omega}\end{cases} \tag{4}$$

$$e^+e^-\to\begin{cases}Z_c(3900)\pi^\mp\to\underline{J/\psi\pi^\pm}\pi^\mp\\ Z_c(4025)\pi^\mp\to\underline{(D^*\bar{D}^*)^\pm}\pi^\mp\\ Z_c(4020)\pi^\mp\to\underline{h_c\pi^\pm}\pi^\mp\\ Z_c(3885)\pi^+\to\underline{(D\bar{D}^*)^-}\pi^+\end{cases} \tag{5}$$

Facing so abundant novel phenomena, a crucial task is to reveal the underlying mechanism behind these phenomena. The observed XYZ states have stimulated extensive discussion of them, which has become a hot research filed in present hadron physics.

2 The hadronic molecular state explanations to $Y(3940)$, $Y(4140)$ and $Y(4274)$

$X(3872)$ is the first reported charmonium-like state in B meson decay $B\to KJ/\psi\pi^+\pi^-$[1]. According to the quark model estimate, the mass of $X(3872)$ is not consistent with that of a 2^3P_1 charmonium (χ'_{c1}) state. Additionally, the observed decay mode $X(3872)\to J/\psi\rho$ is isospin violation. Thus, different theoretical explanations were proposed, which mainly include:

① The molecular state assignment[2-6].

② $X(3872)$ was also explained as the 1^{++} cusp[7].

③ The S-wave threshold effect due to the $D^0\bar{D}^{0*}$ threshold[8].

④ The hybrid charmonium assignment to $X(3872)$[9].

⑤ The diquark anti-diquark bound state[10] and the tetraquark state[11-18].

⑥ $X(3872)$ may have a dominant $c\bar{c}$ component with some admixture of $D^0\bar{D}^{*0}+\bar{D}^0D^{*0}$[19-20].

Thus, further experimental and joint theoretical effort will be helpful to test different theoretical proposals of $X(3872)$.

In the following, I will further introduce the hadronic molecular assignment to $Y(3940)$, $Y(4140)$ and $Y(4274)$ since there exist similarities between $Y(4140)$ and $Y(3940)$. Firstly, the production processes of $Y(4140)$ and $Y(3940)$ through B meson decays are very similar, i.e.,

$$B\to K+\begin{cases}J/\psi\phi\Rightarrow Y(4140)\\ J/\psi\omega\Rightarrow Y(3940)\end{cases}.$$

Secondly, there exits a mass gap relation:

$$M_{Y(4140)}-M_{Y(3930)}\approx M_\phi-M_\omega.$$

Thirdly, $Y(4140)$ and $Y(3940)$ are close to the $D_s^*\bar{D}_s^*$ and $D^*\bar{D}^*$ thresholds, respectively, and satisfy another mass relation

$$M_{Y(4140)}-2M_{D_s^*}\approx M_{Y(3940)}-2M_{D^*}.$$

Just considering these similarities, Liu et al. proposed a uniform molecular picture of $Y(4140)$ and $Y(3940)$ in Ref. [21], where the flavor wave functions of $Y(4140)$ and $Y(3940)$ are[21]

$$|Y(4140)\rangle=|D_s^{*+}D_s^{*-}\rangle,$$

$$|Y(3940)\rangle=\frac{1}{\sqrt{2}}[|D^{*0}\bar{D}^{*0}\rangle+|D^{*+}D^{*-}\rangle],$$

respectively. To test this molecular state assignment to $Y(4140)$ and $Y(3940)$, a dynamical calculation was performed in Ref. [21] via adopting the one boson exchange model, where the pseudoscalar, vector and σ mesons are considered in the calculation, by which the effective potentials of the $D_s^*\bar{D}_s^*$ and $D^*\bar{D}^*$ interactions were obtained. With these effective potentials, Liu et al. found the corresponding bound state solutions, which support the $D_s^*\bar{D}_s^*$ and $D^*\bar{D}^*$ molecular state explanations of $Y(4140)$ and $Y(3940)$[21].

In 2010, CDF reported a charmonium-like state $Y(4274)$ by analyzing the $J/\psi\phi$ invariant mass spectrum[22]. In Ref. [23], Liu et al. suggested $Y(4274)$ to be an S-wave $D_s\bar{D}_{s0}(2317)$ molecular state, and predicted the existence of its partner, an S-wave $D\bar{D}_0(2400)$ molecular state[23].

As shown in Fig. 1, there exist two event clusters around the ranges of $\Delta M\approx 1.27$ GeV and $1.4\ \text{GeV}<\Delta M<1.5$ GeV, which are marked by yellow and pink. The structure around $\Delta M\approx 1.27$ can be related to the $D_s\bar{D}'_{s1}(2460)$ or $D_s^*\bar{D}_{s0}(2317)$ system. The other one in the range $1.4\ \text{GeV}<\Delta M<1.5$ GeV may result from the $D_s\bar{D}_{s1}(2536)$, $D_s\bar{D}_{s2}(2573)$, $D_s^*\bar{D}'_{s1}(2460)$ and $D_s^*\bar{D}_{s1}(2536)$ systems since the event cluster in the range $1.4\ \text{GeV}<\Delta M<1.5$ GeV just overlaps with the corresponding thresholds. Further

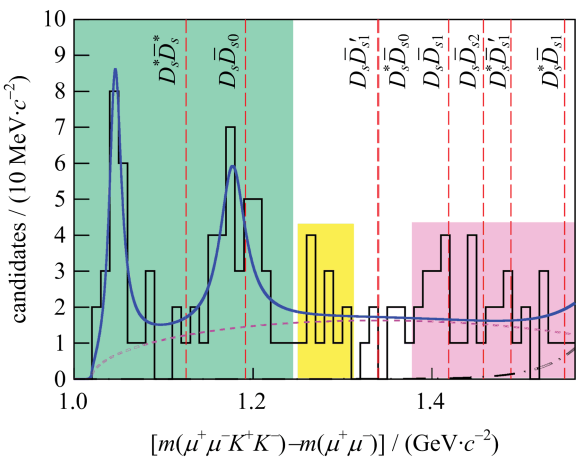

Besides $Y(4140)$, one explicit enhancement appears around 4274 MeV. Here, the purple dashed line is the background from the three-body phase space. The blue solid line is the fitting result with resonance parameters of $Y(4140)$ and $Y(4270)$ resonances in Ref. [22]. The vertical red dashed lines denote the thresholds of $D_s^*\bar{D}_s^*$, $D_s\bar{D}_{s0}(2317)$, $D_s\bar{D}'_{s1}(2460)$, $D_s^*\bar{D}_{s0}(2317)$, $D_s\bar{D}_{s1}(2536)$, $D_s\bar{D}_{s2}(2573)$, $D_s^*\bar{D}'_{s1}(2460)$ and $D_s^*\bar{D}_{s1}(2536)$. Taken from Ref. [23]

Fig. 1 The mass difference $\Delta M=m(\mu^+\mu^-K^+K^-)-m(\mu^+\mu^-)$ distribution (histogram) for events in the B^+ mass window[22]

experimental study of these event clusters will be an interesting task.

3 The non-resonant explanation of $Y(4260)$ and $Y(4360)$

For explaining $Y(4260)$ and $Y(4360)$, different exotic state explanations were proposed in literature, like a charmonium hybird[24-26], diquark-antidiquark state with the component $[cs][\bar{c}\bar{s}]$[27-28], different molecular states[29-34], and a charmonium hybrid state that couples to $D\bar{D}_1$ and $D\bar{D}_0$ channels[35]. Additionally, there were extensive discussions of $Y(4260)$ as conventional charmonium[36-39].

In this paper, I introduce the non-resonant explanation to $Y(4260)$ and $Y(4360)$[40,42].

For $e^+e^- \to J/\psi\pi^+\pi^-$ process, there exists direct production of $J/\psi\pi^+\pi^-$ by the e^+e^- annihilation. Here, the virtual photon from the e^+e^- annihilation directly interacts with $J/\psi\pi^+\pi^-$. Besides the e^+e^- annihilation directly into $J/\psi\pi^+\pi^-$, another important production mechanism of $e^+e^- \to J/\psi\pi^+\pi^-$ is through the intermediate charmonia (see Fig. 2 for more details).

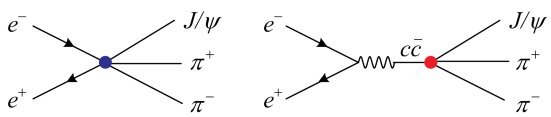

(a) the e^+e^- annihilation directly into $J/\psi\pi^+\pi^-$ (b) from the contributions of intermediate charmonia

Taken from Ref. [42].

Fig. 2 The diagrams relevant to $e^+e^- \to J/\psi\pi^+\pi^-$

The result shown in Fig. 3 indicates that the $Y(4260)$ structure can be reproduced by the interference of production amplitudes of the $e^+e^- \to J/\psi\pi^+\pi^-$ processes via direct e^+e^- annihilation and through intermediate charmonia $\psi(4160)$/$\psi(4415)$[42].

The similar idea was applied to study $Y(4360)$ in Ref. [40], where $Y(4360)$ signals can be described when introducing the interference of $\psi(4160)$ and $\psi(4415)$ with the continuum contribution. This fact shows that $Y(4260)$ and

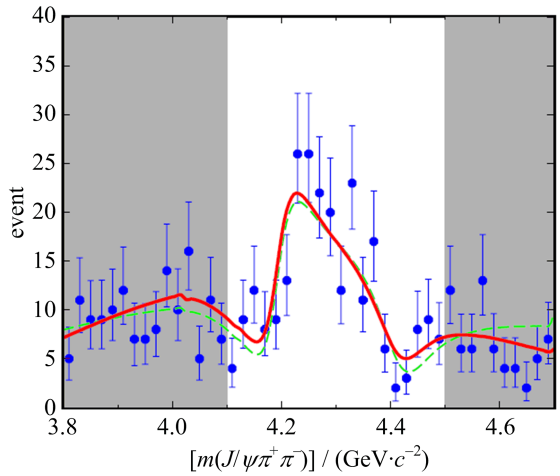

We also give the obtained fitting result by adopting the dipole form for $\mathcal{F}_{NOR}(s)$ (green dashed line). Here, our result is normalized to the experimental data. Taken from Ref. [42].

Fig. 3 The obtained fitting result (red solid line) and the comparison with the experimental data (blue dots with error bar) measured by BaBar[41]

$Y(4360)$ are not genuine resonances. The non-resonant explanation of $Y(4260)$ and $Y(4360)$ can naturally answer why $Y(4260)$ and $Y(4360)$ are still missing in the R value scan and the corresponding open-charm decay channels.

4 The P-wave charmonium assignment to $Y(3915)$, $Z(3930)$ and $X(4350)$

Checking the PDG data[43], we found that there are three P-wave ground states $\chi_{c0}(3415)$, $\chi_{c1}(3510)$ and $\chi_{c2}(3556)$. The observation of $X(3915)$, $X(4350)$ and $Z(3930)$ provides us with a good chance to study the radial excitations of P-wave charmonium family. In the following, I conclusions of the P-wave charmonium assignments to $\chi_{c0}(3415)$, $\chi_{c1}(3510)$ and $\chi_{c2}(3556)$ in Ref. [44]:

① $X(3872)$ and $Z(3930)$ can be regarded as $\chi'_{c1}(2P)$ with $J^{PC}=1^{++}$[19-20] and $\chi'_{c2}(2P)$ with $J^{PC}=2^{++}$, respectively.

② $X(3915)$ can be an χ'_{c0} state[44], since its mass is close to the predicted mass of χ'_{c0} predicted in Ref. [51]. This assignment can explain why the mass difference between $X(3915)$ and $Z(3930)$ is smaller than that between $X(3915)$ and X

(3872)[44].

③ $X(4350)$ was explained as $\chi_{c2}''(2P)$[44].

The above assignment to charmonium-like states observed in $\gamma\gamma$ fusion can be supported by the further study of two-body strong decay of $X(3915)$, $Z(3930)$ and $X(4350)$[44], as shown in Figs. 4 and 5.

5 The initial single pion emission mechanism and the observation of $Z_c(3900)$

Belle observed two charged bottomoniumlike states $Z_b(10610)$ and $Z_b(10650)$ by studying the e^+e^- annihilation into hidden-bottom dipion channels[45]. $Z_b(10610)$ and $Z_b(10650)$ have two interesting properties. Firstly, the masses of $Z_b(10610)$ and $Z_b(10650)$ are close to that of $B\overline{B}^*$ and $B^*\overline{B}^*$, respectively. Secondly, $Z_b(10610)$ and $Z_b(10650)$ are charged states.

The initial single pion emission (ISPE) mechanism[46] was proposed to understand two bottomonium-like structures $Z_b(10610)$ and $Z_b(10650)$. The physical picture is that the emitted pion with continuous energy distribution produces $B^{(*)}$ and $\overline{B}^{(*)}$ with low momentum. Thus, the intermediate $B^{(*)}$ and $\overline{B}^{(*)}$ can easily interact with each other to transit into hidden-charm dipion final states together with one bottomonium. Under the ISPE mechanism, we explained why two bottomonium-like structures $Z_b(10610)$ and $Z_b(10650)$ appear in the $\Upsilon(nS)\pi^{\pm}$ and $h_b(mP)\pi^{\pm}$ invariant mass spectra, and are close to the $B\overline{B}^*$ and $B^*\overline{B}^*$ thresholds, respectively[46].

If the ISPE mechanism is a universal mechanism existing in heavy quarkonium dipion decays, we can naturally apply this mechanism to study the hidden-charm dipion decays of higher charmonia, which is due to the similarity between charmonium and bottomonium[47]. This investigation can provide more predictions for the future experiment as an important test of the ISPE

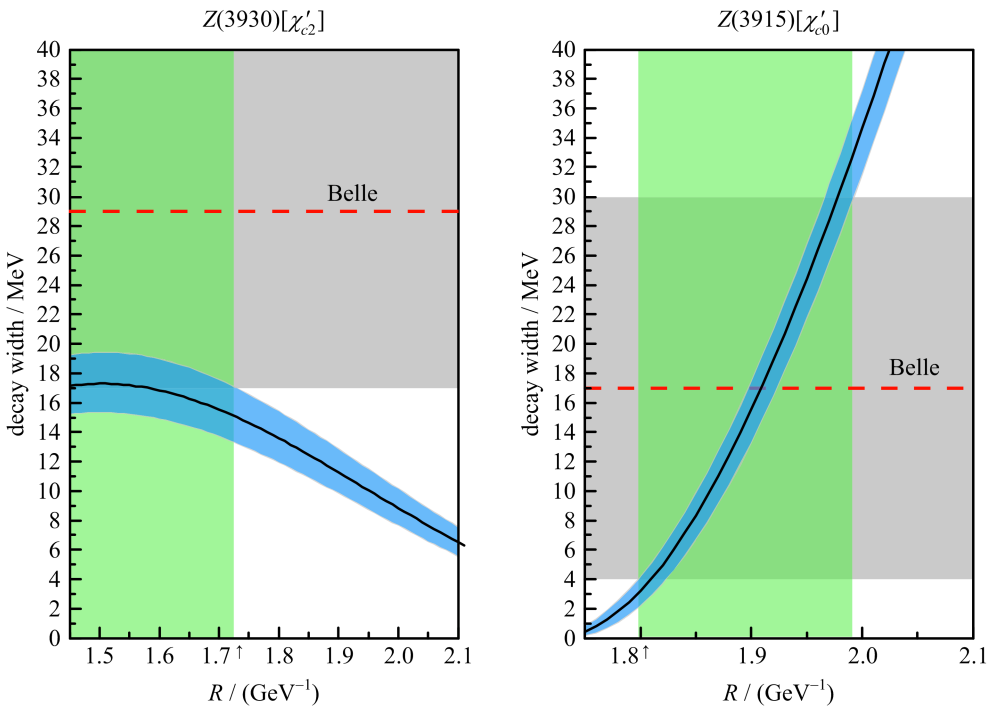

The green band denotes the region of R resulting in the theoretical values consistent with Belle data. The solid lines with blue error bands are our calculation result. Taken from Ref. [44].

Fig. 4 The dependence of the decay width of $Z(3930)$ and $X(3915)$ on R under χ'_{c2} and χ'_{c0} assignment for $Z(3930)$ and $X(3915)$, respectively

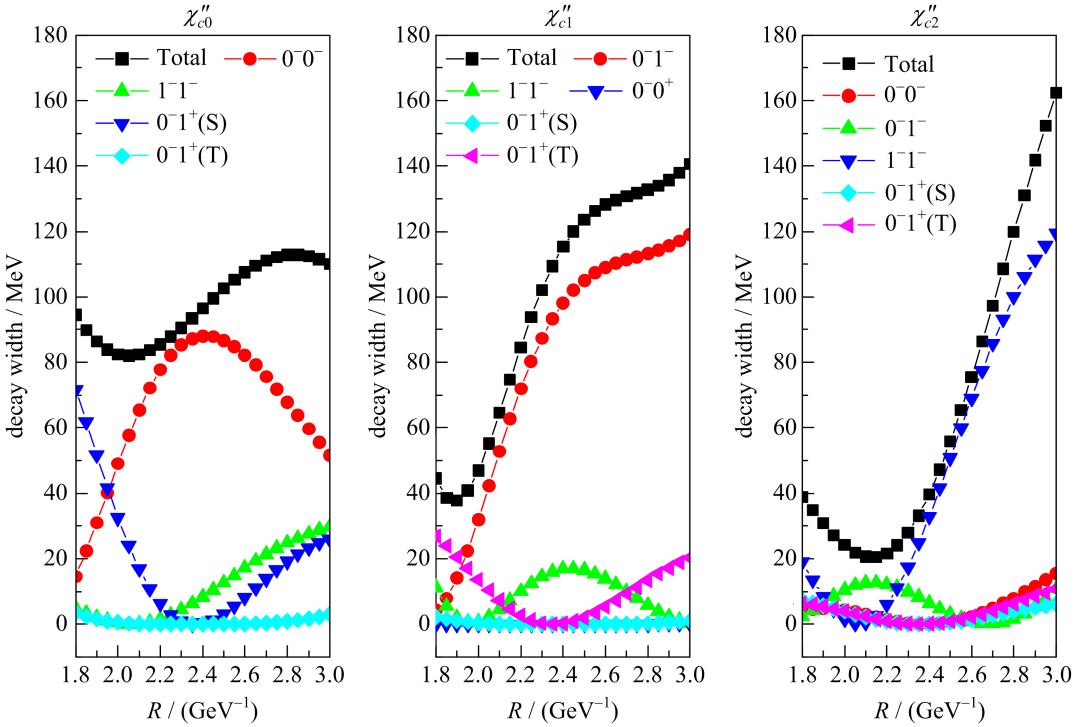

Here, we set the upper limit of the masses of P-wave states with the second radial excitation as 4.35 GeV. The yellow dash line and shaded grey band shown in diagram of χ''_{c2} denote the central value for the error of total width of $X(3915)$ measured by Belle. Taken from Ref. [44].

Fig. 5 The variation of the decay width of χ''_{cJ} ($J=0,1,2$) with R value

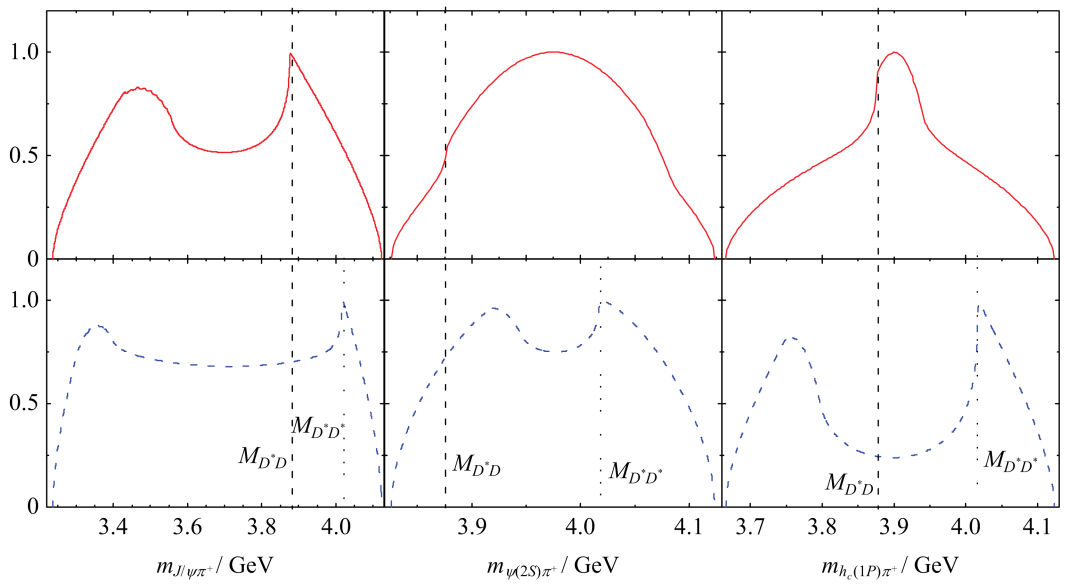

The solid, dashed correspond to the results considering intermediate $D\bar{D}^*+h.c.$ and $D^*\bar{D}^*$ respectively. The vertical dashed lines and the dotted lines denote the threshhold of $D^*\bar{D}$ and $D^*\bar{D}^*$ respectively. The maximum of the line shape is normalized to 1. Taken from Ref. [47].

Fig. 6 The invariant mass spectra of $J/\psi\pi^+$, $\psi(2S)\pi^+$ and $h_c(1P)\pi^+$ for the $Y(4260)$ decays into $J/\psi\pi^+\pi^-$, $\psi(2S)\pi^+\pi^-$ and $h_c(1P)\pi^+\pi^-$

mechanism.

In Ref. [47], we predicted charged charmonium-like structures in the hidden-charm dipion decay of higher charmonia and charmonium-like state $Y(4260)$. The typical peculiarity of predicted charged charmonium-like structures is that they are near the $D\bar{D}^*$ or $D^*\bar{D}^*$ threshold.

In 2013, BESIII announced the observation of a charged charmonium-like structure $Z_c(3900)$ in $e^+e^- \to J/\psi\pi^+\pi^-$ at $\sqrt{s}=4.26$ GeV[48], which is around the $D\bar{D}^*$ threshold. Almost at the same time, Belle also observed $Z_c(3900)$[49]. The observation of $Z_c(3900)$ is consistent with our prediction in Ref. [47].

According to this research status, we studied $Z_c(3900)$ by considering the ISPE mechanism in Ref. [50], where other two mechanisms (the direct production and final state interaction) were included in the calculation. The $Z_c(3900)$ signal can be well reproduced. Thus, it is possible that $Z_c(3900)$ is not a genuine resonance.

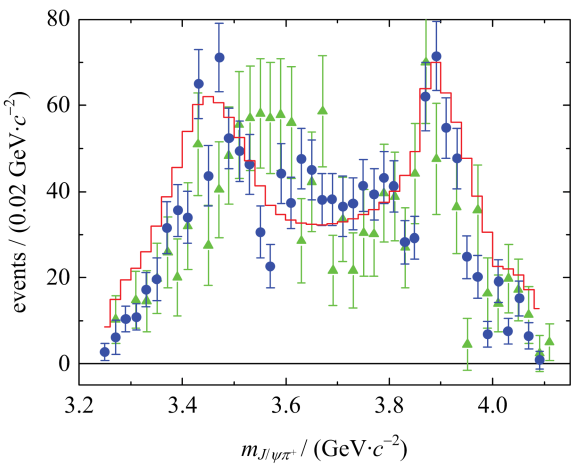

The blue dots and green triangles with error bars are the experimental data given by BESIII[48] and Belle[49], respectively. The red histograms are our results considering contributions of the ISPE mechanism to the $Y(4260)\to\pi^+\pi^- J/\psi$ decay. Taken from Ref. [50].

Fig. 7 The distributions of the $J/\psi\pi^+$ invariant mass spectrum of $Y(4260)\to\pi^+\pi^- J/\psi$

6 Conclusion

In this paper, I gave a brief review of the present research status of *XYZ* states. The conclusions are summarized as follows:

① The hadronic molecular state explanations of $Y(3940)$, $Y(4140)$ and $Y(4274)$ were given in Refs. [21,23].

② The non-resonant explanation of $Y(4260)$ and $Y(4360)$ was suggested in Refs. [40,42].

③ The P-wave charmonium assignment to $Y(3915)$, $Z(3930)$ and $X(4350)$ was proposed in Ref. [44]. Here, $X(3915)$, $Z(3930)$, and $X(4350)$ were explained to be $\chi'_{c0}(2P)$ with $J^{PC}=0^{++}$, $\chi'_{c2}(2P)$ with $J^{PC}=2^{++}$, and $\chi''_{c2}(2P)$, respectively.

④ According to ISPE mechanism, charged charmonium-like state near $D\bar{D}^*$ threshold was predicted in Ref. [47], which may correspond to the observed $Z_c(3900)$[50].

In the years that follow, we still need to make more effort to reveal these underlying mechanisms behind these novel phenomena, which will be an intriguing research issue.

References

[1] CHOI S K, OLSEN S L, ABE K, et al. Observation of a narrow charmonium-like state in exclusive $B^\pm\to K^\pm\pi^+\pi^- J/\psi$ decays [J]. Phys Rev Lett, 2003, 91: 262001.

[2] CLOSE F E, PAGE P R. The $D^{*0}\bar{D}^0$ threshold resonance[J]. Phys Lett B, 2004, 578: 119-123.

[3] VOLOSHIN M B. Interference and binding effects in decays of possible molecular component of $X(3872)$ [J]. Phy Lett B, 2004, 579: 316-320.

[4] WONG C Y. Molecular states of heavy quark mesons [J]. Phys Rev C, 2004, 69: 055202.

[5] SWANSON E S. Short range structure in the $X(3872)$ [J]. Phys Lett B, 2004, 588: 189-195.

[6] TORNQVIST N A. Isospin breaking of the narrow charmonium state of Belle at 3872 MeV as a deuson [J]. Phys Lett B, 2004, 590: 209-215.

[7] BUGG D V. Reinterpreting several narrow "resonances" as threshold cusps[J]. Phys Lett B, 2004, 598: 8-14.

[8] ROSNER J L. Effects of *S*-wave thresholds[J]. Phys Rev D, 2006, 74: 076006.

[9] LI B A. Is $X(3872)$ a possible candidate of hybrid meson[J]. Phys Lett B, 2005, 605: 306-310.

[10] MAIANI L, PICCININI F, POLOSA A D, et al.

Diquark-antidiquarks with hidden or open charm and the nature of $X(3872)$[J]. Phys Rev D, 2005, 71: 014028.

[11] HOGAASEN H, RICHARD J M, SORBA P. Chromomagnetic mechanism for the $X(3872)$ resonance [J]. Phys Rev D, 2006, 73: 054013.

[12] HALLSTEIN Hogaasen, EMI Kou, JEAN-MARC Richard, et al. Isovector and hidden-beauty partners of the $X(3872)$[EB/OL]. (2014-03-14)[2015-11-01]. http://arxiv.org/abs/1309.2049.

[13] EBERT D, FAUSTOV R N, GALKIN V O. Masses of heavy tetraquarks in the relativistic quark model[J]. Phys Lett B, 2006, 634: 214-219.

[14] BARNEA N, VIJANDE J, VALCARCE A. Four-quark spectroscopy within the hyperspherical formalism [J]. Phys Rev D, 2006, 73: 054004.

[15] MATHEUS R D, NARISON S, NIELSEN M, et al. Can the $X(3872)$ be a 1^{++} four-quark state? [J]. Phys Rev D, 2007, 75: 014005.

[16] CHIU T W, HSIEH T H (TWQCD Collaboration). $X(3872)$ in lattice QCD with exact chiral symmetry [J]. Phys Lett B, 2007, 646: 95-99.

[17] CHIU T W, HSIEH T H (TWQCD Collaboration). Pseudovector meson with strangeness and closed charm [J]. Phys Rev D, 2006, 73: 111503(R) (Erratum-ibid. D 2007, 75: 019902).

[18] CUI Y, CHEN X L, DENG W Z, et al. The possible heavy tetraquarks $qQ\bar{q}\bar{Q}$, $qq\bar{Q}\bar{Q}$ and $qQ\bar{Q}\bar{Q}$[J]. High Energy Phys Nucl Phys, 2007, 31: 7-13.

[19] MENG C, GAO Y J, CHAO K T. $B\to\chi_{c1}(1P,2P)K$ decays in QCD factorization and $X(3872)$[J]. Phys Rev D, 2013, 87: 074035.

[20] SUZUKI M. The $X(3872)$ boson: Molecule or charmonium[J]. Phys Rev D, 2005, 72: 114013.

[21] LIU X, ZHU S L. $Y(4143)$ is probably a molecular partner of $Y(3930)$ [J]. Phys Rev D, 2009, 79: 094026.

[22] YI K (for the CDF collaboration). Observation of a narrow near-threshold structure in the $J/\psi\varphi$ mass spectrum in $B^+\to J/\psi\varphi K^+$ decays[J]. PoS ICHEP, 2010, 2010: 182.

[23] LIU X, LUO Z G, ZHU S L. Novel charmonium-like structures in the $J/\psi\phi$ and $J/\psi\omega$ invariant mass spectra [J]. Phys Lett B, 2011, 699: 341-344 (Erratum-ibid. B, 2012, 707: 577).

[24] ZHU S L. The Possible interpretations of $Y(4260)$ [J]. Phys Lett B, 2005, 625: 212-216.

[25] KOU E, PENE O. Suppressed decay into open charm for the $Y(4260)$ being an hybrid[J]. Phys Lett B, 2005, 631: 164-169.

[26] CLOSE F E, PAGE P R. Gluonic charmonium resonances at BaBar and Belle? [J]. Phys Lett B, 2005, 628: 215-222.

[27] MAIANI L, RIQUER V, PICCININI F, et al. Four quark interpretation of $Y(4260)$[J]. Phys Rev D, 2005, 72: 031502.

[28] EBERT D, FAUSTOV R N, GALKIN V O. Relativistic description of heavy tetraquarks[J]. Phys Atom Nucl, 2009, 72: 184-188.

[29] LIU X, ZENG X Q, LI X Q. Possible molecular structure of the newly observed $Y(4260)$[J]. Phys Rev D, 2005, 72: 054023.

[30] YUAN C Z, WANG P, MO X H. The $Y(4260)$ as an $\omega\chi_{c1}$ molecular state[J]. Phys Lett B, 2006, 634: 399-402.

[31] QIAO C F. One explanation for the exotic state $Y(4260)$[J]. Phys Lett B, 2006, 639: 263-265.

[32] DING G J. Are $Y(4260)$ and $Z_2^+(4250)$ D_1D or D_0D^* hadronic molecules? [J]. Phys Rev D, 2009, 79: 014001.

[33] MARTINEZ TORRES A, KHEMCHANDANI K P, GAMERMANN D, et al. The $Y(4260)$ as a $J/\psi K\bar{K}$ system[J]. Phys Rev D, 2009, 80: 094012.

[34] CLOSE F, DOWNUM C, THOMAS C E. Novel charmonium and bottomonium spectroscopies due to deeply bound hadronic molecules from single pion exchange[J]. Phys Rev D, 2010, 81: 074033.

[35] KALASHNIKOVA Y S, NEFEDIEV A V. Spectra and decays of hybrid charmonia [J]. Phys Rev D, 2008, 77: 054025.

[36] LLANES-ESTRADA F J. $Y(4260)$ and possible charmonium assignment[J]. Phys Rev D, 2005, 72: 031503(R).

[37] EICHTEN E J, LANE K, QUIGG C. New states above charm threshold[J]. Phys Rev D, 2006, 73: 014014 (Erratum-ibid. D, 2006, 73: 079903).

[38] SEGOVIA J, YASSER A M, ENTEM D R, et al. $J^{PC}=1^{--}$ hidden charm resonances[J]. Phys Rev D, 2008,78: 114033.

[39] LI B Q, CHAO K T. Higher Charmonia and X, Y, Z states with screened potential[J]. Phys Rev D, 2009, 79: 094004.

[40] CHEN D Y, HE J, LIU X. A Novel explanation of charmonium-like structure in $e^+e^-\to\psi(2S)\pi^+\pi^-$[J]. Phys Rev D, 2011, 83: 074012.

[41] AUBERT B, BARATE R, BOUTIGNY D, et al. Observation of a broad structure in the $\pi^+\pi^-J/\psi$ mass spectrum around 4.26 GeV/c^2 [J]. Phys Rev Lett, 2005, 95: 142001.

(下转第586页)

Article ID:0253-2778(2016)07-0541-08

XYZ at BESIII

ZHANG Jingzhi, YUAN Changzheng (for the BESIII Collaboration)

(*Institute of High Energy Physics, Chinese Academy of Sciences, Beijing* 100049, *China*)

Abstract: With 5.1 fb^{-1} of data taken at $\sqrt{s}=3.8\sim4.6$ GeV, BESIII made a significant contribution to the study of charmonium-like states, i.e., the XYZ states. We review the results of observations of the Z_c states, the $X(3872)$ in e^+e^- annihilation, and charmonium $\psi(1^3D_2)$ state, as well as measurements of the cross-sections of $\omega\chi_{cJ}$ and $\eta J/\psi$.

Key words: charmonium-like; initial state radiation (ISR); exoitic

CLC number: O572.3 **Document code**: A doi:10.3969/j.issn.0253-2778.2016.07.002

Citation: ZHANG Jingzhi, YUAN Changzheng. XYZ at BESIII[J]. Journal of University of Science and Technology of China, 2016,46(7):541-548.

BESIII 上 XYZ 的研究

张景芝,苑长征(BESIII 合作组)

(中国科学院高能物理研究所,北京 100049)

摘要:通过分析质心系能量为3.8~4.6 GeV的5.1 fb^{-1}数据,BESIII在类粲偶素(即XYZ)的研究上取得了重要成果.我们回顾了Z_c的发现,$X(3872)$在e^+e^-湮灭中的产生,粲偶素$\psi(1^3D_2)$的发现,以及$\omega\chi_{cJ}$和$\eta J/\psi$过程界面的测量.

关键词:类粲偶素;初态辐射;奇异态

0 Introduction

In recent years, charmonium physics gained renewed strong interest from both theorists and experimentalists, due to the observation of charmonium-like states[1]. These states do not fit in the conventional charmonium spectroscopy, and could be exotic states that lie outside the quark model. $Y(4260)$ was first seen by BaBar as a peak in the $e^+e^-\to\pi^+\pi^- J/\psi$ cross section at enter-of-mass energy of 4.26 GeV[2]. It was subsequently confirmed by CLEO[3] and Belle[4]. Its production via the electron and positron annihilation process requires the quantum numbers of the $Y(4260)$ to be $J^{PC}=1^{--}$. The absence of any apparent corresponding structure in the cross sections for $e^+e^-\to D^{(*)}D^{(*)}(\pi)$[5] indicates that the $Y(4260)$ is probably not a conventional quarkonium state. To study the charmonium(-like) states above 4 GeV, and to establish the relationship between the charmonium-like states and higher excited charmonium states, BESIII has collected in total 5.1 fb^{-1} data[6-7] during 2013 and 2014 above 3.8 GeV. The results presented in this talk are based

Received:2015-11-30;**Revised**:2016-04-20

Foundation item:Supported by National Natural Science Foundation of China (11235011,11475187).

Biography:ZHANG Jingzhi (corresponding author), PhD/Prof. Research field: experimental particle physics. E-mail: jingzhi@ihep.ac.cn

on these data samples.

1 Observation of $Z_c(3900)$

BESIII studied the $e^+e^-\to\pi^+\pi^- J/\psi$ process at a center-of-mass energy of 4.26 GeV using a 525 pb^{-1} data sample[8]. A structure at around 3.9 GeV/c^2 was observed in the $\pi^\pm J\psi$ mass spectrum with a statistical significance larger than 8σ, which is referred to as the $Z_c(3900)$. A fit to the $\pi^\pm J/\psi$ invariant mass spectrum, shown in Fig. 1, neglecting interference, results in a mass of $(3\,899.0\pm3.6\pm4.9)$ MeV/c^2 and a width of $(46\pm10\pm20)$ MeV. The associated production ratio was measured to be $R=\dfrac{\sigma(e^+e^-\to\pi^\pm Z_c^{\mp}\to\pi^+\pi^- J/\psi)}{\sigma(e^+e^-\to\pi^+\pi^- J/\psi)}=(21.5\pm3.3\pm7.5)\%$.

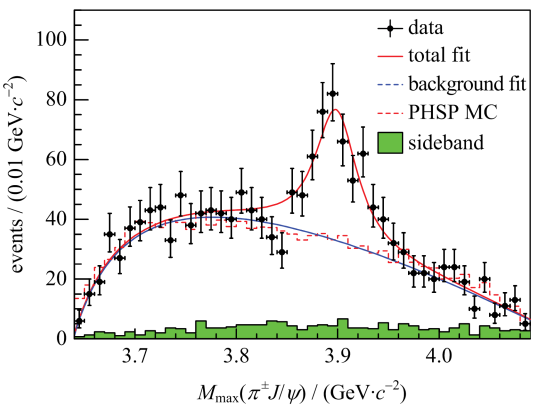

Points with error bars are for data, the curves are the fit results, the dashed histograms are the phase space distributions and the shaded histograms are the non-$\pi^+\pi^- J/\psi$ background estimated from the normalized J/ψ sidebands.

Fig. 1 Unbinned maximum likelihood fit to the distribution of the $M_{\max}(\pi^\pm J/\psi)$

The $Z_c(3900)$ state was confirmed shortly after by Belle[9] and CLEO-c[10] using the initial state radiation (ISR) method. The measured mass and width agreed very well with the BESIII measurements.

A neutral state $Z_c(3900)^0\to\pi^0 J/\psi$ with a significance of 10.4σ was observed at BESIII in $e^+e^-\to\pi^0\pi^0 J/\psi$ with center-of-mass energy ranges from 4.19 to 4.42 GeV[11]. The mass and width were measured to be $(3\,894.8\pm2.3\pm3.2)$ MeV/c^2 and $(29.6\pm8.2\pm8.2)$ MeV, respectively. This state is interpreted as the neutral partner of the $Z_c(3900)^\pm$, as it decays to $\pi^0 J/\psi$ and its mass is close to that of $Z_c(3900)^\pm$. This is in agreement with the previously reported 3.5σ evidence for $Z_c(3900)^0$ in the CLEO-c data[10]. The measured Born cross-sections of $e^+e^-\to\pi^0\pi^0 J/\psi$ were about half of those for $e^+e^-\to\pi^+\pi^- J/\psi$ measured in the Belle experiment[9], which is consistent with the isospin symmetry expectation.

2 Observation of $Z_c(3885)$

With the data sample at $\sqrt{s}=4.26$ GeV, BESIII studied $e^+e^-\to\pi^\pm(D\overline{D}^*)^\mp$. A structure (referred to as $Z_c(3885)$) was observed in the $(D\overline{D}^*)^\pm$ invariant mass distribution[12], as seen in Fig. 2. When fitted to a mass-dependent-width Breit-Wigner (BW) function, the pole mass and width were determined to be $(3\,883.9\pm1.5\pm4.2)$ MeV/c^2 and $(24.8\pm3.3\pm11.0)$ MeV, respectively. The angular distribution of the $Z_c(3885)$ system favors a $J^P=1^+$ assignment for the structure and disfavors 1^- or 0^-. The production rate was measured to be $\sigma(e^+e^-\to\pi^\mp Z_c(3885)^\pm)\times BF(Z_c(3885)^\pm\to(D\overline{D}^*)^\pm)=(83.5\pm6.6\pm22.0)$ pb. The mass and width of $Z_c(3885)$ are 2σ and 1σ, respectively, below those of $Z_c(3900)$, as observed by the BESIII and Belle experiments. However, neither fit considers the possibility of interference with a coherent non-resonant background, which could

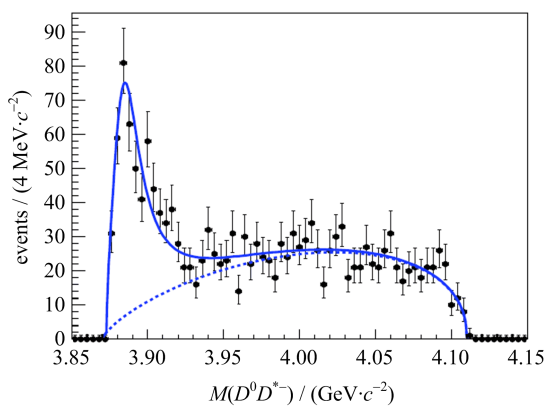

The curves show the best fits.

Fig. 2 Fit to the $M(D^0\ D^{*-})$ distribution for selected events at $\sqrt{s}=4.26$ GeV

shift the results. A spin-parity quantum number determination for $Z_c(3900)$ would provide an additional test of this possibility.

Assuming the $Z_c(3885)$ structure is caused by $Z_c(3900)$, we obtain $\frac{\Gamma(Z_c(3885)\to D\bar{D}^*)}{\Gamma(Z_c(3900)\to\pi J/\psi)}=6.2\pm1.1\pm2.7$. This ratio is much smaller than typical values for decays of conventional charmonium states above the open charm threshold, e. g., $\Gamma(\psi(3770)\to D\bar{D})/\Gamma(\psi(3770)\to\pi^+\pi^- J/\psi)=482\pm84$[13] and $\Gamma(\psi(4040)\to D^{(*)}\bar{D}^{(*)})/\Gamma(\psi(4040)\to\eta J/\psi)=192\pm27$[14]. This suggests very different dynamics in the $Y(4260)-Z_c(3900)$ system.

3 Observation of $Z_c(4020)$

BESIII measured[15] $e^+e^-\to\pi^+\pi^- h_c$ cross-sections at center-of-mass energies of 3.90～4.42 GeV. Intermediate states were studied by examining the Dalitz plot of selected $\pi^+\pi^- h_c$ candidate events. The h_c signal was selected using $3.518\ \mathrm{GeV}/c^2<M(\gamma\eta_c)<3.538$, and $\pi^+\pi^- h_c$ samples of 859 events at 4.23 GeV, 586 events at 4.26 GeV, and 469 events at 4.36 GeV were obtained with purities of 65%. Although there are no clear structures in the $\pi^+\pi^-$ system, there is clear evidence for an exotic charmonium-like structure in the $\pi^\pm h_c$ system in the Dalitz plot. Fig. 3 shows the projection of the $M(\pi^\pm h_c)$ distribution for the signal events, as well as the background events estimated from normalized h_c mass sidebands. There is a significant peak at around $4.02\ \mathrm{GeV}/c^2$ ($Z_c^\pm(4020)$), and there are also some events at around $3.9\ \mathrm{GeV}/c^2$ (inset of Fig. 3), which could be $Z_c(3900)$. The individual datasets at $\sqrt{s}=4.23$, 4.26, and 4.36 GeV show similar structures.

An unbinned maximum likelihood fit was applied to the $M(\pi^\pm h_c)$ distribution summed over the 16 η_c decay modes. The data at 4.23, 4.26, and 4.36 GeV were fitted simultaneously to the same signal function with common mass and width. Fig. 3 shows the fitted results. The mass and width of $Z_c(4020)$ were measured to be

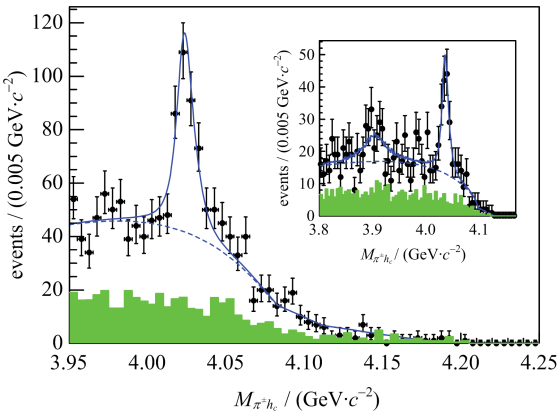

Dots with error bars are data; shaded histograms are normalized sideband background; the solid curves show the total fit; and the dotted curves the backgrounds from the fit.

Fig. 3 Sum of the simultaneous fits to the $M(\pi^\pm h_c)$ distributions at 4.23, 4.26, and 4.36 GeV in the BESIII data; the inset plot shows the sum of the simultaneous fit to the $M_{\pi^+ h_c}$ distributions at 4.23 and 4.26 GeV with $Z_c(3900)$ and $Z_c(4020)$

$(4022.9\pm0.8\pm2.7)\ \mathrm{MeV}/c^2$ and $(7.9\pm2.7\pm2.6)$ MeV, respectively. The statistical significance of the $Z_c(4020)$ signal was found to be greater than 8.9σ.

Adding $Z_c(3900)$ with the mass and width fixed to the BESIII measurements[8], the fit is improved somewhat. But the statistical significance is only 2.1σ (see the inset of Fig. 3). At the 90% confidence level (C. L.), the upper limits on the production cross-sections are set to $\sigma(e^+e^-\to\pi^\pm Z_c^\mp(3900)\to\pi^+\pi^- h_c)<13$ pb at 4.23 GeV and <11 pb at 4.26 GeV. These are lower than those of $Z_c(3900)\to\pi^\pm J/\psi$[8].

BESIII also observed $e^+e^-\to\pi^0\pi^0 h_c$ at $\sqrt{s}=4.23$, 4.26, and 4.36 GeV[16]. The measured Born cross-sections were about half of those for $e^+e^-\to\pi^+\pi^- h_c$, which agree with expectations based on isospin symmetry within systematic uncertainties. A narrow structure with a mass of $(4023.9\pm2.2\pm3.8)\ \mathrm{MeV}/c^2$ (in fit, the width was fixed to that measured in the $e^+e^-\to\pi^+\pi^- h_c$ process[15] due to low statistics) was observed in the $\pi^0 h_c$ mass spectrum. This structure is most likely the neutral isospin partner of the charged $Z_c(4020)$ observed in the $e^+e^-\to\pi^+\pi^- h_c$ process[15]. This observation

indicates that there are no anomalously large isospin violations in $\pi\pi h_c$ and $\pi Z_c(4020)$ systems.

4 Observation of $Z_c(4025)$

We studied[17] the $e^+e^- \to (D^*\overline{D}^*)^\pm\pi^\mp$ process at 4.26 GeV using 827 pb^{-1} of data. Based on a partial reconstruction technique, the Born cross-section was measured to be $(137\pm9\pm15)$ pb. A structure near the $(D^*\overline{D}^*)^\pm$ threshold in the $\pi^\mp$ recoil mass spectrum was observed in Fig. 4, and this is denoted as $Z_c(4025)$. The measured mass and width of the structure were $(4\,026.3\pm2.6\pm3.7)$ MeV/c^2 and $(24.8\pm5.6\pm7.7)$ MeV, respectively, from the fit with a constant-width BW function for the signal. The associated production ratio $\frac{\sigma(e^+e^-\to Z_c^\pm(4025)\pi^\mp\to(D^*\overline{D}^*)^\pm\pi^\mp)}{\sigma(e^+e^-\to(D^*\overline{D}^*)^\pm\pi^\mp)}$ was determined to be $0.65\pm0.09\pm0.06$.

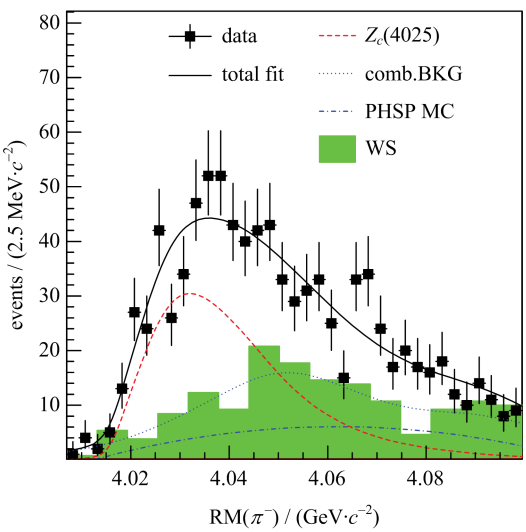

Fig. 4 Unbinned maximum likelihood fit to the $\pi^\mp$ recoil mass spectrum in $e^+e^-\to(D^*\overline{D}^*)^\pm\pi^\mp$ at $\sqrt{s}=4.26$ GeV

Using data at $\sqrt{s}=4.23$ and 4.26 GeV, a structure was observed in the π^0 recoil mass spectrum in the $e^+e^-\to D^{*0}\overline{D}^{*0}(D^{*+}D^{*-})\pi^0$ process[18]. Assuming that the enhancement is due to a neutral state decaying to $D^*\overline{D}^*$, the mass and width of its pole position were determined to be $(4\,025.5^{+2.0}_{-4.7}\pm3.1)$ MeV/c^2 and $\Gamma=(23.0\pm6.0\pm1.0)$ MeV, respectively. The Born cross-section $\sigma(e^+e^-\to Z_c(4025)^0\pi^0\to(D^{*0}\overline{D}^{*0}+D^{*+}D^{*-})\pi^0)$ was measured to be $(61.6\pm8.2\pm9.0)$ pb at 4.23 GeV and $(43.4\pm8.0\pm5.4)$ pb at 4.26 GeV. The ratio $\frac{\sigma(e^+e^-\to Z_c(4025)^0\pi^0\to(D^*\overline{D}^*)^0\pi^0)}{\sigma(e^+e^-\to Z_c(4025)^+\pi^-\to(D^*\overline{D}^*)^+\pi^-)}$ is compatible with unity at $\sqrt{s}=4.26$ GeV, which is expected from isospin symmetry. In addition, $Z_c(4025)^0$ has a mass and width that are very close to those of $Z_c(4025)^\pm$, which couples to $(D^*\overline{D}^*)^\pm$. Therefore, the observed $Z_c(4025)^0$ state is a good candidate for the isospin partner of $Z_c(4025)^\pm$.

As the $Z_c(4025)$ parameters agree to within 1.5σ with those of $Z_c^\pm(4020)$, it is very probable that they are the same state. As the results for $Z_c(4025)^\pm$ are only from data at 4.26 GeV, extending the analysis to 4.23 GeV and 4.36 GeV will probably provide a definite answer.

5 Observation of $Y(4260)\to\gamma X(3872)$

BESIII observed $e^+e^-\to\gamma X(3872)\to\gamma\pi^+\pi^- J/\psi$, with J/ψ reconstructed through its decays into lepton pairs (e^+e^- or $\mu^+\mu^-$)[19]. The $M(\pi^+\pi^- J/\psi)$ distribution (summed over all energy points), as shown in Fig. 5, was fitted to extract the mass and signal yield of $X(3872)$. The ISR $\psi(2S)$ signal was used to calibrate the absolute mass scale and to extract the resolution difference between the data and a Monte Carlo (MC) simulation. Fig. 5 (top) shows the fitting result: the measured mass of $X(3872)$ was $(3\,871.9\pm0.7\pm0.2)$ MeV/c^2. From a fit with a floating width, we obtain a width of $(0.0^{+1.7}_{-0.0})$ MeV, or less than 2.4 MeV at the 90% C. L. The statistical significance of $X(3872)$ is 6.3σ.

The Born-order cross-section was measured, and the results are listed in Tab. 1. For 4.009 and 4.36 GeV data, since the $X(3872)$ signal is not significant, upper limits on the production rates are given at the 90% C. L. The measured cross-sections at around 4.26 GeV are an order of magnitude higher than the NRQCD calculation of continuum production[20], which may suggest the $X(3872)$ events come from resonance decays.

The energy-dependent cross-sections were fitted with a $Y(4260)$ resonance (parameters fixed

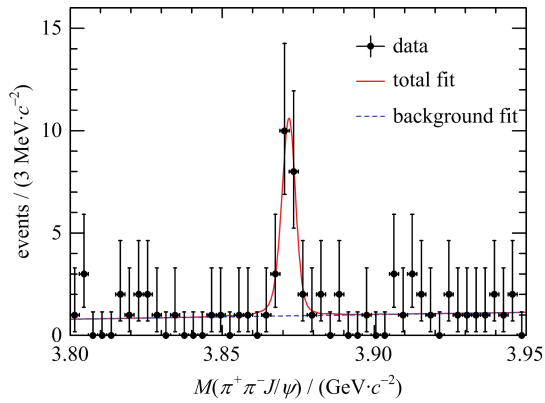

Dots with error bars are data, the curves are the fit results.

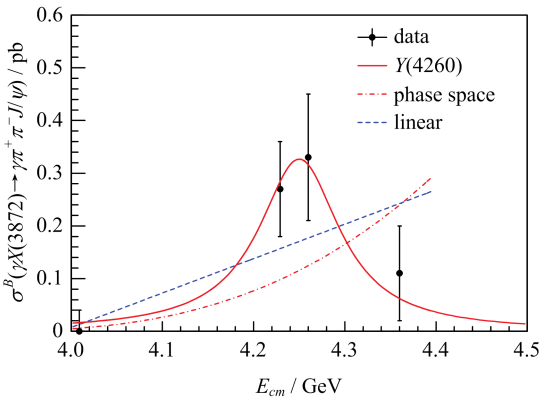

Dots with error bars are data.

Fig. 5 Top: fit to the $M(\pi^+\pi^- J/\psi)$ distribution. Bottom: fit to $\sigma^B[e^+e^-\to\gamma X(3872)]\times\mathcal{B}[X(3872)\to\pi^+\pi^- J/\psi]$ with a $Y(4260)$ resonance (red solid curve), a linear continuum (blue dashed curve), or an $E1$-transition phase space term (red dotted-dashed curve)

Tab. 1 The product of the Born cross section $\sigma^B(e^+e^-\to\gamma X(3872))$ and $\mathcal{B}(X(3872)\to\pi^+\pi^- J/\psi)$ at different energy points

$\sqrt{s}$/GeV	$\sigma^B[e^+e^-\to\gamma X]\cdot\mathcal{B}(X\to\pi\pi J/\psi)$/pb
4.009	$0.00\pm0.04\pm0.01$ or <0.11
4.229	$0.27\pm0.09\pm0.02$
4.260	$0.33\pm0.12\pm0.02$
4.360	$0.11\pm0.09\pm0.01$ or <0.36

【Note】 The upper limits are given at 90% C. L.

to PDG[13] values), linear continuum, or $E1$-transition phase space ($\propto E_\gamma^3$) term. Fig. 5 (bottom) shows all the fitting results, which imply that $\chi^2/\mathrm{ndf}=0.49/3$ (C. L. = 92%), 5.5/2 (C. L. = 6%), and 8.7/3 (C. L. = 3%) for a $Y(4260)$ resonance, linear continuum, and phase space distribution, respectively. Thus, the $Y(4260)$ resonance describes the data better than the other two options. These observations strongly support the existence of the radiative transition process $Y(4260)\to\gamma X(3872)$. The $Y(4260)\to\gamma X(3872)$ process could be another previously unseen decay mode of the $Y(4260)$ resonance.

Combining the above with the $e^+e^-\to\pi^+\pi^- J\psi$ cross-section measurement at $\sqrt{s}=4.26$ GeV from BESIII[8], we obtain $\sigma^B[e^+e^-\to\gamma X(3872)]\cdot BF[X(3872)\to\pi^+\pi^- J/\psi]/\sigma^B(e^+e^-\to\pi^+\pi^- J/\psi)=(5.2\pm1.9)\times10^{-3}$, under the assumption that $X(3872)$ and $\pi^+\pi^- J/\psi$ are only produced from $Y(4260)$ decays. If we take $BF[X(3872)\to\pi^+\pi^- J/\psi]=5\%$[21] (We take 5% from the range presented in the paper of $2.3\%<B[X(3872)\to\pi^+\pi^- J/\psi]<6.6\%$ at 90% C. L.), then $\mathcal{R}=\dfrac{BF[Y(4260)\to\gamma X(3872)]}{BF(Y(4260)\to\pi^+\pi^- J/\psi)}\sim0.1$.

6 Observation of $\psi(1^3D_2)$

BESIII observed $X(3823)$ in the $e^+e^-\to\pi^+\pi^- X(3823)\to\pi^+\pi^-\gamma\chi_{c1}$ process with a statistical significance of 6.2σ in data samples at center-of-mass energies of $\sqrt{s}=4.23$, 4.26, 4.36, 4.42, and 4.60 GeV[22]. Fig. 6 shows the fitting results to $\pi\pi$ recoil mass distributions for events in the χ_{c1} and χ_{c2} signal regions. The fit yields 19 ± 5 $X(3823)$ signal events in the $\gamma\chi_{c1}$ mode, with a measured mass of $X(3823)$ of $(3821.7\pm1.3\pm0.7)$ MeV/c^2, where the first error is statistical and the second systematic. For the $\gamma\chi_{c2}$ mode, no significant $X(3823)$ signal was observed, and an upper limit on its production rate could be determined. The limited statistics do not allow a measurement of the intrinsic width of $X(3823)$. From a fit using the BW function (with a floating width) convolved with Gaussian resolution, it can be determined that $\Gamma[X(3823)]<16$ MeV at the 90% C. L. (including systematic errors). This measurement agrees well with the values found by Belle[23]. The production cross-sections of $\sigma^B(e^+e^-\to\pi^+\pi^- X(3823))\cdot\mathcal{B}(X(3823)\to\gamma\chi_{c1},\ \gamma\chi_{c2})$ were also measured at these center-of-mass energies. The cross-sections

of $e^+e^-\to\pi^+\pi^- X(3823)$ were fitted with the $Y(4360)$ shape or the $\psi(4415)$ shape, with their resonance parameters fixed to the PDG values[13]. Fig. 7 shows the fitting results, both the $Y(4360)$ and $\psi(4415)$ hypotheses are accepted at a 90% C. L.

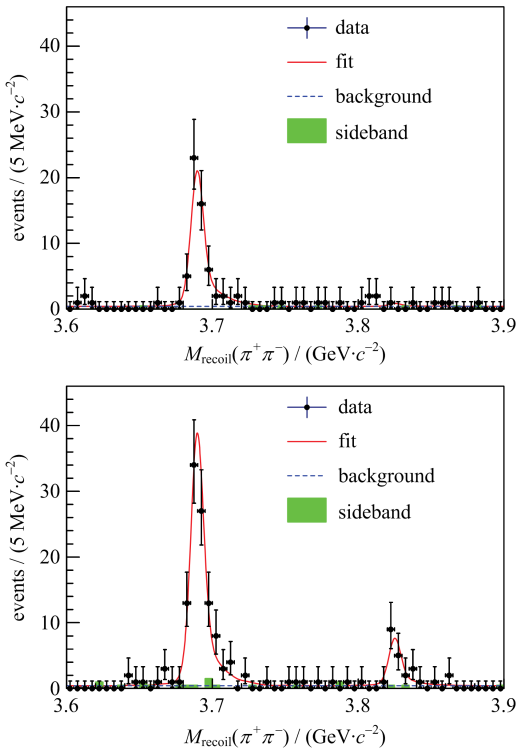

Dots with error bars are data, red solid curves are total fit, dashed blue curves are background, and the green shaded histograms are J/ψ mass sideband events.

Fig. 6 Simultaneous fit to the $M_{\rm recoil}(\pi^+\pi^-)$ distribution of $\gamma\chi_{c1}$ events (top) and $\gamma\chi_{c2}$ events (bottom), respectively

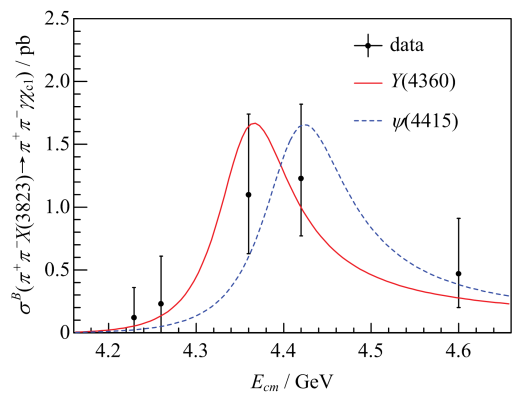

Dots with error bars (statistical only) are data. The red solid (blue dashed) curve shows a fit with the $Y(4360)$ ($\psi(4415)$) line shape.

Fig. 7 Comparison of the energy-dependent cross sections of $\sigma^B[e^+e^-\to\pi\pi X(3823)]\cdot\mathcal{B}(X(3823)\to\gamma\chi_{c1})$ to the $Y(4360)$ and $\psi(4415)$ line shapes

The $X(3823)$ resonance is a good candidate for the $\psi(1^3D_2)$ charmonium state. According to potential models[24-25], the D-wave charmonium states are expected to be within a mass range of 3.82 ~ 3.85 GeV. The $1^1D_2\to\gamma\chi_{c1}$ transition is forbidden because of C-parity conservation, and the amplitude for $1^3D_3\to\gamma\chi_{c1}$ is expected to be small[26]. The mass of $\psi(1^3D_2)$ is in the 3.810 ~ 3.840 GeV/c^2 range predicted by several phenomenological calculations[27]. In this case, the mass of $\psi(1^3D_2)$ was above the $D\bar{D}$ threshold but below the $D\bar{D}^*$ threshold. Because $\psi(1^3D_2)\to D\bar{D}$ violates parity, $\psi(1^3D_2)$ is expected to be narrow, in agreement with the observation, and $\psi(1^3D_2)\to\gamma\chi_{c1}$ is expected to be a dominant decay mode[27-28]. From the cross-section measurement, we obtain the ratio $\frac{\mathcal{B}[X(3823)\to\gamma\chi_{c2}]}{\mathcal{B}[X(3823)\to\gamma\chi_{c1}]}<0.42$ at the 90% C. L., which also agrees with expectations for the $\psi(1^3D_2)$ state[28].

7 Observation of $e^+e^-\to\omega\chi_{c0}$

Based on data samples collected between $\sqrt{s}=4.21$ and 4.42 GeV, the $e^+e^-\to\omega\chi_{c0}$ process was observed at $\sqrt{s}=4.23$ and 4.26 GeV[29]. The Born cross-sections were measured to be $(55.4\pm6.0\pm5.9)$ and $(23.7\pm5.3\pm3.5)$ pb, respectively. For other energy points, no significant signals were found, and upper limits on the cross-section at the 90% C. L. were determined.

The data reveal a sizable $\omega\chi_{c0}$ production at around 4.23 GeV/c^2, as predicted in Ref. [30]. By assuming the $\omega\chi_{c0}$ signals coming from a single resonance, the $\Gamma_{ee}\,\mathcal{B}(\omega\chi_{c0})$, mass, and width of the resonance are fitted to be $(2.7\pm0.5\pm0.4)$ eV, $(4\,230\pm8\pm6)$ MeV/c^2, and $(38\pm12\pm2)$ MeV, respectively (shown in Fig. 8). The parameters are not consistent with the lineshape $Y(4260)\to\pi^+\pi^- J/\psi$ cross-section[2]. This suggests that the observed $\omega\chi_{c0}$ signals are unlikely to originate from $Y(4260)$.

Using data samples collected at energies of 3.81 ~ 4.60 GeV, BESIII analyzed $e^+e^-\to$

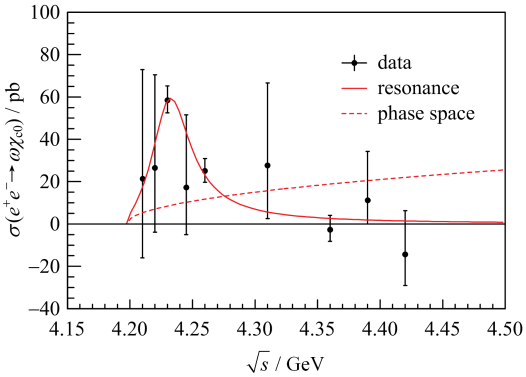

Dots with error bars are the dressed cross sections.
The uncertainties are statistical only.

Fig. 8 Fit to $\sigma(e^+e^-\to\omega\chi_{c0})$ with a resonance (solid curve), or a phase space term (dot-dashed curve)

$\eta J/\psi$[31]. Statistically significant η signals were observed, and the corresponding Born cross-sections were measured. In addition, a search for the $e^+e^-\to\pi^0 J/\psi$ process observed no significant signals, and upper limits at the 90% C. L. on the Born cross-section were set.

A comparison of the Born cross-sections $\sigma(e^+e^-\to\eta J/\psi)$ in this measurement to previous results[14,32] is shown in Fig. 9 (top), indicating very good agreement. The measured Born cross-sections were also compared to those of $e^+e^-\to\pi^+\pi^- J/\psi$ obtained from the Belle experiment[9], as shown in Fig. 9 (bottom). Different line shapes can be observed in these two processes, indicating that the production mechanism of $\eta J/\psi$ differs from that of $\pi^+\pi^- J/\psi$ in the vicinity of $\sqrt{s}$=4.1~4.6 GeV. This could indicate the existence of a rich spectrum of the Y states in this energy region with different coupling strengths to various decay modes.

8 Conclusion

With the world's largest data samples at the center-of-mass energies of 3.8 ~ 4.6 GeV, the BESIII experiment made a significant contribution to the study of the charmonium(-like) states. BESIII will continue to collect and analyse e^+e^- data in the energy region of the putative exotic states of charmonium. Efforts from other experiments, such as LHCb and PANDA, are important to achieve a systematic understanding of

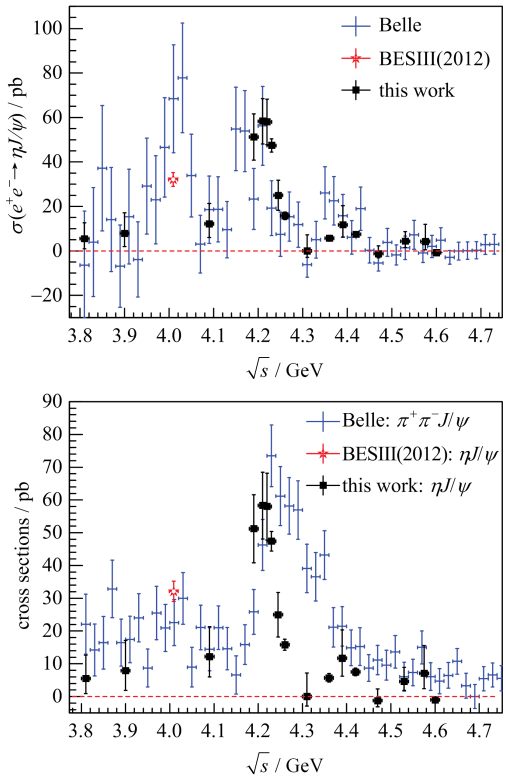

In these two plots, the black square dots and the red star dots are the results of $\eta J/\psi$ obtained from BESIII.
The blue dots are results of $\eta J/\psi$ (top) and $\pi^+\pi^- J/\psi$ (bottom) from Belle.
The errors are statistical only for Belle's results, and are final combined uncertainties for BESIII's results.

Fig. 9 A comparison of the measured Born cross sections of $e^+e^-\to\eta J/\psi$ to those of the previous measurements[14,32] (top), and to those of $e^+e^-\to\pi^+\pi^- J/\psi$ from Belle[9]

the nature of the XYZ states.

References

[1] BRAMBILLA N, EIDELMAN S, HELTSLEY B K, et al. Heavy quarkonium: Progress, puzzles, and opportunities[J]. Eur Phys J C, 2011, 71: 1534.

[2] AUBERT B, BARATE R, BOUTIGNY D, et al. Observation of abroad structure in the $\pi^+\pi^- J/\psi$ mass spectrum around 4.26 GeV/c^2 [J]. Phys Rev Lett, 2005, 95: 142001.

[3] HE Q, INSLER J, MURAMATSU H, et al. Confirmation of the $Y(4260)$ resonance production in initial state radiation[J]. Phys Rev D, 2006, 74: 091104.

[4] YUAN C Z, SHEN C P, WANG P, et al. Measurement of $e^+e^-\to\pi^+\pi^- J/\psi$ cross-section via initial state radiation at Belle[J]. Phys Rev Lett, 2007, 99: 182004.

[5] MO X H, LI G, YUAN C Z, et al. Determining the upper limit of Γ_{ee} for the $Y(4260)$[J]. Phys Lett B,

2006, 640:182.

[6] ABLIKIM M, ACHASOV M N, AI X C, et al. Measurements of the center-of-mass energies at BESIII via the di-muon process[J]. Chin Phys C, 2016, 40(6):063001.

[7] ABLIKIM M, ACHASOV M N, AI X C, et al. Precision measurement of the integrated luminosity of the data taken by BESIII at center of mass energies between 3.810 GeV and 4.600 GeV [EB/OL]. (2015-03-11) [2015-11-01]. http://arxiv.org/abs/1503.03408.

[8] ABLIKIM M, ACHASOV M N, AI X C, et al. Observation of a charged charmoniumlike structure in $e^+e^-\to\pi^+\pi^- J/\psi$ at $\sqrt{s}=4.26$ GeV[J]. Phys Rev Lett, 2013, 110:252001.

[9] LIU Z Q, SHEN C P, YUAN C Z, et al. Study of $e^+e^-\to\pi^+\pi^- J/\psi$ and observation of a charged charmoniumlike state at Belle[J]. Phys Rev Lett, 2013, 110: 252002.

[10] XIAO T, DOBBS S, TOMARADZE A, et al. Observation of the charged hadron $z_c^{\pm}$ (3900) and evidence for the neutral z_c^0(3900) in $e^+e^-\to\pi\pi J/\psi$ at $\sqrt{s}=4$ 170 MeV[J]. Phys Lett B,2013, 72:366-370.

[11] ABLIKIM M, ACHASOV M N, AI XC, et al. Observation of $Z_c(3900)^0$ in $e^+e^-\to\pi^0\pi^0 J/\psi$[J]. Phys Rev Lett,2015, 115: 112003.

[12] ABLIKIM M, ACHASOV M N, ALBAYRAK O, et al. Observation of a charged $(D\overline{D}^*)^{\pm}$ mass peak in $e^+e^-\to\pi D\overline{D}^*$ at $\sqrt{s}=4.26$ GeV [J]. Phys Rev Lett, 2014, 112: 022001.

[13] OLIVE K A, AGASHE K, AMSLER C, et al. Review of particle physics [J]. Chin Phys C, 2014, 38(09): 090001.

[14] ABLIKIM M, ACHASOV M N, AMBROSE D J, et al. Observation of $e^+e^-\to\eta J/\psi$ at center-of-mass energy $\sqrt{s}=$ 4.009 GeV [J]. Phys Rev D,2012, 86: 071101.

[15] ABLIKIM M, ACHASOV M N, ALBAYRAK O, et al. Observation of a charged charmoniumlike structure $Z_c(4020)$ and search for the $Z_c(3900)$ in $e^+e^-\to\pi^+\pi^- h_c$ [J]. Phys Rev Lett,2013, 111: 242001.

[16] ABLIKIM M, ACHASOV M N, AI X C, et al. Observation of $e^+ e^-\to\pi^0\pi^0 h_c$ and a neutral charmoniumlike structure $Z_c(4020)^0$ [J]. Phys Rev Lett,2014, 113: 212002.

[17] Ablikim M, Achasov M N, Albayrak O, et al. Observation of a charged charmoniumlike structure in $e^+e^-\to(D^*\overline{D}^*)^{\pm}\pi^{\mp}$ at $\sqrt{s}=4.26$ GeV [J]. Phys Rev Lett, 2014, 112: 132001.

[18] ABLIKIM M, ACHASOV M N, AI X C, et al. Observation of a neutral charmoniumlike state $Z_c(4025)^0$ in $e^+e^-\to(D^*\overline{D}^*)^0\pi^0$[EB/OL]. (2015-10-08)[2015-11-01]. http://arxiv.org/abs/1507.02404.

[19] ABLIKIM M, ACHASOV M N, AI X C, et al. Observation of $e^+e^-\to\gamma X(3872)$ at BESIII[J]. Phys Rev Lett,2014, 11:092001.

[20] CHAO K T, HE Z G, LI D, et al. Search for $C=+$ charmonium states in $e^+e^-\to\gamma+X$ at BEPCII/BESIII [EB/OL]. (2013-10-31)[2015-11-01]. http://arxiv.org/abs/1310.8597.

[21] YUAN C Z. Exotic Hadrons[EB/OL]. (2009-11-08)[2015-11-01]. http://arxiv.org/abs/0910.3138.

[22] ABLIKIM M, ACHASOV M N, AI X C, et al. Observation of the $\psi(1^3D_2)$ State in $e^+e^-\to\pi^+\pi^-\gamma\chi_{c1}$ at BESIII[J]. Phys Rev Lett,2015, 115: 011803.

[23] BHARDWAJ V, MIYABAYASHI K, ADACHI I, et al. Evidence of a new narrow resonance decaying to $\chi_{c1}\gamma$ in $B\to\chi_{c1}\gamma K$ [J]. Phys Rev Lett, 2013, 111: 032001.

[24] EICHTEN E, GOTTFRIED K, KINOSHITA T, et al. Charmonium: The Model[J]. Phys Rev D, 1978, 17:3090.

[25] EICHTEN E, GOTTFRIED K, KINOSHITA T, et al. Erratum: Charmonium: The model [J]. Phys Rev D, 1980,21:313.

[26] BARNES T, GODFREYS, SWANSON E S. Higher charmonia[J]. Phys Rev D, 2005,72:054026.

[27] GODFREY S, ISGURN. Mesons in a relativized quark model with chromodynamics[J]. Phys Rev D, 1985, 32: 189.

[28] QIAO C F, YUAN F, CHAO K T. Crucial test for color-octet production mechanism in Z^0 decays[J]. Phys Rev D,1997, 55:4001.

[29] ABLIKIM M, ACHASOV M N, AI X C, et al. Study of $e^+e^-\to\omega\chi_{cJ}$ at center of mass energies from 4.21 to 4.42 GeV[J]. Phys Rev Lett,2015, 114:092003.

[30] DAI L Y, SHI M, TANG G Y, et al. Nature of $X(4260)$[J]. Phys Rev D,2015, 92: 014020.

[31] ABLIKIM M, ACHASOV M N, AI X C, et al. Measurement of the $e^+e^-\to\eta J/\psi$ cross section and search for $e^+e^-\to\pi^0 J/\psi$ at center-of-mass energies between 3.810 and 4.600 GeV[J]. Phys Rev D,2015, 91:112005.

[32] WANG X L, HAN Y L, YUAN C Z, et al. Observation of $\psi(4040)$ and $\psi(4160)$ decay into $\eta J/\psi$ [J]. Phys Rev D,2013, 87: 051101.

Article ID:0253-2778(2016)07-0549-08

XYZ states at Belle

SHEN Chengping, LI Zhuang (for the Belle Collaboration)

(*School of Physics and Nuclear Energy Engineering, Beihang University, Beijing* 100191, *China*)

Abstract: Exotic hadronic states beyond the conventional quark model (called charmoniumlike/bottomoniumlike states or XYZ particles) have been searched for and many candidates have been proposed including glueballs, hybrids, multi-quark states, hadron molecules, etc. Dramatic progress was made in the study of them after the running of the B-factories. The most recent results on the XYZ states at Belle are presented, including ① X states: the first observation of $B^0\to X(3872)K^+\pi^-$ and evidence for $B^+\to X(3872)K^0\pi^+$; search for the X_b state; ② Y states: the updated results for the $Y(4360)$ and $Y(4660)$ and cross section measurements of $e^+e^-\to K^+K^-J/\psi$ and $\gamma\chi_{cJ}$; ③ Z states: the evidence for the $Z_c(4050)^\pm\to\pi^\pm\psi(2S)$; search for the Z_{cs} in $e^+e^-\to K^+K^-J/\psi$.

Key words: XYZ; exotic states; Belle

CLC number: O572.3 **Document code**: A doi:10.3969/j.issn.0253-2778.2016.07.003

Citation: SHEN Chengping, LI Zhuang. XYZ states at Belle[J]. Journal of University of Science and Technology of China, 2016,46(7):549-556.

Belle 实验上关于最新的 XYZ 粒子的实验结果

沈成平,李 垚(Belle 合作组)

(北京航空航天大学物理科学与核能工程学院,北京 100191)

摘要:实验上寻找超出传统夸克标准模型的激发态强子(也称为类粲偶素/类底偶素或 XYZ 粒子)已经很多年,建议过很多的激发态强子的候选者,包括胶球、混杂态、多夸克态、强子分子态等. 自从 B 工厂运行以来,这方面的研究已经取得了巨大的进步. 本文给出来自 Belle 实验的关于 XYZ 粒子的最新实验成果,包括① X 态:首次观测到 $B^0\to X(3872)K^+\pi^-$ 过程的信号以及 $B^+\to X(3872)K^0\pi^+$ 过程存在的迹象;寻找 X_b 态;② Y 态:更新的 $Y(4360)$ 和 $Y(4660)$ 共振参数的结果以及更新的测量 $e^+e^-\to K^+K^-J/\psi$ 和 $\gamma\chi_{cJ}$ 过程的散射截面;③ Z 态:发现带电的 $Z_c(4050)^\pm\to\pi^\pm\psi(2S)$ 存在的迹象以及在 $e^+e^-\to K^+K^-J/\psi$ 过程中寻找 Z_{cs} 的态.

关键词:XYZ;激发态强子;Belle 实验

Received:2015-11-30;**Revised**:2016-04-20

Foundation item:Supported by National Natural Science Foundation of China (11575017).

Biography:SHEN Chengping (corresponding author), male, born in 1978, PhD/Prof. Research field: particle physics experiment. E-mail: shencp@buaa.edu.cn

0 Introduction

The study of charmoniumlike states, the so-called "*XYZ*" particles[1-2], has been propering ever since they were observed by many Collaborations, like Belle, BaBar, and BESIII. Most of them are above the open charm threshold and can not be described well by quark potential models, which decay into the final states containing a charmonium and light hadrons, but not into open charm pairs with a detectable rate as expected. Especially the charged charmoniumlike state $Z_c(3900)$ was observed by BESIII[3] and Belle[4] experiments in 2013 in $J/\psi\pi^{\pm}$ system of $e^+e^-\to\pi^+\pi^- J/\psi$ at center-of-mass (CM) energies around 4.26 GeV and very recently the two exotic structures, denoted as pentaquark states of $P_c(4380)^+$ and $P_c(4450)^+$, in the $J/\psi p$ system in $\Lambda_b^0\to J/\psi K^- p$ were observed by LHCb[5].

Their underlying exotic properties have been stimulating significant interest in theoretical studies, and indicate several possible popular interpretations such as tetraquarks, molecules, hybrids, hadrocharmonia, or glueballs[1-2]. Despite the long history of searching for all these kinds of states, no solid conclusion had been reached until the recent discovery of tetraquark and pentaquark states.

Here, We present some most recent results on the *XYZ* states from the Belle experiment.

1 *X* states

More than a decade ago, the Belle Collaboration discovered the $X(3872)$ state[6] in the exclusive reconstruction of $B^+\to X(3872)(\to J/\psi\pi^+\pi^-)K^+$. Considerable effort by both experimentalists and theorists has been invested to clarify its nature. As a result, we know precisely its mass ($3\,871.69\pm0.17$) MeV/c^2[7], have a stringent limit on its width (less than 1.2 MeV at 90% confidence level (C. L.))[8] and have a definitive J^{PC} assignment of 1^{++} determined by LHCb[9]. Due to its mass being close to $D^{*0}\overline{D}^0$ threshold, $X(3872)$ might be a molecule-like bound state of D^{*0} and $\overline{D}^0$ meson[10-11]. Eventually both BaBar[12] and Belle [13] observed conspicuous signals of the $X(3872)\to D^{*0}\overline{D}^0$ process with an order of magnitude higher branching fraction than the $\pi^+\pi^- J/\psi$ mode. Moreover the quantum numbers of $X(3872)$ ($I^G(J^{PC})=0^+(1^{++})$) also suggested that it is possibly a candidate of $\chi_{c1}(2P)$. The generally accepted interpretation at present for the still-fascinating $X(3872)$ is a mixture of a charmonium state $\chi_{c1}(2P)$ and an *S*-wave $D^{*0}\overline{D}^0$ molecule. More experimental information on the production and decays of the $X(3872)$ will shed additional light on its nature.

Based on 711 fb^{-1} of data containing 772×10^6 $B\overline{B}$ events, Belle searched for the $X(3872)$ production via the $B^0\to X(3872)K^+\pi^-$ and $B^+\to X(3872)K_S^0\pi^+$ decay modes, where the $X(3872)$ decays to $J/\psi\pi^+\pi^-$[14].

B candidates were selected using two kinematic variables: the energy difference $\Delta E=E_B-E_{\rm beam}$ and the beam-energy constrained mass $M_{\rm bc}=(\sqrt{E_{\rm beam}^2-p_B{}^2c^2})/c^2$, where $E_{\rm beam}$ is the beam energy and E_B and p_B are the energy and magnitude of momentum, respectively, of the candidate *B* meson, all calculated in the e^+e^- CM frame. To extract the signal yield of $B\to X(3872)(\to J/\psi\pi^+\pi^-)K\pi$, a two-dimensional (2D) unbinned extended maximum likelihood fit to the ΔE and $M_{J/\psi\pi\pi}$ distributions was performed after all the event selections. For the signal, the ΔE distribution is parametrized by the sum of a Crystal Ball and a Gaussian function while the $M_{J/\psi\pi\pi}$ distribution is modeled using the sum of two Gaussians having a common mean. The 2D probability distribution function (PDF) is a product of the individual one-dimensional PDFs.

For the $B^0\to X(3872)K^+\pi^-$ decay mode, a 2D fit is performed. Fig. 1 shows the signal-enhanced projection plots for the $B^0\to X(3872)K^+\pi^-$ decay mode. The curves show the signal (red long-dashed curve) and the background components (black dash-dotted line for the component peaking

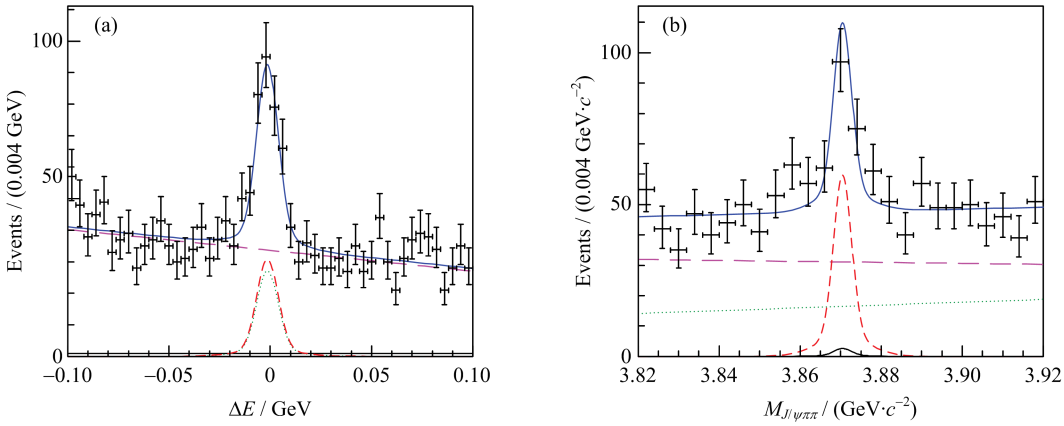

Fig. 1 Projections of the $(\Delta E, M_{J/\psi\pi\pi})$ fit for the $B^0 \to X(3872)K^+\pi^-$ decay mode

in $M_{J/\psi\pi\pi}$ but nonpeaking in ΔE, the green dashed line for the one peaking in ΔE but nonpeaking in $M_{J/\psi\pi\pi}$, and magenta long dash-dotted line for combinatorial background) as well as the overall fit (blue solid curve). The number of signals for $B^0 \to X(3872)K^+\pi^-$ is 116 ± 19, corresponding to a significance of 7.0σ. The product of branching fractions is measured to be $\mathcal{B}(B^0 \to X(3872)K^+\pi^-) \times \mathcal{B}(X(3872) \to J/\psi\pi^+\pi^-) = (7.9 \pm 1.3\ (\text{stat.}) \pm 0.4(\text{syst.})) \times 10^{-6}$.

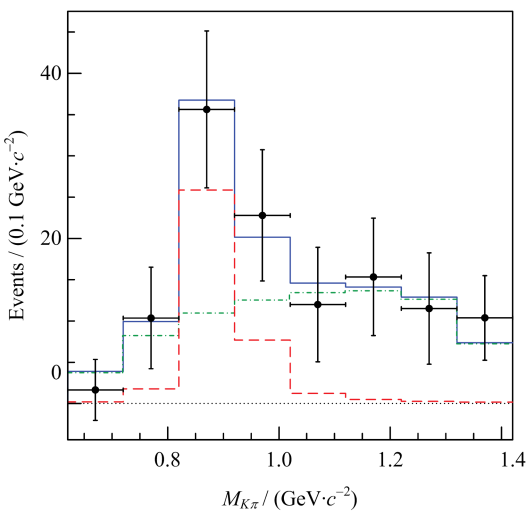

Fig. 2 Fit to the $M_{K\pi}$ distribution for the $B^0 \to X(3872)K^+\pi^-$ decay mode

To obtain the pure $M_{K\pi}$ distribution, a similar 2D fit to ΔE and $M_{J/\psi\pi\pi}$ in each bin of $M_{K\pi}$ was performed. All parameters of the signal PDFs for $M_{J/\psi\pi\pi}$ and ΔE distributions are fixed from the previous 2D fit to all events. Then an χ^2 fit to the $M_{K\pi}$ distribution using $K^*(892)^0$ and $(K^+\pi^-)_{\text{NR}}$ components was done, where the histogram PDFs were obtained from MC samples directly. The possible interference between the $K^*(892)$ and nonresonant component was not considered due to the small statistics. The resulting fit result is shown in Fig. 2. The curves show the $B^0 \to X(3872)K^*(892)^0$ (red long-dashed lines), $B^0 \to X(3872)(K^+\pi^-)_{\text{NR}}$ (green dot-dashed lines), as well as the overall fit (blue solid lines). We obtain $38 \pm 14\ (82 \pm 21)$ signal events for the $B^0 \to X(3872)K^*(892)^0$ ($B^0 \to X(3872)(K^+\pi^-)_{\text{NR}}$) decay mode and a corresponding product of branching fractions of $\mathcal{B}(B^0 \to X(3872)K^*(892)^0) \times \mathcal{B}(X(3872) \to J/\psi\pi^+\pi^-) = (4.0 \pm 1.5(\text{stat.}) \pm 0.3(\text{syst.})) \times 10^{-6}$. The ratio of branching fractions is

$$\frac{\mathcal{B}(B^0 \to X(3872)K^*(892)^0) \times \mathcal{B}(K^*(892)^0 \to K^+\pi^-)}{\mathcal{B}(B^0 \to X(3872)K^+\pi^-)} = 0.34 \pm 0.09(\text{stat.}) \pm 0.02(\text{syst.}).$$

In contrast to $B^0 \to \psi' K^+\pi^-$, $B^0 \to X(3872)K^*(892)^0$ does not dominate in the $B^0 \to X(3872)K^+\pi^-$.

The decays $B^+ \to X(3872)K^0\pi^+$ were also analyzed using the same method. The projections of the 2D fit are shown in Fig. 3. The representations of the curves match those in Fig. 1. The number of fitted signal events is 35 ± 10, corresponding to a 3.7σ significance. The product of branching fractions is $\mathcal{B}(B^+ \to X(3872)K^0\pi^+) \times \mathcal{B}(X(3872) \to J/\psi\pi^+\pi^-) = (10.6 \pm 3.0(\text{stat.}) \pm 0.9(\text{syst.})) \times 10^{-6}$.

It is very natural to search for a similar

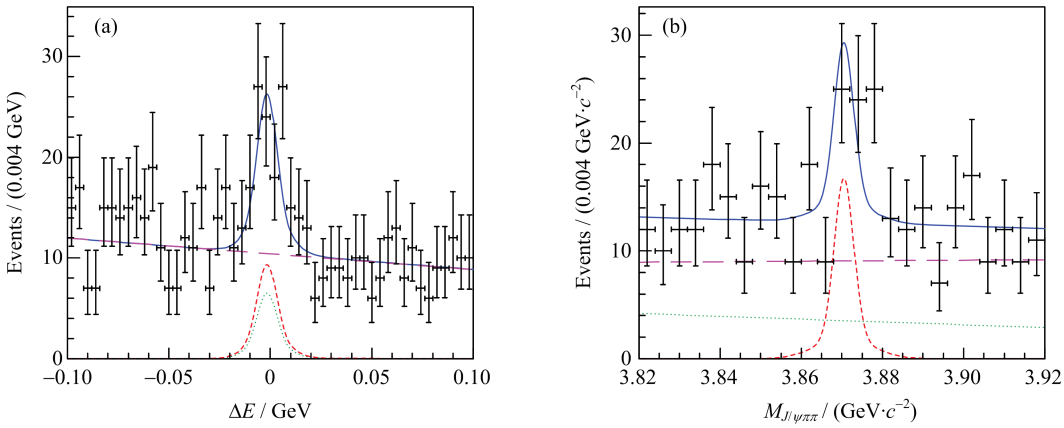

Fig. 3 Projections of the $(\Delta E, M_{J/\psi\pi\pi})$ fit for the $B^{\pm}\to X(3872)K_S{}^0\pi^{\pm}$ decay mode

$X(3872)$ state with $J^{PC}=1^{++}$, called X_b, in the bottomonium system. The search for X_b supplies important information about the discrimination of a compact multiquark configuration and a loosely bound hadronic molecule configuration for the $X(3872)$. The existence of the X_b is predicted in both the tetraquark model[15] and those involving a molecular interpretation[16-18]. The CMS Collaboration ever searched for the X_b decaying to $\pi^+\pi^-\Upsilon(1S)$ based on a sample of pp collisions at $\sqrt{s}=8$ TeV[19]. Except the clear $\Upsilon(2S)$ signal, no evidence for an X_b signal was observed. However, unlike the $X(3872)$, whose decays exhibit large isospin violation, the X_b would decay preferably into $\pi^+\pi^-\pi^0\,\Upsilon(1S)$ rather than $\pi^+\pi^-\Upsilon(1S)$ if it exists[17,20]. So Belle did a search for an X_b signal decaying to $\omega\Upsilon(1S)$ in $e^+e^-\to\gamma X_b$ at a CM energy of 10.867 GeV[21].

Fig. 4 shows the final $\omega\Upsilon(1S)$ invariant mass distribution with the requirement of $M(\pi^+\pi^-\pi^0)$ within the ω signal region; the X_b is searched for from 10.55 to 10.65 GeV/c^2. The dots with error bars are from data, the solid histogram is from the normalized contribution of $e^+e^-\to\omega\chi_{bJ}(J=0,1,2)$ and the shaded histogram is from the normalized ω mass sideband. No obvious X_b signal is observed after applying all the event selection criteria.

An unbinned extended maximum likelihood fit to the $\omega\Upsilon(1S)$ mass distribution is applied, where the signal shape is obtained from MC simulation and the background is parameterized as a first-order polynomial. From the fit, the number of X_b signal events is -0.4 ± 2.0 with a mass at 10.6 GeV/c^2. The upper limit on the yield of the X_b signal events is 4.0 at 90% C. L. with systematic uncertainty included. The dashed histogram in Fig. 4 shows the upper limit on the yield of X_b signal events. The product branching fraction is determined to be $\mathcal{B}(\Upsilon(5S)\to\gamma X_b)\mathcal{B}(X_b\to\omega\Upsilon(1S))<2.9\times10^{-5}$ at 90% C. L.

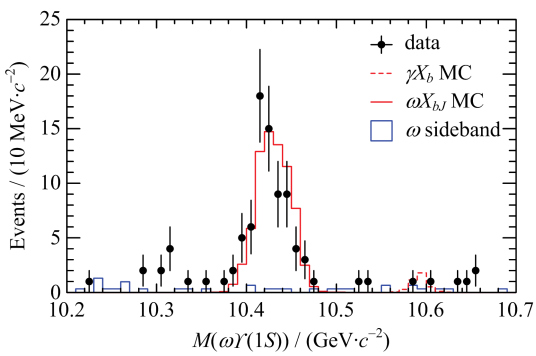

The components shown are described in the text.

Fig. 4 The $\omega\Upsilon(1S)$ invariant mass distribution

2 Y states

The $Y(4260)$ state was first observed by BaBar in the initial-state-radiation (ISR) process $e^+e^-\to\gamma_{ISR}\pi^+\pi^- J/\psi$[22] and then confirmed by the CLEO[23] and Belle experiments[24] using the same technique. An ISR analysis by the Belle experiment with 548 fb^{-1} of data showed a significant $Y(4260)$ signal as well as a broad excess

of $\pi^+\pi^- J/\psi$ event production near 4 GeV — the so-called $Y(4008)$[25].

Later, the BaBar Collaboration reported an updated ISR analysis with 454 fb^{-1} of data and a modified approach for the background description[26]; the $Y(4260)$ state was observed with improved significance, but the $Y(4008)$ structure was not confirmed. Instead, they attributed the structure below the $Y(4260)$ to exponentially falling non-resonant $\pi^+\pi^- J/\psi$ production. In 2013, the Belle Collaboration updated the analysis of $e^+e^-\to\pi^+\pi^- J/\psi$ with a 967 fb^{-1} data sample. Not only was the $Y(4260)$ state observed clearly, but the Y(4008) was also confirmed[4].

In an analysis of the $e^+e^-\to\gamma_{\rm ISR}\pi^+\pi^-\psi(2S)$ process, BaBar found a structure near 4.32 GeV/c^2 (called the $Y(4360)$)[27], while Belle observed two resonant structures at 4.36 and 4.66 GeV/c^2, denoted as the $Y(4360)$ and $Y(4660)$[28]. Recently, BaBar updated their results on $e^+e^-\to\gamma_{\rm ISR}\pi^+\pi^-\psi(2S)$ analysis with its full data sample and confirmed the existence of the $Y(4660)$ state[29].

Very recently, to characterize more precisely the properties of the $Y(4360)$ and $Y(4660)$, Belle updated the $e^+e^-\to\pi^+\pi^-\psi(2S)$ process with the full Belle data 980 fb^{-1}[30]. Fig. 5 shows the invariant mass distribution of $\pi^+\pi^-\psi(2S)$ from the updated measurement. Fitting the mass spectrum of $\pi^+\pi^-\psi(2S)$ with two coherent Breit-Wigner (BW) functions, there are two solutions with identical mass and width but different couplings to electron-positron pairs: $M_{Y(4360)}=(4\ 347\pm6\pm3)$ MeV/c^2, $\Gamma_{Y(4360)}=(103\pm9\pm5)$ MeV, $M_{Y(4660)}=(4\ 652\pm10\pm8)$ MeV/c^2, $\Gamma_{Y(4660)}=(68\pm11\pm1)$ MeV; and $\mathcal{B}[Y(4360)\to\pi^+\pi^-\psi(2S)]\cdot\Gamma^{e^+e^-}_{Y(4360)}=(10.9\pm0.6\pm0.7)$ eV and $\mathcal{B}[Y(4660)\to\pi^+\pi^-\psi(2S)]\cdot\Gamma^{e^+e^-}_{Y(4660)}=(8.1\pm1.1\pm0.5)$ eV for one solution; or $\mathcal{B}[Y(4360)\to\pi^+\pi^-\psi(2S)]\cdot\Gamma^{e^+e^-}_{Y(4360)}=(9.2\pm0.6\pm0.6)$ eV and $\mathcal{B}[Y(4660)\to\pi^+\pi^-\psi(2S)]\cdot\Gamma^{e^+e^-}_{Y(4660)}=(2.0\pm0.3\pm0.2)$ eV for the other. Here, the first errors are statistical and the second systematic.

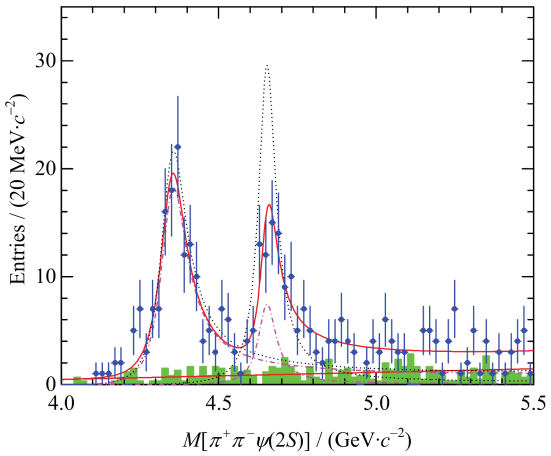

Fig. 5 The $\pi^+\pi^-\psi(2S)$ invariant-mass distributions and the simultaneous fit results described in the text

Belle also noticed there are a few events in the vicinity of the $Y(4260)$ mass that, so an alternative fit with a coherent sum of $Y(4260)$, $Y(4360)$, and $Y(4660)$ amplitudes was also performed. But the signal significance of the $Y(4260)$ is only 2.4σ.

Using a data sample of 673 fb^{-1}, Belle has observed abundant $e^+e^-\to K^+K^- J/\psi$ signal events[31]. There is one very broad structure in the $K^+K^- J/\psi$ mass spectrum; fits using either a single BW function, or the $\psi(4415)$ plus a second BW function yield resonant parameters that are very different from those of the currently tabulated excited ψ states. To examine possible resonant structures in the cross section of the process $e^+e^-\to K^+K^- J/\psi$ as well as in the $K^\pm J/\psi$ and K^+K^- systems, Belle updated measurement of the cross sections for $e^+e^-\to K^+K^- J/\psi$ between threshold and 6.0 GeV/c^2 with an integrated luminosity of 980 fb^{-1}[32].

Fig. 6 shows the measured cross sections for $e^+e^-\to K^+K^- J/\psi$. The maximum likelihood fit was performed to fit the $K^+K^- J/\psi$ invariant mass spectrum using two different parameterizations of the signal shape: ① a single BW function plus a background term; ② a coherent sum of a BW function and a $\psi(4415)$ component with mass and width fixed at their world average values plus a background term. The goodness of the fit ($\chi^2/ndf=$

39/13=3.0 for model (1) and $\chi^2/ndf=30/11=2.7$ for model (2)) is marginal. Thus, these two models can not describe the data well with the increased statistics.

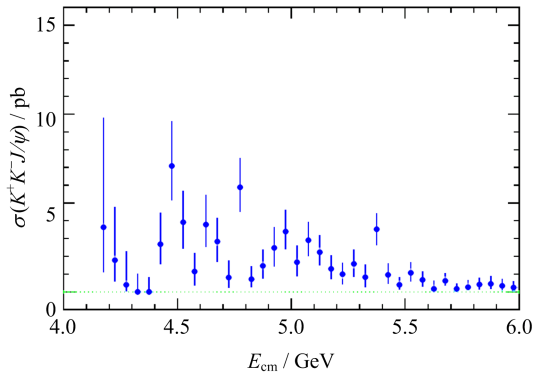

Fig. 6 The measured $e^+e^-\to K^+K^-J/\psi$ cross sections for CM energies up to 6.0 GeV

In order to improve the understanding of the nature of vector charmoniumlike states and search for more new states, Belle studied $e^+e^-\to\gamma\chi_{cJ}$ process using ISR events with χ_{cJ} reconstructed via $\gamma J/\psi$[33]. The integrated luminosity used in this analysis is 980 fb^{-1}.

After all the event selections, no significant signal is observed in either $\gamma\chi_{c1}$ or $\gamma\chi_{c2}$ mode in $M(\gamma\gamma J/\psi)$ distributions for $\gamma\chi_{c1}$ and $\gamma\chi_{c2}$ candidate events as well as the sum of them. The measured upper limits on the cross sections are shown in Fig. 7 and are around a few pb to a few tens of pb.

3 Z states

After the charged charmoniumlike state $Z_c(3900)$ observed by BESIII and Belle experiments, BESIII and Belle also observed a series of charged Z_c states including $Z_c(4020)$[34], $Z_c(4200)$[35], and $Z_c(4430)$[36]. These states seem to indicate that a new class of hadrons has been observed. As there are at least four quarks within these Z_c states, they have been interpreted either as tetraquark states with a pair of charm-anticharm quarks and a pair of light quarks, molecular states of two charmed mesons, or other configurations.

To find more similar charged states, Belle checked the $\pi^\pm\psi(2S)$ system in the updated

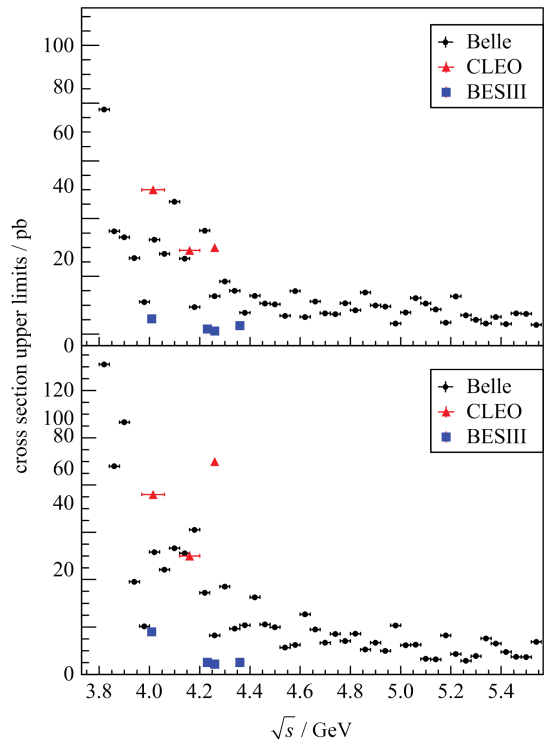

The solid dots show the Belle measurements, the solid triangles are the results from CLEO and the blue squares are from BESIII.

Fig. 7 Measured upper limits on the $e^+e^-\to\gamma\chi_{cJ}$ cross sections at the 90% C.L. for χ_{c1} (top) and χ_{c2} (bottom)

$e^+e^-\to\pi^+\pi^-\psi(2S)$ analysis[30]. There is an excess evident at around 4.05 GeV/c^2 in the $\pi^\pm\psi(2S)$ invariant-mass distributions in the $Y(4360)$ subsample defined as $4.0<M_{\pi^+\pi^-\psi(2S)}<4.5$ GeV/c^2. An unbinned maximum-likelihood fit is performed on the distribution of $M_{\max}(\pi^\pm\psi(2S))$, the maximum of $M(\pi^+\psi(2S))$ and $M(\pi^-\psi(2S))$. The excess is parameterized with a BW function and the non-resonant non-interfering background with a second-order polynomial function. The fit yields a mass of $(4\,054\pm3(\text{stat.})\pm1(\text{syst.}))$ MeV/c^2, a width of $(45\pm11(\text{stat.})\pm6(\text{syst.}))$ MeV and a 3.5σ significance, as shown in Fig. 8. This evident structure is called $Z_c(4050)$.

A strange partner of the $Z_c(3900)^\pm$, called Z_{cs}, may exist in the above scenarios. The mass of a $J^P=1^+$ $D_s\overline{D}^*$ molecular state was first predicted[37] using QCD sum rules with $M(Z_{cs})=(3.97\pm0.08)$ GeV/c^2, which is very close to the $D_s^+\overline{D}^{*0}$ threshold of 3.976 GeV/c^2. Using the same QCD sum rules, the authors of Ref. [38]

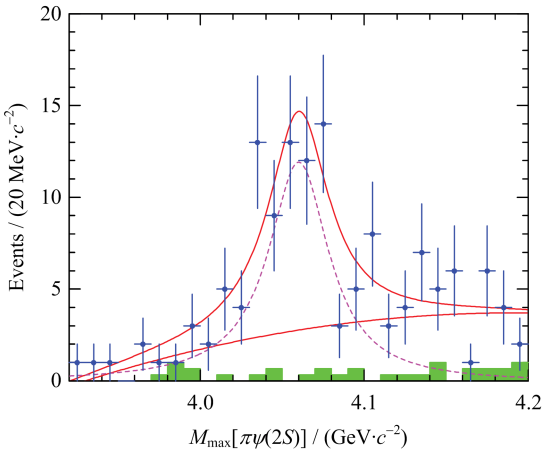

The points with error bars represent the data; the histogram is the normalized sidebands; the solid curve is the best fit and the dashed curve is the signal.

Fig. 8 The distribution of $M_{\max}(\pi^{\pm}\psi(2S))$ from $Y(4360)$ -subsample decays

calculated the decay widths of the Z_{cs}^{+} to $K^{+}J/\psi$, $K^{*+}\eta_c$, $D_s^{+}\overline{D}^{*0}$ and $\overline{D}^{0}D_s^{*+}$, assuming the Z_{cs} to be a tetraquark state. Such a state is also predicted in the single-kaon emission model[39].

Belle tried to search for such a Z_{cs} state in $J/\psi K^{\pm}$ system in the updated process $e^{+}e^{-}\to K^{+}K^{-}J/\psi$[32]. The $M(K^{+}J/\psi)$ and $M(K^{-}J/\psi)$ invariant mass distributions were investigated. No obvious structures were observed in the $J/\psi K^{\pm}$ system. A larger data sample is necessary to obtain more information about possible intermediate structures.

4 Conclusion

In summary, we gave a review of some recent results on XYZ from Belle experiment. With more and more exotic states discovered, especially the recent candidate tetraquark and pentaquark states, a new hadron spectroscopy is being revealed.

Although there has been great progress in the study of the XYZ states, especially Belle and BESIII are still producing more exciting results, we found we have more questions to answer. Further studies along this line may strengthen our understanding of how strong interaction works at low energy and thus result in a better understanding of the matters around us. The Belle-II experiment is going to take data in 2018[40-41]. With a 50 ab^{-1} data sample, the future is very promising.

References

[1] BRAMBILLA N, EIDELMAN S, FOKA P, et al. QCD and strongly coupled gauge theories: Challenges and perspectives[J]. Eur Phys J C, 2014, 74: 2981.

[2] BRAMBILLA N, EIDELMAN S, HELTSLEY B K, et al. Heavy quarkonium: Progress, puzzles, and opportunities[J]. Eur Phys J C, 2011, 71: 1534.

[3] ABLIKIM M, ACHASOV M N, AI X C, et al. Observation of a charged charmoniumlike structure in $e^{+}e^{-}\to\pi^{+}\pi^{-}J/\psi$ at $\sqrt{s}=4.26$ GeV[J]. Phys Rev Lett, 2013, 110: 252001.

[4] LIU Z Q, SHEN C P, YUAN C Z, et al. Study of $e^{+}e^{-}\to\pi^{+}\pi^{-}J/\psi$ and observation of a charged charmoniumlike state at Belle[J]. Phys Rev Lett, 2013, 110: 252002.

[5] RAIJ A, ADEVA B, ADINOLFI M, et al. Observation of $J/\psi p$ resonances consistent with pentaquark states in $\Lambda_b^0\to J/\psi K^{-}p$ decays[J]. Phys Rev Lett, 2015, 115: 072001.

[6] CHOI S K, OLSEN S L, ABE K, et al. Observation of a narrow charmoniumlike state in exclusive $B^{\pm}\to K^{\pm}\pi^{+}\pi^{-}J/\psi$ decays [J]. Phys Rev Lett, 2003, 91: 262001.

[7] OLIVE K A, AGASHE K, AMSLER C, et al. Review of particle physics [J]. Chin Phys C, 2014, 38(09): 090001.

[8] CHOI S K, OLSEN S L, TRABELSI K, et al. Bounds on the width, mass difference and other properties of $X(3872)\to\pi^{+}\pi^{-}J/\psi$ decays[J]. Phys Rev D, 2011, 84: 052004.

[9] AAIJ R, ABELLAN BETETA C, ADEVA B, et al. Determination of the $X(3872)$ meson quantum numbers [J]. Phys Rev Lett, 2013, 110: 222001.

[10] SWANSON E S. Diagnostic decays of the $X(3872)$ [J]. Phys Lett B, 2004, 598: 197-202.

[11] SWANSON E S. The new heavy mesons: A status report[J]. Phys Rep, 2006, 429: 243-305.

[12] AUBERT B, BONA M, BOUTIGNY D, et al. Study of resonances in exclusive B decays to $\overline{D}^{(*)}D^{(*)}$ K[J]. Phys Rev D, 2008, 77: 011102.

[13] AUSHEV T, ZWAHLEN N, ADACHI I, et al. Study of the $B\to X(3872)(\to D^{*0}\overline{D}^{0})K$ decay[J]. Phys Rev D, 2010, 81: 031103.

[14] BALA A, BHARDWAJ V, TRABELSI K, et al. Observation of $X(3872)$ in $B\to X(3872)K\pi$ decays[J].

Phys Rev D,2015, 91:051101(R).

[15] ALI A, HAMBROCK C, AHMED I, et al. A case for hidden $b\bar{b}$ tetraquarks based on $e^+e^-\to b\bar{b}$ cross section between $\sqrt{s}=10.54$ and 11.20 GeV[J]. Phys Lett B, 2010,684: 28-39.

[16] TÖRNQVIST N A. From the deuteron to deusons, an analysis of deuteronlike meson-meson bound states[J]. Z Phys C,1994, 61: 525-537.

[17] GUO F K, HIDALGO-DUQUE C, NIEVES J, et al. Consequences of heavy-quark symmetries for hadronic molecules[J]. Phys Rev D,2013, 88: 054007.

[18] KARLINER M, NUSSINOV S. The doubly heavies: $\bar{Q}\bar{Q}\bar{q}q$ and $QQ\bar{q}\bar{q}$ tetraquarks and QQq baryons[J]. JHEP,2013,2013: 153.

[19] CHATRCHYAN S, KHACHATRYAN V, SIRUNYAN A M, et al. Search for a new bottomonium state decaying to $\gamma(1S)\ \pi^+\ \pi^-$ in pp collisions at $\sqrt{s}=8$ TeV[J]. Phys Lett B,2013, 727: 57-76.

[20] GUO F K, MEIßNER U G, WANG W, et al. Production of the bottom analogs and the spin partner of the $X(3872)$ at hadron colliders[J]. Eur Phys J C, 2014, 74:3063.

[21] HE XH,SHEN C P, YUAN C Z, et al. Observation of $e^+e^-\to\pi^+\ \pi^-\ \pi^0\ \chi_{bJ}$ and search for $X_b\to\omega\Upsilon(1S)$ at $\sqrt{s}=10.867$ GeV [J]. Phys Rev Lett, 2014, 113:142001.

[22] AUBERT B, BARATE R, BOUTIGNY D, et al. Observation of a broad structure in the$\pi^+\pi^- J/\psi$ mass spectrum around 4.26 GeV/c^2 [J]. Phys Rev Lett, 2005, 95: 142001.

[23] HE Q, INSLER J, MURAMATSU H, et al. Confirmation of the $Y(4260)$ resonance production in initial state radiation[J]. Phys Rev D,2006,74: 091104(R).

[24] ABE K, ADACHI I, AIHARA H, et al. Study of the $Y(4260)$ resonance in e^+e^- collisions with initial state radiation at Belle [EB/OL]. (2006-12-04) [2015-11-01]. http://arxiv.org/abs/hep-ex/0612006.

[25] YUAN C Z, SHEN C P, WANG P, et al. Measurement of the $e^+e^-\to\pi^+\pi^- J/\psi$ cross section via initial-state radiation at Belle [J]. Phys Rev Lett, 2007, 99:182004.

[26] LEES J P, POIREAU V, TISSERAND V, et al. Study of the reaction $e^+e^-\to J/\psi\pi^+\pi^-$ via initial-state radiation at BABAR[J]. Phys Rev D,2012, 86:051102(R).

[27] AUBERT B, BARATE R, BONA M, et al. Evidence of a broad structure at an invariant mass of 4.32 GeV/c^2 in the reaction $e^+e^-\to\pi^+\pi^-\psi(2S)$ measured at BABAR[J]. Phys Rev Lett, 2007, 98:212001.

[28] WANG X L, YUAN C Z, SHEN C P, et al. Observation of two resonant structures in $e^+e^-\to\pi^+\pi^-\psi(2S)$ via initial-state radiation at Belle[J]. Phys Rev Lett, 2007, 99: 142002.

[29] AUBERT B, POIREAU V, TISSERAND V, et al. Study of the reaction $e^+e^-\to\psi(2S)\pi^+\pi^-$ via initial-state radiation at BaBar [J]. Phys Rev D, 2014, 89:111103.

[30] WANG X L, YUAN C Z, SHEN C P, et al. Measurement of $e^+e^-\to\pi^+\pi^-\psi(2S)$ via initial state radiation at Belle[J]. Phys Rev D,2015, 91:112007.

[31] YUAN C Z, SHEN C P, WANG P, et al. Observation of $e^+e^-\to K^+K^- J/\psi$ via initial-state radiation at Belle[J]. Phys Rev D, 2008, 77: 011105(R).

[32] SHEN C P, YUAN C Z, WANG P, et al. Updated cross section measurement of $e^+e^-\to K^+K^- J/\psi$ and $K^0_SK^0_S J/\psi$ via initial state radiation at Belle[J]. Phys Rev D,2014, 89: 072015.

[33] HAN Y L, WANG X L, YUAN C Z, et al. Measurement of $e^+e^-\to\to\gamma\chi_{cJ}$ via initial state radiation at Belle[J]. Phys Rev D, 2015, 92: 012011.

[34] ABLIKIM M, ACHASOV M N, ALBAYRAK O, et al. Observation of a charged charmoniumlike structure $Z_c(4020)$ and search for the $Z_c(3900)$ in $e^+e^-\to\pi^+\pi^- h_c$[J]. Phys Rev Lett, 2013:111, 242001.

[35] CHILIKIN K, MIZUK R, ADACHI I, et al. Observation of a new charged charmoniumlike state in $\bar{B}^0\to J/\psi K^-\ \pi^+$ decays [J]. Phys Rev D, 2014, 90:112009.

[36] CHOI S K, OLSEN S L, ADACHI I, et al. Observation of a resonancelike structure in the $\pi^{+-}\psi'$ mass distribution in exclusive $B\to K\pi^{+-}\psi'$ decays[J]. Phys Rev Lett, 2008, 100:142001.

[37] LEE S H, NIELSEN M, WIEDNER U. $D_s\,D^*$ molecule as an axial meson[J]. Jour Korean Phys Soc, 2008,55: 424.

[38] DIAS J M, LIU X, NIELSEN M. Prediction for the decay width of a charged state near the $D_S\,\bar{D}^*/D_S^*\,\bar{D}$ threshold[J]. Phys Rev D,2013, 88: 096014.

[39] CHEN D Y, LIU X, MATSUKI T. Predictions of charged charmoniumlike structures with hidden-charm and open-strange channels[J]. Phys Rev Lett, 2013, 110:232001.

[40] AUSHEV T, BARTEL W, BONDAR A, et al. Physics at Super B Factory[EB/OL]. (2010-02-26)[2015-11-01]. http://arxiv.org/abs/1002.5012.

[41] ABE T, ADACHI I, ADAMCZYK K, et al. Belle II Technical Design Report[EB/OL]. (2010-11-01)[2015-11-01]. http://arxiv.org/abs/1011.0352.

Article ID:0253-2778(2016)07-0557-10

New results on exotic baryon resonances at LHCb

ZHANG Liming (for the LHCb Collaboration)

(*Center for High Energy Physics, Tsinghua University, Beijing* 100084, *China*)

Abstract: Observation of exotic resonant structures decaying into $J/\psi p$ found in the LHCb experiment is discussed. Examination of the $J/\psi p$ system in $\Lambda_b^0 \to J/\psi K^- p$ decays shows two states, each of which must be composed of at least $c\bar{c}uud$ quarks, and are thus consistent with pentaquarks. The significance of each of these resonances is more than 9 standard deviations. Their masses are (4 380±8±29)MeV and (4 449.8±1.7±2.5)MeV, and their corresponding widths are (205±18±86)MeV, and (39±5±19)MeV. The preferred J^P assignments are of opposite parity, with one state having spin 3/2 and the other 5/2.

Key words: LHCb; exotic baryon; hidden-charmonium pentaquark

CLC number: O572.3 **Document code**: A doi:10.3969/j.issn.0253-2778.2016.07.004

Citation: ZHANG Liming. New results on exotic baryon resonances at LHCb[J]. Journal of University of Science and Technology of China, 2016,46(7):557-566.

LHCb 实验上新奇特重子的发现

张黎明(LHCb 合作组)

(清华大学高能物理研究中心,北京 100084)

摘要:介绍了 LHCb 实验上观测到的 $J/\psi p$ 奇特共振结构的实验证据.在 $\Lambda_b^0 \to J/\psi K^- p$ 衰变中,$J/\psi p$ 系统显示出两个共振态,每个至少含有五个夸克 $c\bar{c}uud$,和五夸克态相符.每个态的信号显著度都大于 9 倍的标准差.它们的质量为(4 380±8±29)MeV 和(4 449.8±1.7±2.5)MeV,对应的宽度为(205±18±86)MeV,和(39±5±19)MeV.最有可能自旋一个为 3/2,另一个为 5/2,宇称相反.

关键词:LHCb;奇特重子;隐形粲偶素五夸克态

0 Introduction

In 1964 Gell-Mann[1], and separately Zweig[2], proposed that hadrons were formed from fundamental point-like fractionally-charged objects now called quarks. The minimal quark configuration, that baryon is composed of three quarks and meson a quark and an anti-quark, can explain all well established hadrons for most of the last half-century. However, in the current decade there have been several observations of candidate mesonic states containing two quarks and two anti-quarks, called tetraquarks[3-4], and now, as described here, the observation of two pentaquark candidate baryon states[5]. Such multi-quark configuration were also discussed by the Gell-

Received:2015-11-30;**Revised**:2016-04-20

Foundation item:Supported by Funding of 1000 Young-Talented Plan in China.

Biography:ZHANG Liming, male, born in 1979, PhD/associate professor. Research field: high energy physics. E-mail: liming.zhang@cern.ch

Mann[1] and Zweig[2]. Several pentaquark observations made about ten years ago were all shown to be spurious[6]. Thus, the recent observation of two states decaying into $J/\psi p$, charmonium pentaquarks, found in $\Lambda_b^0 \to J/\psi K^- p$ decays by the LHCb experiment is surprising.

The Λ_b^0 decay mode was first observed by LHCb with an unexpected large yield and have been used to precisely measure the Λ_b^0 baryons lifetime[7-8]. However, one feature of the decay that was not addressed was an anomalous peaking structure in the $J/\psi p$ invariant mass spectrum, evident in the Dalitz plot shown in Fig. 1. While vertical bands correspond to $\Lambda^* \to K^- p$ resonances, shown by Feynman diagram in Fig. 2 (a), the horizontal band can only rise from structures in the $J/\psi p$ mass spectrum, by diagram in Fig. 2 (b). They can also be seen in the invariant mass projections shown in Fig. 3.

To claim such observations, we first addressed the two following questions: could the peak in the $J/\psi p$ mass distribution be caused by an experimental artifact or by an interference of various Λ^* amplitudes?

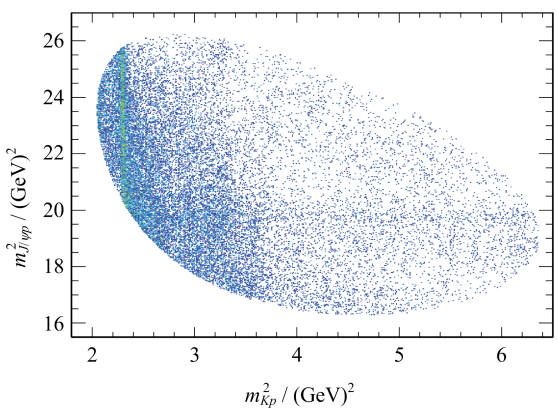

Fig. 1 Invariant mass squared of $K^- p$ versus $J/\psi p$ for candidates within ±15 MeV of the Λ_b^0 mass

1 Analysis and results

For this study LHCb[9] used data corresponding to 3 fb^{-1} of integrated luminosity in 7 and 8 TeV pp collisions. We reconstruct the $\Lambda_b^0 \to J/\psi K^- p$ decays by combining $J/\psi \to \mu^+ \mu^-$

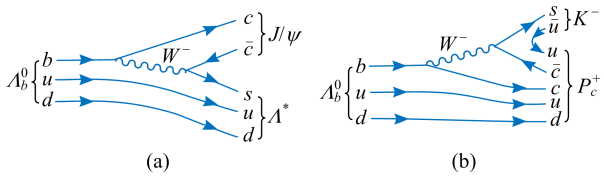

Fig. 2 Feynman diagrams for (a) $\Lambda_b^0 \to J/\psi\Lambda^*$ and (b) $\Lambda_b^0 \to P_c^+ K^-$ decay

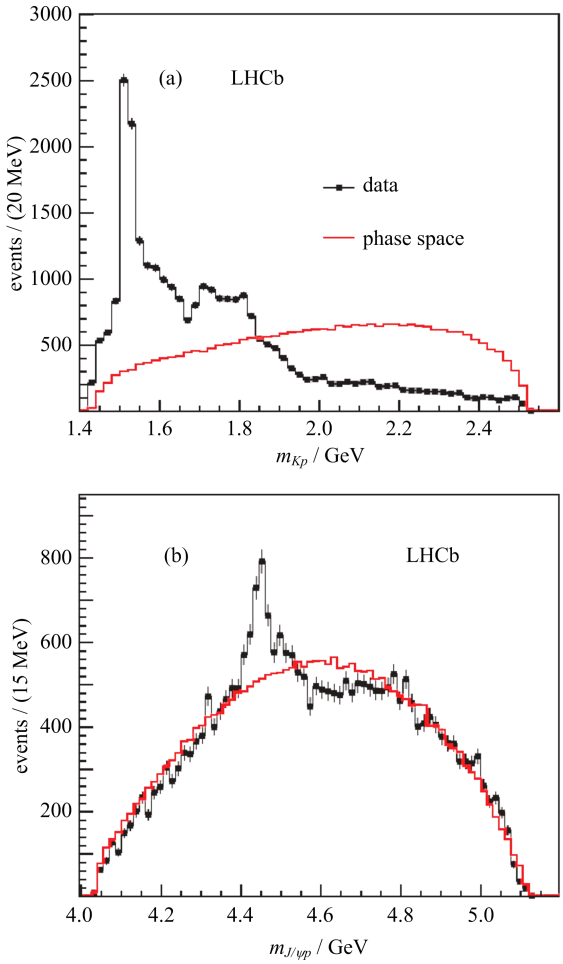

The solid (red) curve is the expectation from phase space. The background has been subtracted.

Fig. 3 Invariant mass of (a) $K^- p$ and (b) $J/\psi p$ combinations from $\Lambda_b^0 \to J/\psi K^- p$ decays

candidates with positive identified K^- and p tracks. The Λ_b^0 vertex is required to be well separated from the primary pp interaction vertex. A dedicated neutral network based selection criteria is optimized to achieve clean signals with high efficiency. The details are thoroughly described in Ref. [5]. In addition, specific backgrounds from $\overline{B}_s^0$ and $\overline{B}^0$ decays are vetoed

where the particle identification fails. We remove combinations that when interpreted as $J/\psi K^+K^-$ fall within ± 30 MeV of the $\overline{B}_s^0$ mass or when interpreted as $J/\psi K^-\pi^+$ fall within ± 30 MeV of the $\overline{B}^0$ mass. This requirement effectively eliminates background from these sources and causes only smooth changes in the detection efficiencies across the Λ_b^0 decay phase space. We have examined that potential backgrounds from Ξ_b decays cannot contribute significantly to our sample; these include Cabibbo-suppressed $\Xi_b^{-(0)} \to J/\psi K^- p\pi^{-(0)}$ and Cabibbo-favoured $\Xi_b^{-(0)} \to J/\psi K^- p K^-(\overline{K}^0)$. The resulting $J/\psi K^- p$ mass spectrum is shown in Fig. 4. There are $26\,007 \pm 166$ signal candidates containing 5.4% background within ± 15 MeV ($\pm 2\sigma$) of the $J/\psi K^- p$ mass peak. For subsequent analysis we constrain the $J/\psi K^- p$ four-vectors to give the Λ_b^0 invariant mass, J/ψ four-vectors to give the J/ψ mass and the Λ_b^0 momentum vector to be aligned with the measured direction from the primary to the Λ_b^0 vertices[10].

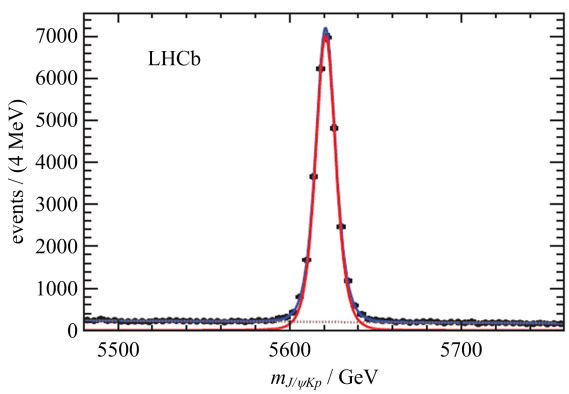

Fig. 4 Invariant mass spectrum of $J/\psi K^- p$ combinations, with the total fit, signal and background components shown as solid (blue), solid (red) and dashed lines, respectively

The overall detection efficiency determined from simulation and background from the sideband both smoothly vary across the Λ_b^0 decay phase space, and thus cannot generate such a narrow peak seen in the invariant mass of $J/\psi p$. In this sample specific tracking artifacts were looked for including fake tracks assembled from mismatched upstream and downstream segments, and multiple reconstructions of the same track. Having found no source of tracking artifacts, we proceeded to analyze the decay sequences represented by the Feynman diagrams shown in Fig. 2.

This requires a full analysis of the amplitude for each of the two decay sequences allowing for their mutual interference. The amplitudes are written using six independent variables; one is the invariant $K^- p$ mass, m_{Kp}, the others are decay angles. These are shown for the decay sequence $\Lambda_b^0 \to J/\psi\Lambda^*$, $\Lambda^* \to K^- p$, $J/\psi \to \mu^+\mu^-$ in Fig. 5. The Λ^* resonances are modeled by Breit-Wigner amplitudes except for the $\Lambda^*(1405)$ which is described by a Flatté function[11].

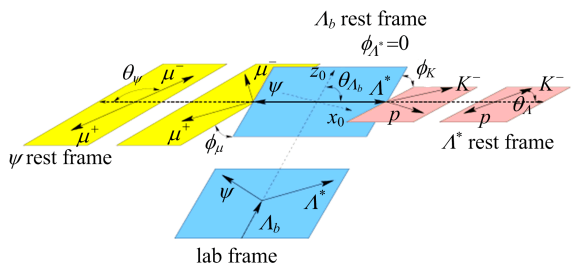

Fig. 5 Definition of the decay angles in the Λ^* decay chain

We first used the conventional resonances Λ^* and Σ^* to fit the data. We consider 14 Λ^* states. In each of their decays there are 4 or 6 independent LS (L is angular momenta and S total spin in Λ_b^0 decays) amplitudes that could be present. Not all of these states are likely to be produced in our final state and not all of the allowable decay angular momenta (LS couplings) are likely to be present. In order to make the most general description possible we first used all the possible states and decay angular momenta. Then data are fit to this model which has 146 free LS coupling coefficiencies, with the masses and widths of the resonant states fixed to their PDG values. Variations are considered later as part of the systematic uncertainties. The results of the fit are shown in Fig. 6. The fit gives a good description of the Λ^* states as can be seen in the m_{Kp} spectrum but fails to reproduce the structure in $m_{J/\psi p}$.

Several other different configurations were

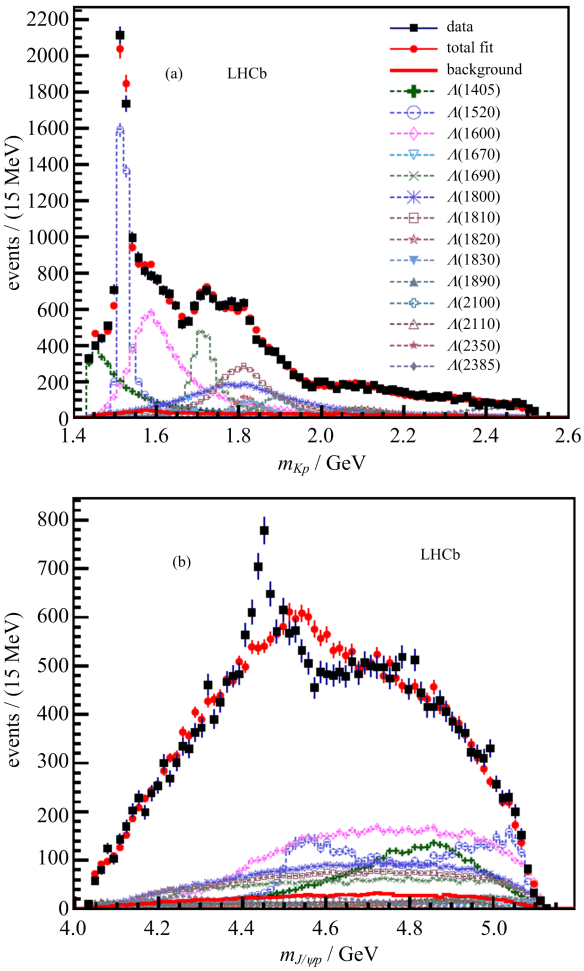

The data are shown as (black) squares with error bars, while the (red) circles show the results of the fit.

Fig. 6 Results for (a) m_{Kp} and (b) $m_{J/\psi p}$ for the extended Λ^* model fit without P_c^+ states

tried to improve the fit, but still none of these fits explains the data. These configurations are ① we added all the possible Σ^* states, ② we added two additional Λ^* allowing their masses and widths to float in the fit and allowed spins up to 5/2 with both parities, and ③ we added four non-resonant components with $J^P = 1/2^+$, $1/2^-$, $3/2^+$, and $3/2^-$.

Having failed to describe the data with conventional resources, we add one state decaying into $J/\psi p$. The matrix element for the decay sequence $\Lambda_b^0 \to P_c^+ K^-$, $P_c^+ \to J/\psi p$ is described by different mass and decay angles shown in Fig. 7. While these quantities can be expressed in terms of the used variables involving only Λ^* decays, thus do not provide additional fit variables. The detailed derivation of the matrix element is given in the arXiv article and the supplementary material for the Physical Review Letters publication[5].

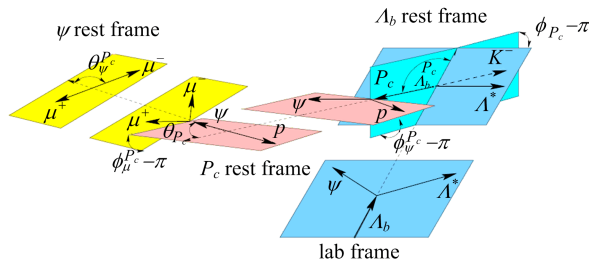

Fig. 7 Definition of the decay angles in the P_c^+ decay sequence

In each fit we minimize $-2\ln\mathscr{L}$ where $\mathscr{L}$ represents the fit likelihood. The $\Delta(-2\ln\mathscr{L})$ between different amplitude models allows to discriminate the models. A preferred model gives the smallest $-2\ln\mathscr{L}$. Separate fits for J^P values of $1/2^\pm$, $3/2^\pm$, $5/2^\pm$ and $7/2^\pm$ were tried. We allowed the mass and width of the putative P_c^+ state to vary. The best fit prefers a $5/2^+$ state, which reduces $-2\ln\mathscr{L}$ by 215. Fig. 8 shows the projections for this fit. Even though the m_{Kp} projection is well described, clear discrepancies in $m_{J/\psi p}$ remain visible.

To improve the fit, a second P_c^+ was added. These fits were performed both with the reduced model and the extended model in order to estimate systematic uncertainties. The best fit projections are shown in Fig. 9. Both m_{Kp} and the peaking structure in $m_{J/\psi p}$ are reproduced by the fit. The reduced model has 64 free parameters for the Λ^* rather than 146 and allows for a much more efficient examination of the parameter uncertainties and, thus, is used for numerical results. The two P_c^+ states are found to have masses of $(4\,380\pm8\pm29)$ MeV and $(4\,449.8\pm1.7\pm2.5)$ MeV, with corresponding widths of $(205\pm18\pm86)$ MeV and $(39\pm5\pm19)$ MeV, and called $P_c(4380)^+$ and $P_c(4450)^+$. Whenever two uncertainties are

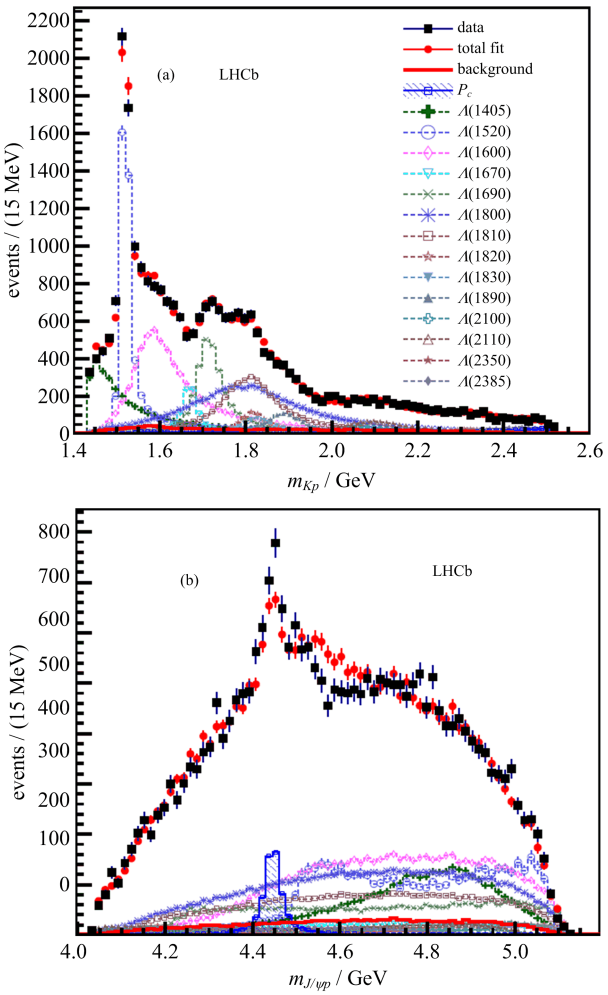

Fig. 8 Results of the fit with one $J^P = 5/2^+$ P_c^+ candidate

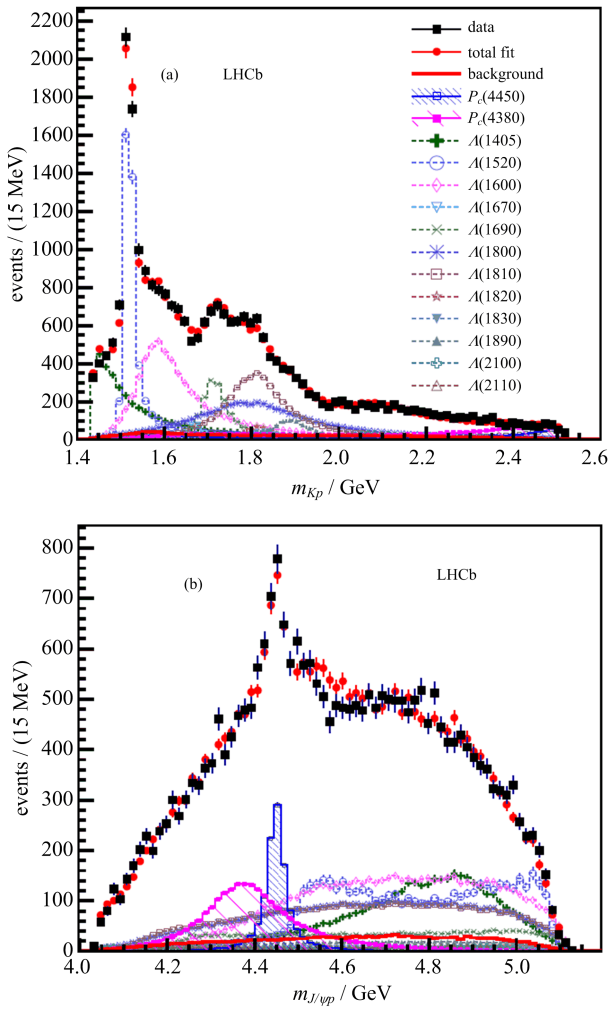

Fig. 9 Results of the fit using the reduced Λ^* model with two P_c^+ states

quoted the first is statistical and the second systematic. The fractions of the total sample due to the lower mass and higher mass states are $(8.4 \pm 0.7 \pm 4.2)\%$ and $(4.1 \pm 0.5 \pm 1.1)\%$, respectively. The overall branching fraction has recently be determined to be[13]

$$\mathcal{B}(\Lambda_b^0 \to J/\psi K^- p) = (3.04 \pm 0.04^{+0.55}_{-0.43}) \times 10^{-4} \tag{1}$$

where the systematic uncertainty is largely due to the normalization procedure, leading to the product branching fractions:

$$\left.\begin{aligned}\mathcal{B}(\Lambda_b^0 \to P_c(4380)^+ K^- p)\mathcal{B}(P_c(4380)^+ \to J/\psi p) = \\ (2.56^{+1.38}_{-1.34}) \times 10^{-5} \\ \mathcal{B}(\Lambda_b^0 \to P_c(4450)^+ K^- p)\mathcal{B}(P_c(4450)^+ \to J/\psi p) = \\ (1.25^{+0.42}_{-0.40}) \times 10^{-5}\end{aligned}\right\} \tag{2}$$

where all the uncertainties have been added in quadrature. Toy simulations are done to more accurately evaluate the statistical significances of the two states, resulting in 9 and 12 standard deviations, for lower mass and higher mass states, using the extended model which gives lower significances to account for systematic uncertainties.

The best fit has spin-parity J^P values of $(3/2^-, 5/2^+)$ for low and high mass states. Acceptable solutions are also found for additional cases with opposite parity, either $(3/2^+, 5/2^-)$ or $(5/2^+, 3/2^-)$. The five angular distributions are also well described by the fit shown in Fig. 10.

The fit projections in different slices of $K^- p$

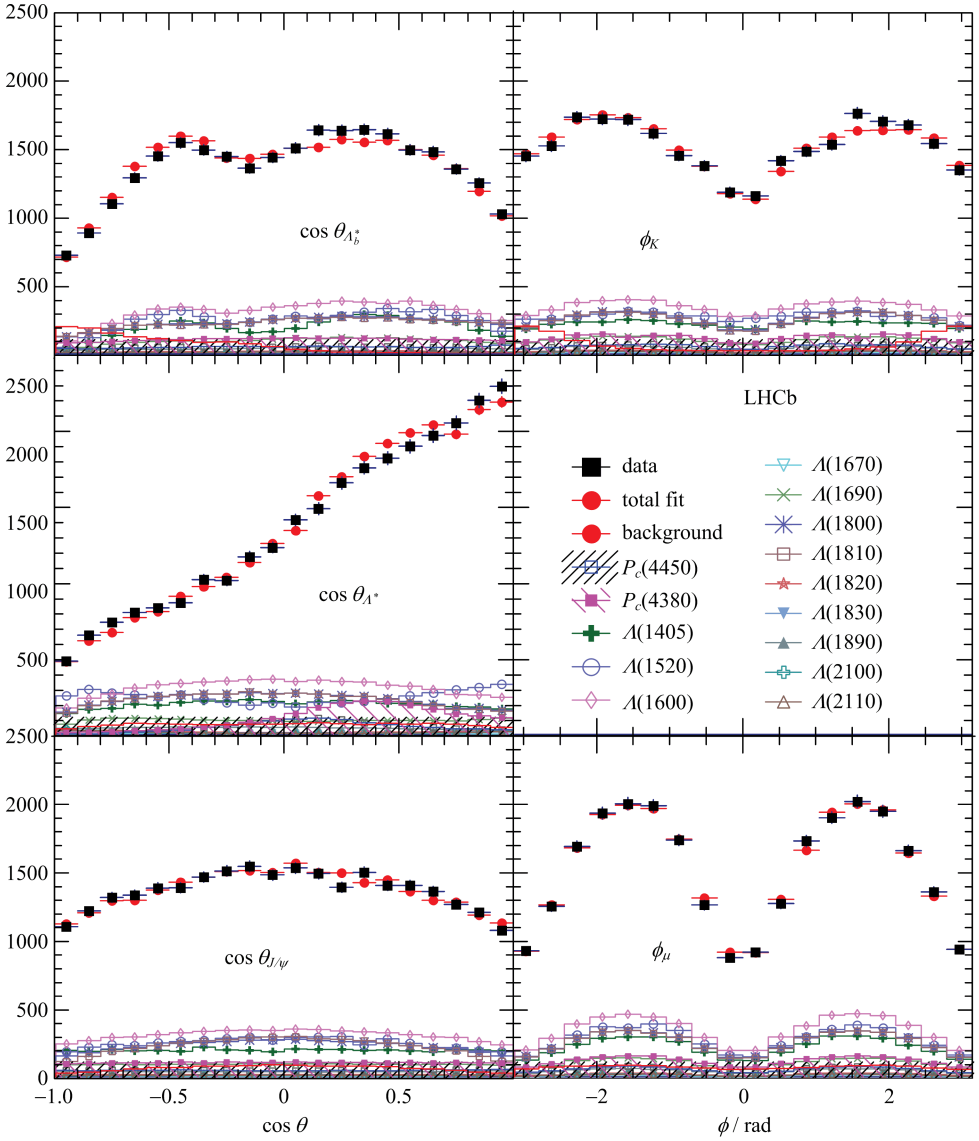

The data are shown as (black) squares, while the (red) circles show the results of the fit. Each fit component is also shown.

Fig. 10 Various decay angular distributions for the fit with two P_c^+ states

invariant mass are given in Fig. 11. In slice (a) the P_c^+ states are not present, as they are outside of the kinematic boundary. In slice (d) both P_c^+ states form a large part of the mass spectrum; there is also a considerable amount of negative interference between them. This can be seen better by examining the helicity angle of the P_c^+, θ_{P_c}, defined in Fig. 7. The efficiency corrected and background subtracted fit projection of the decay angular distribution is shown in Fig. 12 for the entire m_{Kp} range. The summed fit projection agrees very well with the angular distribution in the data, showing that two interfering states are needed to reproduce the asymmetric distribution. It is also shown mathematically that the two states need to be of opposite parity to produce such asymmetric distribution.

Systematic uncertainties are evaluated. The largest contribution comes from Λ^* modeling including the extended versus reduced model, varying the Λ^* masses and widths, and inclusion of a nonresonant amplitude in the fit. Sizable

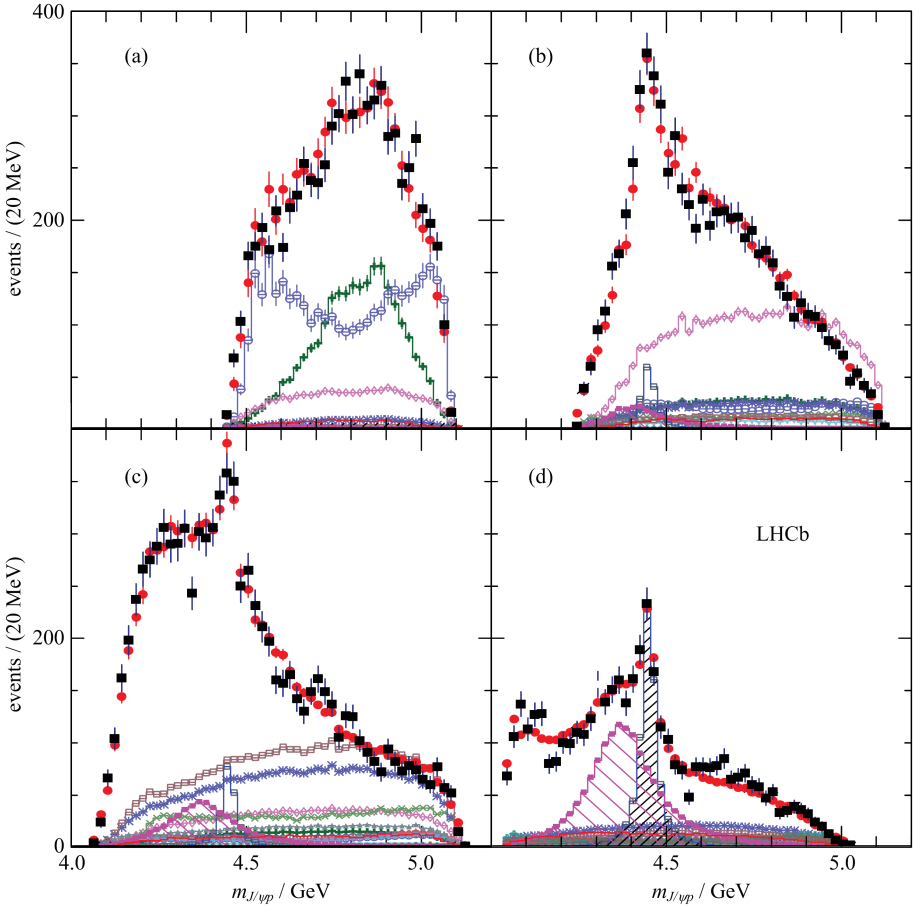

The data are shown as (black) squares with error bars, while the (red) circles show the results of the fit. The blue and purple histograms show the two P_c^+ states. See Fig. 10 for the legend.

Fig. 11 $m_{J/\psi p}$ **in various intervals of** m_{Kp} **for the fit with two** P_c^+ **states: (a)** m_{Kp} **<1.55 GeV, (b) 1.55 GeV<** m_{Kp} **<1.70 GeV, (c) 1.70 GeV<** m_{Kp} **<2.00 GeV, and (d)** m_{Kp} **>2.00 GeV**

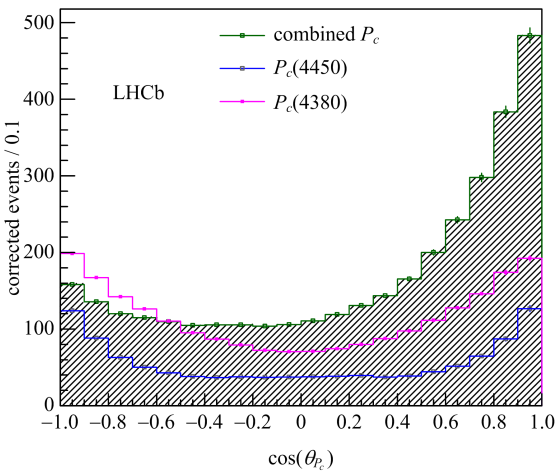

Values of $\cos\theta_{P_c}$ near −1 are correlated with values of m_{Kp} near threshold, while those near +1 are correlated with higher values.

Fig. 12 Efficiency corrected and background subtracted fit projections of the decay angular distributions for the two P_c^+ **states and their sum**

uncertainties are obtained for alternate J^P fits, varying the Blatt-Weisskopf barrier factor and changing the angular momentum L by one or two units. A nonresonant P_c^+ was also included and gave small systematic uncertainty. Consistent results are obtained from two fitters using different methods to account for the background, called "sFit" and "cFit" provided by two institutes.

The stability of the results is cross-checked by comparing the data recorded in 2011/2012, with the LHCb dipole magnet polarity in up/down configurations, $\Lambda_b^0/\overline{\Lambda}_b^0$ decays, and Λ_b^0 produced with low/high values of p_T. The fitters were tested on simulated pseudoexperiments and no biases were found. In addition, selection

requirements are varied, and the vetoes of $\overline{B}_s^0$ and $\overline{B}^0$ are removed and explicit models of those backgrounds added to the fit; all give consistent results.

Further evidence for the resonant character of the higher mass, narrower, P_c^+ state is obtained by viewing the evolution of the complex amplitude in the Argand diagram[12]. In the amplitude fits discussed above, the $P_c(4450)^+$ is represented by a Breit-Wigner amplitude, where the magnitude and phase vary with $m_{J/\psi p}$ according to an approximately circular trajectory in the ($\mathrm{Re}A^{P_c}$, $\mathrm{Im}A^{P_c}$) plane, where A^{P_c} is the $m_{J/\psi p}$ dependent part of the $P_c(4450)^+$ amplitude. We perform an additional fit to the data using the reduced Λ^* model, in which we represent the $P_c(4450)^+$ amplitude as the combination of independent complex amplitudes at six equidistant points in the range $\pm\Gamma=39$ MeV around $M=4\,449.8$ MeV as determined in the default fit. Real and imaginary parts of the amplitude are interpolated in mass between the fitted points. The resulting Argand diagram, shown in Fig. 13(a), is consistent with a rapid counter-clockwise change of the $P_c(4450)^+$ phase when its magnitude reaches the maximum, a behavior characteristic of a resonance. A similar study for the wider state is shown in Fig. 13(b); although the fit does show a large phase change, the amplitude values are sensitive to the details of the Λ^* model and so this latter study is not conclusive.

2 Models of pentaquark structure

All models must explain the J^P of the two states not just one. They also should predict properties of other yet to be observed states: masses, widths, J^P's. There are many explanations of the P_c^+ states.

Let us start with tightly bound quarks ala Jaffe[14]. Early work[15-17] has been expanded upon recently use of diquark-diquark-antiquark models[18-23] and diquark-triquark model[24]. Here each pair of two quarks form a colored object along with the lone antiquark. The three colors then form a colorless state.

Weakly bound "molecules" of a baryon plus a

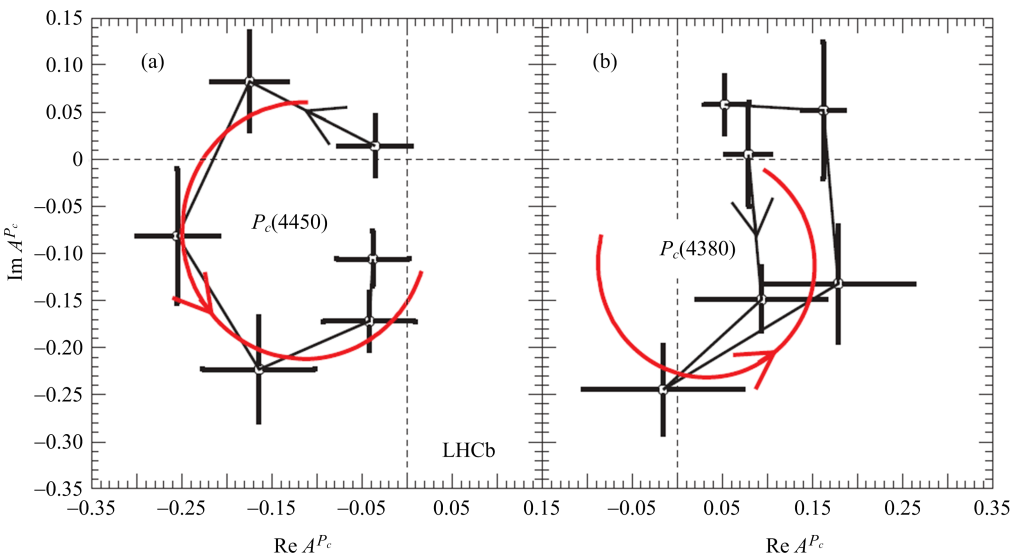

The solid (red) curves are the predictions from the Breit-Wigner formula. Systematic uncertainties are not included.

Fig. 13 Fitted values of the real and imaginary parts of the amplitudes for the baseline ($3/2^-$, $5/2^+$) fit for (a) the $P_c(4450)^+$ state and (b) the $P_c(4380)^+$ state, each divided into six $m_{J/\psi p}$ bins of equal width between $-\Gamma$ and $+\Gamma$ shown in the Argand diagrams as connected points with error bars ($m_{J/\psi p}$ increases counterclockwise)

meson, which are also built on previous work[25-30], have recently received much attention. Models trying to explain the states discussed here have already appeared[31-35], and even been disputed[36].

The $P_c(4450)^+$ is also explained by rescattering of $\chi_{c1}p \to J/\psi p$ as the sum masses of χ_{c1} and p is almost equal to the mass of this state[37-38].

3 Conclusion

After a half century of waiting, pentaquark states have been unmasked. Using a full amplitude fit to the $\Lambda_b^0 \to J/\psi K^- p$ decay, the LHCb collaboration has demonstrated two states of opposite parties decaying into $J/\psi p$, one having a mass of $(4380 \pm 8 \pm 29)$MeV and a width of $(205 \pm 18 \pm 86)$MeV, while the other has a mass of $(4\,449.8 \pm 1.7 \pm 2.5)$MeV and a width of $(39 \pm 5 \pm 19)$MeV. The parities of the two states are opposite with the preferred spins being 3/2 for one state and 5/2 for the other. The detailed binding mechanism of these states are subject to further studies. This work will lead to a better understanding of the strong interactions.

References

[1] GELL-MANN M. A schematic model of baryons and mesons[J]. Phys Lett, 1964,8:214-215.

[2] ZWEIG G. An SU3 model for strong interaction symmetry and its breaking: CERN-TH-401 [R]. [S. l.: s. n.], 1964.

[3] OLSEN S L. A new hadron spectroscopy[J]. Front Phys,2015,10:121-154.

[4] PILLONI A. XYZ: four-quark states? [EB/OL]. (2015-08-16) [2015-11-01]. http://arxiv.org/abs/1508.03823.

[5] AAIJ R, ADEVA B, ADINOLF M, et al. Observation of $J/\psi p$ resonances consistent with pentaquark states in $\Lambda_b^0 \to J/\psi K^- p$ decays[J]. Phys Rev Lett, 2015,115:072001.

[6] HICKS K H. On the conundrum of the pentaquark[J]. Eur Phys J H,2012,37(1): 1-31.

[7] AAIJ R, ADEVA B, ADINOLFI M, et al. Precision measurement of the ratio of the Λ_b^0 to $\overline{B}^0$ lifetimes[J]. Phys Lett B,2014,734:122-130.

[8] AAIJ R, ADEVA B, ADINOLFI M, et al. Precision measurement of the Λ_b^0 baryon lifetime[J]. Phys Rev Lett,2013,111:102003.

[9] ALVES JR A A, ANDRADE FILHO L M, BARBOSA A F, et al. The LHCb detector at the LHC [J/OL]. JINST, 2008, 3: S08005 [2015-11-01]. http://dx.doi.org/10.1088/1748-0221/3/08/S08005.

[10] HULSBERGEN W D. Decay chain fitting with a Kalman filter[J]. Nucl Instrum Meth A,2005,552:566-575.

[11] FLATTÉ S M. Coupled-channel analysis of the $\pi\eta$ and $K\overline{K}$ systems near $K\overline{K}$ threshold[J]. Phys Lett B, 1976,63: 224-227.

[12] OLIVE K A, AGASHE K, AMSLER C, et al. Review of particle physics [J]. Chin Phys C, 2014, 38(09): 090001.

[13] AAIJ R, ADEVA B, ADINOLFI M, et al. Study of the production of Λ_b^0 and $\overline{B}^0$ hadrons in pp collisions and first measurement of the $\Lambda_b^0 \to J/\psi p K^-$ branching fraction[EB/OL]. (2015-09-01)[2015-11-01]. http://arxiv.org/abs/1509.00292.

[14] JAFFE R J. Multiquark hadrons. I. Phenomenology of $Q^2\overline{Q}^2$ mesons[J]. Phys Rev D,1977, 15:267.

[15] STROTTMAN D. Multi-quark baryons and the MIT bag model[J]. Phys Rev D,1979,20: 748.

[16] HÄOGAASEN H, SORBA P. The systematics of possibly narrow quark states with baryon number one [J]. Nucl Phys B,1978,145(1): 119-140.

[17] Rossi G C, Veneziano G. A possible description of baryon dynamics in dual and gauge theories[J]. Nucl Phys B,1977,123(3):507-545.

[18] MAIANI L, POLOSA A D, RIQUER V. The new pentaquarks in the diquark model[J]. Phys Lett B, 2015,749:289-291.

[19] ANISOVICH V V, MATVEEV M A, NYIRI J, et al. Pentaquarks and resonances in the pJ/ψ spectrum [EB/OL]. (2015-07-28)[2015-11-01]. http://arxiv.org/abs/1507.07652.

[20] LI G N, HE M, HE X G. Some predictions of diquark model for hidden charm pentaquark discovered at the LHCb[EB/OL]. (2015-10-08)[2015-11-01]. http://arxiv.org/abs/1507.08252.

[21] GHOSH R, BHATTACHARYA A, CHAKRABARTI B. The masses of $P_c^*(4380)$ and $P_c^*(4450)$ in the quasi particle diquark model[J]. (2015-08-03)[2015-11-01]. http://arxiv.org/abs/1508.00356.

[22] WANG Z G. Analysis of the $P_c(4380)$ and $P_c(4450)$ as pentaquark states in the diquark model with QCD

sum rules[J]. (2015-08-03)[2015-11-01]. http://arxiv.org/abs/1508.01468.

[23] WANG Z G, HUANG T. Analysis of the $\frac{1}{2}^{\pm}$ pentaquark states in the diquark model with QCD sum rules[J]. (2015-08-18)[2015-11-01]. http://arxiv.org/abs/1508.04189.

[24] LEBED R F. The pentaquark candidates in the dynamical diquark picture[J]. Phys Lett B, 2015, 749: 454-457.

[25] VOLOSHIN M B, OKUN L B. Hadron molecules andcharmonium atom[J]. JETP Lett, 1976, 23: 333.

[26] DE RUJULA A, GEORGI H, GLASHOW S L. Molecular charmonium: a new spectroscopy? [J]. Phys Rev Lett, 1977, 38: 317

[27] TÄORNQVIST N A. Possible large deuteronlike meson-meson states bound by pions[J]. Phys Rev Lett, 1991, 67: 556.

[28] TÄORNQVIST N A. From the deuteron to deusons, an analysis of deuteronlike meson-meson bound states [J]. Z Phys C, 1994, 61 (3): 525-537.

[29] YANG Z C, SUN Z F, HE J, et al. The possible hidden-charm molecular baryons composed of anti-charmed meson and charmed baryon[J]. Chin Phys C, 2012, 36: 6-13.

[30] WANG W L, HUANG F, ZHANG Z Y, et al. $\Sigma_c\overline{D}$ and $\Lambda_c\overline{D}$ states in a chiral quark model[J]. Phys Rev C, 2011, 84: 015203.

[31] KARLINER M, ROSNERJ L. New exotic meson and baryon resonances from doubly-heavy hadronic molecules [EB/OL]. (2015-08-24)[2015-11-01]. http://arxiv.org/abs/1506.06386.

[32] ROCA L, NIEVES J, OSET E. The LHCb pentaquark as a $\overline{D}^*\Sigma_c - \overline{D}^*\Sigma_c^*$ molecular state[EB/OL]. (2015-10-21)[2015-11-01]. http://arxiv.org/abs/1507.04249.

[33] CHEN R, LIU X, LI X Q, et al. Identifying exotic hidden-charm pentaquarks [EB/OL]. (2015-08-29)[2015-11-01]. https://arxiv.org/abs/1507.03704.

[34] HE J. $\overline{D}\Sigma_c^*$ and $\overline{D}^*\Sigma_c$ interactions and the LHCb hidden-charmed pentaquarks [EB/OL]. (2015-07-18)[2015-11-01]. https://arxiv.org/abs/1507.05200.

[35] MEIßNER U G, OLLER J A. Testing the $\chi_{c1}p$ composite nature of the $P_c(4450)$[EB/OL]. (2015-08-25) [2015-11-01]. https://arxiv.org/abs/1507.07478.

[36] MIRONOV A, MOROZOV A. Is pentaquark doublet a hadronic molecule? [EB/OL]. (2015-07-16)[2015-11-01]. https://arxiv.org/abs/1507.04694.

[37] GUO F K, MEIßNER U G, WANG W, et al. How to reveal the exotic nature of the $P_c(4450)$[EB/OL]. (2015-10-22)[2015-11-01]. https://arxiv.org/abs/1507.04950.

[38] MIKHASENKO M. A triangle singularity and the LHCb pentaquarks[EB/OL]. (2015-07-23)[2015-11-01]. https://arxiv.org/abs/1507.06552.

Article ID:0253-2778(2016)07-0567-07

Light hadron spectroscopy at BESIII

FANG Shuangshi (for the BESIII Collaboration)

(*Institute of High Energy Physics, Chinese Academy of Sciences*, 100049, *Beijing*, *China*)

Abstract: Based on the samples of 1.3×10^9 J/ψ events and 1.06×10^8 $\psi(3686)$ events taken at the BESIII detector, the recent progress on the light meson spectroscopy, baryon spectroscopy and light meson decays is presented.

Key words: BESIII detector; light hadron spectroscopy; charmonium decays

CLC number: O572.3 **Document code**: A doi:10.3969/j.issn.0253-2778.2016.07.005

Citation: FANG Shuangshi. Light hadron spectroscopy at BESIII[J]. Journal of University of Science and Technology of China, 2016,46(7):567-573.

BESIII 上的轻强子谱

房双世(BESIII 合作组)

(中国科学院高能物理研究所,北京 100049)

摘要:基于 BESIII 探测器采集的 1.3×10^9 个 J/ψ 事例和 1.06×10^8 个 $\psi(3686)$ 事例,报道了关于轻介子谱学、重子谱学和轻介子衰变的最新进展.

关键词:BESIII 探测器;轻强子谱学;粲偶素衰变

0 Introduction

At present our theoretical understanding of the light hadron spectrum remains based largely on the quark model due to the failure of the application of the perturbative theory in the low energy regime. In addition to the coventional hadrons predicted by the quark model, however, one of the clearest predictions of quantum chromodynamics (QCD) is the presence of exotic hadrons, e.g., glueballs, multiquark states and hybrids. The search for these exotic states has been taken for many years and many candidates have been reported by different experiments, but none of them were unambiguously identified to date.

The J/ψ and $\psi(3686)$ decays have provided a wealth of information on the light hadron spectroscopy since it was discovered in 1970s. Since their masses are below the charm meson pair, the direct decay into charmed mesons is forbidden, which offers a clean laboratory to study light hadron spectroscopy. Furthermore the comparison of the radiative and the hadronic decays not only provides insight into the decay mechanisms, but also helps in differentiating between the conventional $q\bar{q}$ states and the new spectroscopy.

In this paper, we present the progress on the

Received:2015-11-30;**Revised**:2016-04-20

Foundation item:Supported by National Natural Science Foundation of China (NSFC) (11175189).

Biography:FANG Shuangshi, male, born in 1977, PhD/Prof. Research field: experimental high energy physics. E-mail: fangss@ihep.ac.cn

light meson spectroscopy, baryon spectroscopy and light meson decays based on the samples of 1.3×10^9 J/ψ events and 1.06×10^8 $\psi(3686)$ events collected with the BESIII detector.

1 Light meson spectroscopy

In 2005 the X(1835) resonance was observed in $J/\psi\to\gamma\pi^+\pi^-\eta'$[1], which stimulated theoretical speculations on its nature. At BESIII, this structure was confirmed in the same decay channel[2] and similar structures around 1.85 GeV/c^2 were observed. To understand their nature, further study is strongly needed, in particular, searching for new decay modes.

In this paper, we present a study of $J/\psi\to\gamma K_SK_S\eta$[3] decays using a sample of $(1\ 310.6\pm10.5)\times10^6$ J/ψ events collected with the BESIII detector. By requiring that $M_{K_SK_S}$ be in the $f_0(980)$ mass region, $M_{K_SK_S}<1.1$ GeV/c^2, the structure around 1.85 GeV/c^2 shown in Fig. 1(a) is clearly seen. A partial wave analysis (PWA) is performed and the spin parity of the $X(1835)$ is determined to be $J^{PC}=0^{-+}$. The mass and width are measured to be $1\ 844\pm9(\text{stat})^{+16}_{-25}(\text{syst})$ MeV/c^2 and $192^{+20}_{-17}(\text{stat})^{+62}_{-43}(\text{syst})$ MeV, respectively, which is consistent with the results obtained by BESIII in $J/\psi\to\gamma\pi^+\pi^-\eta'$[2].

Fig. 1(b) shows the comparison to the BESIII results of the masses and widths of the $X(p\bar{p})$, $X(1835)$, $X(1870)$, $X(1840)$ and $X(1810)$. The mass of $X(1840)$ is in agreement with $X(p\bar{p})$, while its width is significantly broader. Therefore, based on these data, one cannot determine whether $X(1840)$ is a new state or the signal of a $3(\pi^+\pi^-)$ decay mode of $X(p\bar{p})$. Further study, including an amplitude analysis to determine the spin and parity of the $X(1840)$, is needed to establish the relationship between these experimental observations.

In addition, we also performed the model-independent PWA of $J/\psi\to\gamma\pi^0\pi^0$. The results displayed in Fig. 2(b) indicate that the scalar contributions are mainly from $\sigma(600)$, $f_0(1370)$, $f_0(1500)$, $f_0(1710)$ and $f_0(2020)$. The production rate of the pure gauge scalar glueball in J/ψ radiative decays predicted by the lattice QCD[10] was found to be compatible with the production rate of J/ψ radiative decays to $f_0(1710)$, which suggests that $f_0(1710)$ has a larger overlap with the glueball compared to other glueball candidates (e.g., $f_0(1500)$). The tensor components, which is dominantly from $f_2(1270)$, also have a large contribution in $J/\psi\to\gamma\pi^0\pi^0$ decays.

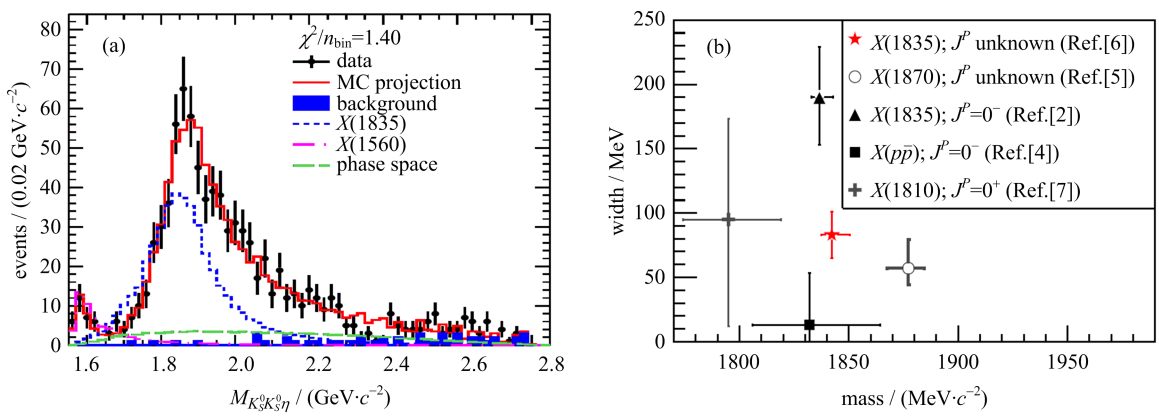

The error bars include statistical, systematic, and, where applicable, model uncertainties.

Fig. 1 (a) $K^0_SK^0_S\eta$ **invariant mass spectrum for events with the requirement** $M_{K^0_SK^0_S}<1.1$ GeV/c^2 **and PWA projections; (b) comparisons of observations at BESIII**

2 Baryon spectroscopy

To search for new excited N^* baryons, we performed a PWA of $\psi(3686)\to p\bar{p}\pi^0$[11] and found that the dominant contributions are from $7N^*$ intermediate resonances. Among these N^* resonances, two new resonances are significant, one $1/2^+$ resonance with a mass of $2300^{+40+109}_{-30-0}$ MeV/c^2 and width of $340^{+30+110}_{-30-58}$ MeV, and one $5/2^-$ resonance with a mass of 2570^{+19+34}_{-10-10} MeV/c^2 and width of 250^{+14+69}_{-24-21} MeV. For the remaining $5N^*$ intermediate resonances, the mass and width values from the PWA are consistent with those from established resonances.

Using a sample of 1.06×10^8 $\psi(3686)$ events collected at the BESIII detector, the processes of $\psi(3686)\to K^-\Lambda\bar{\Xi}^+$ and $\psi(3686)\to\gamma K^-\Lambda\bar{\Xi}^+$[12] are studied for the first time. In the decay $\psi(3686)\to K^-\Lambda\bar{\Xi}^+$, the branching fraction $\mathcal{B}(\psi(3686)\to K^-\Lambda\bar{\Xi}^+)$ is measured, and two structures, around 1 690 and 1 820 MeV/c^2, as indicated in Fig. 4, are observed in the $K^-\Lambda$ invariant mass spectrum with significances of 4.9σ and 6.2σ, respectively. The fitted resonance parameters are consistent with those of $\Xi^-(1690)$ and $\Xi^+(1820)$ in the PDG[13] within one standard deviation. The measured masses and widths are determined to be $M_{\Xi^-(1690)}=(1\,687.7\pm3.8\pm1.0)$ MeV/c^2, $\Gamma_{\Xi^-(1690)}=(27.1\pm10.0\pm2.7)$ MeV, $M_{\Xi^-(1820)}=(1\,826.7\pm5.5\pm1.6)$ MeV/c^2 and $\Gamma_{\Xi^-(1820)}=(54.4\pm15.7\pm4.2)$ MeV. This is the first time that $\Xi^-(1690)$ and $\Xi^-(1820)$ hyperons have been observed in charmonium decays. In the study of the decay $\psi(3686)\to\gamma K^-\Lambda\bar{\Xi}^+$, the branching fractions $\mathcal{B}(\psi(3686)\to K^-\Sigma^0\bar{\Xi}^+)$ and $\mathcal{B}(\chi_{cJ}\to K^-\Lambda\bar{\Xi}^+)$ are measured. The measurements provide new information on charmonium decays to hyperons and on the resonance parameters of the hyperons, and may help in the understanding of the charmonium decay mechanism.

3 Light meson decays

Based on a sample of 1.3 billion J/ψ events taken with the BESIII detector, we report the first

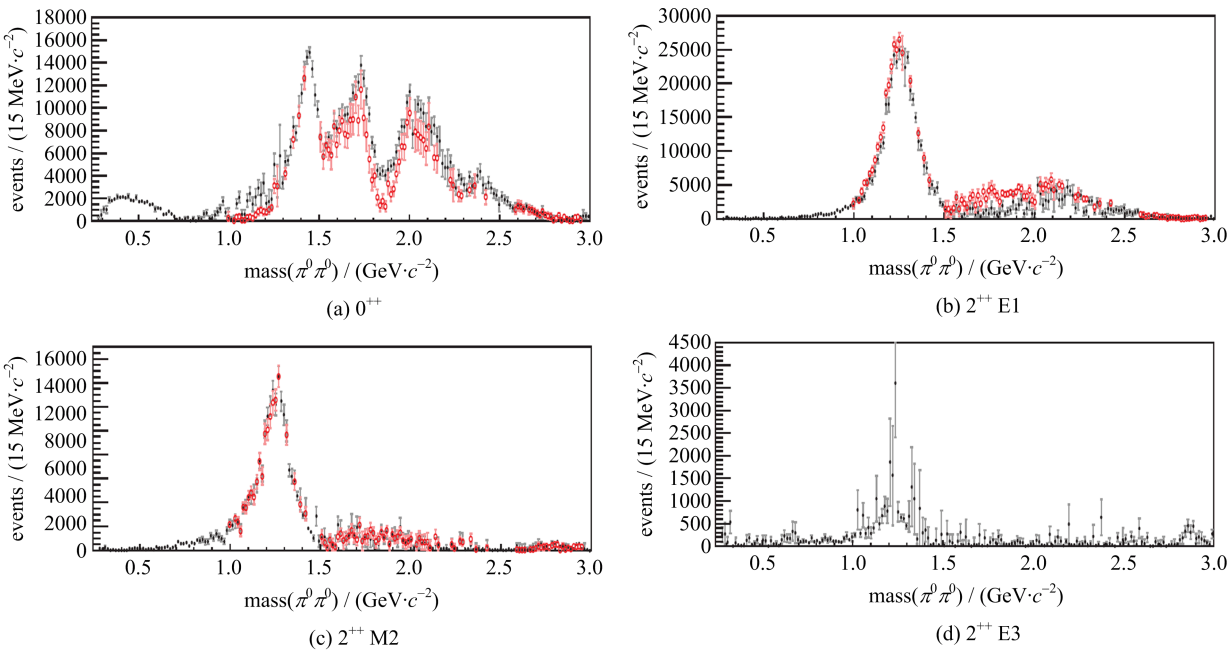

The solid black markers show the intensity calculated fromone set of solutions, while the open red markers represent its ambiguous partner.

Note that the intensity of the 2^{++} E3 amplitude is redundant for the two ambiguous solutions.

Fig. 2 The intensities for the (a) 0^{++}, (b) 2^{++} E1, (c) 2^{++} M2 and (d) 2^{++} E3 amplitudes as a function of $M_{\pi^0\pi^0}$ for the nominal results

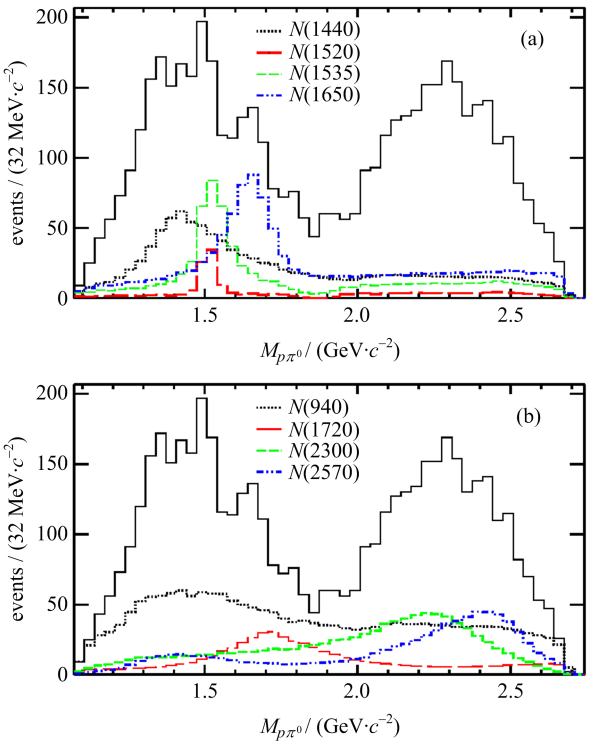

Fig. 3 The contribution of each intermediate resonance in the $p\pi^0$

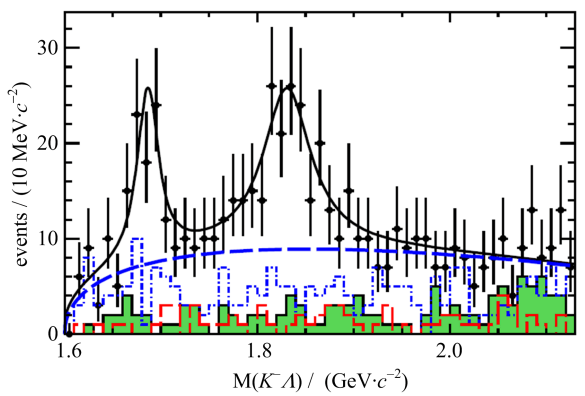

Fig. 4 The contribution of each intermediate resonance in the $p\pi^0$ mass spectra

observation of $\eta' \to \pi^+\pi^-\pi^{+(0)}\pi^{-(0)}$ decays via J/ψ radiative decays[14]. Fig. 5(a) and Fig. 5(b) show the $M_{\pi^+\pi^-\pi^+\pi^-}$ and $M_{\pi^+\pi^-\pi^0\pi^0}$, respectively, where the η' peaks are clearly observed and the dominant background events are from the other η' decays, but none of them contribute to the η' peak. The branching fractions are determined to be $\mathcal{B}(\eta' \to \pi^+\pi^-\pi^+\pi^-) = (8.63 \pm 0.69 \pm 0.64) \times 10^{-5}$ and $\mathcal{B}(\eta' \to \pi^+\pi^-\pi^0\pi^0) = (1.82 \pm 0.35 \pm 0.18) \times 10^{-4}$, which are consistent with the theoretical predictions based on the combination of chiral perturbation theory (ChPT) and vector-meson dominance[15], but could rule out the broken-$SU_6 \times O_3$ quark model.

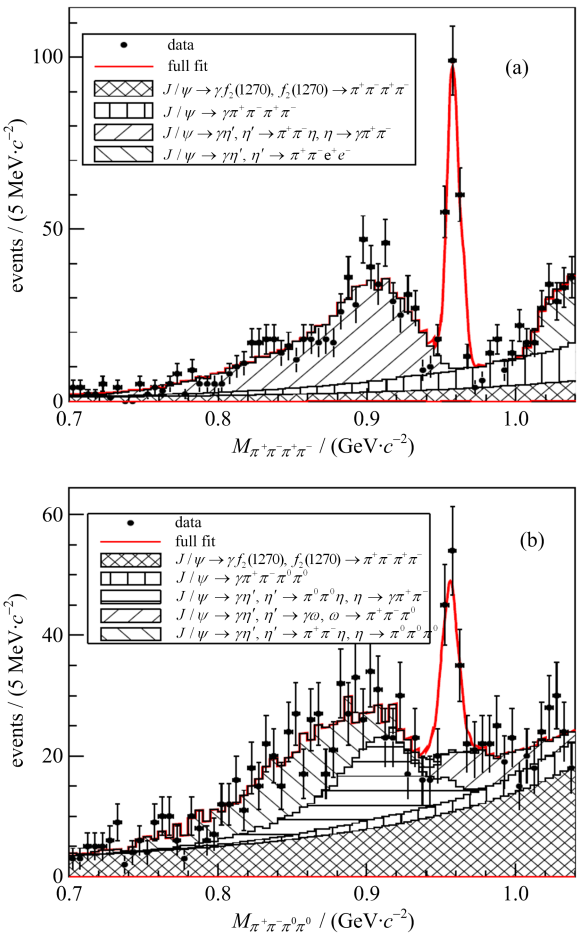

Fig. 5 The invariant mass distributions of (a) $\pi^+\pi^-\pi^+\pi^-$ and (b) $\pi^+\pi^-\pi^0\pi^0$ and the fit results

Recently considerable theoretical efforts to explain the discrepancy that the predicted decay width of $\eta \to \pi^+\pi^-\pi^0$ at the tree level of chiral perturbation theory (ChPT) is much lower than the experimental value of (300 ± 11) eV[13]. To distinguish between the different theoretical approaches, precise measurements of the matrix elements for $\eta \to \pi^+\pi^-\pi^0$ and the decay width are important. At BESIII, a clean sample of 79 625 $\eta \to \pi^+\pi^-\pi^0$[16] candidate events are selected and the background contamination is estimated to be about 0.1%. The distribution of X and Y, two of the Dalitz plot variables defined as $X = \frac{\sqrt{3}}{Q}(T_{\pi^+} - T_{\pi^-})$

and $Y=\frac{m_\eta+2m_\pi}{m_\pi}\frac{T_\eta}{Q}-1$, are shown in Fig. 6 (a) and (b). The Dalitz plot matrix elements for $\eta\to\pi^+\pi^-\pi^0$ are determined to be $a=-1.128\pm0.015\pm0.008$, $b=0.153\pm0.017\pm0.004$, $d=0.085\pm0.016\pm0.009$, $f=0.173\pm0.028\pm0.021$, where the first errors are statistical and the second ones systematic. The results are in reasonable agreement with previous measurements.

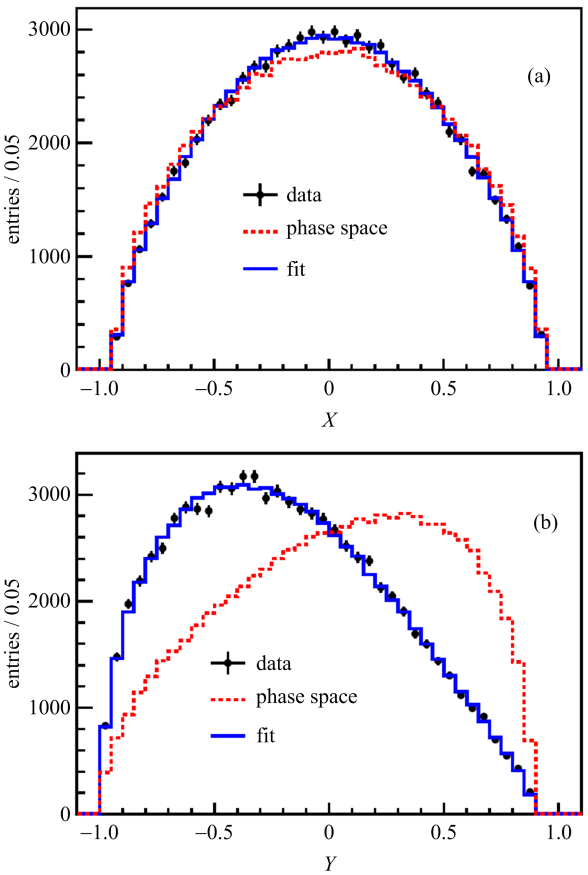

Fig. 6 Projections of the Dalitz plot (a) X and (b) Y for $\eta\to\pi^+\pi^-\pi^0$

For the decays of $\eta\to\pi^0\pi^0\pi^0$, the distribution of the variable Z is displayed in Fig. 7(b). Due to the kinematic boundaries, the interval of $0<Z<0.7$, corresponding to the region of phase space in which the Z distribution is flat, is used to extract the slope parameter from the data. Analogous to the measurement for $\eta\to\pi^+\pi^-\pi^0$, an unbinned maximum likelihood fit, as displayed in the inset of Fig. 7(a), yields the Dalitz plot slope parameter $\alpha=-0.055\pm0.014\pm0.004$, which is compatible with the recent results from other experiments and in agreement with the prediction from ChPT at NNLO within two standard deviations of the theoretical uncertainties.

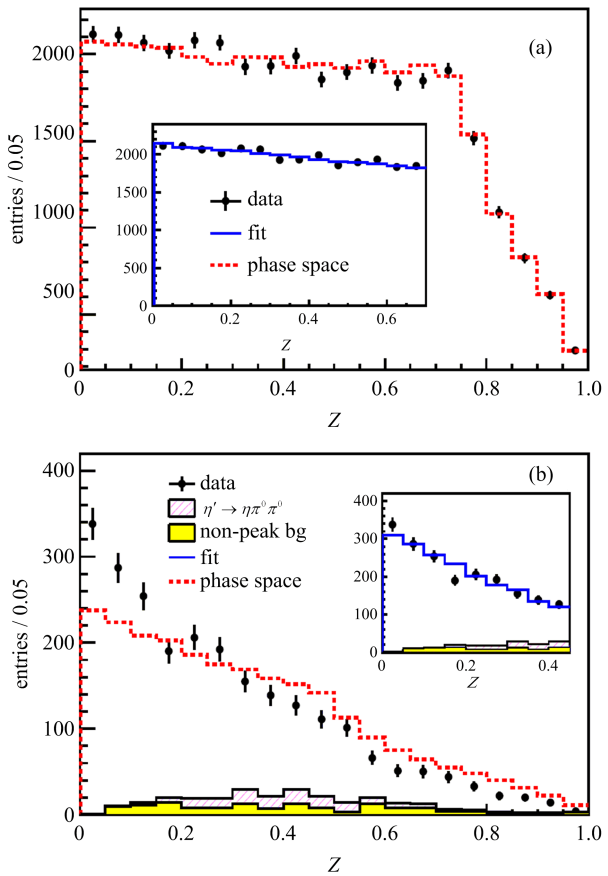

Fig. 7 Distribution of the kinematic variable Z for (a) $\eta\to\pi^0\pi^0\pi^0$ and (b) $\eta'\to\pi^0\pi^0\pi^0$

In the same analysis[16], we also presented the Dalitz plot analysis of $\eta'\to\pi^0\pi^0\pi^0$. The Dalitz plot slope parameter for $\eta'\to\pi^0\pi^0\pi^0$ is measured to be $\alpha=-0.640\pm0.046\pm0.047$, which is consistent with but more precise than previous measurements (Fig. 7(b)). The value deviates significantly from zero. This implies that final state interactions play an important role in the decay. Up to now, there are just a few predictions about the slope parameter of $\eta'\to\pi^0\pi^0\pi^0$. In Ref. [17], the slope parameter is predicted to be less than 0.03, which is excluded by our measurement. More recently, using a chiral unitary approach, an expansion of the decay amplitude up to the fifth and sixth order of X and Y has been used to parameterize the Dalitz plot of

$\eta' \to \pi^0\pi^0\pi^0$[18]. The coefficient, which corresponds to in this paper, is found to be in the range between -2.7 and 0.1, consistent with our measurement.

Theoretically the non-resonant part of coupling in $\eta' \to \gamma\pi^+\pi^-$ is accounted for by the higher term of Wess-Zumino-Witten (WZW) ChPT Lagrangian[4] (also known as the box anomaly). However the decay dynamics of $\eta' \to \gamma\pi^+\pi^-$ has been explored with very limited statistics only and new measurements are needed to clarify the scenario. In this work, a sample of 9 106 $\eta' \to \gamma\pi^+\pi^-$ events is selected to investigate its decay dynamics and the $\pi^+\pi^-$ mass spectrum is shown in Fig. 6 with a background level of 1%. The shape of the $M_{\pi^+\pi^-}$ spectrum is analyzed in parameterizations with the model-dependent and model-independent approaches respectively. For the model-dependent approach, the results show that only $\rho(770)$ resonance is insufficient to describe the data even considering $\rho(770)$, ω resonances and the interference between them. The fit performance get much better after including the box anomaly (Fig. 8(a)) with a statistical significance of larger than 37 s. We also try to replace the box anomaly with $\rho(1450)$ (Fig. 8(b)) by fixing its mass the width to be the world average values. The fit also can provide a reasonable description of data. Therefore, we conclude that in addition to $\rho(770)$ and ω, the box anomaly is necessary, but the contribution from $\rho(1450)$ could not be ruled out.

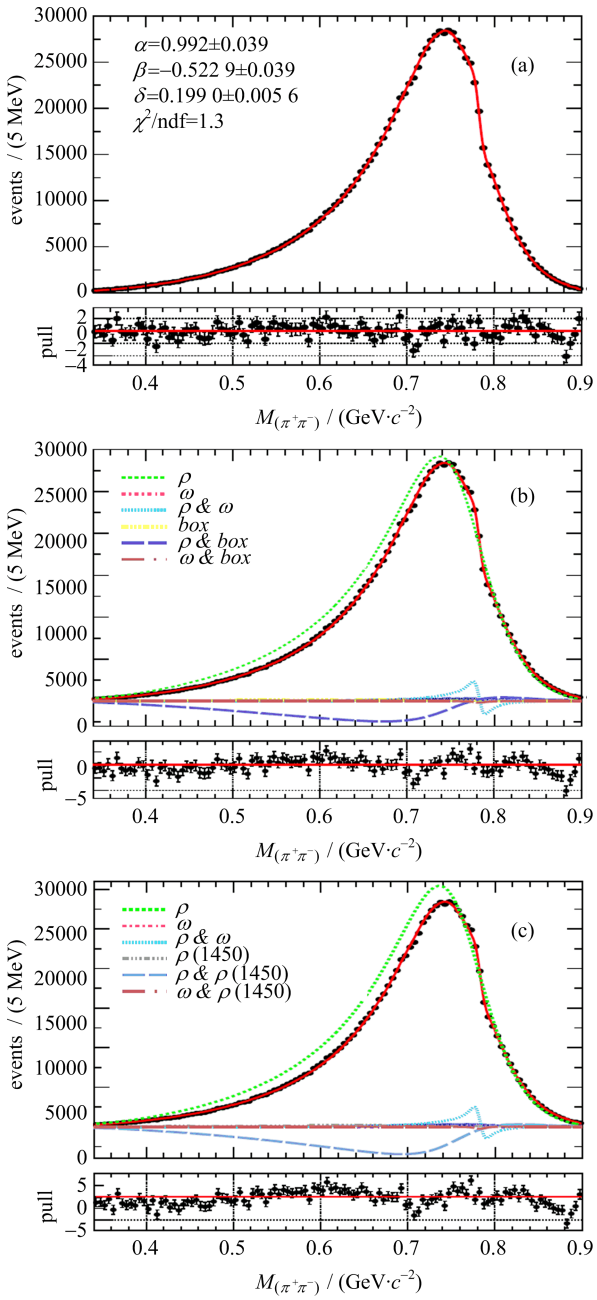

Fig. 8 The fit results for different cases: (a) $\rho(770)-\omega$, (b) $\rho(770)-\omega-box$ and (c) $\rho(770)-\omega-\rho(1450)$

4 Conclusion

Based on the data samples taken at the peak of J/ψ, $\psi(3686)$, the recent progress on the hadron spectroscopy is presented in this paper.

For the light hadron spectroscopy, besides the confirmation of $X(1835)$ in J/ψ radiative decays, the $X(1840)$, is observed in $J/\psi \to \gamma K_S^0 K_S^0 \eta$. Its spin-parity is determined to be $J^{PC} = 0^{-+}$, which implies that $X(1835)$ is a pseudoscalar resonance. The mass and with are consistent with the previous measurements. In addition, the PWA of $J/\psi \to \gamma\pi^0\pi^0$ is performed. For the baryon spectroscopy, two new excited N^* states, $N(2300)$ and $N(2570)$, were observed based on the the PWA of $\psi(3686) \to p\bar{p}\pi^0$. In addition, significant progress on η/η' decays was achieved, including observation of $\eta' \to \pi^+\pi^-\pi^{+(0)}\pi^{-(0)}$, Dalitz plot of $\eta \to \pi^+\pi^-\pi^0$, $\eta/\eta' \to 3\pi^0$, and $\eta' \to \gamma\pi^+\pi^-$.

The interesting results not only underline the

importance of the study of hadron spectroscopy, but also demonstrate the effectiveness of a programmatic approach to studying hadron spectroscopy at BESIII. With the high statistical data accumulated at the BESIII detector, more interesting results are expected to arrive soon.

References

[1] Ablikim M, Bai J Z, Ban Y, et al. Observation of a resonance $X(1835)$ in $J/\psi\to\gamma\pi^+\pi^-\eta'$[J]. Phys Rev Lett,2005, 95: 262001.

[2] ABLIKIM M, ACHASOV M N, AN L, et al. Confirmation of the $X(1835)$ and observation of the resonances $X(2120)$ and $X(2370)$ in $J/\psi\to\gamma\pi^+\pi^-\eta'$ [J]. Phys Rev Lett,2011, 106: 072002 .

[3] ABLIKIM M, ACHASOV M N, AI X C, et al. Observation and spin-parity determination of the $X(1835)$ in $J/\psi\to\gamma K^0_S K^0_S\eta$ [J]. Phys Rev Lett, 2015, 115: 091803.

[4] ABLIKIM M, ACHASOV M N, ALBERTO D, et al. Spin-parity analysis of $p\bar{p}$ mass threshold structure in J/ψ and $\psi(3686)$ radiative decays[J]. Phys Rev Lett, 2012, 108:112003.

[5] ABLIKIM M , ACHASOV M N, ALBERTO D, et al. $\eta\pi^+\pi^-$ Resonant Structure around 1.8 GeV/c^2 and $\eta(1405)$ in $J/\psi\to\omega\eta\pi^+\pi^-$ [J]. Phys Rev Lett, 2011, 107: 182001.

[6] ABLIKIM M, ACHASOV M N, ALBAYRAK O, et al. Observation of a structure at 1.84 GeV/c^2 in the 3$(\pi^+\pi^-)$ mass spectrum in $J/\psi\to\gamma3(\pi^+\pi^-)$ decays[J]. Phys Rev D,2013, 88: 091502.

[7] ABLIKIM M, ACHASOV M N, ALBAYRAK O, et al. Study of the near-threshold $\omega\phi$ mass enhancement in doubly OZI-suppressed $J/\psi\to\gamma\omega\phi$ decays[J]. Phys Rev D,2013, 87:032008 .

[8] ABLIKIM M, BAI J Z, BAN Y, et al. Observation of a near-threshold enhancement in the $\omega\phi$ mass spectrum from the doubly OZI-suppressed decay $J/\psi\to\gamma\omega\phi$ [J]. Phys Rev Lett, 2006,96: 162002.

[9] ABLIKIM M, ACHASOV M N, AI X C, et al. Amplitude analysis of the $\pi^0\pi^0$ system produced in radiative J/ψ decays [J]. Phys Rev D, 2015, 92:052003.

[10] Gui L C , Chen Y, Li G, et al. Scalar glueball in radiative J/ψ decay on the lattice[J]. Phys Rev Lett, 2013,110: 021601 .

[11] ABLIKIM M, ACHASOV M N, AMBROSE D J, et al. Observation of two new N^* resonances in the decay $\psi(3686)\to p\bar{p}\pi^0$ [J]. Phys Rev Lett, 2013, 110:022001.

[12] ABLIKIM M, ACHASOV M N, AI X C, et al. Measurements of $\psi(3686)\to K^-\Lambda\bar{\Xi}^+ +$ c. c. and $\psi(3686)\to\gamma K^-\Lambda\bar{\Xi}^+ +$ c. c. [J]. Phys Rev D, 2015, 91: 092006.

[13] OLIVE K A, AGASHE K, AMSLER C, et al. Review of particle physics [J]. Chin Phys C, 2014, 38(09): 090001.

[14] ABLIKIM M, ACHASOV M N, AI X C, et al. Observation of $\eta'\to\pi^+\pi^-\pi^+\pi^-$ and $\eta'\to\pi^+\pi^-\pi^0\pi^0$ [J]. Phys Rev Lett,2014, 112: 251801 .

[15] GUO F K, KUBIS B, WIRZBA A. Anomalous decays of η' and η into four pions[J]. Phys Rev D, 2012, 85: 014014.

[16] ABLIKIM M, ACHASOV M N, AI X C, et al. Measurement of the matrix elements for the decays $\eta\to\pi^+\pi^-\pi^0$ and $\eta/\eta'\to\pi^0\pi^0\pi^0$ [J]. Phys Rev D, 2015, 92: 012014.

[17] ROIESNEL C, TRUONG TN. $\eta,\eta'\to3\pi$ decays[J]. Paris Ec Polytech A, 1982,515:0982.

[18] BORASOY B, NISSLER R. Hadronic η and η' decays [J]. Eur Phys J A, 2005,26: 383-398.

Article ID:0253-2778(2016)07-0574-06

Towards the nature of $X(3872)$ resonance

ACHASOV N. N.[1], ROGOZINA E. V.[2]

(1. *Laboratory of Theoretical Physics, Sobolev Institute for Mathematics, Novosibirsk* 630090, *Russian*;
2. *Novosibirsk State University, Novosibirsk* 630090, *Russian*)

Abstract: The spectra of decays of resonance $X(3872)$ with good analytical and unitary properties are constructed, which allows to define the branching ratio of the $X(3872)\to D^{*0}\overline{D}^0+c.c.$ decay by studying only one more decay, for example, the $X(3872)\to\pi^+\pi^- J/\psi(1S)$ decay, and it is shown that the spectra are an effective means of selection of models for the resonance $X(3872)$. Then the scenario is discussed where the $X(3872)$ resonance is the $c\bar{c}=\chi_{c1}(2P)$ charmonium which "sits on" the $D^{*0}\overline{D}^0$ threshold. An explanation is given of the shift of the mass of the $X(3872)$ resonance with respect to the prediction of a potential model for the mass of the $\chi_{c1}(2P)$ charmonium by the contribution of the virtual $D^*\overline{D}+c.c.$ intermediate states into the self energy of the $X(3872)$ resonance. This allows us to estimate the coupling constant of the $X(3872)$ resonance with the $D^{*0}\overline{D}^0$ channel, the branching ratio of the $X(3872)\to D^{*0}\overline{D}^0+c.c.$ decay, and the branching ratio of the $X(3872)$ decay into all non-$D^{*0}\overline{D}^0+c.c.$ states. A significant number of unknown decays of $X(3872)$ via two gluons: $X(3872)\to gluon\ gluon\to hadrons$ are predicted.

Key words: Charmonium; molecule; two-gluon decays

CLC number: O572.3 **Document code**: A doi:10.3969/j.issn.0253-2778.2016.07.006

Citation: ACHASOV N N, ROGOZINA E V. Towards the nature of $X(3872)$ resonance[J]. Journal of University of Science and Technology of China, 2016,46(7):574-579.

走近 $X(3872)$ 共振态的本质

ACHASOV N. N.[1], ROGOZINA E. V.[2]

(1. 索博列夫数学学院理论物理实验室,新西伯利亚 630090,俄罗斯;
2. 新西伯利亚州立大学,新西伯利亚 630090,俄罗斯)

摘要:构造了具有良好解析性和幺正性的共振态 $X(3872)$ 衰变谱,能够定义衰变反应 $X(3872)\to D^{*0}\overline{D}^0+c.c.$ 的分支比,而只需要多研究另外一个衰变,比如说 $X(3872)\to\pi^+\pi^- J/\psi(1S)$ 衰变,这表明构造谱是筛选共振态 $X(3872)$ 模型的有效工具.之后讨论了共振态 $X(3872)$ 是粲偶素 $c\bar{c}=\chi_{c1}(2P)$ 的情形,此时它处在 $D^{*0}\overline{D}^0$ 的阈上.根据由粲偶素 $\chi_{c1}(2P)$ 的质量的势能模型的预言解释了共振态 $X(3872)$ 的质量偏移.这个势能模型是依据衰变产物 $D^*\overline{D}+c.c.$ 的中间态计入共振态 $X(3872)$ 的质量的贡献而构造的.这使得我们能够研究共

Received: 2015-11-30; **Revised**: 2016-04-20

Foundation item: Supported by Russian Fundation for Basic Research(13-02-00039), Interdisciplinary Project of Siberian Division of RAS (102).

Biography: ACHASOV N. N. (corresponding author), male, born in 1941, Prof. Research field: high energy physics. E-mail: achasov@math.nsc.ru

振态 $X(3872)$和衰变道$D^{*0}\overline{D}^0$的耦合常数，$X(3872)\to D^{*0}\overline{D}^0+c.c.$的衰变分支比以及共振态 $X(3872)$衰变到所有不含$D^{*0}\overline{D}^0+c.c.$的过程的分支比. 预言了一个共振态 $X(3872)$通过双胶子衰变的重要常数.

关键词：粲偶素；分子；双胶子衰变

0 Introduction

The $X(3872)$ resonance became the first in discovery of the resonant structures XYZ ($X(3872)$, $Y(4260)$, $Z_b^+(10610)$, $Z_b^+(10650)$, $Z_c^+(3900)$), the interpretations of which as hadron states assumes existence in them at least pair of heavy and pair of light quarks in this or that form.

Thousands of articles on this subject have been published in spite of the fact that many properties of new resonant structures are not defined yet and not all possible mechanisms of dynamic generation of these structures are studied, in particular, the role of the anomalous Landau thresholds is not yet studied. Consequently, this spectroscopy took the central place in the physics of hadrons.

Below we give reasons that $X(3872)$, $I^G(J^{PC})=0^+(1^{++})$, is the $\chi_{c1}(2P)$ charmonium and suggest a physically clear program of experimental researches for the verification of our assumption.

1 How to learn the branching ratio $X(3872)\to D^{*0}\overline{D}^0+c.c.$ [1]

The mass spectrum $\pi^+\pi^- J/\psi(1S)$ looks like the ideal Breit-Wigner one in the $X(3872)\to\pi^+\pi^- J/\psi(1S)$ decay, see Fig. 1(a).

The mass spectrum $\pi^+\pi^-\pi^0 J/\psi(1S)$ in the $X(3872)\to\pi^+\pi^-\pi^0 J/\psi(1S)$ decay looks similar[3-4]. The mass spectrum $D^{*0}\overline{D}^0+c.c.$ in the $X(3872)\to D^{*0}\overline{D}^0+c.c.$ decay[5] looks like the typical resonance threshold enhancement, see Fig. 2.

If structures in the above channels are a manifestation of the same resonance, it is possible to define the branching ratio $BR(X(3872)\to D^{*0}\overline{D}^0+c.c.)$ treating data of the two above decay channels only.

We believe that the $X(3872)$ is the axial vector, 1^{++}[6-7]. In this case the S wave dominates in the $X(3872)\to D^{*0}\overline{D}^0+c.c.$ decay and hence is described by the effective Lagrangian

$$L_{XD^{*0}D^0}(x)=g_A X^\mu(D^0_\mu(x)\,\overline{D}^0(x)+\overline{D}^0_\mu(x)D^0(x)) \tag{1}$$

The width of the $X\to D^{*0}\overline{D}^0+c.c.$ decay

$$\Gamma(X\to D^{*0}\,\overline{D}^0+c.c.,m)=\frac{g_A^2}{8\pi}\frac{\rho(m)}{m}\left(1+\frac{\boldsymbol{k}^2}{3m^2_{D^{*0}}}\right) \tag{2}$$

where $\boldsymbol{k}$ is the momenta of D^{*0}(or $\overline{D}^0$) in the $D^{*0}\overline{D}^0$ center mass system, and m is the invariant mass of the $D^{*0}\overline{D}^0$ pair,

$$\rho(m)=\frac{2\,|\,\boldsymbol{k}\,|}{m}=\frac{\sqrt{(m^2-m_+^2)(m^2-m_-^2)}}{m^2},$$

$$m_\pm=m_{D^{*0}}\pm m_{D^0}.$$

The second term in the right side of Eq. (2) is very small in our energy region and can be

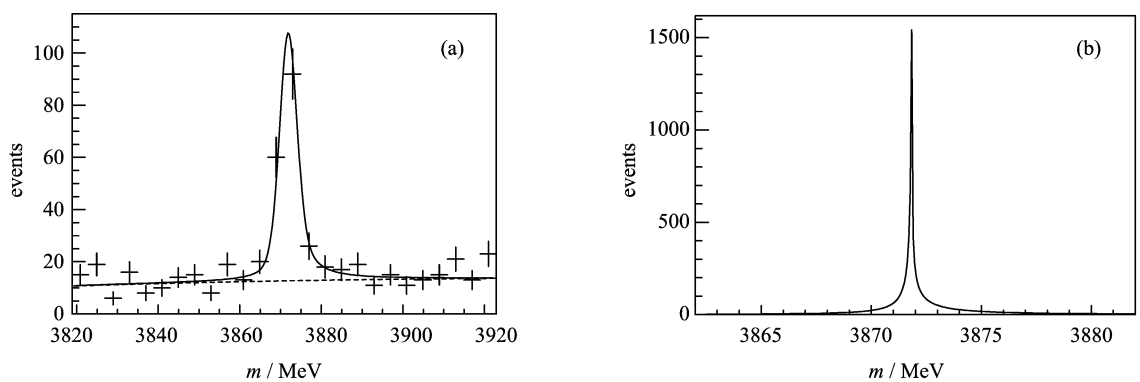

The solid line is our theoretical one taking into account the Belle energy resolution.

The dotted line is the second-order polynomial for the incoherent background.

Fig. 1　The Belle data[2] on the invariant $\pi^+\pi^- J/\psi(1S)$ mass (m) distribution (a) and our undressed theoretical line (b)

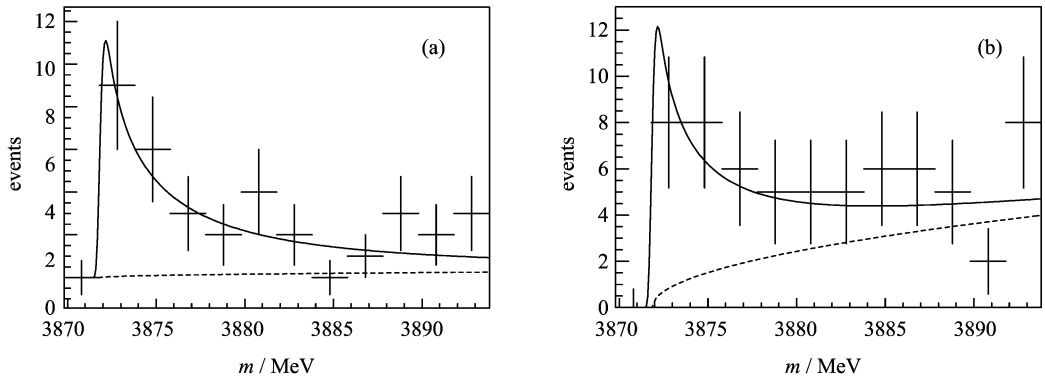

(a) $D^{*0}\to D^0\pi^0$ (b) $D^{*0}\to D^0\gamma$

The solid line represents our theoretical prediction taking into account the Belle energy resolution.

The dotted line is a square root function for the incoherent background.

Fig. 2 The Belle data[5] on the invariant $D^{*0}\overline{D}^0+c.c.$ mass (m) distribution

neglected. This gives us an opportunity to construct the mass spectra for the $X(3872)$ decays with the good analytical and unitary properties as in the scalar meson case[8-9].

The mass spectrum in the $D^{*0}\overline{D}^0+c.c.$ channel

$$\frac{\mathrm{d}BR(X\to D^{*0}\overline{D}^0+c.c.,m)}{dm}=4\frac{1}{\pi}\frac{m^2\Gamma(X\to D^{*0}\overline{D}^0,m)}{|D_X(m)|^2} \tag{3}$$

The branching ratio of $X(3872)\to D^{*0}\overline{D}^0+c.c.$

$$BR(X\to D^{*0}\overline{D}^0+c.c.)=4\frac{1}{\pi}\int_{m_+}^{\infty}\frac{m^2\Gamma(X\to D^{*0}\overline{D}^0,m)}{|D_X(m)|^2}\mathrm{d}m \tag{4}$$

In other $\{i\}$ (non-$D^{*0}\overline{D}^0$) channels the $X(3872)$ state is seen as a narrow resonance, which is why we write the mass spectrum in the i channel in the form

$$\frac{\mathrm{d}BR(X\to i,m)}{\mathrm{d}m}=2\frac{1}{\pi}\frac{m_X^2\Gamma_i}{|D_X(m)|^2} \tag{5}$$

where Γ_i is the width of the $X(3872)\to i$ decay.

The branching ratio of $X(3872)\to i$

$$BR(X\to i)=2\frac{1}{\pi}\int_{m_0}^{\infty}\frac{m_X^2\Gamma_i}{|D_X(m)|^2}\mathrm{d}m \tag{6}$$

where m_0 is the threshold of the i channel.

The inverse propagator $D_X(m)$

$$D_X(m)=m_X^2-m^2+Re(\Pi_X(m_X^2))-\Pi_X(m^2)-\imath m_X\Gamma \tag{7}$$

where $\Gamma=\Sigma\Gamma_i<1.2$ MeV is the total width of the $X(3872)$ decay into all non-($D^{*0}\overline{D}^0+c.c.$) channels.

$$\Pi_X(s)=\frac{g_A^2}{8\pi^2}(I^{D^{*0}\overline{D}^0}(s)+I^{D^{*+}D^-}(s)),\ m^2=s \tag{8}$$

When $m_+=m_{D^*}+m_D\leqslant m$,

$$I^{D^*\overline{D}}(m^2)=\frac{(m^2-m_+^2)}{m^2}\frac{m_-}{m_+}\ln\frac{m_{D^*}}{m_D}+\rho(m)\left[\imath\pi+\ln\frac{\sqrt{m^2-m_-^2}-\sqrt{m^2-m_+^2}}{\sqrt{m^2-m_-^2}+\sqrt{m^2-m_+^2}}\right] \tag{9}$$

where $m_-=m_{D^*}-m_D$.

When $m_-\leqslant m\leqslant m_+$,

$$I^{D^*\overline{D}}(m)=\frac{(m^2-m_+^2)}{m^2}\frac{m_-}{m_+}\ln\frac{m_{D^*}}{m_D}-2|\rho(m)|\arctan\frac{\sqrt{m^2-m_-^2}}{\sqrt{m_+^2-m^2}} \tag{10}$$

where $|\rho(m)|=\sqrt{(m_+^2-m^2)(m^2-m_-^2)}/m^2$.

When $m\leqslant m_-$ and $m^2\leqslant 0$,

$$I^{D^*\overline{D}}(m)=\frac{(m^2-m_+^2)}{m^2}\frac{m_-}{m_+}\ln\frac{m_{D^*}}{m_D}-\rho(m)\ln\frac{\sqrt{m_+^2-m^2}-\sqrt{m_-^2-m^2}}{\sqrt{m_+^2-m^2}+\sqrt{m_-^2-m^2}} \tag{11}$$

Our branching ratios satisfy the unitarity

$$1=BR(X\to D^{*0}\overline{D}^0+c.c.)+BR(X\to D^{*+}\overline{D}^-+c.c.)+\sum_i BR(X\to i) \tag{12}$$

Fitting the Belle data[2], we take into account the Belle results[2]: $m_X=3\,871.84$ MeV$=m_{D^{*0}}+m_{D^0}=m_+$ and $\Gamma_{X(3872)}<1.2$ MeV 90% CL, that corresponds to $\Gamma<1.2$ MeV, which controls the

width of the $X(3872)$ signal in the $\pi^+\pi^- J/\psi(1S)$ channel and in every non-$(D^{*0}\overline{D}^0+c.c.)$ channel. The results of our fit are in the Tab. 1.

Tab. 1 BR_{seen} **is a branching ratio for** $m \leqslant 3\,891.84$ **MeV,** Γ **in MeV,** g_A **in GeV**

Γ	$1.2_{-0.4}$	mode	$D^{*0}\overline{D}^0+c.c.$	$D^{*+}D^-+c.c.$	Others
$g_A^2/8\pi$	1.4^{+5}_{-1}	BR	$0.6^{+0.02}_{-0.1}$	$0.31^{+0.13}_{-0.16}$	$0.1^{+0.3}_{-0.1}$
χ^2/Ndf	45/42	BR_{seen}	$0.3^{+0.1}_{-0.2}$	$0.03^{+0.004}_{-0.02}$	$0.09^{+0.3}_{-0.1}$

Our approach can serve as a guide to the selection of theoretical models for the $X(3872)$ resonance. Indeed, if $3\,871.68\ \text{MeV} < M_X < 3\,871.95$ MeV and $\Gamma_{X(3872)} = \Gamma < 1.2$ MeV then for $g_A^2/4\pi < 0.2\ \text{GeV}^2$ $BR(X \to D^{*0}\overline{D}^0 + c.c.;\ m \leqslant 3\,891.84\ \text{MeV}) < 0.3$. That is, unknown decays of $X(3872)$ into non-$D^{*0}\overline{D}^0$ states are considerable or dominant.

For example, in Ref. [10] the authors considered $m_X = 3\,871.68$ MeV, $\Gamma = 1.2$ MeV and $g_{XDD^*} = g_A\sqrt{2} = 2.5$ GeV, that is, $g_A^2/8\pi = 0.1\ \text{GeV}^2$. In this case $BR(X \to D^{*0}\overline{D}^0 + c.c.) \approx 0.2$, that is, unknown decays $X(3872)$ into non-$(D^{*0}\overline{D}^0+c.c.)$ states are dominant. For details see Tab. 2.

Tab. 2 Branching ratios for the model from Ref. [10]

m_X	3 871.68	mode	$X \to D^{*0}\overline{D}^0+c.c.$	$X \to D^{*+}D^-+c.c.$	$X \to$ Others
Γ	1.2	BR	0.176	0.045	0.779
$g_A^2/8\pi$	0.1	BR_{seen}	0.14	0.011	0.761

【Note】 Γ in MeV, m_X in MeV, g_A in GeV

2 $X(3872)$, $I^G(J^{PC}) = 0^+(1^{++})$, as the $\chi_{c1}(2P)$ charmonium[11]

Contrary to the almost standard opinion that the $X(3872)$ resonance is the $D^{*0}\overline{D}^0 + c.c.$ molecule or the $qc\bar{q}\bar{c}$ four-quark state, we discuss the scenario where the $X(3872)$ resonance is the $c\bar{c} = \chi_{c1}(2P)$ charmonium which "sits on" the $D^{*0}\overline{D}^0$ threshold.

The two dramatic discoveries have generated a stream of the $D^{*0}\overline{D}^0 + D^0\overline{D}^{*0}$ molecular interpretations of the $X(3872)$ resonance.

The mass of the $X(3872)$ resonance is 50 MeV lower than predictions of the most lucky naive potential models for the mass of the $\chi_{c1}(2P)$ resonance,

$$m_X - m_{\chi_{c1}(2P)} = -\Delta \approx -50\ \text{MeV} \tag{13}$$

and the relation between the branching ratios

$$BR(X \to \pi^+\pi^-\pi^0 J/\psi(1S)) \approx BR(X \to \pi^+\pi^- J/\psi(1S)) \tag{14}$$

that is interpreted as a strong violation of isotopic symmetry.

But the bounding energy is small, $\epsilon_B < (1\sim3)$ MeV. That is, the radius of the molecule is large, $r_{X(3872)} > (3\sim5)\ \text{fm} = (3\sim5)\times10^{-13}$ cm. As for the charmonium, its radius is less one fermi, $r_{\chi_{c1}(2P)} \approx 0.5\ \text{fm} = 0.5\times10^{-13}$ cm. That is, the molecule volume is 100～1 000 times as large as the charmonium volume, $V_{X(3872)}/V_{\chi_{c1}(2P)} > 100\sim1\,000$.

How to explain sufficiently abundant inclusive production of the rather extended molecule X (3872) in a hard process $pp \to X(3872) + anything$ with rapidity in the range 2.5～4.5 and transverse momentum in the range 5～20 GeV[12]? Actually,

$$\sigma(pp \to X(3872) + anything) \cdot BR(X(3872) \to \pi^+\pi^- J/\psi) = 5.4\ \text{nb}$$

and

$$\sigma(pp \to \psi(2S) + anything) \cdot BR(\psi(2S) \to \pi^+\pi^- J/\psi) = 38\ \text{nb} \tag{16}$$

But, according to Ref. [7]

$$BR(\psi(2S) \to \pi^+\pi^- J/\psi) = 0.34 \tag{17}$$

while

$$0.023 < BR(X(3872) \to \pi^+\pi^- J/\psi) < 0.066 \tag{18}$$

according to Ref. [13].

So,

$$0.74 < \frac{\sigma(pp \to X(3872) + anything)}{\sigma(pp \to \psi(2S) + anything)} < 2.1 \tag{19}$$

The extended molecule is produced in the hard process as intensively as the compact charmonium. It's a miracle.

As for the problem of the mass shift, Eq. (13), the contribution of the D^-D^{*+} and $\overline{D}^0D^{*0}$ loops, see Fig. 3, into the self energy of the $X(3872)$ resonance, $\Pi_X(s)$, solves it easily.

Let us calculate $I^{D^*\overline{D}}(s)$ in Eq. (8) with the

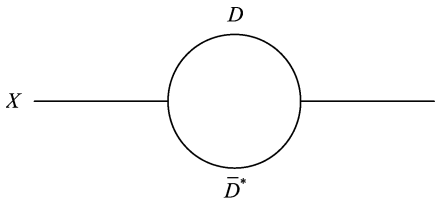

Fig. 3 The contribution of the $\bar{D}^0 D^{*0}$ and $D^- D^{*+}$ loops into the self energy of the $X(3872)$ resonance

help of a cut-off Λ.

$$I^{D^*\bar{D}}(s) = \int_{m_+^2}^{\Lambda^2} \frac{\sqrt{(s'-m_+^2)(s'-m_-^2)}}{s'(s'-s)} \mathrm{d}s' \approx$$

$$2\ln\frac{2\Lambda}{m_+} - 2\sqrt{\frac{m_+^2-s}{s}}\arctan\sqrt{\frac{s}{m_+^2-s}} \qquad (20)$$

where $s<m_+^2$, $\Lambda^2 \gg m_+^2$.

The inverse propagator of the $X(3872)$ resonance

$$D_X(s) = m_{\chi_{c1}(2P)}^2 - s - \Pi_X(s) - \imath m_X \Gamma \qquad (21)$$

The renormalization of mass

$$m_{\chi_{c1}(2P)}^2 - m_X^2 - \Pi_X(m_X^2) = 0 \qquad (22)$$

results in

$$\Delta(2m_X + \Delta) = \Pi_X(m_X^2) \approx (g_A^2/8\pi^2)4\ln(2\Lambda/m_+) \qquad (23)$$

If $\Delta = m_{\chi_{c1}(2P)} - m_X \approx 50$ MeV, then $g_A^2/8\pi \approx 0.2$ GeV^2 for $\Lambda = 10$ GeV and $BR(X \to D^0 \bar{D}^{*0} + \bar{D}^0 D^{*0}) \approx 0.3$[①].

Thus, we expect that a number of unknown mainly two-gluon decays of $X(3872)$ into non-$D^{*0}\bar{D}^0 + c.c.$ states are considerable[②]. The discovery of these decays would be a strong (if not decisive) confirmation of our scenario.

As for $BR(X \to \omega J/\psi) \approx BR(X \to \rho J/\psi)$, Eq. (14), this could be a result of dynamics. In our scenario the $\omega J/\psi$ state is produced via the three gluons, see Fig. 4.

As for the $\rho J/\psi$ state, it is produced both via the one photon, see Fig. 5, and via the three gluons (via the contribution $\approx m_u - m_d$), see Fig. 4.

Close to our scenario is an example of the $J/\psi \to \rho\eta'$ and $J/\psi \to \omega\eta'$ decays. According to Ref. [7]

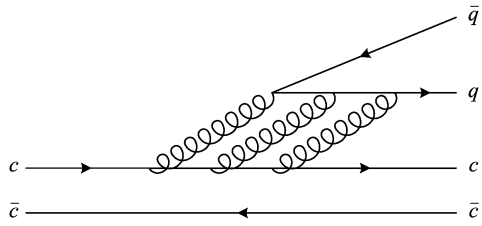

All possible permutations of gluons are assumed.

Fig. 4 The three-gluon production of the ω and ρ mesons (the ρ meson via the contribution $\approx m_u - m_d$)

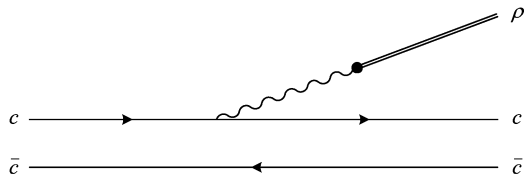

All possible permutations of photon are assumed.

Fig. 5 The one-photon production of the ρ meson

$$BR(J/\psi \to \rho\eta') = (1.05 \pm 0.18) \times 10^{-4}$$

and

$$BR(J/\psi \to \omega\eta') = (1.82 \pm 0.21) \times 10^{-4} \qquad (24)$$

Note that in the $X(3872)$ case the ω meson is produced on its tail ($m_X - m_{J/\psi} = 775$ MeV), while the ρ meson is produced on a half.

It is well known that the physics of charmonium ($\bar{c}c$) and bottomonium ($\bar{b}b$) is similar. Let us compare the already known features of $X(3872)$ with the ones of $\Upsilon_{b1}(2P)$.

Recently, the LHCb Collaboration published a landmark result[14]

$$\frac{BR(X \to \gamma\psi(2S))}{BR(X \to \gamma J/\psi)} = C_X\left(\frac{\omega_{\psi(2S)}}{\omega_{J/\psi}}\right)^3 = 2.46 \pm 0.7 \qquad (25)$$

where $\omega_{\psi(2S)}$ and $\omega_{J/\psi}$ are the energies of the photons in the $X \to \gamma\psi(2S)$ and $BR(X \to \gamma J/\psi)$ decays, respectively.

On the other hand, it is known[7] that

$$\frac{BR(\chi_{b1}(2P) \to \gamma\Upsilon(2S))}{BR(\chi_{b1}(2P) \to \gamma\Upsilon(1S))} = C_{\chi_{b1}(2P)}\left(\frac{\omega_{\Upsilon(2S)}}{\omega_{\Upsilon(1S)}}\right)^3 = 2.16 \pm 0.28 \qquad (26)$$

① The assumption of the determining role of the $D^*\bar{D} + c.c.$ channels in the shift of the mass of the $\chi_{c1}(2P)$ meson is based on the following reasoning. Let us imagine that D and D^* mesons are light, for example, like the K and K^* mesons. Then the width of $X(3872)$ meson is equal 50 MeV for $g_A^2/8\pi = 0.2$ GeV^2, which is much more than the width of its decay into all non-($D^{*0}\bar{D}^0 + $c.c.) channels, $\Gamma < 1.2$ MeV. That is, to our case the coupling of the $X(3872)$ meson with the $D^*\bar{D} + c.c.$ channels is rather strong.

② Note that in the $\chi_{c1}(1P)$ case the width of the two-gluon decays equals 0.56 MeV[7], which agrees with $\Gamma < 1.2$ MeV satisfactory.

where $\omega_{\Upsilon(2S)}$ and $\omega_{\Upsilon(1S)}$ are the energies of the photons in the $\chi_{b1}(2P)\to\gamma\Upsilon(2S)$ and $\chi_{b1}(2P)\to\gamma\Upsilon(1S)$ decays, respectively.

Consequently,

$$C_X = 136.78 \pm 38.89 \tag{27}$$

and

$$C_{\chi_{b1}(2P)} = 80.00 \pm 10.37 \tag{28}$$

as all most lucky versions of the potential model predicted for the quarkonia $C_{\chi_{c1}(2P)} \gg 1$ and $C_{\chi_{b1}(2P)} \gg 1$.

According to Ref. [7]

$$BR(\chi_{b1}(2P) \to \omega\Upsilon(1S)) = (1.63 \pm^{0.4}_{0.34})\% \tag{29}$$

If the one-photon mechanism dominates in the $X(3872)\to\rho J/\psi$ decay, see Fig. 5, then one should expect

$$BR(\chi_{b1}(2P) \to \rho\Upsilon(1S)) \approx (e_b/e_c)^2 \times 1.6\% = (1/4) \times 1.6\% = 0.4\% \tag{30}$$

where e_c and e_b are the charges of the c and b quarks, respectively.

If the three-gluon mechanism (its part $\approx m_u - m_d$) dominates in the $X(3872)\to\rho J/\psi$ decay, see Fig. 4, then one should expect

$$BR(\chi_{b1}(2P) \to \rho\Upsilon(1S)) \approx 1.6\% \tag{31}$$

3 Conclusion

We believe that the discovery of a significant number of unknown decays of the $X(3872)$ into non-$D^{*0}\overline{D}^0 + c.\,c.$ states via two gluons and discovery of the $\chi_{b1}(2P)\to\rho\Upsilon(1S)$ decay could decide the destiny of X(3872).

Once more, we discuss the scenario where the $\chi_{c1}(2P)$ charmonium sits on the $D^{*0}\overline{D}^0$ threshold but not a mixing of the giant $D^*\overline{D}$ molecule and the compact $\chi_{c1}(2P)$ charmonium, see, for example, Refs. [15-16] and references cited therein. Note that the mixing of such states requests special justification. That is, it is necessary to show that the transition of the giant molecule into the compact charmonium is considerable at insignificant overlapping of their wave functions. Such a transition $\approx\sqrt{V_{\chi_{c1}(2P)}/V_{X(3872)}}$ and a branching ratio of a decay via such a transition $\approx V_{\chi_{c1}(2P)}/V_{X(3872)}$.

References

[1] ACHASOV NN, ROGOZINA E V. How learn the branching ratio $X(3872)\to D^{*0}\overline{D}^0 + c.\,c.$ [J]. JETP Lett, 2014, 100: 227-231.

[2] CHOI S K, OLSEN S L, TRABELSI K, et al. Bounds on the width, mass difference and other properties of $X(3872)\to\pi^+\pi^- J/\psi$ decays[J]. Phys Rev D, 2011, 84: 052004.

[3] ABE K, ADACHI I, AIHARA H, et al. Evidence for $X(3872)\to\gamma J/\psi$ and the sub-threshold decay $X(3872)\to\omega J/\psi$[EB/OL]. (2005-05-14)[2015-11-01]. http://arxiv.org/abs/hep-ex/0505037.

[4] DEL AMO SANCHEZ P, LEES J P, POIREAU V, et al. Evidence for the decay $X(3872)\to J/\psi\omega$ [J]. Phys Rev D, 2010, 82: 011101 (R).

[5] AUSHEV T, ZWAHLEN N, ADACHI I, et al. Study of the $B\to X(3872)(\to D^{*0}\overline{D}^0)K$ decay[J]. Phys Rev D, 2010, 81: 031103.

[6] AAIJ R, ABELLAN BETETA C, ADEVA B, et al. Determination of the $X(3872)$ meson quantum numbers [J]. Phys Rev Lett, 2013, 110: 222001.

[7] OLIVE K A, AGASHE K, AMSLER C, et al. Review of particle physics [J]. Chin Phys C, 2014, 38(09): 090001.

[8] ACHASOV NN, DEVYANIN S A, SHESTAKOV G N. Nature of scalar resonances[J]. Sov J Nucl Phys, 1980, 32: 566-573.

[9] ACHASOV NN, KISELEV A V. Propagators of light scalar mesons[J]. Phys Rev D, 2004, 70: 111901 (R).

[10] MAIANI L, RIQUER V, FACCINI R, et al. $J^{PG} = 1^{++}$ charged resonance in the $\Upsilon(4260)\to\pi^+\pi^- J/\psi$ decay? [J]. Phys Rev D, 2013, 87: 111102 (R).

[11] ACHASOV N N, ROGOZINA E V. $X(3872)$, $I^G(J^{PC}) = 0^+(1^{++})$, as the $\chi_{c1}(2P)$ charmonium[J]. Mod Phys Lett A, 2015, 30: 1550181.

[12] AAIJ R, ABELLAN BETETA C, ADEVA B, et al. Observation of $X(3872)$ production in pp collisions at $\sqrt{s}=7$ TeV [J]. Eur Phys J C, 2012, 72: 1972.

[13] YUAN C Z (Belle Collaboration). Exotic Hadrons [EB/OL]. (2009-11-08)[2015-11-01]. http://arxiv.org/abs/0910.3138.

[14] AAIJ R, ADEVA B, ADINOLFI M, et al. Evidence for the decay $X(3872)\to\psi(2S)\gamma$[J]. Nucl Phys B, 2014, 886: 665-680.

[15] KARLINER M, ROSNER J L. $X(3872)$, X_b, and the $\chi_{b1}(3P)$ state[J]. Phys Rev D, 2015, 91: 014014.

[16] BUTENSCHOEN M, HE Z G, KNIEHL B A. Next-to-leading-order nonrelativistic QCD disfavors the interpretation of $X(3872)$ as $\chi_{c1}(2P)$ [J]. Phys Rev D, 2013, 88: 011501 (R).

Article ID:0253-2778(2016)07-0580-07

Status of the Monte Carlo generators for low energy $e^+ e^-$ scattering

CZYŻ Henryk

(*Institute of Physics, University of Silesia, Uniwersytecka* 4, 40-007 *Katowice, Poland*)

Abstract: A short review of the existing Monte Carlo generators used for luminosity measurements at meson factories and simulating reactions $e^+ e^- \to$ hadrons, $e^+ e^- \to$ hadrons + photons or $e^+ e^- \to e^+ e^-$ + hadrons is presented, and the physical accuracy of the codes with emphasis on QED radiative corrections is discussed.

Key words: Monte Carlo generators; radiative corrections; low energy $e^+ e^-$ scattering

CLC number: O572.3 **Document code**: A doi:10.3969/j.issn.0253-2778.2016.07.007

Citation: CZYŻ H. Status of the Monte Carlo generators for low energy $e^+ e^-$ scattering[J]. Journal of University of Science and Technology of China, 2016,46(7):580-586.

低能正负电子散射蒙特卡洛产生子现状

CZYŻ Henryk

(西里西亚大学物理学院,卡托维兹 40-007,波兰)

摘要:简要评述了现有蒙特卡洛产生子,这些产生子被用于介子工厂中亮度的测量和模拟正负电子淹没产生强子、产生强子与光子或者产生正负电子与强子等反应.讨论了这些产生子的物理精度,着重强调量子电动力学辐射修正.

关键词:蒙特卡洛产生子;辐射修正;低能正负电子散射

0 Introduction

With the LHC running and no new physics found so far, the role of precise observables like anomalous magnetic moment of the muon $(g-2)_\mu$ is becoming increasingly important. The quest for precision, initiated many years ago by the community attending the PHIPSI Workshops and on the field of Monte Carlo generators and radiative corrections pursued by Working Group on Radiative Corrections and Monte Carlo Generators for Low Energies[1], started to pay off. Precise data on hadronic cross sections, with the most important $\sigma(e^+ e^- \to \pi^+ \pi^-)$, as well as on meson transition form factors, are coming up. More data are analysed by BaBar experiment[2]. New data are coming from BES-III[3], CMD-3[4] and SND[5] experiments. KLOE2 will produce results on $\gamma-\gamma$

Received: 2015-11-30; **Revised**: 2016-04-20

Foundation item: Supported by the Polish National Science Centre (DEC-2012/07/B/ST2/03867) and German Research Foundation DFG under Collaborative Research Center (CRC-1044).

Biography: CZYŻ Henryk, male, PhD/Prof. Research field: elementary particle physics. E-mail: czyz@us.edu.pl

form factors[6] making use of their newly installed low angle detectors. We will soon have the new $(g-2)_\mu$ experiment running at Fermilab[7], which is going to improve the already impressive accuracy[8] by about factor 4. In some years from now we could also expect data coming from a completely independent method developed at J-PARC[9] and new precise hadronic cross section measurements by BELLE-2[10]. Also on the theory side continuous efforts towards improving the accuracy of calculations of the $(g-2)_\mu$ are to be acknowledged. A summary and perspectives in this field can be found in a short resume[11] of two very busy workshops held at Mainz last year (April 1～10, 2014 in Mainz, Germany). Concluding their outcome in one sentence one can say that it will be difficult to reach the precision of the new $(g-2)_\mu$ Fermilab experiment, but with new emerging ideas a significant improvement is guarantied.

This paper is a short review of the current status of Monte Carlo generators used at meson factories and scan experiments. The generators are used there for many purposes helping in luminosity measurements, in measuring the hadronic cross section using scan and radiative return method, and in measuring meson transition form factors in virtual $\gamma-\gamma$ scattering. In Sec. 1 the status of radiative corrections is given. It is discussed whether one still needs to improve the radiative corrections and/or its tests in view of the improving experimental accuracy. Another accuracy limiting factor, especially for accuracy of efficiencies and acceptance corrections, might be the wrong modelling of the hadron-photon interactions. This issue is discussed in Sec. 2. Conclusions are presented in Sec. 3.

1 Radiative corrections

The radiative corrections are the most crucial for the physical accuracy of Monte Carlo codes. For low energies the most important, and for most of the applications the only important, corrections are the ones coming from quantum electrodynamics (QED).

1.1 Monte Carlo generators used for luminosity measurements

The experiments use mostly the Bhabha scattering at large angles for luminosity monitoring. As the considered energy is only up to 10～11 GeV the weak corrections are almost negligible and definitively well under control. The Monte Carlo generators used by the experimental groups BabaYaga @ NLO[12], BHWIDE[13] and MCGPJ[14] have been well established and stable for a long time. The comparisons between them made by various groups (see for example[15]) show that they agree between themselves at about 0.1% for the integrated cross sections, but in some corners of the phase space they might disagree up to 1%. This accuracy is adequate for the precision required at the low energy experiments and it looks that right now further progress here is not needed.

The reaction $e^+ e^- \to \gamma\gamma$ used for cross checks of the Bhabha luminosity measurements is also generated by BabaYaga@NLO[16], by MCGPJ[17-19] and a BKQED[20]. Here no extensive comparisons were made and for the accuracy one has to rely on the authors estimates. The BKQED has a declared precision of about 1%, the MCGPJ 0.2%, and BabaYaga@NLO 0.1%.

The reaction $e^+ e^- \to \mu^+ \mu^- \gamma$ is used as a luminometer in some of the low energy experiments using the radiative return method. The generator PHOKHARA[21] now including complete NLO corrections[22] was compared with KKMC generator. The biggest differences for muon invariant mass distribution were found[24-25] to be 0.25%, well contained in the PHOKHARA estimated precision[26]. It is difficult to assess an error of the generator AfkQed used by BaBar experiment[27]. The accuracy of the structure function approach used in this generator was discussed in Ref. [26]. It is very sensitive to event selections used by an experiment as photons spectra are partly integrated in the generator and its typical value is from a few per mile to a few

percent.

1.2 Monte Carlo generators used in scan measurements

For low hadron multiplicities the already mentioned generators: BabaYaga@NLO, KKMC, MCGPJ, and PHOKHARA provide the possibility of generation of the reactions $e^+e^- \to$ hadrons and $e^+e^- \to \mu^+\mu^-$ with the accuracy estimated by authors of the codes at a similar level as discussed in the previous subsection. Yet there are limitations: in BabaYaga@NLO from hadrons only $\pi^+\pi^-$ channel is generated and only initial state corrections (ISR) are included; in KKMC the hadronic final states are modelled with low accuracy; in MCGPJ only $\pi^+\pi^-$ and K^+K^- channels include radiative corrections going beyond ISR and in PHOKHARA also only ISR corrections are included. No systematic comparisons of the codes was performed. A limited sample of comparisons can be found in Ref. [25]. It would be desirable to make such comparisons in future and disentangle the radiative correction effects from the modelling of photon-hadron interactions. Due to the lack of final state emission (FSR) modelling in the original generators most of the experiments use PHOTOS[28] as a source of additional FSR emission. With this approach one neglects ISR-FSR interference unless a dedicated "fine tuning" of the PHOTOS is performed.

Monte Carlo generators used in inclusive measurements have a completely different philosophy as it is impossible to make a dedicated fine tuning (form factors modelling) for all separate multi-hadron final states. Instead, hadronisation models are used like in LUARLW generator[29] or methods based on structure function approach with a combination of Lund model and decay chains based on the measured branching fractions are deployed, like in ZRC generator[30]. Unfortunately no comparisons between these generators are available. It is also difficult to assess an error to the simulated distributions. Another possibility of progress in this direction might be offered by automatising the cross section calculations like in Carlomat 3.0 generator[31] if a better modelling of hadron production is provided.

1.3 Monte Carlo generators used for radiative return measurements

For the radiative return measurements essentially only two generators were used: AfkQed and PHOKHARA. At the early stage a precursor of the PHOKHARA generator, EVA generator[32-33], was used, but its development was abandoned as the PHOKHARA approach provides with much better theoretical accuracy. The structure functions used in EVA[34] are the ones used in AfkQed. The accuracy stated for PHOKHARA in Subsection 1.1 is valid also for hadronic final states as far as the ISR radiative corrections are concerned. In principle the estimated 0.5% might look conservative as the biggest difference with KKMC, which was found, is 0.25%. Yet the tests were performed for inclusive event selection and some event selections might enhance the relative size of higher order corrections neglected in PHOKHARA event generator. So without detailed dedicated studies the conservative estimate of of 0.5% has to be taken. In Ref. [24] the observed difference was guessed to have come from third order corrections neglected in PHOKHARA. It is indeed true as shown in Fig. 1. The test was performed using analytic results with no cuts imposed, thus it is only indicative and the event selection might change the output. Yet it confirms the "guess" from Ref. [24]. Relative differences between differential, in the invariant mass of the muon pair (Q^2), cross sections of the reaction $e^+e^- \to \mu^+\mu^-\gamma$ calculated using NLO formulae from Refs. [35-36] (marked as Ber in Fig. 1) and the semi-analytic ones available in KKMC based on Ref. [37] are shown in Fig. 1. The semi-analytic KKMC result is expanded and: ① only NLO terms are kept (marked as KKMC(al) in Fig. 1); ② up to NNLO terms are kept (marked as KKMC(al2) in Fig. 1); ③ the complete semi-analytic result of KKMC is

used (marked as KKMC in Fig. 1). In Ref. [38] it was shown that PHOKHARA is numerically equivalent to the semi-analytic results of Refs. [35-36], if one integrates over the whole phase space with the exception of the muon pair invariant mass. Thus the comparison shown in Fig. 1 proves that the bulk of the difference between KKMC and PHOKHARA is coming from the NNLO corrections and that beyond this level the corrections are well below 0.1% level. From Fig. 1 it is also clear that the PHOKHARA generator in its radiative return mode cannot be used close to the nominal energy of the experiment as it lacks the exponentiation.

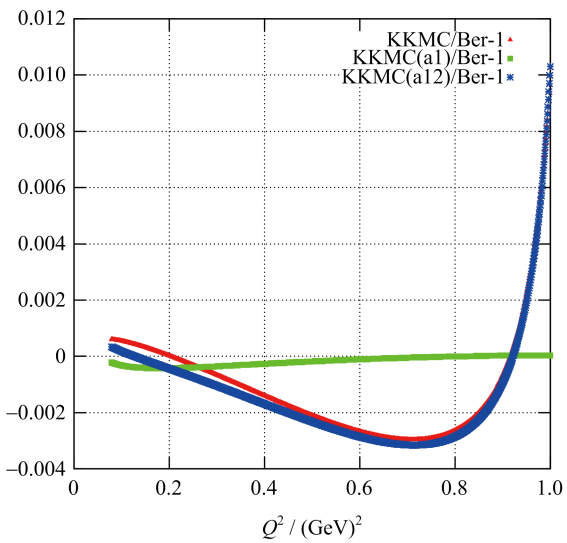

See text for details

Fig. 1 Numerical comparisons between four analytic results concerning ISR radiative corrections to the reaction $e^+e^-\to\mu^+\mu^-\gamma$

The FSR corrections are included in PHOKHARA only for some of the final states. For the $e^+e^-\to\mu^+\mu^-\gamma$ reaction they are exact at NLO level[22] and the code includes also ISR-FSR interference at the same level. For the $e^+e^-\to\pi^+\pi^-\gamma$ reaction an improved scalar QED was used[39] and supplemented with contributions coming from radiative ϕ decays[40]. A similar approach was adopted for the $e^+e^-\to K^+K^-\gamma$ reaction supplemented with the modeling of the J/ψ and $\psi(2S)$ contributions to this process[41]. The modeling of the final state emission for the reaction $e^+e^-\to\bar{p}p\gamma$ was added to the code recently[42]. For other final states FSR corrections are not included.

1.4 Monte Carlo generators used for reactions $e^+e^-\to e^+e^-$ hadrons

Some of the experiments have their own, "home made", generators not relying on theoretical groups. KLOE was using the generator of the reaction $e^+e^-\to e^+e^-\pi^0\pi^0$[43] relying on equivalent photon approximation (EPA) of the matrix element. This approximation works well if both virtual photons are quasi real and might be wrong by large factors if this is not fulfilled. CLEO was using TwoGam generator by D. Coffman and V. Savinov not well documented in publicly available sources and based on EPA. BELLE was using TREPS[44] again using EPA. Publicly available generators were developed a long time ago. The reaction $e^+e^-\to e^+e^-\pi^+\pi^-$ was generated in Ref. [45], and in the QED part there was no approximation, while for the modeling of the $\gamma^*-\gamma^*\to\pi^+\pi^-$ amplitude the quark model was used. Other amplitudes contributing to this process were neglected. Aiming at being used at LEP, a GALUGA generator of processes $e^+e^-\to e^+e^-X$ with X being a meson produced in $\gamma^*-\gamma^*$ was developed[46]. The modeling of the $\gamma^*-\gamma^*-X$ part used in this generator is quite involved and will not be discussed here. The EKHARA generator of the process $e^+e^-\to e^+e^-\pi^+\pi^-$ was born[47] as a tool to provide a background for the pion form factor measurement by KLOE. The two photon amplitudes were negligible, as compared to other amplitudes, for the KLOE event selection used in the pion form factor measurement and the generator was not optimised for event selections relevant for the $\gamma^*-\gamma^*\to\pi^+\pi^-$ amplitude measurement. Other modes $e^+e^-\to e^+e^-\pi^0$, $e^+e^-\to e^+e^-\eta$ and $e^+e^-\to e^+e^-\eta'$ were added to this generator later[48] aiming at simulation of the $\gamma^*-\gamma^*$ processes. The phase space simulation was adopted from Ref. [46] and the modeling of the transition form factors relies now, after the

recent update, on the model developed in Ref. [49] based on the resonance chiral perturbation theory. All the generators mentioned above do not contain radiative corrections. The only generator containing radiative corrections through structure function method is GGRESRC[50] developed for a single tag experiment and used by BaBar[51]. Unfortunately there exist no other generator containing radiative corrections to allow for independent tests of the code.

2 The importance of modeling of hadron-photon interactions

A modeling of the hadron-photon interactions, as well as the internal structure of the form factors and transition form factors, is crucial for the quality of event generators. Even if the QED radiative corrections are included with care, providing in principle a decent accuracy, a generator can be completely wrong if the hadronic part is modeled losely. This might affect for example acceptance corrections giving wrong extrapolation to the regions not covered by a detector. In this respect a continuous improvement of the generators and feedback experiment-theory is necessary.

3 Conclusion

Existing Monte Carlo generators used for luminosity measurements at meson factories and simulating reactions $e^+e^- \to$ hadrons, $e^+e^- \to$ hadrons+photons or $e^+e^- \to e^+e^-$ +hadrons were reviewed with emphasis on physical accuracy of the codes.

References

[1] ACTIS S, ARBUZOV A, BALOSSINI G, et al. Quest for precision in hadronic cross sections at low energy: Monte Carlo tools vs. experimental data[J]. Eur Phys J C, 2010, 66: 585-686.

[2] LEES J P, POIREAU V, TISSERAND V, et al. Measurement of initial-state-final-state radiation interference in the processes $e^+e^- \to \mu^+\mu^-\gamma$ and $e^+e^- \to \pi^+\pi^-\gamma$[J]. Phys Rev D, 2015, 92: 072015.

[3] ABLIKIM M, ACHASOV M N, AI X C, et al. Measurement of the $e^+e^- \to \pi^+\pi^-$ cross section between 600 and 900 MeV using initial state radiation [EB/OL]. (2015-11-17)[2015-11-20]. http://arxiv.org/abs/1507.08188.

[4] AKHMETSHIN R R, AMIRKHANOV A N, ANISENKOV A V, et al. Study of the process $e^+e^- \to p\bar{p}$ in the c. m. energy range from threshold to 2 GeV with the CMD-3 detector[EB/OL]. (2015-07-29)[2015-11-20]. http://arxiv.org/abs/1507.08013.

[5] AULCHENKO V M, ACHASOV M N, YU A, et al. Measurement of the $e^+e^- \to \eta\pi^+\pi^-$ cross section in the center-of-mass energy range 1.22~2.00 GeV with the SND detector at the VEPP-2000 collider[J]. Phys Rev D, 2015, 91: 052013.

[6] GAUZZI P (for the KLOE-2 Collaboration). Gamma-gamma physics and transition form factor measurements at KLOE/KLOE-2[EB/OL]. (2015-11-30)[2015-12-02]. http://arxiv.org/abs/1511.09253.

[7] GRAY F (for the Fermilab E989 Muon $g-2$ Collaboration). Muon $g-2$ experiment at Fermilab [EB/OL]. (2015-10-01)[2015-11-10]. http://arxiv.org/abs/1510.00346.

[8] BENNETT G W, BOUSQUET B, BROWN H N, et al. Final report of the E821 muon anomalous magnetic moment measurement at BNL[J]. Phys Rev D, 2006, 73: 072003.

[9] Saito N. (J-PARC ($g-2$)/EDM Collaboration). A novel precision measurement of muon $g-2$ and EDM at J-PARC[J]. AIP Conf Proc, 2012, 1467: 45-46.

[10] ABE T, ADACHI I, ADAMCZYK K, et al. Belle II Technical Design Report [EB/OL]. (2010-11-01)[2015-11-20]. http://arxiv.org/abs/1011.0352.

[11] BENAYOUN M, BIJNENS J, BLUM T, et al. Hadronic contributions to the muon anomalous magnetic moment Workshop. $(g-2)_\mu$: Quo vadis? Workshop. Mini proceedings[EB/OL]. (2014-07-21)[2015-11-10]. http://arxiv.org/abs/1407.4021.

[12] BALOSSINI G, CARLONI CALAME C M, MONTAGNA G, et al. Matching perturbative and parton shower corrections to Bhabha process at flavour factories[J]. Nucl Phys B, 2006, 758: 227-253.

[13] JADACH S, PLACZEK W, WARD B F L. BHWIDE 1.00: $O(\alpha)$ YFS exponentiated Monte Carlo for Bhabha scattering at wide angles for LEP1/SLC and LEP2[J]. Phys Lett B, 1997, 390: 298-308.

[14] ARBUZOV A B, FEDOTOVICH G V, IGNATOV F V, et al. Monte-Carlo generator for e^+e^- annihilation into lepton and hadron pairs with precise radiative corrections[J]. Eur Phys J C, 2006, 46: 689-703.

[15] BALOSSINI G, BIGNAMINI C, CARLONI CALAME C M, et al. Mini-review on Monte Carlo programs for Bhabha scattering[J]. Nucl Phys Proc Suppl, 2008, 183: 168-173.

[16] BALOSSINI G, BIGNAMINI C, CALAME C M C, et al. Photon pair production at flavour factories with per mille accuracy[J]. Phys Lett B, 2008, 663: 209-213.

[17] FEDOTOVICH G V, KURAEV E A, SIBIDANOV A L. Monte Carlo generator photon jets used for luminosity at e^+e^- colliders[J]. Chin Phys C, 2010, 34: 877-882.

[18] ARBUZOV A B, ASTAKHOV V A, FEDOROV A V, et al. Radiative corrections for pion and kaon production at e^+e^- colliders of energies below 2 GeV [J]. JHEP, 1997, 9710: 006.

[19] ARBUZOV A B, FEDOTOVICH G V, KURAEV E A, et al. Large angle QED processes at e^+e^- colliders at energies below 3 GeV[J]. JHEP, 1997, 9710: 001.

[20] BERENDS F A, KLEISS R. Distributions for electron-positron annihilation into two and three photons[J]. Nucl Phys B, 1981, 186: 22-34.

[21] CZYZ H, GRZELINSKA A, KUHN J H, et al. Radiative return at Φ- and B-factories: FSR for muon pair production at next-to-leading order[J]. Eur Phys J C, 2005, 39: 411.

[22] CAMPANARIO F, CZYZ H, GLUZA J, et al. Complete QED NLO contributions to the reaction $e^+e^-\to\mu^+\mu^-\gamma$ and their implementation in the event generator PHOKHARA[J]. JHEP, 2014, 1402: 114.

[23] JADACH S, WARD B F L, WAS Z. The precision Monte Carlo event generator KK for two-fermion final states in e^+e^- collisions[J]. Comput Phys Commun, 2000, 130: 260-325.

[24] JADACH S. Studies of μ-pair and π-pair production at the electron-positron low energy colliders[J]. Acta Phys Polon B, 2005, 36: 2387.

[25] CZYZ H, GUNIA M, KUHN J H. Simulation of electron-positron annihilation into hadrons with the event generator PHOKHARA [J]. JHEP, 2013, 1308: 110.

[26] RODRIGO G, CZYZ H, KUHN J H, et al. Radiative return at NLO and the measurement of the hadronic cross-section in electron-positron annihilation[J]. Eur Phys J C, 2002, 24: 71-82.

[27] LEES J P, POIREAU V, TISSERAND V, et al. Precise measurement of the $e^+e^-\to\pi^+\pi^-(\gamma)$ cross section with the initial-state radiation method at BABAR[J]. Phys Rev D, 2012, 86: 032013.

[28] BARBERIO E, VAN EIJK B, WAS Z. Photos: A universal Monte Carlo for QED radiative corrections in decays [J]. Comput Phys Commun, 1991, 66: 115-128.

[29] ANDERSSON B, HU H M. Few-Body States in Lund String Fragmentation Model[EB/OL]. (1999-10-08) [2015-11-10]. http://arxiv.org/abs/hep-ph/9910285.

[30] ZHANG D, GANG R, CHEN J C. Monte Carlo generator for full simulation of $e^+e^-\to$hadrons cross section scan experiment[J]. Phys Rev D, 2006, 74: 054012 .

[31] KOLODZIEJ K. carlomat_3.0, an automatic tool for the electron-positron annihilation into hadrons at low energies [J]. Comput Phys Commun, 2015, 196: 563-568.

[32] BINNER S, KÜHN J H, MELNIKOV K. Measuring $\sigma(e^+e^-\to$hadrons) using tagged photons[J]. Phys Lett B, 1999, 459: 279-287.

[33] CZYZ H, KUHN J H. Four pion final states with tagged photons at electron positron colliders[J]. Eur Phys J C, 2001, 18: 497-509.

[34] CAFFO M, CZYZ H, REMIDDI E. Order-α^2 leading-logarithmic corrections in Bhabha scattering at LEP/SLC energies[J]. Phys Lett B, 1994, 327: 369-376.

[35] BERENDS F A, BURGERS G J H, VAN NEERVEN W L. QED radiative corrections to the reaction $e^+e^-\to Z\gamma$[J]. Phys Lett B, 1986, 177: 191-194.

[36] BERENDS F A, VAN NEERVEN W L, BURGERS G J H. Higher order radiative corrections at LEP energies [J]. Nucl Phys B, 1988, 297: 429-478 (Erratum: Nucl Phys B, 1988, 304: 921).

[37] JADACH S, SKRZYPEK M, WARD B F L. Is there a better way of exponentiating QED corrections? [J]. Phys Lett B, 1991, 257: 173-178.

[38] CZYZ H, GRZELINSKA A, KUHN J H, et al. The radiative return at ϕ- and B-factories: small-angle photon emission at next-to-leading order[J]. Eur Phys J C, 2003, 27: 563-575.

[39] CZYZ H, GRZELINSKA A, KUHN J H, et al. The radiative return at Φ- and B-factories: FSR at next-to-leading order[J]. Eur Phys J C, 2004, 33: 333-347.

[40] CZYZ H, GRZELINSKA A, KUHN J H. Charge asymmetry and radiative ϕ decays[J]. Phys Lett B, 2005, 611: 116-122.

[41] CZYZ H, GRZELINSKA A, KUHN J H. Narrow resonances studies with the radiative return method [J]. Phys Rev D, 2010, 81: 094014.

[42] CZYZ H, KUHN J H, TRACZ S. Nucleon form factors and final state radiative corrections to $e^+e^-\to\bar{p}p\gamma$[J]. Phys Rev D, 2014, 90: 114021.

[43] NGUYEN F, PICCININI F, POLOSA A D. $e^+e^-\to e^+e^-\pi^0\pi^0$ at DAPHNE[J]. Eur Phys J C, 2006, 47:

65-70.
[44] UEHARA S. TREPS: A Monte-Carlo event generator for two-photon processes at e^+e^- colliders using an equivalent photon approximation[EB/OL]. (2013-10-01)[2015-11-10]. http://arxiv.org/abs/1310.0157.
[45] KRASEMANN H, VERMASEREN J A M. The 2γ reaction $e^+e^-\to e^+e^-\pi^+\pi^-$ in the resonance region[J]. Nucl Phys B, 1981, 184: 269-282.
[46] SCHULER G A. Two-photon physics with GALUGA 2.0[J]. Comput Phys Commun, 1998, 108: 279-303.
[47] CZYZ H, NOWAK-KUBAT E. The reaction $e^+e^-\to e^+e^-\pi^+\pi^-$ and the pion form factor measurements via the radiative return method[J]. Phys Lett B, 2006, 634: 493-497.
[48] CZYZ H, IVASHYN S. EKHARA: A Monte Carlo generator for $e^+e^-\to e^+e^-\pi^0$ and $e^+e^-\to e^+e^-\pi^+\pi^-$ processes[J]. Comput Phys Commun, 2011, 182: 1 338-1 349.
[49] CZYZ H, IVASHYN S, KORCHIN A, et al. Two-photon form factors of the π^0, η, and η' mesons in the chiral theory with resonances[J]. Phys Rev D, 2012, 85: 094010.
[50] DRUZHININ V P, KARDAPOLTSEV L V, TAYURSKY V A. GGRESRC: A Monte Carlo generator for the two-photon process $e^+e^-\to e^+e^-R$ ($J^{pc}=0^{+-}$) in the single-tag mode[J]. Comput Phys Commun, 2014, 185: 236-243.
[51] AUBERT B, KARYOTAKIS Y, LEES J P, et al. (BaBar Collaboration). Measurement of the $\gamma\gamma^*\to\pi^0$ transition form factor [J]. Phys Rev D, 2009, 80: 052002.

(上接第540页)

[42] CHEN D Y, HE J, LIU X. Nonresonant explanation for the $Y(4260)$ structure observed in the $e^+e^-\to J/\psi\pi^+\pi^-$ process[J]. Phys Rev D, 2011, 83: 054021.
[43] BERINGER J, ARGUIN J F, Barnett R M, et al. Review of Particle Physics (RPP)[J]. Phys Rev D, 2012, 86: 010001.
[44] LIU X, LUO Z G, SUN Z F. $X(3915)$ and $X(4350)$ as new members in P-wave charmonium family[J]. Phys Rev Lett, 2010, 104: 122001.
[45] BONDAR A, GARMASH A, MIZUK R, et al. Observation of two charged bottomonium-like resonances in $\Upsilon(5S)$ decays[J]. Phys Rev Lett, 2012, 108: 122001.
[46] CHEN D Y, LIU X. $Z_b(10610)$ and $Z_b(10650)$ structures produced by the initial single pion emission in the $\Upsilon(5S)$ decays [J]. Phys Rev D, 2011, 84: 094003.
[47] CHEN D Y, LIU X. Predicted charged charmonium-like structures in the hidden-charm dipion decay of higher charmonia[J]. Phys Rev D, 2011, 84: 034032.
[48] ABLIKIM M, ACHASOV M N, AI X C, et al. Observation of a charged charmoniumlike structure in $e^+e^-\to\pi^+\pi^- J/\psi$ at $\sqrt{s}=4.26$ GeV[J]. Phys Rev Lett, 2013, 110: 252001.
[49] LIU Z Q, SHEN C P, YUAN C Z, et al. Study of $e^+e^-\to\pi^+\pi^- J/\psi$ and observation of a charged charmonium-like state at Belle[J]. Phys Rev Lett, 2013, 110: 252002.
[50] CHEN D Y, LIU X, MATSUKI T. Reproducing the $Z_c(3900)$ structure through the initial-single-pion-emission mechanism [J]. Phys Rev D, 2013, 88: 036008.
[51] BARNES T, GODFREY S, SWANSON E S. Higher charmonia[J]. Phys Rev D, 2005, 72: 054026.

Article ID:0253-2778(2016)07-0587-07

Dark mediator searches at KLOE/KLOE-2

PÉREZ DEL RÍO Elena (for the KLOE-2 Collaboration)

(*INFN-Laboratori Nazionali di Frascati*, *Via E. Fermi* 40, 00044 *Frascati* (*RM*), *Italy*)

Abstract: The existence of a new vector boson has been postulated in different scenarios where the coupling to the SM can be achieved either via a kinetic mixing term, the U boson, or by coupling to the baryon number, the B boson. Direct searches for these dark matter mediators are performed at accelerator facilities. The KLOE detector at the DAϕNE Φ-factory has been prolific in searches for the U boson in both Dalitz decays of the ϕ meson, $\phi\to\eta U$ with $U\to e^+e^-$, and continuum events, $e^+e^-\to U\gamma$. For all of these processes, an upper limit for the U boson coupling ε^2 of 10^{-7} to 10^{-5} has been established in the mass range 4 MeV $\cdot c^{-2}<M_U<980$ MeV $\cdot c^{-2}$. KLOE has also sought the U boson in the dark Higgsstrahlung process $e^+e^-\to Uh'$, $U\to\mu^+\mu^-$, setting limits on m_U and $m_{h'}$ in the parameter space from $2m_\mu<m_U<1\,000$ MeV $\cdot c^{-2}$ and 10 MeV $\cdot c^{-2}<m_{h'}<500$ MeV $\cdot c^{-2}$. In the meantime a new data campaign has started with the KLOE-2 setup, with the aim of collecting more than 5 fb^{-1} in the next three years. The new setup and goal statistics could further improve the current limits on the dark coupling constant.

Key words: dark matter; dark forces; U boson; A'; dark Higgsstrahlung; h'; upper limit

CLC number: O572.3 **Document code**: A doi:10.3969/j.issn.0253-2778.2016.07.008

Citation: PÉREZ DEL RÍO E. Dark mediator searches at KLOE/KLOE-2[J]. Journal of University of Science and Technology of China, 2016,46(7):587-593.

在 KLOE/KLOE-2 实验中寻找暗传播子

PÉREZ DEL RÍO Elena (KLOE-2 合作组)

(弗拉斯卡蒂国家实验室—核物理研究所,弗拉斯卡蒂 00044,意大利)

摘要:一个新的矢量玻色子的存在已经在不同的背景下被提出,这个新矢量玻色子与标准模型粒子的耦合可以通过动力学混合,对U玻色子,或者通过耦合到重子数,对B玻色子.暗物质传播子的直接寻找可以在加速器上进行.DAϕNE Φ-工厂中的KLOE探测器大量研究了U玻色子参与的两种过程:ϕ介子的达利兹衰变,即伴随$\phi\to\eta U$,$U\to e^+e^-$过程,以及连续统事件$e^+e^-\to U\gamma$过程.在所有这些过程中,对于质量区间在4 MeV/$c^2<M_U<980$ MeV/c^2,我们可以给出U玻色子耦合参数ε^2上限在10^{-7}到10^{-5}.KLOE也在暗希格斯辐射过程$e^+e^-\to Uh'$,$U\to\mu^+\mu^-$中寻找U玻色子,m_U和$m_{h'}$在参数空间中被分别限定在$2m_\mu<m_U<1\,000$ MeV/c^2和10 MeV/$c^2<m_{h'}<500$ MeV/c^2的范围内.同时新的数据采集已经在KLOE-2设备上运行,未来3

Received:2015-11-30;**Revised**:2016-04-20

Foundation item:Supported in part by the EU Integrated Infrastructure Initiative Hadron Physics Project(RII3-CT-2004-506078), the European Commission under the 7th Framework Programme through the "Research Infrastructures" Action of the "Capacities" Programme FP7-INFRASTRUCTURES-2008-1(227431), the Polish National Science Centre (2011/03/N/ST2/02652, 2013/08/M/ST2/00323, 2013/11/B/ST2/04245, 2014/14/E/ST2/00262, 2014/12/S/ST2/00459).

Biography:PÉREZ DEL RÍO Elena, female, born in 1981, PhD. Research field: high energy physics. E-mail: eperez@lnf.infn.it

年采集目标将在 5 fb^{-1}以上. 新的大数据样本将进一步提高暗耦合常数的上限.

关键词:暗物质;暗能量;U 玻色子;A';希格斯辐射; h';上限

0 Introduction

Recent observations, such as the 511 keV gamma-ray signal from the galactic center[1], the CoGeNT results[2], the DAMA/LIBRA annual modulation[3-4], the total e^+e^- flux[5-8] and the discrepancy between the calculated and measured magnetic moment of the muon, a_μ, serve as examples of possible physics beyond the Standard Model. To explain the aforementioned anomalies, extensions of the SM[9-13] by dark matter models, with a weakly interacting massive particle (WIMP) belonging to a secluded gauge sector, have been proposed. The new gauge interaction would be mediated by a new vector gauge boson, the U boson or dark photon, which could interact with the photon via a kinetic mixing term,

$$\mathscr{L}_{mix} = -\frac{\varepsilon}{2}F^{EM}_{\mu\nu}F^{\mu\nu}_{DM} \tag{1}$$

where the parameter, ε, represents the mixing strength and is defined as the ratio of the dark photon to the SM electroweak coupling, α_D/α_{EM}. U boson searches are conducted in e^+e^- colliders via different processes: $e^+e^- \to U\gamma$, $V \to P\gamma$ decays, where V and P are vector and pseudoscalar mesons, and $e^+e^- \to h'U$, where h' is a Higgs-like particle responsible for the breaking of the hidden symmetry. Some of these searches, which are reported in the following, have been performed by the KLOE experiment.

1 The KLOE detector at DAϕNE

The KLOE detector is operated at the DAϕNE ϕ-factory, located at the INFN-LNF in Frascati. It consists of three main parts, a cylindrical drift chamber (DC)[14] surrounded by an electromagnetic calorimeter (EMC)[15], all embedded in a magnetic field of 0.52 T, provided along the beam axis by a superconducting coil located around the calorimeter. The EMC energy and time resolutions are $\sigma_E/E = 5.7\%/\sqrt{E[\mathrm{GeV}]}$ and $\sigma_t(E) = 57\ \mathrm{ps}/\sqrt{E[\mathrm{GeV}]} \oplus 100\ \mathrm{ps}$, respectively. The EMC consists of a barrel and two end-caps of lead/scintillating fibers, which cover 98% of the solid angle. The all-stereo drift chamber, 4 m in diameter and 3.3 m long, operates with a light gas mixture (90% helium, 10% isobutane). The position resolutions are $\sigma_{xy} \approx 150\ \mu$m and $\sigma_z \approx 2$ mm. Momentum resolution, $\sigma_{p_\perp}/p_\perp$, is better than 0.4% for large-angle tracks.

2 $\phi \to \eta U$ with $U \to e^+e^-$

The U boson decay $U \to e^+e^-$ in the process $\phi \to \eta U$ was the first search to be conducted at KLOE. A total of 13000 events of $\eta \to \pi^+\pi^-\pi^0$ from 1.5 fb^{-1} and 31000 events of $\eta \to \pi^0\pi^0\pi^0$ from 1.7 fb^{-1} taken in 2004 ~ 2005 were selected. The corresponding background contributions were of the order of ~2%[16] and ~3%[17], respectively. The irreducible background from the Dalitz decay $\phi \to \eta\gamma^* \to \eta e^+e^-$ was directly extracted from the data by a fit to the M_{ee} distribution parameterized according to the Vector Meson Dominance model[18].

No resonant signal was observed in the M_{ee} distributions of both analyses, see Fig. 1. The peak around 400 MeV $\cdot\ c^{-2}$ is due to background from the decay $\phi \to K_S K_L$. The confidence levels (CLs) technique[19] was used to set an upper limit on the kinetic mixing parameter, as a function of the U boson mass, using the signal cross section given by Ref. [20],

$$\sigma(\phi \to \eta U) = \varepsilon^2 \mid F_{\eta\phi}(m_U^2) \mid^2 \cdot \frac{\lambda^{3/2}(m_\phi^2, m_\eta^2, m_U^2)}{\lambda^{3/2}(m_\phi^2, m_\eta^2, 0)}\sigma(\phi \to \eta\gamma) \tag{2}$$

In Eq. (2), $|F_{\eta\phi}(m_U^2)|^2$ is the form factor of the $\phi \to \eta\gamma$ decay evaluated at the U mass and the quotient corresponds to the ratio of the kinematic functions of the decays involved in the process. In

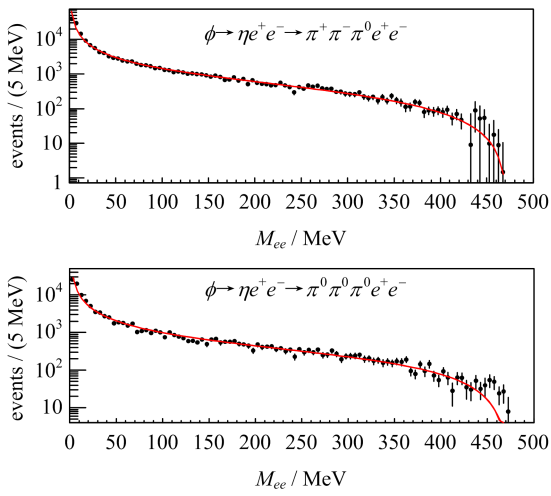

The red lines are the fits to the measured data.

Fig. 1 Di-electron invariant mass distributions, M_{ee}, for $\phi \to \eta e^+ e^-$ with $\eta \to \pi^+ \pi^- \pi^0$ (top) and $\eta \to \pi^0 \pi^0 \pi^0$ (bottom)

Fig. 2 the 90% confidence level limit is presented along with results from KLOE and other various experiments.

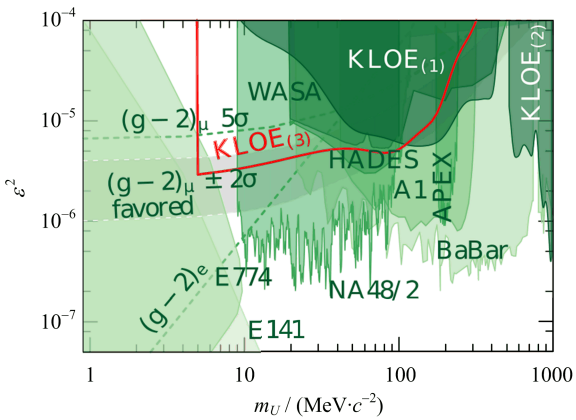

The results are compared with the limits from E141, E774[28], MAMI/A1[29], APEX[30], WASA[31], HADES[32], NA48/2[33] and BaBar[34]. The gray band indicates the parameter space favored by the $(g_\mu-2)$ discrepancy.

Fig. 2 Exclusion limits on the kinetic mixing parameter, ε^2, from KLOE (in red): $KLOE_1$, $KLOE_2$ and $KLOE_3$ correspond to the combined limits from the analysis of $\phi \to \eta e^+ e^-$, $e^+ e^- \to \mu^+ \mu^- \gamma$ and $e^+ e^- \to e^+ e^- \gamma$, respectively

3 $e^+ e^- \to U\gamma$ with $U \to \mu^+ \mu^-$

The next of the U boson searches carried out at KLOE was studying the reaction $e^+ e^- \to U\gamma$ with $U \to \mu^+ \mu^-$, in a sample of 239.3 pb^{-1} of data collected in 2002[21]. The expected signal would show up as a narrow resonance in the di-muon mass spectrum. The process $e^+ e^- \to \mu^+ \mu^- \gamma$ receives a very large contribution from the reaction $e^+ e^- \to \mu^+ \mu^-$, where photons are radiated by the initial-state electrons (ISR) or the final-state muons (FSR). The FSR process is highly suppressed by kinematical and geometrical cuts. The requirement to select the candidate events was to find two opposite-charged tracks emitted at large polar angles, with an initial-state radiation photon emitted at small angles and thus undetected. The photon was later kinematically reconstructed from the charged leptons.

A variable called "track mass", M_{trk} was reconstructed using energy and momentum conservation and used to separate muons from pions and electrons. The M_{trk} was calculated assuming two opposite charged tracks of equal mass and an unobserved photon in the final state. Residual backgrounds, consisting of $e^+ e^- \to e^+ e^- \gamma$, $e^+ e^- \to \pi^+ \pi^- \gamma$ and $e^+ e^- \to \phi \to \pi^+ \pi^- \pi^0$ were determined using Monte Carlo simulation by fitting the observed M_{trk} spectrum. The resulting invariant mass spectrum was obtained after subtracting residual backgrounds and being divided by efficiency and luminosity. Fig. 3 shows the di-muon invariant mass, which is in excellent agreement with the PHOKARA Monte Carlo simulation. Since no resonant peak was observed, the CLs technique was used to estimate the number of U boson signal events excluded at 90% confidence level, N_{CLs} and then the limit on the kinetic mixing parameter,

$$\varepsilon^2 = \frac{\alpha_D}{\alpha_{EM}} = \frac{N_{CLs}}{\varepsilon_{eff}} \frac{1}{H \cdot I \cdot L_{integrated}} \qquad (3)$$

where ε_{eff} is the overall efficiency, I is the effective cross section, $L_{integrated}$ the integrated luminosity and H is the radiator function, which is extracted from the differential cross section, $d\sigma_{\mu\mu\gamma}/dM_{\mu\mu}$. A systematic uncertainty of about 2% was estimated. The 90% confidence level limit is shown in Fig. 2.

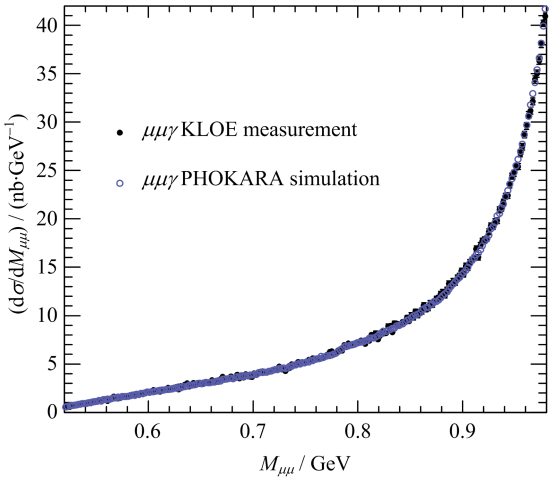

Fig. 3 Di-muon invariant mass distributions, $M_{\mu\mu}$. Comparison of data (full blue circles) and simulation (open red circles)

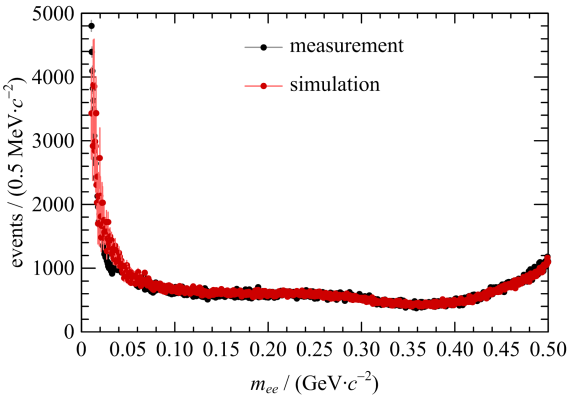

Fig. 4 Di-electron invariant mass distribution, M_{ee}, for the process $e^+e^-\to e^+e^-\gamma$ (black circles) compared to the MC simulated spectra (red circles)

4 $e^+e^-\to U\gamma$ with $U\to e^+e^-$

Similar to the previous analyses, the reaction $e^+e^-\to U\gamma$, $U\to e^+e^-$ was investigated. This process offers the possibility of investigating the low mass region close to the di-electron mass threshold[22]. For the event selection three separated energy depositions in the barrel of the calorimeter were required, corresponding to two opposite charged tracks and the ISR photon, which is explicitly detected.

To reduce the background contamination from $e^+e^-\to\mu^+\mu^-$, $e^+e^-\to\pi^+\pi^-\gamma$, $e^+e^-\to\gamma\gamma$, with a photon converting into an e^+e^-—pair, $e^+e^-\to\phi\to\pi^+\pi^-\pi^0$, a pseudo-likelihood discriminant was used to separate electrons from muons and pions, and then the "track mass" variable, M_{trk}, was also used to further discriminate the background sources. The resulting background contamination was less than 1.5%. Fig. 4 compares the di-electron invariant mass with MC BABAYAGA-NLO simulation[23] modified to allow the Bhabha radiative process to proceed only via the annihilation channel, in which the U boson signal would occur, showing an excellent agreement.

In an analogous way as the $e^+e^-\to\mu^+\mu^-\gamma$ study, the upper limit of the kinetic mixing parameter ε^2 as a function of m_U was evaluated with the CLs technique. The limit on the U boson signal was evaluated at 90% confidence level and the limit in the kinetic parameter was calculated using Eq. (3). In this case the selection efficiency amounts to $\varepsilon_{eff}\approx 1.5\%\sim 2.5\%$ and the integrated luminosity corresponds to $L_{integrated}=1.54\ \text{fb}^{-1}$ from the 2004～2005 data campaign.

5 $e^+e^-\to h'U$ with $U\to\mu^+\mu^-$

Given the fact that the U boson has mass, a natural consequence is the breaking of the U_D hidden symmetry associated by a Higgs-like mechanism through an additional scalar particle, called h' or dark Higgs, giving rise to the so-called "dark Higgsstrahlung" process. The production cross section of $e^+e^-\to h'U$ with $U\to\mu^+\mu^-$, would be proportional to the product $a_D\times\varepsilon^2$[24]. Thus this process is suppressed by a factor ε compared with the previous processes, already suppressed by a factor ε^2. Depending on the ratio of the masses of the h' and the U boson there are two possible decay scenarios: if $m_{h'}>2m_U$, the dark Higgs could decay via $h'\to UU\to 4l$, 4π, $2l+2\pi$, where l denotes lepton. This scenario was studied by Babar[25] and Belle[26] Collaborations in recent experiments. If $m_{h'}<2m_U$, then the dark Higgs would have a large lifetime and would escape any detection. This scenario was the one studied by

KLOE[27].

To perform the analysis a sample of 1.65 fb^{-1} of data collected during 2004～2005 data campaign at a center of mass energy at the ϕ-peak and also a data sample of 0.2 fb^{-1} at a center of mass energy of ～1 000 MeV were used. The expected signal would show up as a sharp enhancement in the missing mass, M_{miss}, versus $\mu\mu$ invariant mass, $M_{\mu\mu}$, two-dimensional spectra, shown in Fig. 5.

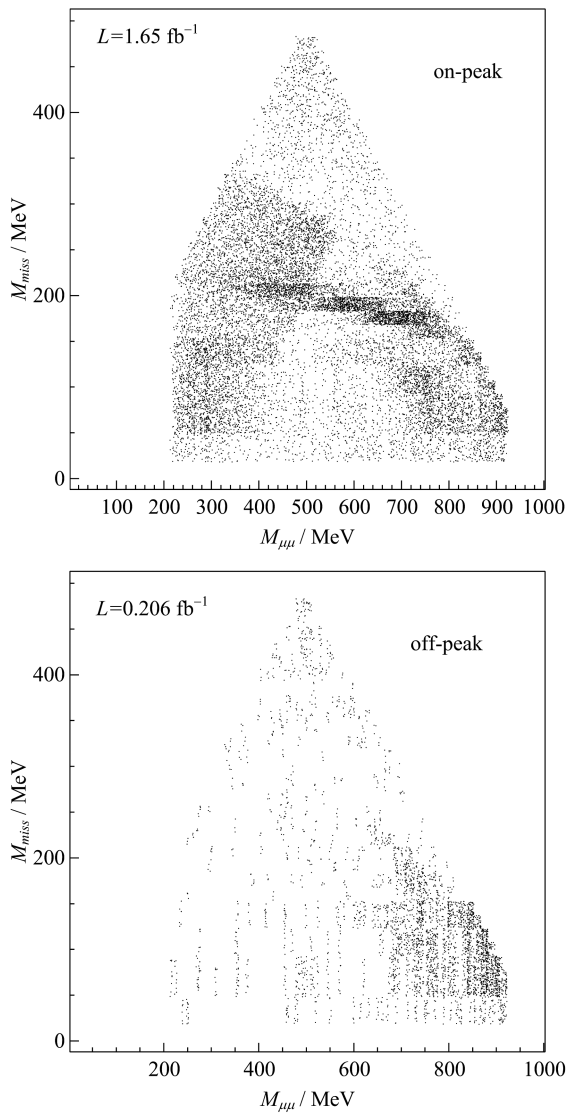

Fig. 5 Missing mass, M_{miss}, versus di-muon mass, $M_{\mu\mu}$, for the 1.65 fb^{-1} on-peak data sample (top) and the 0.2 fb^{-1} off-peak sample (bottom)

The candidate event selection required two opposite charged tracks with associated calorimeter clusters and missing momentum exceeding 40 MeV. Since most of the signal is expected to be in just one bin, a sliding matrix of 5×5 bins was built and used with data and Monte Carlo to check the presence of a possible signal in the central bin while the neighboring cells were used to estimate the background. The selection efficiencies were found to be about 15%～25%.

Different sources of background can be identified in the upper plot of Fig. 5. The left region of the on-peak data is populated by $\phi\to K^+K^-$, $K^\pm\to\mu^\pm\nu$. The central horizontal band corresponds to $\phi\to\pi^+\pi^-\pi^0$ contribution. Continuum backgrounds $e^+e^-\to\mu^+\mu^-$, $\pi^+\pi^-$ populate the right lower side of the spectra and the top point of the distribution is mostly due to $e^+e^-\to e^+e^-\mu^+\mu^-$ and $e^+e^-\to e^+e^-\pi^+\pi^-$. In the lower plot of Fig. 5 (off-peak sample), all the backgrounds from the ϕ decays are strongly suppressed.

A Bayesian limit on the number of signal events, $N_{90\%}$, was derived for both samples separately since no signal of the dark Higgsstrahlung process was observed. The product $\alpha_D\times\varepsilon^2$ was then calculated with,

$$\alpha_D\,\varepsilon^2_{90\%CL}=\frac{N_{90\%}}{\varepsilon_{eff}}\frac{1}{\sigma_{h'U}(\alpha_D\varepsilon^2)\cdot L_{integrated}} \tag{4}$$

with

$$\sigma_{h'U}\propto\frac{1}{s}\frac{1}{(1-m_U^2/s)^2} \tag{5}$$

where $N_{90\%}$ is the signal events excluded at the 90% confidence level, ε_{eff} the signal efficiency, $\sigma_{h'U}(\alpha_D\varepsilon^2)$ corresponds to the dark Higgsstrahlung cross section for $\alpha_D\,\varepsilon^2=1$ and $L_{integrated}$ is the integrated luminosity. The combined 90% confidence level limits for both on-and off-peak data samples are presented in Fig. 6, as a function of m_U(left) and of $m_{h'}$(right). The limit values of $\alpha_D\times\varepsilon^2$ of $10^{-9}\sim10^{-8}$ at 90% confidence level transform into a limit on the kinetic parameter, ε^2, of $10^{-6}\sim10^{-8}$ ($\alpha_D=\alpha_{EM}$). A conservative 10% of systematic uncertainty was considered.

6 Conclusion

The KLOE Collaboration has extensively

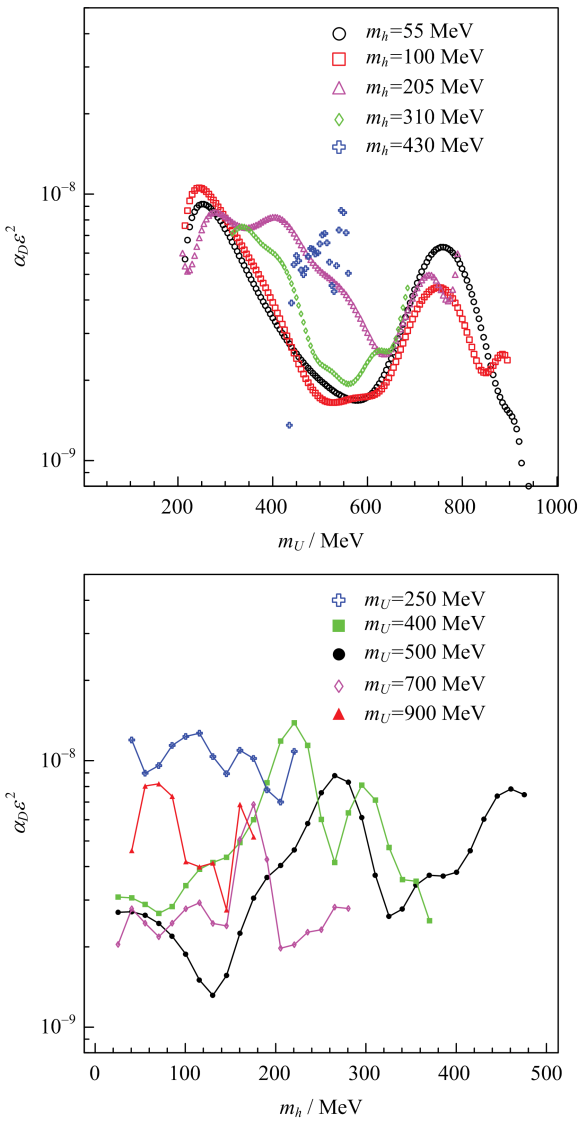

Fig. 6 Combined 90% confidence level upper limits in $\alpha_D \times \varepsilon^2$ as a function of m_U for different $m_{h'}$ values (top) and as a function of $m_{h'}$ for different m_U (bottom)

contributed to the U boson searches by analyzing four different production processes. Up to now, no evidence for a U boson or dark Higgs boson was found and limits at the 90% confidence level were set on the kinetic mixing parameter, ε^2, in the mass range 5 MeV$<m_U<$980 MeV. For the dark Higgsstrahlung process, limits on $\alpha_D \times \varepsilon^2$ at the 90% confidence level in the parameter space $2m_\mu<m_U<1\,000$ eV with $m_{h'}<m_U$ have been extracted. In the meantime a new data campaign has started with the KLOE-2 setup, which will collect more than 5 fb^{-1} in the next three years. The new setup and the enlarged statistics could further improve the sensitivity on the dark coupling constant measurement by at least a factor of two.

Acknowledgments We warmly thank our former KLOE colleagues for the access to the data collected during the KLOE data taking campaign. We thank the DA NE team for their efforts in maintaining low background running conditions and their collaboration during all data taking. We want to thank our technical staff: G. F. Fortugno and F. Sborzacchi for their dedication in ensuring efficient operation of the KLOE computing facilities; M. Anelli for his continuous attention to the gas system and detector safety; A. Balla, M. Gatta, G. Corradi and G. Papalino for electronics maintenance; M. Santoni, G. Paoluzzi and R. Rosellini for general detector support; C. Piscitelli for his help during major maintenance periods.

References

[1] JEAN P, KNÖDLSEDER J, LONJOU V, et al. Early SPI/INTEGRAL measurements of 511 keV line emission from the 4th quadrant of the galaxy[J]. Astronomy and Astrophysics, 2003 407: L55-L58.

[2] AALSETH C E, BARBEAU P S, COLARESI J, et al. Search for an annual modulation in a *p*-type point contact germanium dark matter detector[J]. Physical Review Letters, 2011, 107: 141301.

[3] BERNABEI R, BELLI P, CAPPELLA F, et al. Dark matter particles in the Galactic halo: Results and implications from DAMA/NaI [J]. International Journal of Modern Physics D, 2004, 13: 2127-2160.

[4] BERNABEI R, BELLI P, CAPPELLA F, et al. First results from DAMA/LIBRA and the combined results with DAMA/NaI[J]. The European Physical Journal C, 2008, 56: 333-355.

[5] CHANG J, ADAMS J H, AHN H S, et al. An excess of cosmic ray electrons at energies of 300～800 GeV [J]. Nature, 2008, 456: 362-365.

[6] AHARONIAN F, AKHPERJANIAN A G, DE ALMEIDA U B, et al. Energy spectrum of cosmic-ray electrons at TeV energies [J]. Physical Review Letters, 2008, 101: 261104.

[7] AHARONIAN F, AKHPERJANIAN A G,

ANTONG , et al. Probing the ATIC peak in the cosmic-ray electron spectrum with H. E. S. S. [J]. Astronomy and Astrophysics, 2009, 508:561-564.
[8] ABDO AA, ACKERMANN M, AJELLO M, et al. Measurement of the cosmic ray $e^+ + e^-$ spectrum from 20 GeV to 1 TeV with the Fermi Large Area Telescope [J]. Physical Review Letters, 2009, 102:181101.
[9] HOLDOM B. Two U(1)'s and ε charge shifts[J]. Physics Letters B, 1985, 166:196-198.
[10] BOEHM C, FAYET P. Scalar dark matter candidates [J]. Nuclear Physics B, 2004, 683:219-263.
[11] FAYET P. U-boson production in e^+e^- annihilations, ψ and Υ decays, and light dark matter[J]. Physical Review D, 2007,75: 115017.
[12] POSPELOV M, RITZ A, VOLOSHIN M B. Secluded WIMP dark matter[J]. Physics Letters B, 2008, 662: 53-61.
[13] MAMBRINI Y. The kinetic dark-mixing in the light of CoGENT and XENON100[J]. Journal of Cosmology and Astroparticle Physics, 2010, 2010:022.
[14] ADINOLFIA M, AMBROSINOB F, ANDRYAKOV A, et al. The tracking detector of the KLOE experiment[J]. Nuclear Instruments and Methods in Physics Research A, 2002, 488:51-73.
[15] ADINOLFIA M, AMBROSINOB F, ANTONELLI A, et al. The KLOE electromagnetic calorimeter[J]. Nuclear Instruments and Methods in Physics Research A, 2002, 482:364-386.
[16] ARCHILLI F, BABUSCIF D, BADONI D, et al. Search for a vector gauge boson in ϕ meson decays with the KLOE detector[J]. Physics Letters B, 2012, 706: 251-255.
[17] BABUSCIH D, BADONIR D, BALWIERZ-PYTKO I, et al. Limit on the production of a light vector gauge boson in ϕ meson decays with the KLOE detector[J]. Physics Letters B, 2013, 720:111-115.
[18] LANDSBERG L G. Electromagnetic decays of light mesons[J]. Physics Reports, 1985, 128:301-376.
[19] FELDMAN G J, COUSINS R D. Unified approach to the classical statistical analysis of small signals[J]. Physical Review D, 1998, 57:3873
[20] REECE M, WANG L T. Searching for the light dark gauge boson in GeV-scale experiments[J]. Journal of High Energy Physics, 2009, 2009:051.
[21] BABUSCI D, BALWIERZ-PYTKOG I, BENCIVENNI G, et al. Search for light vector boson production in $e^+e^- \to \mu^+\mu^-\gamma$ interactions with the KLOE experiment [J]. Physics Letters B, 2014, 736:459-464.
[22] ANASTASI A, BABUSCID D, BENCIVENNI G, et al. Limit on the production of a low-mass vector boson in $e^+e^- \to U\gamma$, $U \to e^+e^-$ with the KLOE experiment [J]. Physics Letters B, 2015, 750:633-637.
[23] BARZÈ L, BALOSSINI G, BIGNAMINI C, et al. Radiative events as a probe of dark forces at GeV-scale e^+e^- colliders[J]. The European Physical Journal C, 2011, 71:1680.
[24] BATELL B, POSPELOV M, Ritz A. Probing a Secluded U(1) at *B* factories[J]. Physical Review D, 2009, 79:115008.
[25] LEES J P, POIREAU V, TISSERAND V, et al. Search for low-mass dark-sector higgs bosons [J]. Physical Review Letters, 2012, 108:211801.
[26] JAEGEL I. Search for the "Dark Photon" and the "Dark Higgs" at Belle [J]. Nuclear Physics B: Proceedings Supplements, 2013, 234:33-36.
[27] ANASTASI A, BABUSCIF D, BENCIVENNI G, et al. Search for dark Higgsstrahlung in $e^+e^- \to \mu^+\mu^-$ and missing energy events with the KLOE experiment [J]. Physics Letters B, 2015, 747:365-372.
[28] BJORKEN J D, ESSIG R, SCHUSTER P, et al. New fixed-target experiments to search for dark gauge forces [J]. Physical Review D, 2009, 80:075018.
[29] MERKEL H, ACHENBACH P, AYERBE GAYOSO C, et al. Search at the Mainz Microtron for light massive gauge bosons relevant for the muon $g-2$ anomaly [J]. Physical Review Letters, 2014, 112:221802.
[30] ABRAHAMYAN S, AHMED Z, ALLADA K, et al. Search for a new gauge boson in electron-nucleus fixed-target scattering by the APEX experiment [J]. Physical Review Letters, 2011, 107:191804.
[31] ADLARSON P, AUGUSTYNIAKB W, BARDAN W, et al. Search for a dark photon in the $\pi^0 \to e^+e^-\gamma$ decay [J]. Physics Letters B, 2013, 726:187-193.
[32] AGAKISHIEV G, BALANDA A, BELVER D, et al. Searching a dark photon with HADES[J]. Physics Letters B, 2014, 731:265-271.
[33] BATLEY J R, KALMUS G, LAZZERONI C, et al. Search for the dark photon in π^0 decays[J]. Physics Letters B, 2015, 746:178-185.
[34] LEES J P, POIREAU V, TISSERAND V, et al. Search for a dark photon in e^+e^- collisions at BaBar [J]. Physical Review Letters, 2014, 113:201801.

Article ID:0253-2778(2016)07-0594-07

Search for dark photons in π^0 decays at NA48 and NA62

GONNELLA Francesco (for the NA48/2 Collaboration)

(*INFN-Laboratori Nazionali di Frascati, via E. Fermi* 40, 00044 *Frascati, Italy*)

Abstract: The NA48/2 experiment at CERN collected, between 2003 and 2004, 1.69×10^7 fully reconstructed $\pi^0\to\gamma e^+e^-$ in the kinematic range $m_{ee}>10$ MeV/c^2, with a negligible background contamination. The sample is analysed to search for the presence of dark photons (A') via the decay chain $\pi^0\to\gamma A'$, $A'\to e^+e^-$. No signal has been observed, and the exclusion limits on space of the dark photon mass $m_{A'}$ and the mixing parameter ϵ^2 are reported.

Key words: dark photon; NA48; NA62

CLC number: O572.3 **Document code**: A doi:10.3969/j.issn.0253-2778.2016.07.009

Citation: GONNELLA F. Search for dark photons in π^0 decays at NA48 and NA62[J]. Journal of University of Science and Technology of China, 2016,46(7):594-600,624.

NA48 和 NA62 实验在 π^0 衰变中寻找暗光子

GONNELLA Francesco (NA48/2 合作组)

(意大利国家核物理研究院弗拉斯卡蒂国家实验室,弗拉斯卡蒂 00044 ,意大利)

摘要:2003 到 2004 年间,CERN 的 NA48/2 实验收集了 1.69×10^7 个完全重建的 $\pi^0\to\gamma e^+e^-$ 事例,动量范围在 $m_{ee}>10$ MeV/c^2,本底污染可忽略.该样本通过分析衰变链 $\pi^0\to\gamma A'$,$A'\to e^+e^-$ 来寻找暗光子.然而并没有观测到信号,本文给出暗光子质量 $m_{A'}$ 和混合参数 ϵ^2 的排除限.

关键词:暗光子;NA48;NA62

0 Introduction

Kaons are a source of tagged neutral pion decays; the opportunity for precision studies on π^0 decay physics mainly proceeds via $K^\pm\to\pi^\pm\pi^0$ and $K^\pm\to\mu^\pm\pi^0\nu$ processes. One of the high-intensity kaon experiments focusing on such physics is the NA48/2 experiment at CERN SPS, which collected, between 2003 and 2004, a large sample of charged kaon ($K^\pm$) decays in flight, that is about 2×10^{11} $K^\pm$[1]. Analysing a large set of π^0 mesons decaying in the fiducial volume allows for a high-sensitivity search of the dark photon (A'), a hypothetical gauge boson appearing in hidden sectors of new physics models with an extra U(1) gauge symmetry. In such models, dark photons interact with the visible sector through kinetic mixing with the Standard Model (SM) hypercharge[2]. The observed rise in measurements of the cosmic-ray positron fraction with energy and of the $(g-2)$ of the muon could possibly be explained by scenarios involving GeV-scale dark

Received:2015-11-30;**Revised**:2016-04-20

Biography:GONNELLA Francesco, PhD. Research field: high energy physics. E-mail: francesco.gonnella@lnf.infn.it

matter and therefore dark photons[3]. A recent review of the status of dark photon searches can be found in Ref. [4]. Experimentally, two parameters characterise the dark photon and are unknown a priori: the mixing parameter ϵ^2 and the dark photon mass $m_{A'}$. A' production in NA48/2 occurs through neutral pions coming from $K^\pm \to \pi^\pm \pi^0$ ($K_{2\pi}$) and $K^\pm \to \mu^\pm \pi^0 \nu$ ($K_{\mu 3}$). Dark photons may be produced and decay with the following:

$$\pi^0 \to \gamma A', \ A' \to e^+ e^- \tag{1}$$

Three charged particles and a photon are produced in the final state. The expected branching ratio of the π^0 decay is[5]:

$$BR(\pi^0 \to \gamma A') = 2\epsilon^2 \left(1 - \frac{m_{A'}^2}{m_{\pi^0}^2}\right)^3 BR(\pi^0 \to \gamma\gamma) \tag{2}$$

where $m_{A'}$ approaches m_{π^0}, the branching fraction is kinematically suppressed. In the mass range accessible in this analysis, $2m_e \ll m_{A'} < m_{\pi^0}$, the dark photon lies below threshold for each decay into SM fermions, except for $A' \to e^+ e^-$, whereas the $A' \to 3\gamma$ and $A' \to \nu\bar{\nu}$ processes, which are allowed loop-induced decays, are strongly suppressed. Therefore, assuming that dark photons only decay into SM particles, the only allowed fermions are two opposite-charged electrons, this leading to $BR(A' \to e^+ e^-) \approx 1$. The expected total decay width of the dark photon is[6]:

$$\Gamma(A' \to e^+ e^-) = \frac{1}{3}\alpha\epsilon^2 m_{A'} \sqrt{1 - \frac{4m_e^2}{m_{A'}^2}} \left(1 + \frac{2m_e^2}{m_{A'}^2}\right) \tag{3}$$

Thus, for $2m_e \ll m_{A'} < m_{\pi^0}$, the dark photon mean lifetime $\tau_{A'}$ fulfils the relation:

$$c\tau_{A'} \approx 0.8\mu m \left(\frac{10^{-6}}{\epsilon^2}\right)\left(\frac{100 \text{ MeV}}{m_{A'}}\right) \tag{4}$$

The NA48/2 analysis is performed assuming that dark photons decay at the production point (prompt decay), which is valid under two conditions: A' mass has to be sufficiently large ($m_{A'} > 10$ MeV/c^2), as well as the mixing parameter ($\epsilon^2 > 5 \times 10^{-7}$). Provided these, the dark photon signature is undistinguishable from the Dalitz decay $\pi^0 \to \gamma e^+ e^-$ which, therefore, represents an irreducible background and determines the sensitivity of the measurement. The largest π_D^0 sample is obtained through the reconstruction of the $K_{2\pi}$ and $K_{\mu 3}$ processes. Furthermore, the $K^\pm \to \pi^\pm \pi^0 \pi^0$ decay ($K_{3\pi}$) is considered a background in the $K_{\mu 3}$ sample.

1 The NA48/2 experiment

A primary beam of 400 GeV/c protons was extracted from the CERN SPS; two simultaneous K^+ and K^- beams of narrow momentum band were delivered to the NA48/2 beam line, following a common beam axis derived from the primary beam; secondary beams with central momenta of (60±3) GeV/c (r. m. s.) were used. A 114 m-long cylindrical vacuum tank contained the fiducial volume, with a length of 98 m, in which the beam kaons decayed. A magnetic spectrometer, housed in a tank filled with helium and placed after the decay volume, measured the momenta of charged decay products. The spectrometer was made of four drift chambers (DCHs), with eight planes of sense wires each; the chambers were placed two upstream and two downstream of a dipole magnet, which provided a horizontal transverse momentum kick of 120 MeV/c to single charged particles. After the spectrometer, a plastic scintillator hodoscope (HOD) was positioned in order to produce fast trigger signals and provide precise time measurements of charged particles. Further downstream, a liquid krypton electromagnetic calorimeter (LKr) was placed; the LKr was an almost-homogeneous ionisation chamber, $27X_0$ deep, with an active volume of 7 m^3 filled with liquid krypton; such a chamber was transversally segmented into 13248 projective 2×2 cm^2 cells, without longitudinal segmentation. The LKr information was used for photon energy measurements and charged particle identification. A hadronic calorimeter made of alternated iron and scintillator layers was located downstream, together with a muon detector system. A dedicated two-level trigger operated to collect three-track

decays with an efficiency of about 98%. A detailed description of the NA48/2 experimental apparatus can be found in Ref. [7].

2 Event selection

For the analysis presented in this paper, the whole NA48/2 data sample was used. The $K_{2\pi}$ and $K_{\mu 3}$ selections, with the following $\pi^0 \to \gamma e^+ e^-$ event, require a three-track vertex to be reconstructed in the fiducial decay region; the vertex has to be formed by the tracks originated from a pion or muon candidate and two opposite-charged electron ($e^{\pm}$) candidates. The identification of charged particles is based on the ratio of energy deposition in the LKr calorimeter to the momentum measured by the spectrometer, E/p. Pions and muons are kinematically constrained above 5 GeV/c momenta, while the momentum spectra of electrons originating from π^0 decays are soft, with a peak at 3 GeV/c. Thus, the requirements for the kinematics of the process are: $p>5$ GeV/c and $E/p<0.85$ ($E/p<0.4$) for the pion (muon) candidate; $p>2.75$ GeV/c and $(E/p)_{\min}<E/p<1.15$ for the electron candidates, where $(E/p)_{\min}=0.80$ for $p<5$ GeV/c and $(E/p)_{\min}=0.85$ otherwise. Moreover, a single insulated cluster of energy deposition in the LKr is associated with the photon candidate. The reconstructed invariant mass of the $e^+e^-\gamma$ system is required to be compatible with the π^0 mass ($|m_{e^+e^-\gamma}-m_{\pi^0}|<8$ MeV/c^2), an interval corresponding to ± 5 times the resolution on $m_{e^+e^-\gamma}$.

As far as the $K_{2\pi}$ selection is concerned, the invariant mass of the $\pi^{\pm}e^+e^-\gamma$ system (Fig. 1) is to be compatible with the $K^{\pm}$ mass, that is 474 MeV/$c^2<m_{\pi e^+e^-\gamma}<514$ MeV/c^2. Regarding the $K_{\mu 3}$ selection, the squared missing mass $m^2_{miss}=(P_K-P_{\mu}-P_{\pi^0})^2$ (Fig. 2) is required to be compatible with zero, i.e. $|m^2_{miss}|<0.01$ GeV$^2/c^4$, where P_{μ} and P_{π^0} are the reconstructed four-momenta of $\mu^{\pm}$ and π^0, and P_K is the nominal four-momentum of the kaon.

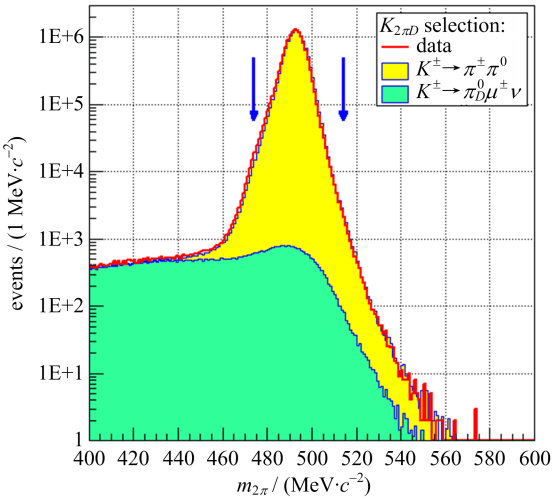

The cuts on the selection are represented by the arrows.

Fig. 1 Data and Monte Carlo (MC) reconstructed invariant mass of $\pi^{\pm}\pi^0_D$ for events passing the $K_{2\pi}$ selection

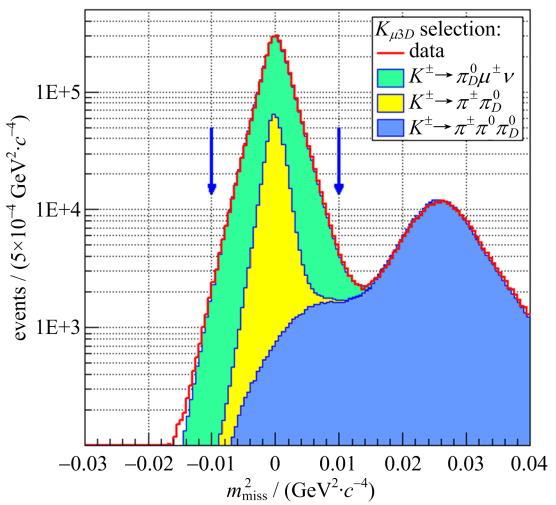

The cuts on the selection are represented by the arrows.

Fig. 2 Data and MC reconstructed invariant mass of $\pi^{\pm}\pi^0_D$ for events passing the $K_{\mu 3}$ selection

After the two selections are applied, a sample of 1.38×10^7 (0.31×10^7) fully reconstructed π^0_D decay candidates, coming from $K_{2\pi}$ ($K_{\mu 3}$) with a negligible background, is selected. Two parameters are used to correct the observed number of candidates: the acceptance and the trigger efficiency of the apparatus; eventually, the total number of $K^{\pm}$ decays in the 98 m-long fiducial region for the analysed data sample is found to be $N_K=(1.57\pm0.05)\times10^7$, where the external uncertainty on the π^0_D decay branching fraction dominates the error on N_K.

Fig. 3 shows the reconstructed spectra of the e^+e^- invariant mass for the $K_{2\pi}$ selection, while Fig. 4 displays the same reconstructed spectra for the $K_{\mu 3}$ selection; in addition to the two single selections, a joint dark photon selection is taken into account and considered passed whenever an event fulfils either the $K_{2\pi}$ or the $K_{\mu 3}$ requirements. The acceptance of the joint selection for any process is equal to the sum of the acceptances of the two mutually exclusive individual selections.

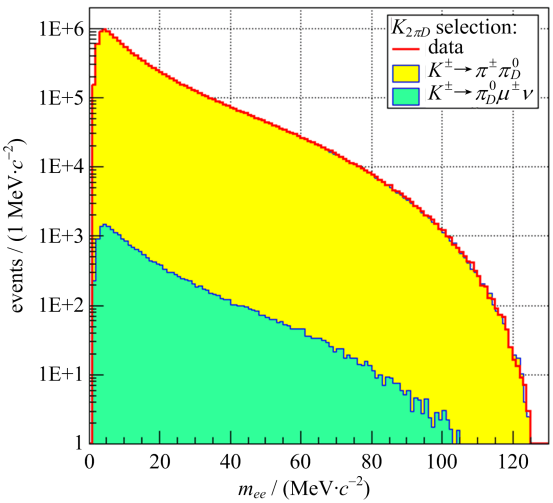

Fig. 3　Data and MC reconstructed invariant mass m_{ee} for events passing the $K_{2\pi}$ selection

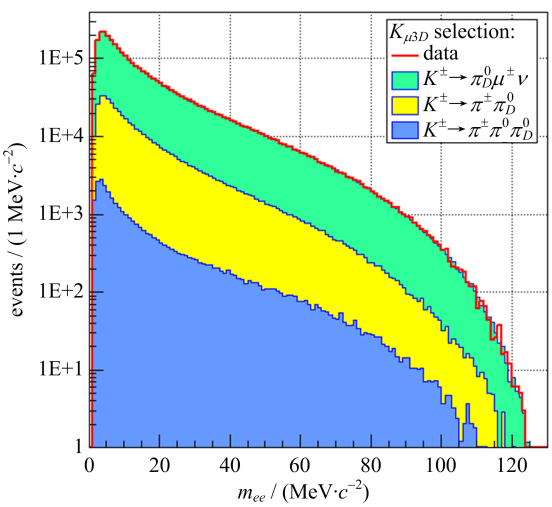

Fig. 4　Data and MC reconstructed invariant mass m_{ee} for events passing the $K_{\mu 3}$ selection

3　The π^0 Dalitz simulation

The π^0_D decay is simulated using the following lowest-order differential decay rate:

$$\frac{\mathrm{d}^2\Gamma}{\mathrm{d}x\mathrm{d}y}=\Gamma_0\frac{\alpha}{\pi}\mid F(x)\mid^2\frac{(1-x)^3}{4x}\left(1+y^2+\frac{r^2}{x}\right) \tag{5}$$

where x and y are two kinematic variables defined as:

$$x=\frac{(q_1+q_2)^2}{m_\pi^2}=\frac{m_{ee}^2}{m_{\pi^0}^2},\ y=\frac{2p(q_1-q_2)}{m_{\pi^0}(1-x)} \tag{6}$$

In these definitions, $r=2m_e/m_{\pi^0}$, whereas q_1, q_2 and p are the four-momenta of the opposite-charged electrons and the neutral pion; Γ_0 is the rate of the $\pi^0\to\gamma\gamma$ decay, and $F(x)$ is the transition form factor (TFF) of the pion.

According to the classical approach of Mikaelian and Smith[8], one can implement radiative corrections to the differential decay rate, which is thereby modified using the following formula:

$$\frac{\mathrm{d}^2\Gamma^{rad}}{\mathrm{d}x\mathrm{d}y}=\delta(x,y)\frac{\mathrm{d}^2\Gamma}{\mathrm{d}x\mathrm{d}y} \tag{7}$$

which does not take into account the emission of inner bremsstrahlung photons.

The TFF is conventionally parametrised as $F(x)=1+ax$, where the slope parameter of the TFF, a, is expected to be of about 0.03, according to vector meson dominance models; detailed theoretical computations based on the dispersion theory yield $a=0.030\,7\pm0.000\,6$[9]. Experimentally, the Particle Data Group provides a measurement of $a=0.032\pm0.004$[10], mainly determined by the CELLO experiment[11], which measured the rate of the $e^+e^-\to e^+e^-\pi^0$ process in the space-like region.

However, the precision on the Mikaelian and Smith radiative corrections to the π^0_D decay is limited. Indeed, the measured TFF slope lacks a further correction, due to two-photon exchange, which is estimated to be $\Delta a=+0.005$[12]. For this reason, the description of the backgrounds cannot benefit from precise inputs on the TFF slope[9-10]; therefore, by fitting the data of the m_{ee} spectrum itself, an effective TFF slope is obtained and used to get a satisfactory background description, as evaluated by a χ^2 test, over the range $m_{ee}>10$ MeV/c^2, the one used in the search for the dark

photon. The acceptance computation in the m_{ee} region is less robust due to two reasons: the abruptly falling geometrical acceptance at low values of m_{ee} and the decreasing efficiency in identifying electrons at low momentum; this accounts for the fact that the m_{ee} region is not considered for the aforementioned purpose.

4 Search for the dark photon

In the mass range 9 MeV/$c^2 \leqslant m_{A'} <$ 120 MeV/c^2, a scan to search for dark photon signals is performed. The limited precision of MC simulations on backgrounds at low mass affects the lower extent of the considered mass range, whereas the signal acceptance drops to zero at the upper limit of the range. The mass step of the scan and the width of the mass window for the dark photon signal, around the assumed mass, are determined by the resolution δm_{ee} on the $e^+ e^-$ invariant mass, which is a function of m_{ee} to be evaluated with MC simulations; this function is parametrised as $\sigma_m(m_{ee}) = 0.067\ \text{MeV}/c^2 + 0.010\ 5 m_{ee}$, and varies between 0.16 MeV/c^2 and 1.33 MeV/c^2 over the mass range of the scan, whose mass step is set to be $\sigma_m/2$, while the mass window of the signal region, for each hypothesis on the dark photon mass, is defined as $\pm 1.5\sigma_m$ around the assumed mass. The width of such a mass window has been optimised via MC simulations, in order to obtain the highest possible sensitivity to the dark photon signal; both the fluctuation of π^0_D background and the signal acceptance contribute to the determination of the sensitivity.

Each mass value of the dark photon is considered, studying the number of observed events passing the joint selection, N_{obs}, and comparing them to the expected number of background events, N_{exp}. The latter is evaluated from MC simulations and corrected for the trigger efficiency, as measured from control data samples passing the joint selection. Fig. 5 shows the numbers of observed and expected events for each mass value and their estimated uncertainties, δN_{obs} and δN_{exp}, the former being equal to $\sqrt{N_{obs}}$, because of its statistical origin; on the other hand, the generated MC sample is rather limited, contributing to the determination of δN_{exp}, together with the statistical errors on the trigger efficiencies, measured in the signal region of the dark photon. One can evaluate the local statistical significance of the dark photon signal for each mass value (Fig. 6):

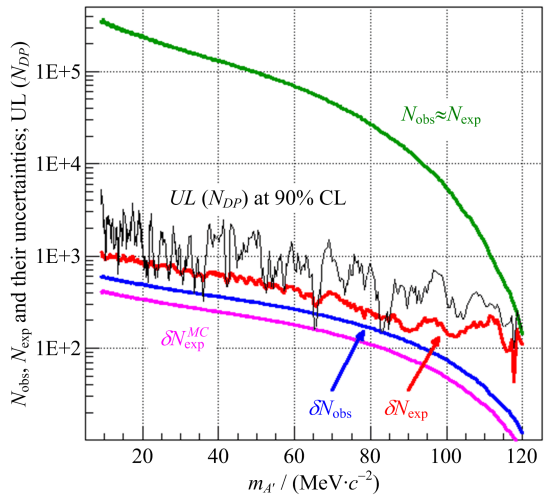

Fig. 5 Numbers of observed data events and expected π^0_D background events passing the joint selection (indistinguishable in a logarithmic scale), estimated uncertainties and obtained upper limits at 90% CL on the numbers of dark photon candidates (N_{DP}) for each mass value $m_{A'}$

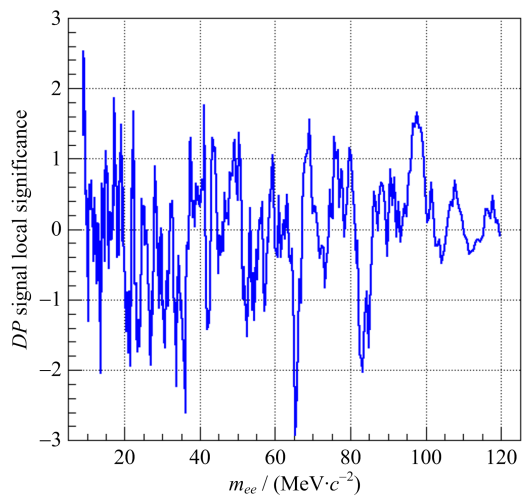

Fig. 6 Estimated local significance of the dark photon signal for each A' mass value

$$Z = (N_{obs} - N_{exp}) / \sqrt{(\delta N_{obs})^2 + (\delta N_{exp})^2} \quad (8)$$

The measurements of N_{obs}, N_{exp} and δN_{exp} allow for the computation of confidence intervals at

90% CL on the number of $A' \to e^+ e^-$ decay candidates, called N_{DP}, for each mass hypothesis; this calculation is performed by using the Rolke-Lopez method[13], assuming Poissonian (Gaussian) errors on the number of observed (expected) events.

Furthermore, under the assumption $BR(A' \to e^+ e^-) = 1$, one can also compute upper limits at 90% CL on the branching fraction $BR(\pi^0 \to A'\gamma)$, considering each mass value of the dark photon; the above-mentioned presumption is a good approximation for $m_{A'} < 2m_\mu$, in case that A' decays to SM fermions only. Said upper limits are calculated making use of the following relation:

$$BR(\pi^0 \to A'\gamma) = \frac{N_{DP}}{N_K e_1 e_2 [BR(K_{2\pi}) A_{DP}(K_{2\pi}) + BR(K_{\mu 3}) A_{DP}(K_{\mu 3}) + 2BR(K_{3\pi}) A_{DP}(K_{3\pi})]} \quad (9)$$

where $A_{DP}(K_{2\pi})$, $A_{DP}(K_{\mu 3})$ and $A_{DP}(K_{3\pi})$ are the acceptances of the joint selection for $K_{2\pi}$, $K_{\mu 3}$ and $K_{3\pi}$ decays, respectively, followed by the $\pi^0 \to A'\gamma$, $A' \to e^+ e^-$ decay chain; e_1 and e_2 are the trigger inefficiencies, which have been taken into account neglecting their variations over the m_{ee} invariant mass.

One can consider the angle between the e^+ momentum (in the e^+e^- rest-frame) and the e^+e^- momentum (in the π^0 rest-frame); studying the distribution of the angle between the two momenta, one can observe that they are identical for both the dark photon (that is $\pi^0 \to A'\gamma$, $A' \to e^+e^-$) and the π^0_D decays, up to a negligible effect of the radiative corrections, which does not have to be applied in the former case, since the acceptance was found to be affected by 1% by it. Therefore, MC samples for background description are used to evaluate the dark photon acceptances, so that no dedicated MC productions are required in this analysis.

Fig. 7 displays the resulting signal acceptances for the $\pi^0 \to A'\gamma$ decay, while Fig. 8 shows the upper limits on the branching ratio of the latter process, these being $O(10^{-6})$ and not exhibiting a strong dependence on $m_{A'}$.

In Fig. 9, one can observe the upper limits at 90% CL on the mixing parameter ϵ^2, for each mass value of the dark photon, as computed from the upper limits on $BR(\pi^0 \to A'\gamma)$, by using Eq. (2); in the same figure, one can also have a glance on the constraints obtained by SLAC E141 and

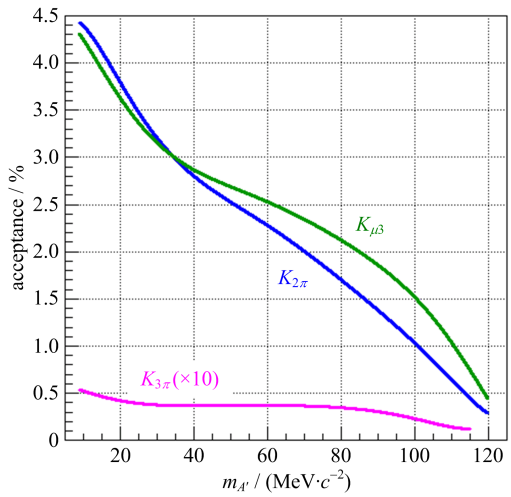

The $K_{3\pi}$ acceptance is scaled by 10 for visibility purposes.

Fig. 7　Acceptances of the joint dark photon selection for $K_{2\pi}$, $K_{\mu 3}$ and $K_{3\pi}$, depending on the assumed mass of the dark photon, evaluated with MC simulations

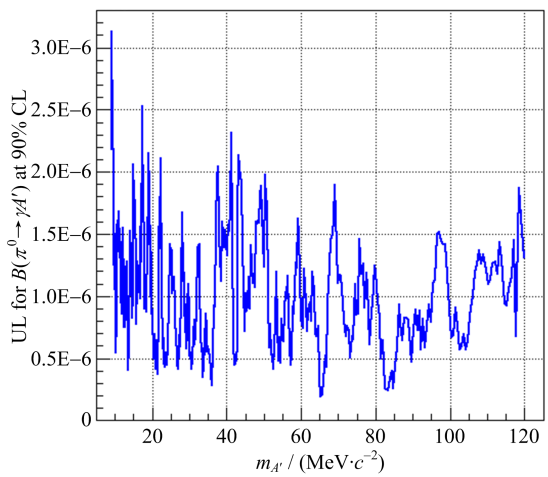

Fig. 8　Obtained upper limits on $BR(\pi^0 \to A'\gamma)$ at 90% CL, for each mass value of A'

FNAL E774[15], KLOE[16], WASA[17], HADES[18], A1[19], APEX[20] and BaBar[21]

experiments. On the ($m_{A'}$, ϵ^2) plane, a band between the two curved lines is displayed; if the discrepancy between the measured and the calculated values for the anomalous magnetic moment of the muon lies in the $\pm 2\sigma$ range, the anomaly could be explained taking into account scenarios involving the presence of dark photons. Likewise, a region accounting for the anomalous magnetic moment of the electron is visible[3,22].

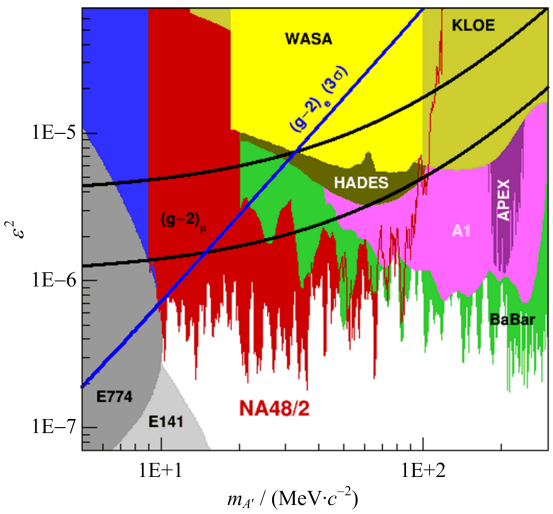

Between the black lines, the band accounts for the muon anomalous magnetic moment ($(g-2)_\mu$), whereas the blue line marks the region which could explain the anomaly of the magnetic moment of the electron ($(g-2)_e$)[14].

Fig. 9 The NA48/2 upper limits at 90% CL on the mixing parameter ϵ^2 versus $m_{A'}$, compared to the results on exclusion limits from meson decays, as published by SLAC E141, FNAL E774, KLOE, WASA, HADES, A1, APEX and BaBar experiments

The upper limits on ϵ^2 obtained from the present analysis represent an improvement over the existing data in the dark-photon mass range 9～70 MeV/c^2 and exclude the whole region of $(g-2)_\mu$[14], in the hypothesis that the dark photon can only decay into SM particles. The irreducible π^0_D background limits the sensitivity of the search for the prompt A' decay. Moreover, the achievable upper limit on ϵ^2 scales as the inverse square root of the integrated beam flux; this means that the technique with which this analysis was carried out, if applied to larger samples of K^+, as will be collected by the NA62 experiment at CERN[23] in 2015 ～ 2018, could lead to rather modest improvements in future results.

References

[1] BATLEY J R, CULLING A J, KALMUS G, et al. Search for direct CP violating charge asymmetries in $K^\pm \to \pi^\pm \pi^+ \pi^-$ and $K^\pm \to \pi^\pm \pi^0 \pi^0$ decays[J]. Eur Phys J C, 2007,52: 875-891.

[2] HOLDOM B. Two U(1)'s and ε charge shifts[J]. Phys Lett B,1996,166: 196-198.

[3] POSPELOV M. Secluded U(1) below the weak scale [J]. Phys Rev D,2009,80: 095002.

[4] RAGGI M, KOZHUHAROV V. Results and perspectives in dark photon physics [J]. Riv Nuovo Cimento,2015, 38(10): 449-505.

[5] BATELL B, POSPELOV M, RITZ A. Exploring portals to a hidden sector through fixed targets[J]. Phys Rev D,2009,80:095024.

[6] BATELL B, POSPELOV M, RITZ A. Direct detection of multicomponent secluded WIMPs[J]. Phys Rev D, 2009,79: 115019.

[7] FANTI V, LAI A, MARRAS D, et al. The beam and detector for the NA48 neutral kaon CP violation experiment at CERN[J]. Nucl Instrum Meth A,2007, 574 :433-471.

[8] MIKAELIAN K O, SMITH J. Radiative Corrections to the Decay $\pi^0 \to \gamma e^+ e^-$ [J]. Phys Rev D, 1972, 5: 1763.

[9] HOFERICHTER M , KUBIS B, LEUPOLD S, et al. Dispersive analysis of the pion transition form factor [J]. Eur Phys J C,2014,74: 3180.

[10] OLIVE K A, AGASHE K, AMSLER C, et al. Review of particle physics [J]. Chin Phys C, 2014, 38 (09): 090001.

[11] BEHREND H J, CRIEGEE L, FIELD J H, et al. A measurement of the π^0, η and η' electromagnetic form factors[J]. Z Phys C,1991,49: 401-409.

[12] KAMPF K, KNECHT M, NOVOTN J. The Dalitz decay$\pi^0 \to e^+ e^- \gamma$ revisited[J]. Eur Phys J C, 2006, 46:191-217.

[13] ROLKE W A, LOPEZ A M. Confidence intervals and upper bounds for small signals in the presence of background noise [J]. Nucl Instrum Meth A, 2001, 458:745-758.

[14] BATLEY J R, KALMUS G, LAZZERONI C, et al. Search for the dark photon in π^0 decays[J]. Phys Lett B,2015,746:178-185.

(下转第 624 页)

Article ID:0253-2778(2016)07-0601-07

Search for dark photon and long-lived particles at BaBar

LUSIANI A.[1,2](for the BaBar Collaboration)

(1. *Scuola Normale Superiore*, *piazza dei Cavalieri* 7, *Pisa PI* 56125, *Italy*;
2. *Instituto Nazionale di Fisica Nucleare*, *sezione di Pisa*, *Largo Bruno Pontecorvo* 3, 56127 *Pisa PI*, *Italy*)

Abstract: The complete large and clean sample of e^+e^- collisions recorded by the BaBar detector at PEP-II at the SLAC National Laboratory was used to search for a photon-like particle with mass and decaying into an e^+e^- or $\mu^+\mu^-$ pair, which is proposed in some Dark Matter theory models, and to search for a long-lived particle that decays into an oppositely charged fermion pair, predicted in a number of New Physics models. We do not observe a significant signal and we set 90% confidence level upper limits of several production rates and on the parameters of some proposed New Physics models.

Key words: New Physics; Dark Matter; B-factory

CLC number: O572.3 **Document code**: A doi:10.3969/j.issn.0253-2778.2016.07.010

Citation: LUSIANI A. Search for dark photon and long-lived particles at BaBar[J]. Journal of University of Science and Technology of China, 2016,46(7):601-607.

BaBar 实验寻找暗光子和长寿命粒子

LUSIANI A.[1,2](BaBar 合作组)

(1. 高等师范学校,比萨 56125,意大利;2. 意大利国家核物理研究院,比萨 56127,意大利)

摘要:我们用 SLAC 国家实验室 PEP-II 上的 BaBar 探测器记录的全部大量干净的 e^+e^- 对撞事例,寻找一些暗物质理论模型提出的一种具有质量、衰变到e^+e^-或$\mu^+\mu^-$对的类光子粒子,并寻找很多新物理模型中预言的衰变到带相反电荷的费米子对的长寿命粒子.我们没有观测到信号,因此我们在 90%的置信度下给出了几种产生率和一些新物理模型参数的上限.

关键词:新物理;暗物质;B 工厂

0 Introduction

Well motivated New Physics (NP) models predict the existence of several new particles that are not yet excluded by experiment. The BaBar experiment has collected large samples of clean e^+e^- collisions with a general purpose full solid-angle detector at and around the $\Upsilon(4S)$ on the PEP-II storage ring at the SLAC National Laboratory. This data sample is well suited to search for kinematically allowed NP particles that are rarely produced and may have escaped previous searches. The results of two recent searches for NP light particles with BaBar are reported in the following.

Received:2015-11-30;**Revised**:2016-04-20

Biography:LUSIANI A., PhD. Research field: high energy physics. E-mail: alberto.lusiani@pi.infn.it

1 Search for dark photon into $e^+ e^-$ or $\mu^+ \mu^-$

Light NP particles may be loosely coupled with ordinary matter through "portals"[1], which provide interactions between the Standard Model (SM) fields and "dark" fields, which can be scalar, pseudoscalar, vector or spin 1/2 fermions. A model for weakly interacting Dark Matter particles predicts[2] the existence of a "Dark Photon" A' with mass around 1 GeV, which interacts with the SM particles via a "kinetic mixing" term $\Delta\mathscr{L}=(\epsilon/2)F^{Y,\mu\nu}F'_{\mu\nu}$, with a coupling constant $\epsilon \ll 1$.

A search for A' production in the process $e^+e^- \to \gamma A' \to \gamma l^+ l^-$ ($l^\pm = e^\pm$ or $\mu^\pm$, as shown in Fig. 1) has been conducted on the whole BaBar data sample of 514 fb^{-1}[3]. The A' branching ratios into $l^+ l^-$ are expected to be sizeable over the whole hypothetical mass range[4] (see also Fig. 2). With respect to the process $e^+e^- \to \gamma\gamma$, the cross-section for this process is reduced by a factor ϵ^2.

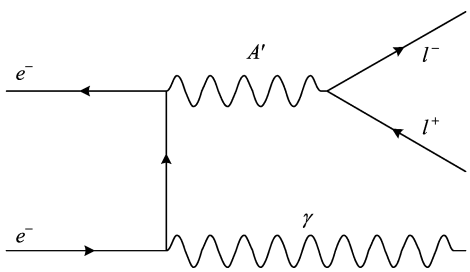

Fig. 1 Diagram for $e^+ e^- \to \gamma A' \to \gamma l^+ l^-$

We select events with a final state containing two oppositely-charged leptons and a photon and do a kinematic fit of the reconstructed track parameters to match the center-of-mass (CM) energy with the constraint that all three particles come from the interaction point (IP). We suppress background removing events consistent with having an electron conversion and requiring a good-quality photon. According to simulation, which is consistent with the data, the selection efficiency is typically 15% (35%) for the electron pair (muon pair) channel.

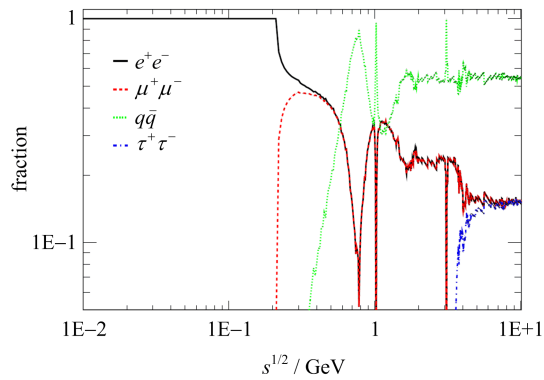

Fig. 2 Branching fraction predictions for $A' \to l^+ l^-$ and $A' \to q\bar{q}$ as a function of $m_{A'}$ [4]

We search for a signal peak on top of a smooth background in the lepton pair invariant mass. The SM background yield is fitted from the sidebands, to avoid the need of an accurate simulation. We nevertheless perform a Monte Carlo (MC) simulation and find that the simulation is reasonably accurate except in the m_{ee} low-mass region, where radiative Bhabha simulation (performed with BHWIDE[5]) is known to be relatively less reliable. Further details are in the BaBar publication[3]. In order to get a smoother behaviour at threshold, we consider for muons the reduced mass $m_R = \sqrt{(m^2_{l^+\mu^-} - 4\,m^2_\mu)}$ rather than the invariant mass. Fig. 3 shows the mass and reduced mass distributions in data and simulation.

We fit the signal yield on about 5 500 steps in the mass m, with a variable step size close to half the mass resolution, and on mass intervals 20～30 times broader than the mass resolution. We use a likelihood function that includes a signal peak centered on m over a polynomial background. The signal peak shape depends on the mass and is interpolated from simulated events, which are tuned by comparing data and simulation on known resonances.

In the vicinity of known resonances [ω, ϕ, J/ψ, $\psi(2S)$, $\Upsilon(1S,2S)$], the resonance peaks are excluded from the scan, the resonance is fitted on data, and the resonance tails are added to the likelihood in addition to the signal and non-peaking background components. For the ω and ϕ

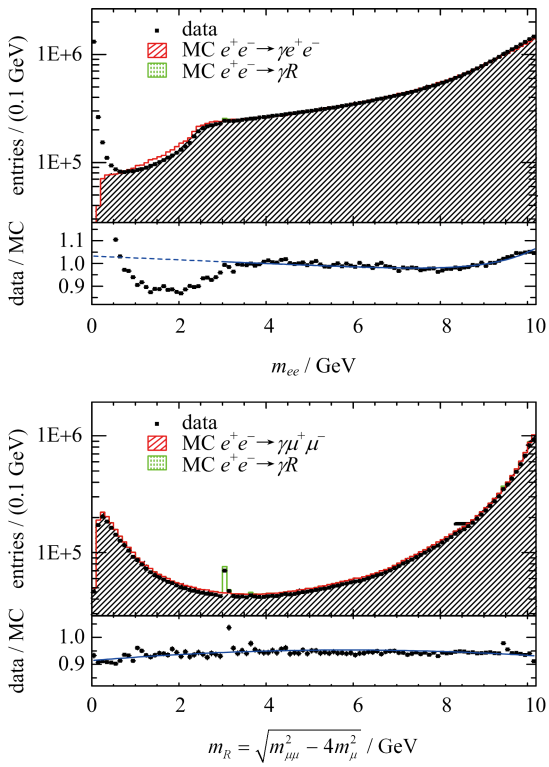

On the bottom the data/simulation ratio is reported.

Fig. 3 Electron pair mass spectrum (top) and muon pair reduced mass spectrum (bottom) for data and simulation

resonances, their interference with the non-resonant channel is also fitted and used in the maximum likelihood fits of the neighouring masses.

In the fit, the signal component can be negative, but the total probability density is constrained to be non-negative. We determine the "local" significance of each fit as $S=\sqrt{2\log(L/L_0)}$, where L and L_0 are the maximum likelihood values for fits with and without freely varying signal, respectively. The largest local significance is 3.4σ (2.9σ) for electron pairs (muon pairs). Since we search for signal in many mass hypotheses, we estimate the significance of the whole scan by determining the trial factors with a large sample of simulated Monte Carlo experiments. With this correction, the "global" significance of the two scans is 0.57 (0.94) for electron pairs (muon pairs).

In absence of signal evidence, we compute 90% confidence level (CL) Bayesian upper limits on the cross-section $e^+e^-\to\gamma A'$, combining both channels. The determination uses the BaBar luminosity (with $\sim$ 0.6% uncertainty), the estimated efficiency (with 0.5%$\sim$4% uncertainty) and the predicted branching fractions in Ref. [4] (with 0.1%$\sim$4% uncertainty) and models the respective uncertainties with Gaussian distributions. The muon pair final state search is significantly more powerful than the electron pair for $m>212$ MeV because its backgrounds are smaller. From the cross-section limits we derive limits on the Dark Photon coupling constant ϵ as a function of its mass m according to Ref. [4]. Results are shown in Fig. 4.

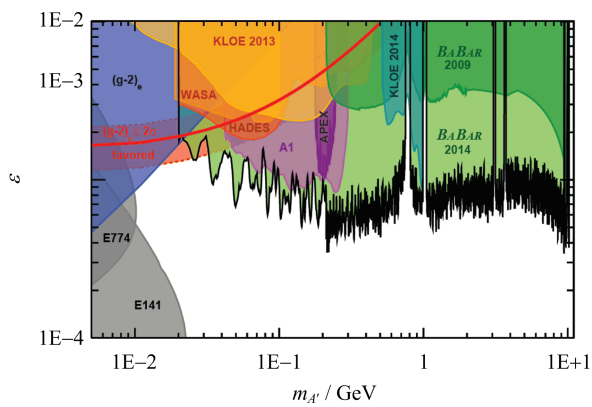

The values required to explain the discrepancy between the calculated and measured anomalous magnetic moment of the muon[6] are displayed as a red line.

Fig. 4 Upper limit (90% CL) on the mixing strength ϵ as a function of the dark photon mass

Bounds in the range $10^{-4}\sim10^{-3}$ for $0.02<m_{A'}<10.2$ GeV are set, significantly improving previous constraints derived from beam-dump experiments[7-9], the electron anomalous magnetic moment[10], KLOE[11-12], WASA-at-COSY[13], HADES[14], A1 at MAMI[15], and the test run from APEX[16].

These results improve and supersede existing constraints obtained from a BaBar search for a light *CP*-odd Higgs boson[17-18] using a smaller dataset. We reduce the experimentally allowed parameter space that could explain with a Dark Photon the discrepancy between the calculated and measured

anomalous magnetic moment of the muon[6].

2 Search for long-lived particles in e^+e^- collisions

When NP particles are weakly coupled to standard matter, they can be long-lived if they are restricted to decay to SM particles[19]. Recent anomalous astrophysical observations have induced the elaboration of several NP models that include low-mass, long-lived hidden-sector states, such as dark photons[19-22], an inflaton[23], supersymmetry[24-25], a dark Higgs boson[26] and with other dark-sector states[27].

Experiments have mostly searched for such long-lived particles at small masses under 1 GeV[8,28-29] and in the multi-GeV mass range[30-34]. The BaBar collaboration has completed a search that is sensitive to masses O(GeV)[35].

At the B factories, a hidden-sector scalar particle may be produced in an Υ radiative decay or in a B penguin decay and, in turn, may decay into a pair of fermions as shown in Fig. 5.

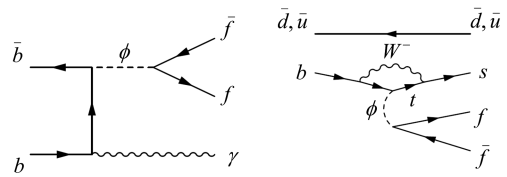

Fig. 5 Lowest-order diagrams for the production of a long-lived dark scalar particle in radiative Υ decays (left) and in penguin decays of B mesons (right)

We completed a model-independent search for inclusive production of a long-lived particle L in the process $e^+e^-\to LX$, where L decays at a displaced vertex into any of six different final states, e^+e^-, $\mu^+\mu^-$, $e^\pm\mu^\mp$, $\pi^+\pi^-$, K^+K^- and $K^\pm\pi^\mp$. Except for 20 fb^{-1} taken at the Υ(4S), which where used to test the analysis, we use the entire BaBar data collected at the Υ(4S), 40 MeV below the Υ(4S) peak, at the Υ(2S), and Υ(3S), corresponding to a luminosity of 489.1 fb^{-1}.

We reconstruct L from two oppositely-charged tracks that originate from a common vertex with distance to the beam line in the transverse plane from 1 to 50 cm. The resolution on the radial distance of the fitted vertex must be smaller than 0.2 cm. We require that both tracks have impact parameters with respect to the beam line larger than 3 times the resolution. We reject background from K^0_S and Λ decays, and we skip searching for signal in several low-mass regions with problematic structures in the mass distribution by requiring, depending on the final state, that $m_{e^+e^-}>0.44$ GeV, $m_{\mu^+\mu^-}<0.37$ GeV or $m_{\mu^+\mu^-}>0.5$ GeV, $m_{e^\pm\mu^\mp}>0.48$ GeV, $m_{\pi^+\pi^-}>0.86$ GeV, $m_{K^+K^-}>1.35$ GeV, and $m_{K^\pm\pi^\mp}>1.05$ GeV. According to a Monte Carlo simulation, surviving background consists primarily of hadronic events with high track multiplicity, where large-d_0 tracks originate mostly from K^0_S, Λ, $K^\pm$, and $\pi^\pm$ decays, as well as particle interactions with detector material. Random overlaps of such tracks comprise the majority of the background candidates.

Fig. 6 shows the mass distributions of the signal candidates (with uniform mass bins) together with the respective background PDFs.

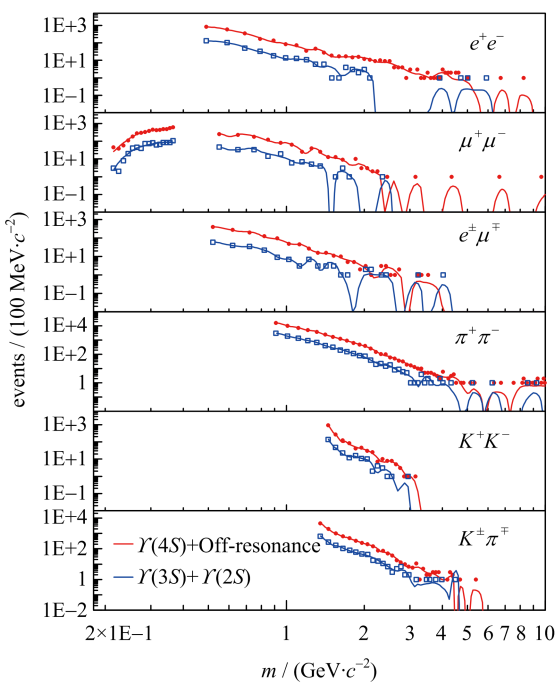

Fig. 6 Observed mass distribution for Υ(4S) +off-resonance data (red solid points), for Υ(3S) + Υ(2S) data (blue open squares) as a function of mass m for each final state with the background PDF P_B overlaid (red, blue solid lines)

We scan for a signal mass peak over a smooth background with an extended unbinned maximum likelihood fit with a polynomial background and a signal peak corresponding to a mass m whose shape and width we determine from a Monte Carlo simulation for 11 mass hypotheses. We repeat the fit in steps of 2 MeV. We determine the significance of the signal yield as $S = \sqrt{2\log(L / L_0)}$, where L and L_0 are the maximum likelihood values for fits with and without freely varying signal, respectively.

For each final state mass scan, we determine the background-only hypothesis p-values of the largest found signal significances with positive signal yields using a large amount of background-only toy Monte Carlo simulations. No evidence of signal was found, hence we compute upper limits on the product $\sigma(e^+e^-\to LX)\mathcal{B}(L\to f)\epsilon(f)$ using the signal yield and the estimated BaBar integrated luminosity. We determine the signal yield profile likelihood using convolutions with Gaussians to account for systematic uncertainties on the signal efficiency (obtained from a Monte Carlo simulation) and on the background likelihood term. We obtain Bayesian 90% CL upper limits using a flat prior, shown in Fig. 7.

For the purpose of testing specific NP models, the signal efficiency has been estimated with a Monte Carlo simulation using 11 L masses. The simulation used lifetime large enough to populate the acceptance in the radial distance of the displaced vertex. With appropriate weighting, shorter signal lifetimes are then properly simulated. The estimated signal efficiencies as a function of the mass, the lifetime and the transverse momentum are provided to allow model testing[35].

We used the results to set constraints on a specific model where L is produced in B decays via $B\to L\ X_s$ where X_s is a hadronic state with strangeness $S=-1$ as in Higgs portal[23-26] and axion-portal[36] models of dark matter. By

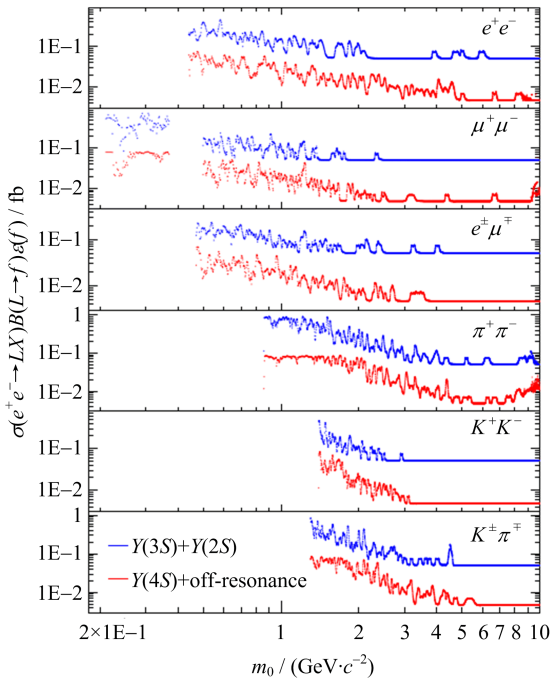

Fig. 7 90% CL upper limits on $\sigma(e^+e^-\to LX)\mathcal{B}(L\to f)\varepsilon(f)$ for each final state f as a function of L mass for $\Upsilon(4S)$ data (lower red curves) and for $\Upsilon(3S)+\Upsilon(2S)$ data (upper blue curves)

simulating the detection efficiency with this production model, we obtained limits on the product branching fraction $\mathcal{B}_{Lf}=\mathcal{B}(B\to L\ X_s)\cdot\mathcal{B}(L\to f)$, shown in Fig. 8. These limits exclude a significant region of the parameter space of the inflaton model[23].

3 Conclusion

The e^+e^- collision data recorded by BaBar have been used to search for new particles that are predicted by several New Physics models. We did not find evidence for any signal beyond the Standard Model and we obtained significant experimental constraints to present and future theory models.

No dark photon has been found in the 0.02～10.2 GeV mass region, constraining the kinetic mixing parameter ϵ to be less than 10^{-4} to 10^{-3} depending on the dark photon mass.

We did not find evidence of non-SM long-lived particle in the 0.2 GeV$<m<$10 GeV mass range and proper decay lengths of 0.5 cm$<c\tau<$100 cm

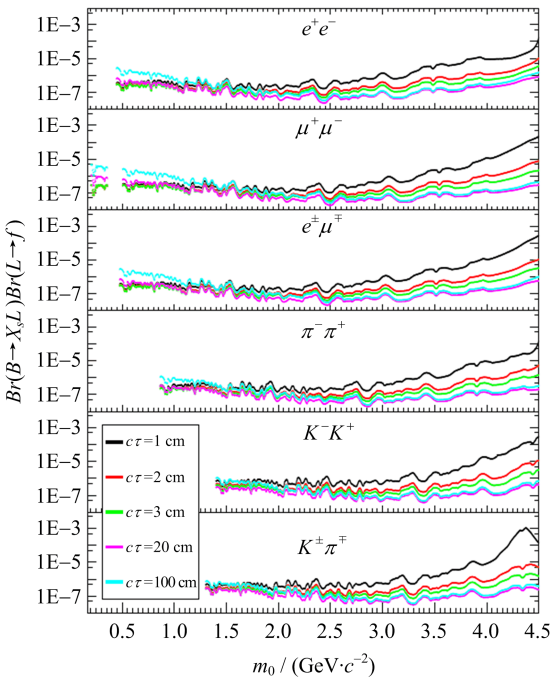

Fig. 8 Upper limits on $\mathcal{B}_{Lf} = \mathcal{B}(B\to L X_s)\cdot\mathcal{B}(L\to f)$ as a function of the L mass for a selection of lifetimes

and we published appropriate 90% CL upper limits on the product $\sigma(e^+e^-\to LX)\cdot\mathcal{B}(L\to f)\cdot\epsilon_f$.

Belle has collected about twice the amount of BaBar events, and has good prospects of improving part of the above measurements. BelleII with 50 ab^{-1} and an improved trigger for light New Physics searches will be able to ameliorate all the presented limits by one order of magnitude or more.

References

[1] ESSIG R, JAROS J A, WESTER W, et al. New light, weakly-coupled particles[C]//Planning the Future of U. S. Particle Physics: SLAC-PUB-15960. Menlo Park, CA, USA: SLAC, 2013: 71-76.

[2] HOLDOM B. Two U(1)'s and Charge Shifts[J]. Phys Lett B, 1986, 166: 196-198.

[3] LEES J P, POIREAU V, TISSERAND V, et al. Search for a dark photon in e^+e^- collisions at BaBar [J]. Phys Rev Lett, 2014, 113(20): 201801.

[4] POSPELOV M, RITZ A, VOLOSHIN M B. Secluded WIMP darkmatter[J]. Phys Lett B, 2008, 662: 53-61.

[5] JADACH S, PLACZEK W, WARD B F L. BHWIDE 1.00: O(α) YFS exponentiated Monte Carlo for Bhabha scattering at wide angles for LEP1 / SLC and LEP2[J]. Phys Lett B, 1997, 390: 298-308.

[6] POSPELOV M. Secluded U(1) below the weak scale [J]. Phys Rev D, 2009, 80: 095002.

[7] BLÜMLEIN J, BRUNNER J. New exclusion limits for dark gauge forces from beam-dump data[J]. Phys Lett B, 2011, 701: 155-159.

[8] ANDREAS S, NIEBUHR C, RINGWALD A. New limits on hidden photons from past electron beamdumps [J]. Phys Rev D, 2012, 86: 095019.

[9] BLÜMLEIN J, BRUNNER J. New exclusion limits on dark gauge forces from proton Bremsstrahlung in beam-dump data[J]. Phys Lett B, 2014, 731: 320-326.

[10] ENDO M, HAMAGUCHI K, MISHIMA G. Constraints on hidden photon models from electron $g-2$ and hydrogen spectroscopy[J]. Phys Rev D, 2012, 86: 095029.

[11] BABUSCI D, BADONIR D, BALWIERZ-PYTKO I, et al. Limit on the production of a light vector gauge boson in ϕ meson decays with the KLOE detector[J]. Phys Lett B, 2013, 720: 111-115.

[12] BABUSCI D, BALWIERZ-PYTKOG I, BENCIVENNI G, et al. Search for light vector boson production in $e^+e^-\to\mu^+\mu^-\gamma$ interactions with the KLOE experiment [J]. Phys Lett B, 2014, 736: 459-464.

[13] ADLARSON P, AUGUSTYNIAK W, BARDAN W, et al. Search for a dark photon in the $\pi^0\to e^+e^-\gamma$ decay [J]. Phys Lett B, 2013, 726: 187-193.

[14] AGAKISHIEV G, BALANDAC A, BELVER D, et al. Searching a dark photon with HADES[J]. Phys Lett B, 2014, 731: 265-271.

[15] MERKEL H, ACHENBACH P, AYERBE GAYOSO C, et al. Search at the Mainz Microtron for light massive gauge bosons relevant for the muon $g-2$ anomaly[J]. Phys Rev Lett, 2014, 112(22): 221802.

[16] ABRAHAMYAN S, AHMED Z, ALLADA K, et al. Search for a new gauge boson in electron-nucleus fixed-target scattering by the APEX experiment[J]. Phys Rev Lett, 2011, 107: 191804.

[17] AUBERT B, KARYOTAKIS Y, LEES J P, et al. Search for dimuon decays of a light scalar boson in radiative transitions $\Upsilon\to\gamma A^0$ [J]. Phys Rev Lett, 2009, 103: 081803.

[18] BJORKEN J D, ESSIG R, SCHUSTER P, et al. New fixed-target experiments to search for dark gauge forces [J]. Phys Rev D, 2009, 80: 075018.

[19] SCHUSTER P, TORO N, YAVIN I. Terrestrial and solar limits on long-lived particles in a dark sector[J]. Phys Rev D, 2010, 81: 016002.

[20] BATELL B, POSPELOV M, RITZ A. Probing a Secluded U(1) at B factories[J]. Phys Rev D, 2009, 79: 115008.

[21] ESSIG R, SCHUSTER P, TORO N. Probing dark

forces and light hidden sectors at low-energy e^+e^- colliders[J]. Phys Rev D, 2009, 80:015003.

[22] BOSSI F. Dark photon searches using displaced vertices at low energy e^+e^- colliders[J]. Adv High Energy Phys, 2014,2014:891820.

[23] BEZRUKOV F, GORBUNOV D. Light inflaton after LHC8 and WMAP9 results [J]. JHEP, 2013, 1307:140.

[24] CHEUNG C, NOMURA Y. Singlet portal to the hidden sector[J]. JHEP, 2010, 2010:103.

[25] SCHMIDT-HOBERG K, STAUB F, WINKLER M W. Constraints on light mediators: Confronting dark matter searches with B physics [J]. Phys Lett B, 2013, 727:506-510.

[26] CLARKE J D, FOOT R, VOLKAS RR. Phenomenology of a very light scalar (100 MeV$<m_h<$ 10 GeV) mixing with the SM Higgs[J]. JHEP, 2014, 1402:123.

[27] NELSON A E, SCHOLTZ J. Heavy flavor and dark sector[J]. Phys Rev D, 2015, 91:014009.

[28] GNINENKO S N. Stringent limits on the $\pi^0\to\gamma X$, $X\to e^+e^-$ decay from neutrino experiments and constraints on new light gauge bosons[J]. Phys Rev D, 2012, 85:055027.

[29] ADAMS T, ALTON A, AVVAKUMOV S, et al. Observation of an anomalous number of dimuon events in a high energy neutrino beam[J]. Phys Rev Lett, 2001,87:041801.

[30] ABAZOV V M, ABBOTT B, ABOLINS M, et al. Search for neutral, long-lived particles decaying into two muons in $p\bar{p}$ collisions at $\sqrt{s}=1.96$ TeV[J]. Phys Rev Lett, 2006, 97:161802.

[31] ABE F, AKIMOTO H, AKOPIAN A, et al. Search for long-lived parents of Z^0 bosons in $p\bar{p}$ collisions at $\sqrt{s}=1.8$ TeV[J]. Phys Rev D, 1998, 58:051102.

[32] AAD G , ABAJYAN T, ABBOTT B, et al. Searches for heavy long-lived sleptons and R-hadrons with the ATLAS detector in pp collisions at $\sqrt{s}=$ 7 TeV[J]. Phys Lett B, 2013, 720:277-308.

[33] AAD G, ABBOTT B, ABDALLAH J, et al. Search for a light Higgs boson decaying to long-lived weakly-interacting particles in proton-proton collisions at $\sqrt{s}=7$ TeV with the ATLAS detector[J]. Phys Rev Lett, 2012,108:251801.

[34] AAD G, ABAJYAN T, ABBOTT B, et al. Search for long-lived, heavy particles in final states with a muon and multi-track displaced vertex in proton-proton collisions at $\sqrt{s}=7$ TeV with the ATLAS detector[J]. Phys Lett B,2013, 719:280-298.

[35] LEES J P, POIREAU V, TISSERAND V, et al. Search for long-lived particles in e^+e^- collisions[J]. Phys Rev Lett, 2015, 114(17):171801.

[36] FREYTSIS M, LIGETI Z, THALER J. Constraining the axion portal with $B\to Kl^+l^-$ [J]. Phys Rev D, 2010, 81:034001.

Article ID:0253-2778(2016)07-0608-09

Precision hadron physis at the Mainz Microtron MAMI and MESA

DENIG Achim

(*Institute for Nuclear Physics and PRISMA Cluster of Excellence, Johannes Gutenberg University Mainz, 55099 Mainz, Germany*)

Abstract: The Mainz Microtron MAMI is a high-intensity electron accelerator for fixed-target experiments in the fields of hadron and low-energy particle physics. It provides a polarized beam of up to 1.6 GeV beam energy. Two major installations are currently in operation at MAMI: the high-resolution spectrometer setup A1 as well as the A2 detector setup, which consists of the Crystal Ball detector in conjunction with the TAPS calorimeter. Highlights of the research program at MAMI are measurements of the electromagnetic form factors and polarizabilities of the proton, which are related to the proton radius puzzle, the measurement of the transition form factors and slope parameters of the eta meson, as well as the search for hypothetical gauge bosons of the dark sector, also denoted as dark photons. Currently, the new electron accelerator MESA is in preparation at Mainz, which will allow for a precision measurement of the electroweak mixing angle at low momentum transfer as well as measurements of low-energy electron-nucleon/nucleus scattering for various applications in nuclear, hadron, and particle physics.

key words: hadron physics; electron scattering; electromagnetic form factors; polarizability; meson decays; proton radius; electroweak mixing angle; dark photon

CLC number: O572.3 **Document code**: A doi:10.3969/j.issn.0253-2778.2016.07.011

Citation: DENIG A. Precision hadron physis at the Mainz Microtron MAMI and MESA[J]. Journal of University of Science and Technology of China, 2016,46(7):608-616.

美因茨电子回旋加速器 MAMI 和 MESA 上的精细强子物理

DENIG Achim

(核物理研究所和 PRISMA 卓越中心,美因茨大学,美因茨 55099,德国)

摘要:美因茨电子回旋加速器 MAMI 是用于强子和低能粒子物理领域固定靶实验的高流强电子加速器.它提供了能量高达 1.6GeV 的极化束流.目前 MAMI 上两个主要的装置正在安装:高分辨谱仪 A1 和由晶体球探测器连同 TAPS 量能器组成的探测器 A2.在 MAMI 上研究规划的亮点是:测量质子的电磁形状因子和极化度,这会涉及质子半径困惑;η 介子的跃迁形状因子和斜率参数的测量;以及寻找假想的暗物质规范玻色子即暗光子.目前,美因茨的新电子加速器 MESA 正在准备之中,它将允许低动量传递下电弱混合角的精确测量及核、强子和粒子物理中各种低能电子—核子/原子核散射的测量.

关键词:强子物理;电子散射;电磁形状因子;极化度;介子衰变;质子半径;电弱混合角;暗光子

Received:2015-11-30;**Revised**:2016-04-20

Foundation item:Supported by German Research Foundation DFG under Collaborative Research Centre (CRC-1044).

Biography:DENIG Achim, male, born in 1968, PhD/Prof. Research field: nuclear and particle physics. E-mail: denig@kph.uni-mainz.de

1 The MAMI and MESA facilities

1.1 The MAMI facility

The Mainz Microtron MAMI is a continuous-wave (CW) electron accelerator for beam energies of up to 1.604 GeV[1-2]. It is operated as a university accelerator by the Institute for Nuclear Physics of the Johannnes Gutenberg University (JGU) of Mainz. MAMI is constructed as a cascade of four microtrons, of which the last stage, the harmonic double-sided microtron MAMI-C, represents a new concept in microtron accelerator technology. The beam intensity (up to ≈100 μA), the beam polarization (up to 85%), and the energy resolution (0.1 MeV) are among the highest in the world. Also, the availability of the accelerator, which is routinely operated by students, is very high with approximately 7000 hours of beam delivered for the users per year. Currently, two major installations are operated at MAMI, the electron scattering experiment A1 as well as the A2 experiment at the tagged photon beam facility.

1.1.1 The A1 electron scattering experiment

The A1 experiment consists of three high-resolution magnetic spectrometers, allowing for coincidence electron scattering experiments[3]. The spectrometers with a weight of 300 tons each, can be rotated around a common pivot. They have a maximum momentum coverage of up to 870 MeV/c, spatial acceptances of 28 msr and an outstanding momentum resolution of 10^{-4}. The focal planes of the spectrometers comprise drift chambers, scintillators as timing detectors, Cherenkov detectors, and a proton polarimeter. In addition, a compact spectrometer (KAOS) for the detection of kaons is available. At present, a highly segmented large solid angle neutron detector is under construction. High-power cryogenic targets for liquid hydrogen and deuterium, pressurized ^{3}He and ^{4}He as well as a polarized ^{3}He target are available as well.

1.1.2 The A2 photon scattering setup

The A2 collaboration runs a facility for energy tagging of bremsstrahlung photons[4]. An additional end point tagger was built to cover the high-energy part of the photon energy spectrum and to access the η' threshold. The primary detector arrangement consists of the Crystal Ball and TAPS detectors. This setup is particularly suitable for the detection of photons with a solid angle of almost 4π with high resolution and high count rate capabilities. A set of two inner multiwire proportional chambers and a barrel of scintillation detectors serve for tracking and particle identification. A recoil proton polarimeter is also available. A polarized frozen-spin target for protons and deuterons with longitudinal and transverse polarization is operating successfully[5]. Very high relaxation times of up to 3 000 h have been obtained.

1.2 The future MESA facility

In addition to MAMI, a new accelerator, the Mainz Energy Recovering Superconducting Accelerator (MESA), a compact CW linear accelerator using superconducting cavities and the energy-recovering linac (ERL) concept[6], is currently under construction at Mainz, see Fig. 1. It will be housed in existing underground halls as well as a new hall and will run in parallel to MAMI. MESA exhibits a beam energy of maximum 155 MeV, however with beam intensities (at least 1 mA) which exceed the intensities achieved at MAMI by more than one order of magnitude when running in the ERL mode. The commissioning of the MESA accelerator as well as the experiments P2 (operated in the extracted beam mode) and MAGIX (an internal target experiment for the ERL mode) is foreseen for 2019. The MESA beam can be polarized both in the external as well as the ERL operation mode.

1.2.1 The P2 experiment

The major goal of the P2 experiment is a new precision measurement of the electroweak mixing

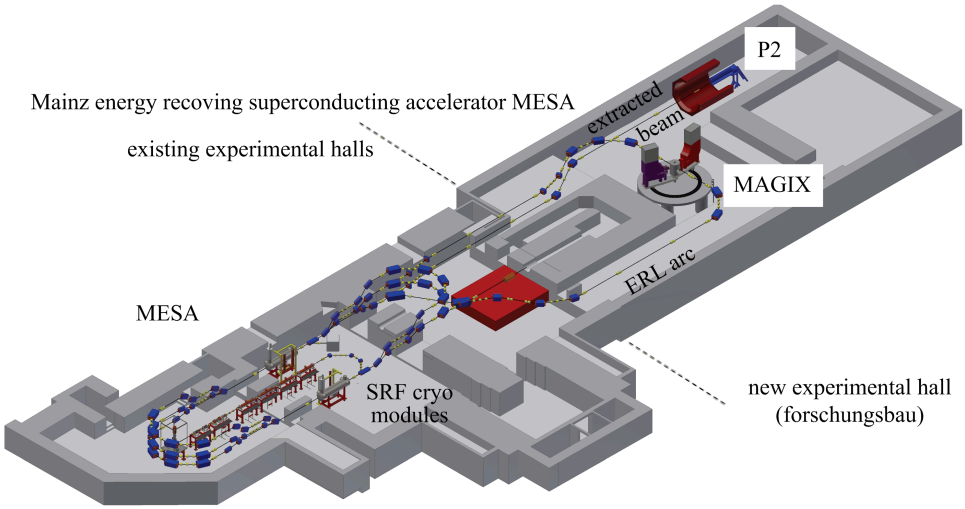

Fig. 1 The future MESA accelerator facility with the accelerator itself (left) and the two experiments P2 and MAGIX (right)

angle, $\sin^2\Theta_W$ at low momentum transfer. The P2 experiment is described in detail in a dedicated contribution to these proceedings, see Ref. [7]. A measurement of this kind has the potential to probe New Physics scenarios at a mass scale of up to 49 TeV, hence being complementary to searches for New Physics at the Large Hadron Collider. The P2 experiment might also be used for a measurement of the neutron skin[8] of nuclei with important implications for astrophysics and a detailed understanding of neutron stars.

1.2.2 The MAGIX experiment

The operation of a high-intensity ERL beam with intensities of at least 1 mA in conjunction with an internal gas target is a novel experimental approach and will yield competitive luminosities of 10^{35} $cm^{-2} \cdot s^{-1}$. To fully exploit the physics opportunities of such a setup, the MAGIX high-resolution double-arm spectrometers will be constructed. MAGIX will allow to continue the search for a hypothetical gauge boson γ' (dark photon), which is predicted in the context of dark matter models. Furthermore, precision measurements of the electromagnetic form factors of the nucleon at low momentum transfers will be possible at MAGIX, as motivated by the proton radius puzzle. The MAGIX spectrometers will be equipped with large area GEM-based focal plane detectors. For the internal target, a supersonic gas jet target as well as a T-shaped target with the option of target polarization are prepared.

2 Experiments related to the proton radius puzzle

The charge radius of the proton currently is determined using different methods[9]: ① by measuring the electromagnetic form factor of the proton in electron-proton scattering experiments at low momentum transfer; ② by measuring various atomic transitions in hydrogen; ③ by measuring the lamb shift of the $2S-2P$ transition in muonic hydrogen. The latter method comes out to provide an extremely precise determination of the proton radius on the permille level. It however shows a dramatic difference with respect to the first two methods, which themselves are consistent with each other and provide measurements on the percent level. This surprising situation was dubbed the proton radius puzzle. It has triggered in the past years a large number of theoretical investigations, which have tried to explain the discrepancy by unaccounted hadronic uncertainties in the muonic hydrogen measurement. In the meantime, there is however consensus in the community that the hadronic correction associated with the two-photon exchange diagram represents

by far the largest hadronic correction. Nonetheless, it, amounts to only about 10% of the total discrepancy, and, furthermore, is known with approximately 10% accuracy and therefore by no means can be the sole reason for the proton radius puzzle. There are speculations whether the proton radius puzzle might indicate physics beyond the Standard Model of particle physics. Before coming to this conclusions, the experiments both in electron-proton scattering as in electronic and muonic atomic spectroscopy need to be scrutinized.

The most precise measurement of the proton radius according to method ① has been performed at A1/MAMI[10]. A momentum range of as low as few 10^{-3} GeV^2 has been covered, yielding a proton radius of $\langle r\rangle = 0.879(8)$ fm. This deviates by approximately 5 standard deviations from the muonic hydrogen value, obtained at PSI with $\langle r\rangle = 0.840\ 9(4)$ fm[11]. It has been speculated whether the momentum range covered by A1 might not be low enough for a precise determination of the proton radius as an extrapolation to essentially zero momentum transfer has to be made[12] (see also the reply in Ref. [13] to this critism). In the following, we present two new approaches to achieving extremely low ranges of momentum transfer, either by utilizing the method of initial state radiation, or, by carrying out dedicated measurements at the low-energy facility MESA.

2.1 Initial state radiation measurement at A1

The radiation of a high-energetic photon from the incoming electron, involved in the electron-proton scattering process, leads to a reduction of the effective momentum transfer probing the proton. In fact, for a given setup of beam energies and polar angles of the A1 spectrometers, values of momentum transfer down to 2×10^{-4} GeV^2 can be probed. The method of course needs a good theoretical understanding of the effects of final state radiation, or of the radiation of photons from the protons. While the former is a pure QED process and is therefore known precisely, the latter requires an a priori knowledge of the electromagnetic form factors of the proton, which shall be measured. The present accuracy of the form factor measurements is however sufficient for the purpose of subtracting this background process.

At A1/MAMI, data at beam energies of 495 MeV, 330 MeV, and 195 MeV has been taken. The analysis of the data is currently ongoing. Preliminary results can be seen for the two higher energy points in Fig. 2. In the upper panel the counting rate for the two energy settings is shown, along with the background expected from inelastic processes. Both the data spectrum and the detector simulation are shown as a function of the energy of the electron in the final state. A very good agreement between data and simulation on the sub-percent level is found, as displayed in the lower panel. The main limitation is presently given by the systematic effects associated with the background from the target walls. The current results indicate that a precision measurement with a competitive accuracy of the low-momentum region can be carried out with the initial state radiation method.

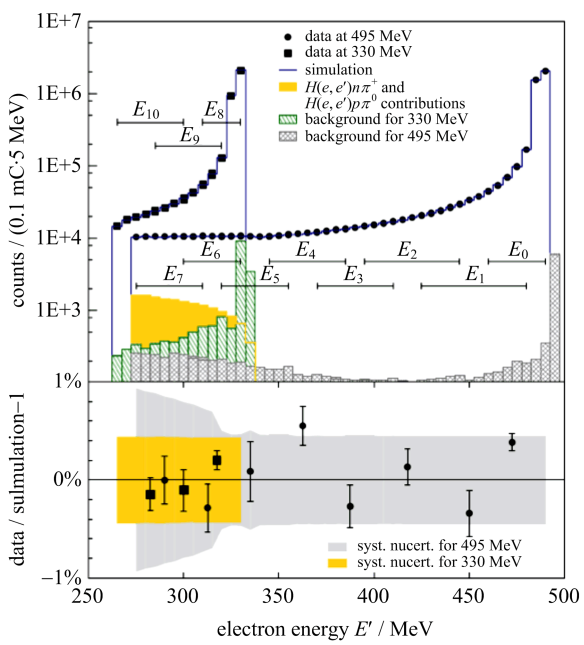

See text for explanations.

Fig. 2 Initial state radiation analysis of the elastic process $ep \to e'p'$

2.2 Future opportunities at MAGIX/MESA

The low beam energy of MESA in combination with the high resolution of the MAGIX double arm spectrometer setup will be ideal for the measurement of electromagnetic form factors at low momentum transfer. It will also be possible to measure the ratio of the electric to the magnetic form factors, $\mu_p G_E/G_M$, using the double polarization method, developed at BLAST/MIT-Bates. A simulation has been carried out, assuming a polarized MESA beam (1 mA beam current), along with a target polarization of 80% (target density 3×10^{15} cm^{-2} as in the BLAST target). Fig. 3 shows the results of the simulation with the projected error bars of the MAGIX measurement (red points), together with the currently existing world data set. The high accuracy of the data and the fact that a low momentum transfer can be achieved, will lead to new insights regarding the structure of the nucleon.

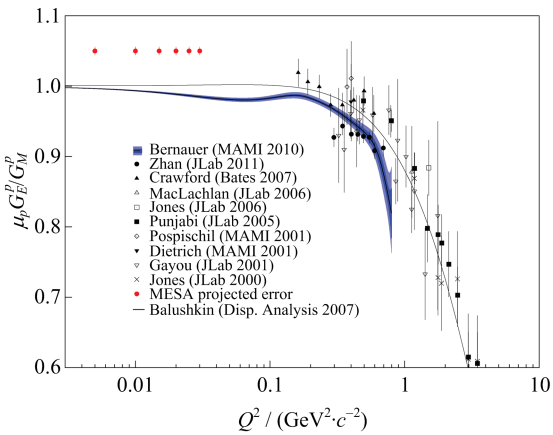

Fig. 3 Ratio of the electric to the magnetic form factor, $\mu_p G_E/G_M$, as a function of momentum transfer: projected error bars of the future measurement at MAGIX (red data points) from a simulation, assuming a polarized MESA beam and target. Shown is also the currently existing world data set of this ratio

3 Investigations of proton and meson structure using tagged photons

3.1 Proton polarizabilites at A2

As mentioned above, the largest uncertainty for the determination of the proton radius from the muonic hydrogen Lamb shift measurement arises from the two-photon exchange diagram. This effect can be related to the forward Compton scattering amplitude, which in turn is related to the magnetic polarizability β_{M1}. At MAMI, measurements of polarizabilities of the proton are possible at the tagged photon beam line with the A2 setup and a major program of polarizability measurements is currently ongoing. The use of single polarization as well as double polarization variables indeed provides new and exciting opportunities for precision measurements, as will be discussed below.

Proton polarizabilities describe the response of the nucleon on an external electromagnetic field and provide fundamental information on the proton structure. We distinguish between the electric polarizability α_{E1} and the magnetic polarizability β_{M1}. At higher orders also the four spin polarizabilities enter: γ_{E1E1}, γ_{M1M1}, γ_{E1M2}, and γ_{M1E2}. Fig. 4 shows the current PDG[14] average of the electric and the magnetic polarizability along with several theoretical predictions from (heavy) baryon chiral perturbation theory, dispersion relations, and sum rules. Obviously, a precise measurement of the polarizabilities has the

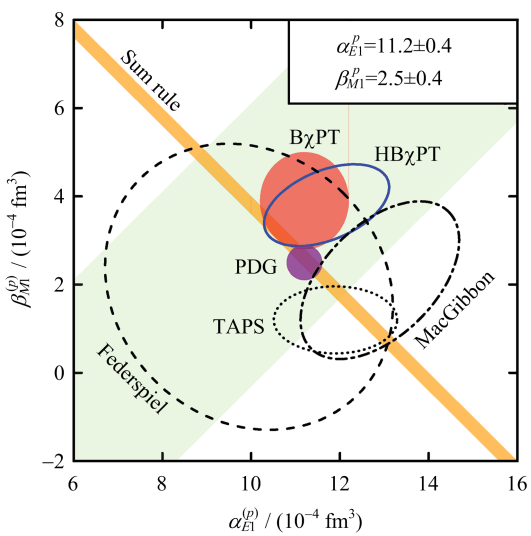

Fig. 4 PDG average and theoretical predictions for the scalar polarizabilities

potential to distinguish between the various theoretical models.

The A2 collaboration has carried out for the very first time a pilot experiment and has taken data on the cross section beam asymmetry Σ_3,

$$\Sigma_3 = \frac{d\sigma_\perp - d\sigma_\parallel}{d\sigma_\perp + d\sigma_\parallel} \quad (1)$$

in Compton scattering on protons below pion threshold. Linearly polarized photons, either parallel ($\parallel$) or perpendicular ($\perp$) to the scattering plane, are used for the measurement together with an unpolarized target. It was recently shown by the Mainz theory group[15] that in a model-independent framework Σ_3 can be related to β_{M1}, since the term containing the electric polarizability is negligible at low photon energies.

Using an 883 MeV electron beam the degree of linear polarization reached about 75% at photon energies around 130 MeV. Since the recoil proton has energies too low to be detected in the Crystal Ball, one neutral hit was required in the trigger. After subtraction of random events and background from empty target measurements, a clean missing mass distribution was obtained.

The data analysis is almost complete and a publication of this pilot experiment is in preparation. Clearly more data are necessary to improve the accuracy of β_{M1} significantly. The A2 collaboration plans to take additional data in 2016 to reduce the error on β_{M1} to a level of 10%. Such an increase in accuracy will also be possible due to the replacement of the photo multipliers for the focal plane of the tagging detector in addition to the recently installed new DAQ system.

In addition to the work related to the scalar polarizabilities, the A2 collaboration has also performed a measurement of the spin polarizabilities by using the double polarization variable Σ_{2x},

$$\Sigma_{2x} = \frac{\sigma^R_{+x} - \sigma^L_{+x}}{\sigma^R_{+x} + \sigma^L_{+x}} = \frac{\sigma^R_{+x} - \sigma^R_{-x}}{\sigma^R_{+x} + \sigma^R_{-x}} \quad (2)$$

where a right-handed (R) or left-handed (L) circularly polarized beam is scattered on a transversally ($\pm x$) polarized target. The variable Σ_{2x} is particularily sensitive to the spin polarizability γ_{E1E1}, which is found to be $\gamma_{E1E1} = (4.6 \pm 1.6) \times 10^{-4}$ fm^3, see Ref. [16]. Again, with the improvements in the data taking rate for the A2 data taking, a significant improvement will be possible in the upcoming years.

3.2 Timelike electromagnetic form factor measurements of η and η' at A2

A new determination of the electromagnetic transition form factor (TFF) from the $\eta \to e^+ e^- \gamma$ Dalitz decay was carried out at A2/MAMI[18]. Experimentally, such a determination can be done by measuring the decay rate of $\eta \to \gamma^* \gamma \to e^+ e^- \gamma$ as a function of a dilepton invariant mass $m_{ee} = q$ and by normalizing it to the partial decay width $\Gamma(\eta \to \gamma\gamma)$:

$$\frac{d\Gamma(\eta \to e^+ e^- \gamma)}{q\Gamma(\eta \to \gamma\gamma)} = [QED] \cdot |F_\eta(q)|^2 \quad (3)$$

where F_η is the TFF of the η meson, and $[QED]$ is the analytic QED expression of the decay ratio assuming structureless mesons, which depends on q, the mass of the η meson and the fine structure constant α only. Assuming Vector Meson Dominance (VMD), TFFs are usually parametrized within a pole description:

$$F(q^2) = \frac{1}{1 - q^2/\Lambda^2} \quad (4)$$

where Λ is the effective mass of the virtual vector mesons, with Λ^{-2} the FF slope at $q^2 = 0$.

The statistical accuracy achieved in this work surpasses all previous measurements of $\eta \to e^+ e^- \gamma$ and matches the NA60 result[17] based on $\eta \to \mu^+ \mu^- \gamma$ decays from peripheral In-In collisions. Compared to the former determination of the η TFF by the A2 collaboration[19] from 2011, an increase by more than one order of magnitude in statistics has been achieved. This was accomplished by an analysis of three times more data and the use of a kinematic-fit technique, which allowed for a higher selection efficiency and for exploiting the full η production range available at MAMI-C.

Our extracted slope parameter $b=\Lambda^{-2}=(1.95\pm 0.15_{\text{stat}} \pm 0.10_{\text{syst}})$ GeV^{-2} agrees within the uncertainties with the results from all recent measurements of the η TFF. The pole-approximation fit to the MAMI data shows almost perfect agreement with the model-independent calculation of Ref. [20], which was discussed above in the theory section. The calculation by Terschlüsen and Leupold[21] and the dispersion theory calculation[22] by Hanhart et al. deviate slightly from the fit, but the statistical accuracy is still not sufficient to rule out any of the theoretical predictions, see Fig. 5.

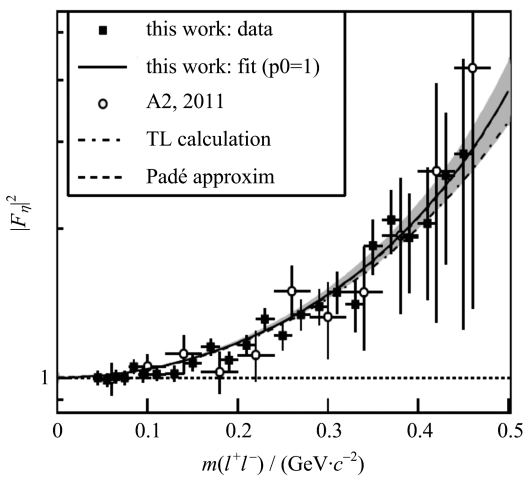

Shown are two measurements from A2 (this work from 2013, 2011) together with a fit to the more recent measurement and two theoretical calculations (TL calculation, Pade approxim.), see text.

Fig. 5 Timelike η transition form factor measurement at A2/MAMI

4 Search for the dark photon

Extra U(1) bosons-so-called dark photons, γ'-naturally appear in most string compactifications and essentially in any extensions of the SM. A prediction for the mass and the couplings is in general not possible. As a consequence, dedicated searches span a wide range of masses and couplings, exploiting very different experimental techniques (from atomic physics experiments to experiments at the LHC).

Recently, the focus of dark photon searches has moved to γ' masses in the MeV to GeV mass range. As Arkani-Hamed et al. in Ref. [23] have pointed out, dark photons in that mass range could be related to Dark Matter phenomena. In fact, γ' particles coupling to ordinary matter via so-called kinetic mixing give an elegant explanation for a number of astrophysical anomalies, such as the PAMELA/FERMI/AMS discovery of a positron excess in the cosmic ray flux.

Furthermore, it has been realized that dark photons with masses in the MeV to GeV range could also explain the presently seen deviation between the direct measurement of $(g-2)_\mu$ and its Standard Model prediction. Given the present size of the effect, a firm prediction for the dark photon parameter range (coupling parameter ε versus Dark Photon mass $m_{\gamma'}$) can be made[24].

4.1 Dark photon search at A1

The experimental technique for the 2014 A1/MAMI measurement[25] is similar to the one used for the 2011 precursor experiment[26]. A high-intensity MAMI beam was scattered on a tantalum target. Electron-positron pairs are produced in QED processes, in which a virtual photon couples either in a timelike or a space like proecess to an e^+e^- pair. A dark photon could be produced by exchanging an ordinary photon with a dark photon. This would show up in the experiment as a bump over the QED background in the e^+e^- invariant mass spectrum.

In total, 22 kinematic settings were chosen with beam energies ranging from 180 MeV to 855 MeV. Depending on the setting, a 99.99% pure single foil ^{181}Ta target or a stack of these foils was used. The result, which is shown in Fig. 6 in pink, was the most stringent limit below 400 MeV prior to a publication by BABAR[27].

4.2 Future opportunities at MAGIX/MESA

The dual-arm high-resolution spectrometers in combination with a windowless internal gas target are ideally suited for the detection of low-momentum tracks and as such also for the dark photon search at low masses. A simulation has been carried out and it was found, that the

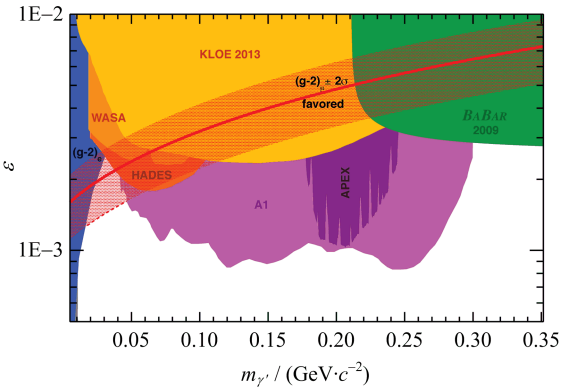

The red (shaded) band shows the parameter range, in which a dark photon would explain the presently seen deviation between Standard Model prediction and direct measurement of $(g-2)_\mu$. The figure shows the parameter range after the publication of the A1 results; new BABAR data of Ref. [27] is not yet included.

Fig. 6 Dark photon exclusion plot in the parameter range dark photon coupling (ε) versus dark photon mass ($m_{\gamma'}$)

MAGIX measurement will extend existing dark photon limits by almost an order of magnitude for masses below 50 MeV. A luminosity of 10^{35} $cm^{-2} \cdot s^{-1}$ has been assumed for the simulation, as also expected for a MESA ERL beam of 1 mA in conjunction with the high-density gas jet target.

According to current plannings, the excellent resolution of the MAGIX spectrometers should also allow for a highly competitive dark photon search with an invisible decay of the dark photon into dark matter particles or neutrinos. This represents an extension of the Mainz dark photon program.

5 Conclusion

We have presented in this paper several typical measurements, which can be carried out at low-energy facilities as MAMI and at the future MESA facility. It is the low beam energy (or low energy transfer) together with world class luminosities, which allows for competitive measurements in the field of hadron and low-energy particle physics. In future, MESA will allow to extend this low-energy frontier further.

References

[1] HERMINGHAUS H, FEDER A, KAISER K H, et al. The design of a cascaded 800 MeV normal conducting C. W. race track microtron [J]. Nucl Instrum Meth, 1976, 138(1): 1-12.

[2] KAISER K H, AULENBACHER K, CHUBAROV O, et al. The 1.5 GeV harmonic double-sided microtron at Mainz University[J]. Nucl Instrum Meth A, 2008, 593(3): 159-170.

[3] BLOMQVIST K I, BOEGLIN W U, BÖHM R, et al. The three-spectrometer facility at the Mainz microtron MAMI[J]. Nucl Instrum Meth A, 1998, 403 (2/3): 263-301.

[4] MCGEORGE J C, KELLIE J D, ANNAND J R M, et al. Upgrade of the Glasgow photon tagging spectrometer for Mainz MAMI-C[J]. Eur Phys J A, 2008, 37(1): 129-137.

[5] THOMAS A. Polarised targets for 4π detectors at MAMI [J]. Eur Phys J ST, 2011, 198: 171.

[6] AULENBACHER K. The MESA accelerator[J]. AIP Conf Proc, 2013, 1563: 5.

[7] BERGER N, AULENBACHER K, BAUNACK S, et al. Measuring the weak mixing angle with the P2 experiment at MESA [J]. Journal of University of Science and Technology of China, 2016, 46 (6): 481-487.

[8] SFIENTI C, BECKER D, FERRETTI BONDY M I, et al. Status and prospects of R_n measurements at Mainz[J]. AIP Conf Proc, 2013, 1563: 231.

[9] CARLSON C E, VANDERHAEGHEN M. Constraining off-shell effects using low-energy Compton scattering [J]. (2011-09-17) [2015-11-01]. http://arxiv.org/abs/1109.3779.

[10] BERNAUER J C, ACHENBACH P, AYERBE GAYOSO C, et al. High-precision determination of the electric and magnetic form factors of the proton[J]. Phys Rev Lett, 2010, 105: 242001.

[11] POHL R, GILMAN R, MILLER G A, et al. Muonic hydrogen and the proton radius puzzle[J]. Ann Rev Nucl Part Sci, 2013, 63: 175-204.

[12] GRIFFIOEN K, CARLSON C, MADDOX S. Are electron scattering data consistent with a small proton radius? [J]. (2015-10-26)[2015-11-01]. http://arxiv.org/abs/1509.06676.

[13] DISTLER M O, WALCHER T, BERNAUER J C. Solution of the proton radius puzzle? Low momentum transfer electron scattering data are not enough [J]. (2015-11-02) [2015-11-10]. http://arxiv.org/abs/1511.00479.

[14] OLIVE K A, AGASHE K, AMSLER C, et al.

Review of particle physics [J]. Chin Phys C, 2014, 38 (09): 090001.

[15] KRUPINA N, PASCALUTSA V. Separation of proton polarizabilities with the beam asymmetry of compton scattering [J]. Phys Rev Lett, 2013, 110:262001.

[16] MARTEL PP, MISKIMEN R, AGUAR-BARTOLOME P, et al. Measurements of double-polarized compton scattering asymmetries and extraction of the proton spin polarizabilities[J]. Phys Rev Lett,2015,114: 112501.

[17] AGUAR-BARTOLOME P, ANNAND J R M, ARENDS H J, et al. New determination of the η transition form factor in the Dalitz decay $\eta \to e^+ e^- \gamma$ with the Crystal Ball/TAPS detectors at the Mainz Microtron [J]. Phys Rev C,2014, 89:044608.

[18] ARNALDI R, BANICZ K, CASTOR J, et al. Study of the electromagnetic transition form-factors in $\eta \to \mu^+ \mu^- \gamma$ and $\omega \to \mu^+ \mu^- \pi^0$ decays with NA60[J]. Phys Lett B,2009, 677:260-266.

[19] BERGHAUSER H, METAG V, STAROSTIN A, et al. Determination of the η-transition form factor in the $\gamma p \to p\eta \to p\gamma e^+ e^-$ reaction[J]. Phys Lett B, 2011, 701: 562-567.

[20] ESCRIBANO R, MASJUAN P, SANCHEZ-PUERTAS P. η and η' transition form factors from rational approximants [J]. Phys Rev D, 2014, 89:034014.

[21] TERSCHLÜSENA C, LEUPOLD S. Electromagnetic transition form factors of light vector mesons[J]. Phys Lett B, 2010,691:191-201.

[22] HANHART C, KUPŚĆ A, MEIßNER U G, et al. Dispersive analysis for $\eta \to \gamma\gamma *$ [J]. Eur Phys J C, 2013, 73: 2668.

[23] ARKANI-HAMED N, FINKBEINER D P, SLATYER T R, et al. A theory of dark matter[J]. Phys Rev D, 2009,79: 015014.

[24] POSPELOV M. Secluded U(1) below the weak scale [J]. Phys Rev D,2009, 80: 095002.

[25] MERKEL H, ACHENBACH P, AYERBE GAYOSO C, et al. Search at the Mainz Microtron for light massive gauge bosons relevant for the muon $g-2$ anomaly[J]. Phys Rev Lett,2014, 112: 221802.

[26] MERKEL H, ACHENBACH P, AYERBE GAYOSO C, et al. Search for light gauge bosons of the dark sector at the Mainz Microtron [J]. Phys Rev Lett, 2011,106: 251802.

[27] LEES J P, POIREAU V, TISSERAND V, et al. Search for a dark photon in $e^+ e^-$ collisions at BaBar [J]. Phys Rev Lett,2014, 113: 201801.

Article ID:0253-2778(2016)07-0617-08

The Belle II experiment and SuperKEKB upgrade

WANG Boqun (for the Belle II Collaboration)

(*Department of Physics, University of Cincinnati, Cincinnati, OH* 45221, *USA*)

Abstract: The Belle II/SuperKEKB experiment is an e^+e^- collider running at the $\Upsilon(4S)$ resonance energy to produce B meson pairs. As an upgrade of the Belle/KEKB experiment, it will start physics data taking from 2018 and with ~40 times luminosity. Its goal is to accumulate 50 ab^{-1} of e^+e^- collision data. Now the upgrade of the sub-detector systems is on-going in KEK. The physics program has a wide range of areas, including searches for direct CP violation (CPV), lepton flavour violation and dark matter. The current upgrade status of Belle II and SuperKEKB is reviewed and some physics opportunities at this facility are introduced.

Key words: Belle II; SuperKEKB; e^+e^- collider; New Physics

CLC number: O572.3 **Document code**: A doi:10.3969/j.issn.0253-2778.2016.07.012

Citation: WANG Boqun. The Belle II experiment and SuperKEKB upgrade[J]. Journal of University of Science and Technology of China, 2016,46(7):617-624.

Belle II 实验和超级 KEKB 升级

王博群(Belle II 合作组)

(辛辛那提大学物理系,辛辛那提 45221,美国)

摘要:Belle II/超级 KEKB 实验是一个在 $Y(4S)$ 共振态能量点运行产生 B 介子对的正负电子对撞机.作为 Belle/KEKB 实验的升级,它将从 2018 年开始以大约 40 倍的亮度取数,目标是收集 50 ab^{-1} 的正负电子对撞数据.现在子探测器系统的升级正在 KEK 进行.物理项目涉及范围很宽,包括寻找直接 CP 破坏、轻子味破缺、暗物质.本文回顾当前 Belle II 和超级 KEKB 升级状况并介绍该设施带来的物理机遇.

关键词:Belle II;超级 KEKB;正负电子对撞机;新物理

0 Introduction

The so-called B factory is an e^+e^- collider running at the $\Upsilon(4S)$ resonance energy to produce B meson pairs. The major B factories are Belle running at KEKB in Japan and BaBar running at PEP-II in US. The total data set collected by these two facilities is ~1.5 ab^{-1} of e^+e^- collision data. With that data sample, they've reached physics achievements in areas like the CKM angle measurement, $|V_{cb}|$ and $|V_{ub}|$ measurement, semileptonic and leptonic B decays, rare B decays, τ physics, D^0 mixing and CPV, B physics at the $\Upsilon(5S)$, two-photon physics and new resonances[1].

To search for the New Physics (NP), which

Received:2015-11-30;**Revised**:2016-06-27

Foundation item:Supported by DOE Grant (DE-SC0011784).

Biography:WANG Boqun, male, born in 1984, PhD. Research field: experimental high energy physics. E-mail: boqunwg@ucmail.uc.edu

is physics beyond the Standard Model (SM), the Belle/KEKB experiment will be upgraded to Belle II/SuperKEKB[2]. The upgraded detector is planning to take ~50 ab^{-1} of e^+e^- collision data. The SuperKEKB asymmetric electron-positron collider can provide a clean environment for producing B meson pairs via $\Upsilon(4S)$ resonance decay. Its designed luminosity is 8×10^{35} $cm^{-2}\cdot s^{-1}$, which is about 40 times larger than the KEKB collider. The 50 ab^{-1} overall integrated luminosity corresponds to 55 billion $B\overline{B}$ pairs, 47 billion $\tau^+\tau^-$ pairs, and 65 billion $c\bar{c}$ states.

In this article, we introduce the Belle II/SuperKEKB experiment, the current status and the future plan of the experiment, and the opportunities for New Physics.

1 SuperKEKB

Many sub-systems of the SuperKEKB accelerator need to be upgraded for achieving the 40 times luminosity compared with KEKB. The most important part is the beam size. By using the so-called nano-beam technology[3], the beam bunches are significantly squeezed to 60 nm thick at the collision point as shown in Fig. 1. The beam energies of positron and electron will be changed slightly, from 3.5 GeV/8 GeV to 4 GeV/7 GeV,

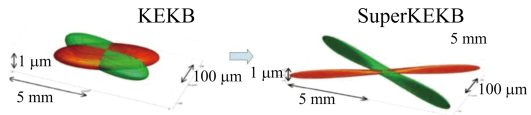

Fig. 1 The beam size comparison between KEKB (left) and SuperKEKB (right)

to achieve a less boosted center-of-mass system.

2 Belle II detector

As shown in Fig. 2, most sub-detectors of Belle will be upgraded for Belle II. This includes the newly designed vertex detection system (PXD and SVD), a drift chamber with longer arms and smaller cells, a completely new PID system which consists of TOP detector in the central region and ARICH detector in the forward end, the electromagnetic calorimeter (ECL) with upgraded crystals and electronics, and upgraded $K_L-\mu$ detection system (KLM). More details will be introduced in the following sections.

2.1 VXD

The vertex detector (VXD) consists of two parts: PXD in the inner part[4] and SVD in the outer part[5]. PXD consists of two layers of DEPFET (DEPleted p-channel Field Effect Transistor) and SVD consists of four layers of DSSD (Double Sided Strip Detectors), as shown in

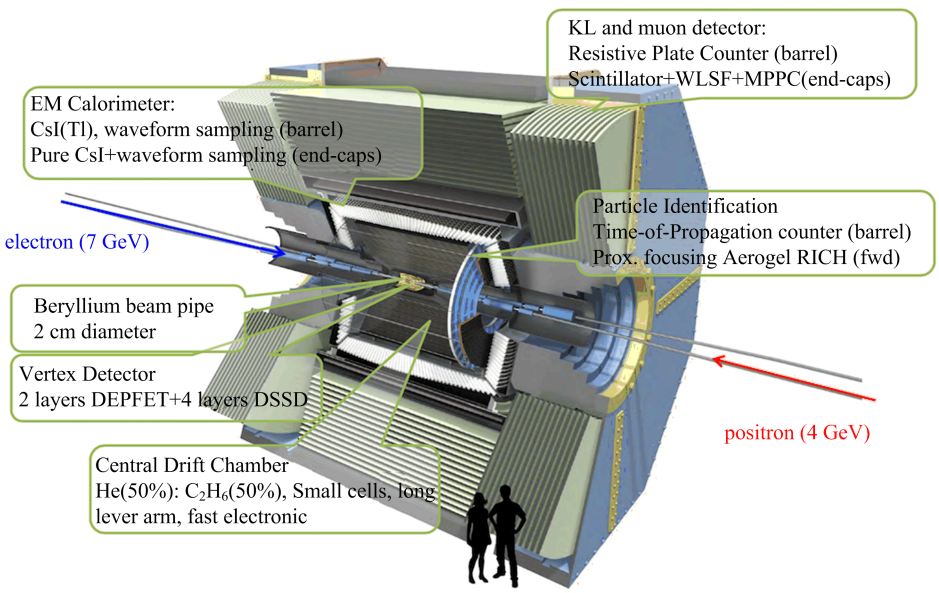

Fig. 2 Overview of the Belle II detector and its sub-detectors

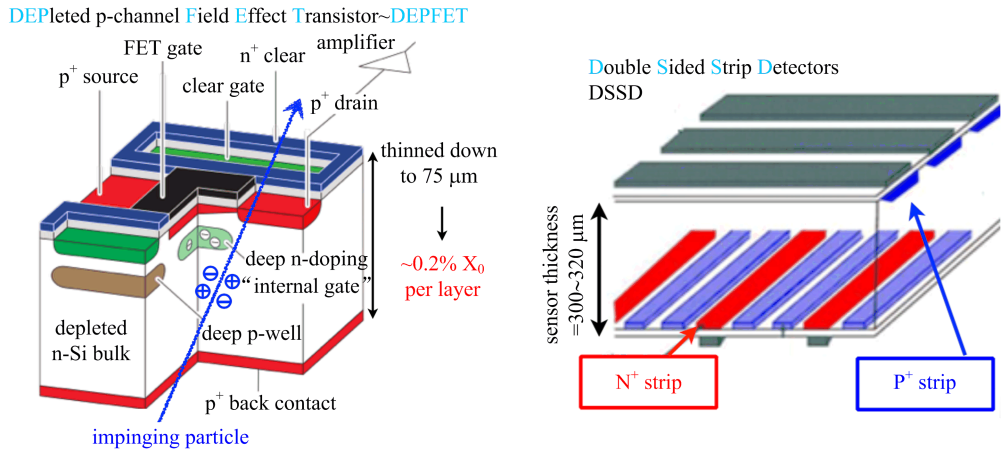

Fig. 3 The structure of the DEPFET (left) and DSSD (right)

Fig. 3. These two sub-detectors combined should have a good vertex resolution for charged tracks. Now the system integration is on-going, and a beam test for VXD has just finished in the spring of 2016.

2.2 CDC

As the main tracking device for charged tracks, the CDC in Belle II is larger than that in Belle and it has a smaller cell size, as shown in Fig. 4. This should improve the momentum and dE/dx resolution. The stringing for the CDC was finished in January of 2014 with 51456 wires and now it is being commissioned with cosmic rays.

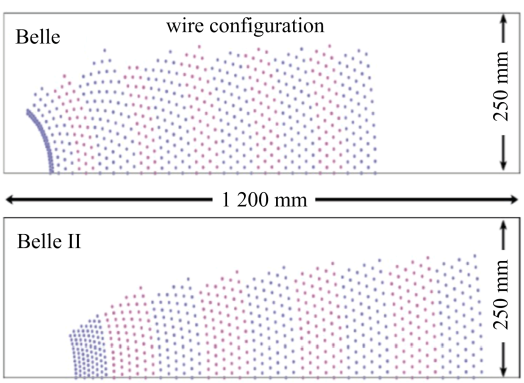

Fig. 4 The comparison of CDC wire configurations between Belle (top) and Belle II (bottom)

2.3 TOP

The imaging Time of Propagation sub-detector (TOP or iTOP) will be used for particle identification in the barrel region of Belle II[6]. There are 16 TOP modules, and each one consists of two quartz bars, one mirror, one prism, and an array of photo-detectors to collect Cerenkov photons generated by charged tracks going through the radiator, as shown in Fig. 5. To distinguish between kaons and pions, the photo-detectors have excellent position and timing resolution. This is achieved by using multi-channel-plate photomultiplier tubes (MCP-PMTs) and new waveform sampling electronics.

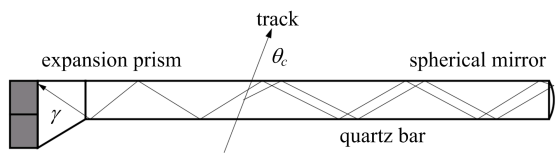

Fig. 5 The structure of the TOP detector

Prototype TOP modules have been tested during the beam test at SPring-8 at LEPS in 2013, and good agreement between data and MC simulation has been obtained[7], with timing requirement $\sim O(100\ \text{ps})$, as shown in Fig. 6.

As of May 2016, all TOP modules have been assembled, tested and installed to the Belle II detector. The commissioning of all modules is underway.

2.4 ARICH

Aerogel Ring Imaging Cerenkov (ARICH) detector will be used for particle identification in the forward end-cap. Two layers of aerogel with different indices of refraction will be used to improve the resolution of the detector[8]. For

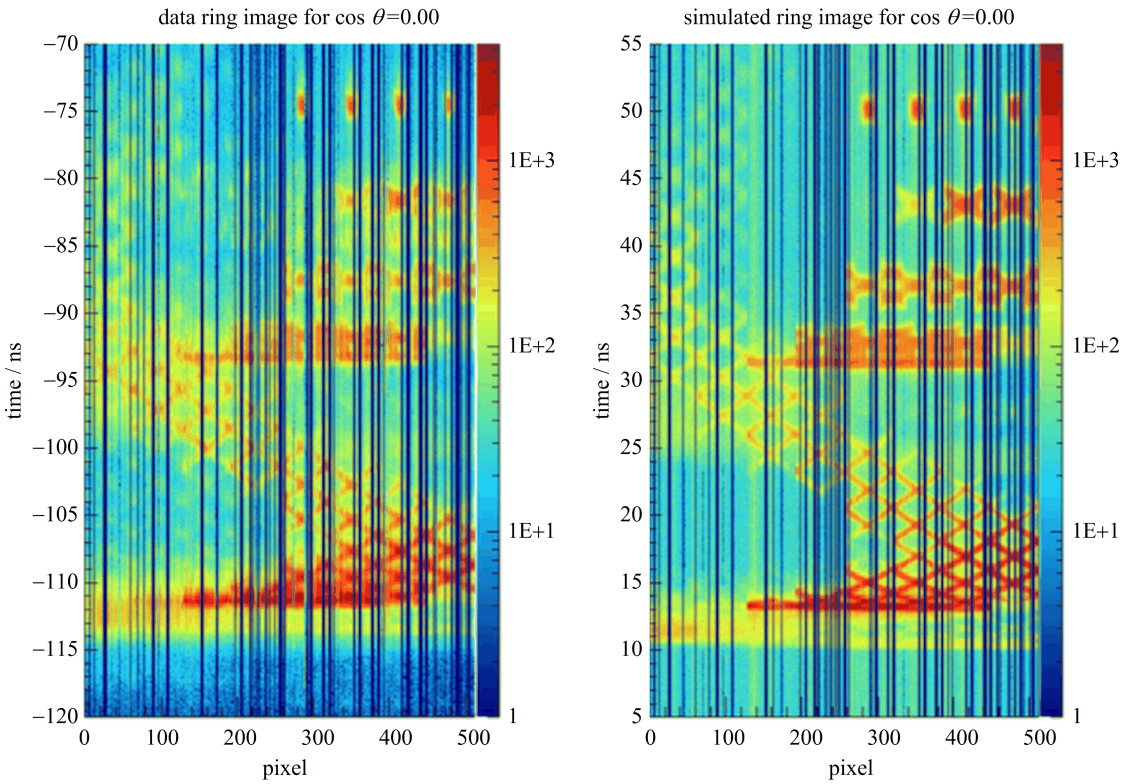

Fig. 6 The TOP beam test data (left) and simulated MC sample (right)

readout, 420 Hybrid Avalanche Photo Detectors (HAPD), each with 144 channels, will be used, as shown in Fig. 7.

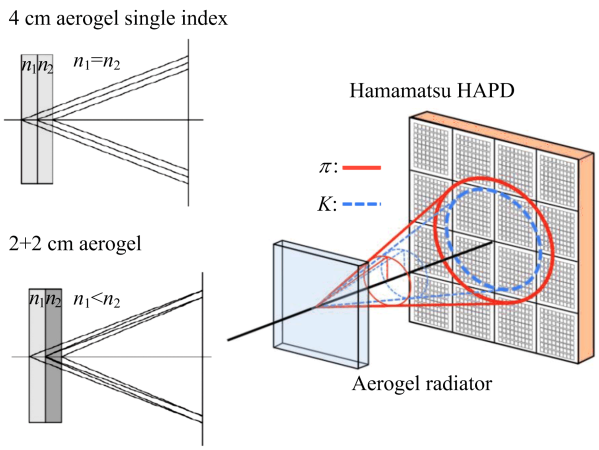

Fig. 7 The focusing mechanism (left) and the structure (right) of ARICH

2.5 ECL

For the upgrade of the ECL detector, the crystals in barrel side will be re-used and the crystals in the end-cap will be refurbished. New electronics, such as bias filter and waveform sampling will be used for the upgraded detector[9]. Now the cosmic ray test is underway. The expected performance for ECL is shown in Fig. 8[10].

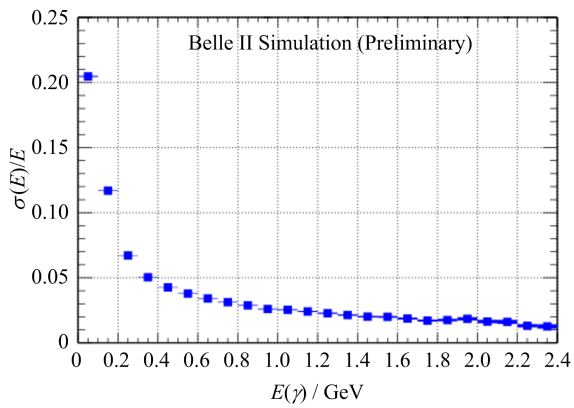

Fig. 8 The expected performance of the ECL detector[10]

2.6 KLM

The endcaps and the inner layers of the barrel resistive plate chambers (RPCs) of KLM has been replaced with scintillators due to increased backgrounds expected in Belle II, as shown in Fig. 9. The barrel KLM was the first sub-detector

to be installed in Belle II.

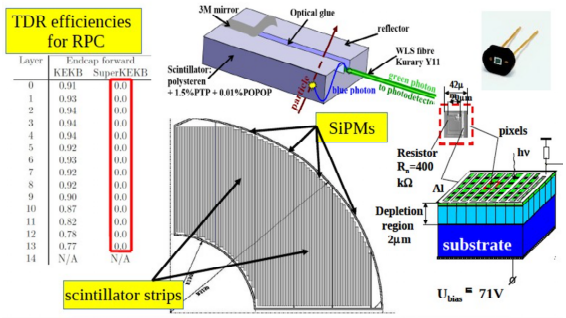

Fig. 9 The structure of the KLM detector

3 Physics opportunities

There should be many potential signals for new physics in Belle II, such as the flavor changing neutral currents, probing charged Higgs, new sources of CPV, lepton flavour violation decays, and searches for a dark photon. With the much larger data set compared with Belle and BaBar, Belle II will contribute to the search for new physics, together with the upgraded LHCb. For example, the CKM Unitarity Triangle should be significantly improved, as shown in Fig. 10[11].

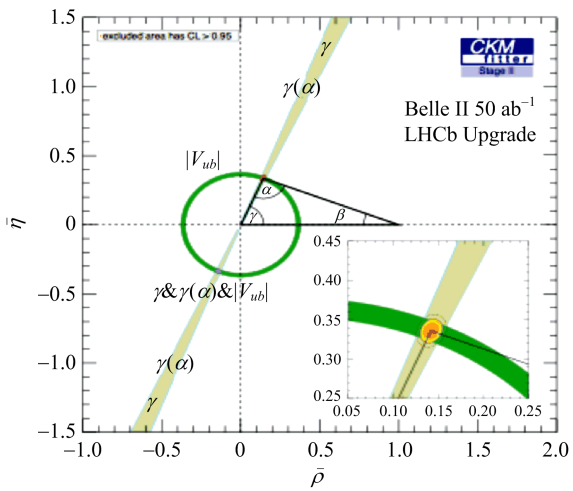

This is a fit to the tree level measurements of the CKM UT angles.

Fig. 10 The predicted accuracy of CKM Unitarity Triangle with data taken by LHCb and Belle II, from Ref. [11]

3.1 Direct CPV in $D^0 \to \phi\gamma$, $\rho^0\gamma$

The direct CPV in radiative decays can be enhanced to exceed 1%[12] over standard model. The A_{CP} for $D^0 \to \phi\gamma$ could be up to 2%, and the A_{CP} for $D^0 \to \rho^0\ \gamma$ could be up to 10%. The decay for $D^0 \to \phi\gamma$ was first observed by Belle with 78 fb^{-1} of data, with the relative error on yield of about 25%[13]. For Belle II, with 50 ab^{-1} of data, the A_{CP} sensitivity will be reduced to 1%.

3.2 $D^0 \to \gamma\gamma$

The branching fraction of the decay $D^0 \to \gamma\gamma$ is predicted by SM as $\approx 10^{-8} \sim 10^{-11}$. Although the rate is low, New Physics (NP) processes can lead to significant enhancements[14].

This decay has been searched for by BaBar① and the upper limit with 470 fb^{-1} of data is 2.2×10^{-6} with 90% CL[16], as shown in Fig. 11.

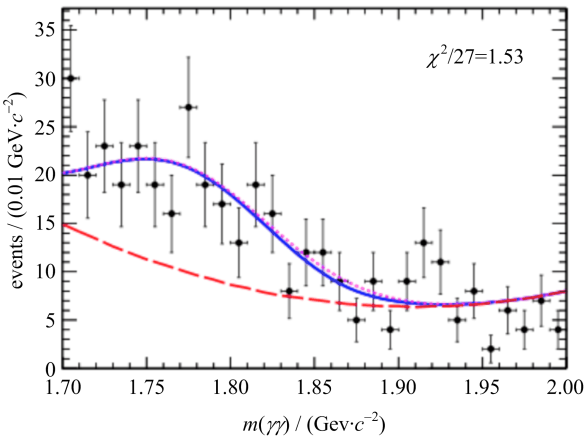

Fig. 11 The decay of $D^0 \to \gamma\gamma$ from BaBar[16]

With 50 ab^{-1} of data by Belle II, the upper limit could be improved to $\sim 2 \times 10^{-8}$, if it scales with luminosity L, or $\sim 2 \times 10^{-7}$, if it scales with $\sqrt{L}$.

3.3 τ Lepton Flavour Violation

The lepton flavour violation decays are highly suppressed by SM, with a branching fraction of $\sim 10^{-25}$. But they could be enhanced in certain New Physics scenarios, such as supersymmetry (SUSY)[17], little Higgs models[18] and extra dimensions[19].

Belle has searched for LFV[20-21], but no trace of NP has been found. As shown in Fig. 12, the red dots show the sensitivity for some LFV decays in Belle II[22]. The branching fraction of the decays

① Recently, Belle has presented an upper limit on this decay; see Ref. [15].

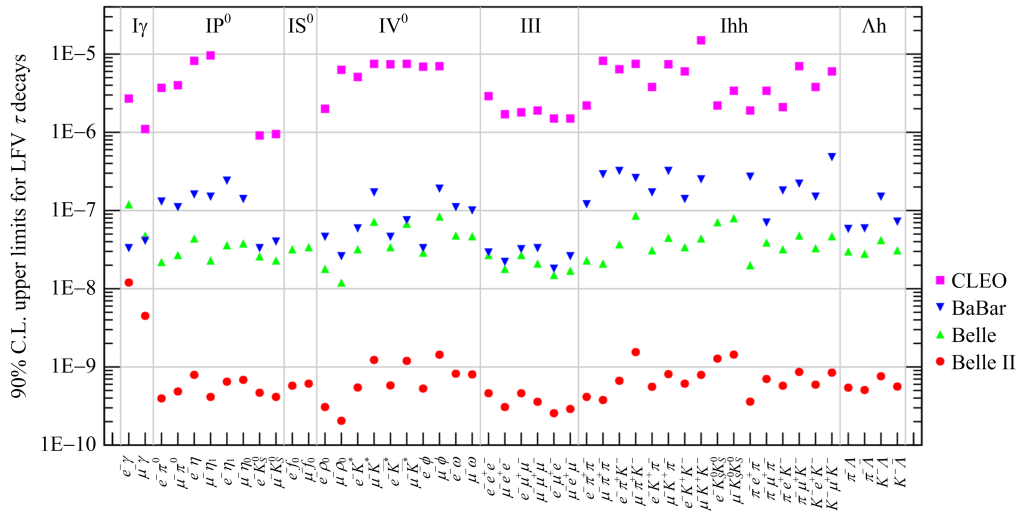

Fig. 12 The comparison of LFV upper limit by different experiments for different decay channels, from Ref. [22]

is within the capability of the Belle II experiment. Belle II will push many limits below 10^{-9}.

3.4 Dark sector

The dark photon A' is one candidate for dark matter that could be searched for at an accelerator. Its mass is predicted to be in the range of MeV to GeV[23]. The dark photon could be searched for in the reaction $e^+e^-\to\gamma_{ISR}A'$. There are two ways to detect a dark photon: probing leptonically decaying dark photons through mixing, or probing sub-GeV dark matter in invisible decays. In the latter case, the signature for the decay is a single energetic photon in the event, which requires the single photon trigger. The single photon trigger was not available in Belle but will be implemented in Belle II.

The upper limits of dark photon measurement for different experiments are shown in Fig. 13[24]. Belle II has an advantage to search for dark photon A' with much higher integrated luminosity.

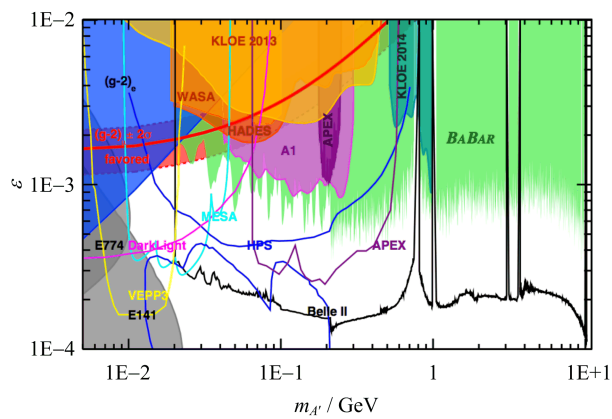

Fig. 13 The upper limit by different experiments in search of the dark photon, from Ref. [24]

4 Schedule

The SuperKEKB accelerator is now at the final stage of construction and the upgrade of the Belle II detector is on-going. As shown in Fig. 14, there are three phases in the commission and operation of Belle II. In Phase 1, which begins in early 2016, the commissioning of various components will start without rolling-in the detector. In Phase 2, which begins in the autumn of 2017, Belle II detector will be partly commissioned to take test physics data without the vertex detector. Finally, in Phase 3, which is expected to start at the end of 2018, the Belle II detector with full apparatus will take physics data.

The plan for instantaneous and integrated luminosity is shown in Fig. 15. According to this plan, the target integrated luminosity of 50 ab^{-1} will be achieved by 2024.

5 Conclusion

Belle and BaBar as B factories have made many contributions for flavour physics. As an upgrade, the Belle II/SuperKEKB experiment should play an important role in the search for New Physics. With

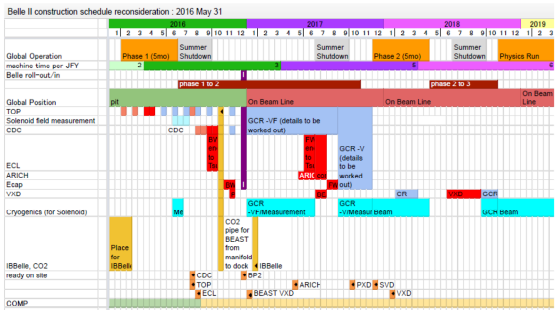

Fig. 14 The current Belle II commissioning schedule

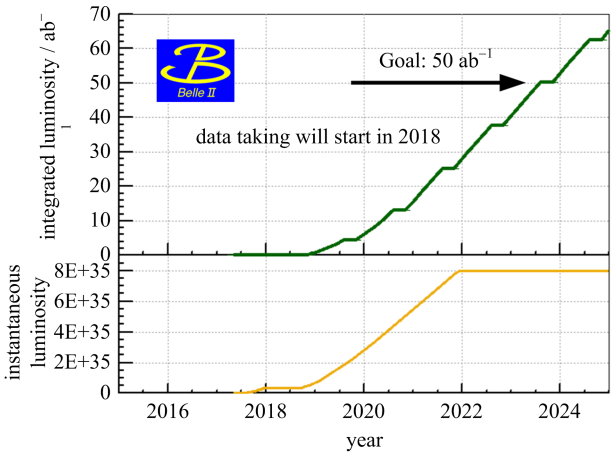

Fig. 15 The plan for Belle II data taking

the upgraded accelerator and detector, the experiment will have much higher luminosity and much better performance for detecting final state particles.

With the much larger data set collected with the upgraded detector, Belle II has a rich physics program, which makes it possible to study the channels with missing energy and neutral particles in the final states. Now the accelerator and detector are under construction, and the physics data taking will start at the end of 2018.

Acknowledgments I'd like to thank the organizers of the PhiPsi15 conference for inviting me to introduce this work. I'd like to express my gratitude to the Belle II collaboration and the HEP group of the University of Cincinnati.

References

[1] BEVAN A J, GOLOB B, MANNEL Th, et al. The physics of the *B* factories[J]. Eur Phys J C, 2014, 74: 3026

[2] ABE T, ADACHI I, ADAMCZYK K, et al. Belle II technical design report[EB/OL]. (2010-11-01)[2015-11-01]. http://arxiv.org/abs/1011.0352v1.

[3] RAIMONDI P. Status on SuperB effort: Talk given at the 2nd SuperB workshop, Frascati, 2006[R/OL]. (2006-03-16)[2015-11-01]. http://www.lnf.infn.it/conference/superb06/talks/raimondi1.ppt.

[4] SCHIECK J. DEPFET pixels as a vertex detector for the Belle II experiment [J]. Nucl Instrum Meth A, 2013, 732:160-163.

[5] FRIEDL M, ACKERMANNF K, AIHARAI H, et al. The Belle II silicon vertex detector[J]. Nucl Instrum Meth A, 2013, 732: 83-86

[6] INAMI K. TOP counter for particle identification at the Belle II experiment[J]. Nucl Instrum Meth A, 2014, 766: 5-8

[7] STARIC M. Performance studies of the Belle II TOP counter[J]. Nucl Instrum Meth A, 2014, 766: 237-240.

[8] NISHITA S, ADACHIA I, HAMADA N, et al. Aerogel RICH forder3wsdxew34ert6y7u8i90pkkilkikjui the Belle II forward PID[J]. Nucl Instrum Meth A, 2014, 766: 28-31

[9] V AULCHENKO, BOBROV A, BONDAR A, et al. Electromagnetic calorimeter for Belle II [J]. Journal of Physics: Conference Series, 2015, 587: 012045.

[10] MIYABAYASHI K. ECL reconstruction: Photons, pi0s [C]//16th B2GM, KEK, Japan. [S. l.: s. n.], 2013.

[11] CKMfitter[EB/OL]. [2015-11-01]. http://ckmtter.in2p3.fr/.

[12] ISIDORI G, KAMENIK J F. Shedding Light on *CP* Violation in the Charm System via $D \to V\gamma$ Decays[J]. Phys Rev Lett, 2012, 109: 171801.

[13] TAJIMA O, ABE K, AIHARA H, et al. Observation of the radiative decay $D^0 \to \phi\gamma$[J]. Phys Rev Lett, 2004, 92: 101803.

[14] PRELOVSEK S, WYLER D. $c \to u\gamma$ in the minimal supersymmetric standard model [J]. Phys Lett B, 2001, 500: 304-312.

[15] NISAR N K, MOHANTY G B, TRABELSI K, et al. Search for the rare decay $D^0 \to \gamma\gamma$ at Belle[J]. Phys Rev D, 2016, 93: 051102(R).

[16] LEES JP, POIREAU V, PRENCIPE E, et al. Search for the decay $D^0 \to \gamma\gamma$ and measurement of the branching fraction for $D^0 \to \pi^0\pi^0$[J]. Phys Rev D, 2012, 85: 091107(R).

[17] HERRERO M J, PORTOLÉS J, RODRÍGUEZ-SÁNCHEZ A M. Sensitivity to the Higgs sector of

supersymmetric-seesaw models in the lepton flavor violating $\tau \to \mu f^0(980)$ decay[J]. Phys Rev D, 2009, 80: 015023.

[18] YUE C X, ZHAO S. Lepton flavor violating signals of a little Higgs model at high energy linear e^+e^- colliders [J]. Eur Phys J C, 2007, 50 (4): 897-903.

[19] DE GOUVEA A, GIUDICE G F, STRUMIA A, et al. Phenomenological implications of neutrinos in extra dimensions[J]. Nucl Phys B, 2002, 623: 395-420.

[20] HAYASAKA K, ABEAR K, ADACHI I, et al. New search for $\tau \to \mu\gamma$ and $\tau \to e\gamma$ decays at Belle[J]. Phys Lett B, 2008, 666(1): 16-22.

[21] HAYASAKA K, INAMI K, MIYAZAKI Y, et al. Search for lepton-flavor-violating τ decays into three leptons with 719 million produced $\tau^+\tau^-$ pairs[J]. Phys Lett B, 2010, 687: 139-143.

[22] Ciuchini M. Belle II Flavour Prospects[C]// B2TIP 2014, KEK, Japan. [S. l.: s. n.], 2014.

[23] ARKANI-HAMED N, FINKBEINER D P, SLATYER T R, et al. A theory of dark matter[J]. Phys Rev D, 2009, 79: 015014.

[24] HEARTY C. Current and projected limits, radiative production of dark photon, decay to SM particles[C]// B2TIP 2014, KEK, Japan. [S. l.: s. n.], 2014.

(上接第600页)

[15] ANDREAS S, NIEBUHR C, RINGWALD A. New limits on hidden photons from past electron beam dumps[J]. Phys Rev D, 2012, 86: 095019 .

[16] BABUSCI D, BADONI D, BALWIERZ-PYTKO I, et al. Limit on the production of a light vector gauge boson in ϕ meson decays with the KLOE detector[J]. Phys Lett B, 2013, 720: 111-115.

[17] ADLARSON P, AUGUSTYNIAK W, BARDAN W, et al. Search for a dark photon in the $\pi^0 \to e^+e^-\gamma$ decay [J]. Phys Lett B, 2013, 726: 187-193.

[18] AGAKISHEVG, BALANDA A, BELVER D, et al. Searching a dark photon with HADES [J]. Phys Lett B, 2014, 731: 265-271.

[19] MERKEL H, ACHENBACH P, AYERBE GAYOSO C, et al. Search at the Mainz Microtron for light massive gauge bosons relevant for the muon $g-2$ anomaly[J]. Phys Rev Lett, 2014, 112: 221802.

[20] ABRAHAMYAN S, AHMED Z, ALLADA K, et al. Search for a new gauge boson in electron-nucleus fixed-target scattering by the APEX experiment[J]. Phys Rev Lett, 2011, 107: 191804 .

[21] LEES J P, POIREAU V, TISSERAND V, et al. Search for a dark photon in e^+e^- collisions at BaBar [J]. Phys Rev Lett, 2014, 113: 201801.

[22] DAVOUDIASL H, LEE H S, MARCIANo W J. Muon $g-2$, rare kaon decays, and parity violation from dark bosons[J]. Phys Rev D, 2014, 89: 095006.

[23] CECCUCCI A, AMBROSINO F , ANELLI G, et al. Proposal to measure the rare decay $K^+ \to \pi^+ \bar{\nu\nu}$ at the CERN SPS: CERN-SPSC-2005-013 [R]. [S. l.: s. n.], 2005.

List of Talks

Opening Address	Liang Han (USTC, Hefei)
Session 1. *R*-measurements	Chaired by Xiaoyan Shen (IHEP, Beijing)
Overview of the CMD-3 results	Gennady Fedotovich (BINP)
BaBar ISR measurements	Evgeny Kozyrev (Novosibirsk)
Study of e^+e^- annihilation to hadrons below 2 GeV with SND	Tatyana Dimova (BINP)
Precise measurement of $e^+e^-\to K^+K^-$ at SND	Konstantin Beloborodov (BINP)
Session 2. *R*-measurements	Chaired by Paolo Gauzzi (INFN)
Recent results from the KEDR detector at the VEPP-4M	Korneliy Todyshev (BINP)
KLOE/KLOE2 results	Veronica De Leo (INFN)
BESIII R scan	Haiming Hu (IHEP, Beijing)
BESIII $2\pi/3\pi$ ISR	Yaqian Wang (JGU Mainz)
Session 3. Form Factors	Chaired by Rinaldo Baldini (IHEP & INFN)
Theory review on form factors	Simone Pacetti (Perugia)
Experimental review on form factors	Tord Johansson (Uppsala)
Preliminary results on $e^+e^-\to\pi^+\pi^-$ form factor at CMD-3	Fedor Ignatov (BINP)
Measurement of the time-like neutron and proton form factors at VEPP-2000	Aleksandr Korol (Novosibirsk)
Session 4. Form Factors	Chaired by Alberto Lusiani (Pisa)
BaBar form factor measurements	Evgeny Kozyrev (Novosibirsk)
BESIII form factor measurements	Yadi Wang (HIM-GSI)
Form factor measurements at WASA	Andrzej Kupsc (Uppsala)
Form factor measurements at JLAB	Bogdan Wojtsekhowsk(remote)
Session 5. Flavor Physics	Chaired by Tatyana Dimova (BINP)
Charm physics at Belle	Longke Li (USTC, Hefei)
Flavour physics at LHCb	Sergey Barsuk (Orsay)
Charm physics at BESIII	Hailong Ma (IHEP, Beijing)
BaBar measurement of the $D^0\to\pi^-\ e^+\nu$	Konrad Griessinger (JGU Mainz)
Session 6. Tau Physics	Chaired by Andrzej Czarnecki (U. Alberta)
A new look at V_{us} from inclusive flavor-breaking hadronic τ decay sum rules	Kim Maltman (York University)
Radiative tauleptonic decays	Matteo Fael (U. Bern)
Five-lepton lepton decays in the SM and beyond	Pablo Roig (Mexico)
Combined analysis of the decays $\tau^-\to K_S\pi^-\nu$ and $\tau^-\to K^-\eta\nu$	Rafel Escribano (U. Barcelona)
Session 7. Muon $g-2$	Chaired by Massimo Passera (Padova)
Theoretical review on $g-2$	Andrzej Czarnecki (U. Alberta)
$g-2$ experiment at FNAL	Seung Cheon Kim (Cornell)
$g-2$ experiment at J-PARC	Boris Shwartz (BINP)
Space-like measurement for a_μ	Carlo Carloni Calame (Pavia)
Session 8. Gamma-gamma/HLbL	Chaired by Achim Denig (JGU Mainz)
Gamma-gamma analysis at KLOE/KLOE-2	Paolo Gauzzi (INFN)
Two-photon physics studies at Belle	Qingnian Xu (UCAS, Beijing)

Gamma-gamma analysis at BESIII	Christoph Redmer (JGU Mainz)
Hadronic contribution from light by light processes in $(g-2)_\mu$ in nonlocal quark model	Alexey Zhevlakov (Tomsk)
The η transition form factor from space- and time-like experimental data	Rafel Escribano (U. Barcelona)
Session 9. Proton Radius Puzzle	Chaired by Gennady Fedotovich (BINP)
Proton radius QED theory	Savely Karshenboim (MPQ)
New electronic atomic physics measurements	Axel Beyer (MPQ)
New JLab experiment (PRad) on proton charge radius	Haiyan Gao (Duke Kunshan)
Session 10. Electroweak	Chaired by Bradley Lee Roberts (U. Boston)
sin2theta theory and New Physics	Hye-Sung Lee (Daejeon)
Perspectives for sin2theta at BelleII	Boris Shwartz (BINP)
P2 measurement at Mainz	Niklaus Berger (JGU Mainz)
Dalitz decay studies at BESIII	Dayong Wang (PKU, Beijing)
Comprehensive study of η/η' physics in chiral effective field theory	Zhihui Guo (HNU, Shijiazhuang)
Poster Session	
$e^+e^-\to\phi\eta$ reaction with CMD-3 detector	Vecheslav Ivanov (BINP)
$e^+e^-\to\overline{K}K$ (K_SK_L, K^+K^-) reactions with CMD-3 Detector	Evgeny Kozyrev (Novosibirsk)
$e^+e^-\to\eta\pi^+\pi^-$, $\omega\pi^+\pi^-$ reactions with CMD-3 Detector	Alexsander Popov (BINP)
$e^+e^-\to VP$ reactions at the VEPP-2000 e^+e^- collider with the SND detector	Alexander Botov (BINP)
Search for $\eta'\to e^+e^-$ and $\eta\to e^+e^-$ at the VEPP-2000 e^+e^- collider	Leonid Kardapoltsev (BINP)
Study of interference effects in the decays of ψ mesons into K^+K^-	Alberto Lusiani (Pisa)
Advertising of Chinese Physics C	Caitriana Nicholson (IHEP, Beijing)
Session 11. Spectroscopy	Chaired by Changzheng Yuan (IHEP, Beijing)
Theoretical review of *XYZ*	Xiang Liu (LZU)
XYZ at BESIII	Jingzhi Zhang (IHEP, Beijing)
XYZ at Belle	Chengping Shen (Beihang)
New results on exotic baryon resonances at LHCb	Liming Zhang (TSU)
Session 12. Spectroscopy & Radiative Corrections	Chaired by Savely Karshenboim (MPQ)
BESIII light hadron spectroscopy	Shuangshi Fang (IHEP, Beijing)
Towards nature of the X(3872) resonance	Nikolay Achasov (Sobolev)
Status of MC generators	Henryk Czyz (U. Silesia)
Session 13. Dark Photon	Chaired by Henryk Czyz (U. Silesia)
Dark mediator searches at KLOE/KLOE-2	Elena Perez Del Rio (INFN)
Search for the dark photon in π^0 decays at NA48/NA62	Francesco Gonnella (INFN)
Search for dark photon and long-lived particles at BaBar	Alberto Lusiani (Pisa)
Session 14. Machines and Detectors	Chaired by Zhengguo Zhao (USTC, Hefei)
Facility at JLAB for hadron physics	Haiyan Gao (Duke Kunshan)
MAMI & MESA	Achim Denig (JGU Mainz)
The BelleII experiment and superKEKB upgrade	Boqun Wang (U. Cincinnati)
Status and prospects of e^+e^- colliders at BINP	Pavel Piminov (BINP)
Post BEPCII in China: HIEPA	Jianbei Liu (USTC, Hefei)
Closing Remarks	Guangshun Huang (USTC, Hefei)

List of Participants

Name	E-mail	Institution	City	Country
Prof. ACHASOV, Nikolay	achasov@math. nsc. ru	Sobolev Institute for Mathematics	Novosibirsk	Russian
Prof. AN, Qi	anqi@ustc. edu. cn	USTC	Hefei	China
Dr. BALDINI FERROLI, Rinaldo	baldini@lnf. infn. it	INFN-LNF	Frascati	Italy
Dr. BARSUK, Sergey	sergey. barsuk@cern. ch	Laboratoire de l'Accélérateur Linéaire (FR)	Orsay	France
Mr. BELOBORODOV, Konstantin	K. I. Beloborodov@inp. nsk. su	NSU / BINP	Novosibirsk	Russian
Prof. BERGER, Niklaus	niberger@uni-mainz. de	JGU Mainz	Mainz	Germany
Mr. BEYER, Axel	axel. beyer@mpq. mpg. de	MPQ	Garching	Germany
Mr. BOTOV, Alexander	a. a. botov@inp. nsk. su	BINP	Novosibirsk	Russian
Prof. CAI, Hao	hcai@whu. edu. cn	Wuhan University	Wuhan	China
Mr. CAO, Zheng	caoz@ihep. ac. cn	IHEP	Beijing	China
Dr. CARLONI CALAME, Carlo	carlo. carloni. calame@pv. infn. it	University of Pavia	Pavia	Italy
Mr. CHEN, Rui	chenr2012@lzu. edu. cn	Lan Zhou University	Lanzhou	China
Prof. CHEN, Shenjian	sjchen@nju. edu. cn	Nanjing University	Nanjing	China
Dr. CZARNECKI, Andrzej	andrzejc@ualberta. ca	University of Alberta	Edmonton	Canada
Prof. CZYZ, Henryk	czyz@us. edu. pl	University of Silesia	Katowice	Poland
Dr. DE LEO, Veronica	veronica. deleo@roma3. infn. it	INFN Sezione Roma 3	Roma	Italy
Prof. DENIG, Achim	denig@kph. uni-mainz. de	JGU Mainz	Mainz	Germany
Dr. DIMOVA, Tatyana	baiert@inp. nsk. su	NSU / BINP	Novosibirsk	Russian
Dr. DING, Guijun	dinggj@ustc. edu. cn	USTC	Hefei	China
Prof. DRUZHININ, Vladimir	druzhinin@inp. nsk. su	NSU / BINP	Novosibirsk	Russian
Dr. ESCRIBANO, Rafel	rafel. escribano@ifae. es	U. Barcelona	Barcelona	Spain
Dr. FAEL, Matteo	fael@itp. unibe. ch	University of Bern	Bern	Switzerland
Ms. FANG, Xin	fangx@mail. ustc. edu. cn	USTC	Hefei	China
Mr. FANG, Shuangshi	fangss@ihep. ac. cn	IHEP	Beijing	China
Prof. FEDOTOVICH, Gennady	fedotovich@inp. nsk. su	BINP	Novosibirsk	Russian
Prof. GAO, Daoneng	gaodn@ustc. edu. cn	USTC	Hefei	China
Prof. GAO, Haiyan	yijun. gu@dku. edu. cn	Duke Kunshan University	Kunshan	China
Mr. GAO, Xinlei	gaoxinl@mail. ustc. edu. cn	USTC	Hefei	China
Mr. GAO, Zhen	gaozhen@mail. ustc. edu. cn	USTC	Hefei	China
Dr. GAUZZI, Paolo	paolo. gauzzi@roma1. infn. it	U. Roma / INFN Roma	Rome	Italy
Prof. GOLTERMAN, Maarten	maarten@sfsu. edu	SF State U.	San Francisco	United States
Dr. GONNELLA, Francesco	francesco. gonnella@lnf. infn. it	INFN	Frascati	Italy
Mr. GRIESSINGER, Konrad	griess@slac. stanford. edu	Mainz University	Mainz	Germany
Dr. GUO, Zhihui	dr_guozhihui@163. com	Hebei Normal University	Shijiazhuang	China
Prof. HUANG, Guangshun	hgs@ustc. edu. cn	USTC	Hefei	China
Prof. HU, Haiming	huhm@ihep. ac. cn	IHEP	Beijing	China
Dr. IGNATOV, Fedor	ignatov@inp. nsk. su	BINP	Novosibirsk	Russian
Mr. IVANOV, Vyacheslav	vyacheslav_lvovich_ivanov@mail. ru	BINP	Novosibirsk	Russian
Dr. JIAO, Jianbin	jiaojb@sdu. edu. cn	Shandong University	Jinan	China
Prof. JOHANSSSON, Tord	tord. johansson@physics. uu. se	Uppsala University	Uppsala	Sweden
Mr. KARDAPOLTSEV, Leonid	l. v. kardapoltsev@inp. nsk. su	BINP / NSU	Novosibirsk	Russian
Dr. KARSHENBOIM, Savely	savely. karshenboim@mpq. mpg. de	MPQ	Garching	Germany
Dr. KIM, SeungCheon	sk2528@cornell. edu	Cornell University	Ithaca	United States
Dr. KISELEV, Alexey	kiselev@math. nsc. ru	Sobolev Institute for Mathematics / NSU	Novosibirsk	Russian
Mrs. KONG, HUI	kid007@mail. ustc. edu. cn	USTC	Hefei	China
Dr. KOROL, Aleksandr	a. a. korol@inp. nsk. su	NSU / BINP	Novosibirsk	Russian
Mr. KOZYREV, Evgeny	eakozyrev09@gmail. com	NSU / BINP	Novosibirsk	Russian
Dr. KUPSC, Andrzej	Andrzej. Kupsc@physics. uu. se	Uppsala University	Uppsala	Sweden
Dr. LEE, Hye-Sung	hyesung. lee@cern. ch	IBS CTPU	Daejeon	Republic of Korea
Dr. LI, Cui	cui. li@physics. uu. se	Uppsala University	Uppsala	Sweden
Prof. LI, Haibo	lihb@ihep. ac. cn	IHEP	Beijing	China
Dr. LI, Lei	lilei@ihep. ac. cn	BIPT	Beijing	China
Mr. LI, Longke	lilongke@mail. ustc. edu. cn	USTC	Hefei	China

Ms. LI, Peilian	lipl@mail. ustc. edu. cn	USTC	Hefei	China
Mr. LI, Peirong	lipeirong11@mails. ucas. ac. cn	UCAS	Beijing	China
Mr. LIU, Dong	dliu13@mail. ustc. edu. cn	USTC	Hefei	China
Prof. LIU, Jianbei	liujianb@ustc. edu. cn	USTC	Hefei	China
Dr. LIU, Landiao	liulandiao@gmail. com	Peking University	Beijing	China
Prof. LIU, Shubin	liushb@ustc. edu. cn	USTC	Hefei	China
Prof. LIU, Xiang	xiangliu@lzu. edu. cn	Lanzhou University	Lanzhou	China
Prof. LIU, Yanwen	yanwen@ustc. edu. cn	USTC	Hefei	China
Prof. LU, Caidian	lucd@ihep. ac. cn	IHEP	Beijing	China
Dr. LUSIANI, Alberto	alberto. lusiani@pi. infn. it	Scuola Normale Superiore	Pisa	Italy
Dr. LYU, Xiaorui	xiaorui@ucas. ac. cn	UCAS	Beijing	China
Prof. MAGGIORA, Marco	marco. maggiora@to. infn. it	INFN-TO	Turin	Italy
Dr. MA, Hailong	mahl@ihep. ac. cn	IHEP	Beijing	China
Prof. MALTMAN, Kim	kmaltman@yorku. ca	York University	Toronto	Canada
Dr. MASSRI, Karim	karim. massri@cern. ch	University of Liverpool	Liverpool	UK
Dr. NICHOLSON, Caitriana	c. nicholson@ihep. ac. cn	IHEP	Beijing	China
Mr. NIU, Pengyu	niupengyu14@mails. ucas. ac. cn	IHEP	Beijing	China
Dr. PACETTI, Simone	simone. pacetti@pg. infn. it	U. Perugia / INFN	Perugia	Italy
Dr. PASSERA, Massimo	passera@pd. infn. it	INFN Padova	Padova	Italy
Mr. PENG, Junbo	vortex@mail. ustc. edu. cn	USTC	Hefei	China
Dr. PEREZ DEL RIO, Elena	eperez@lnf. infn. it	INFN Frascati	Frascati	Italy
Dr. PIMINOV, Pavel	piminov@inp. nsk. su	BINP SB RAS	Novosibirsk	Russian
Mr. POPOV, Alexandr	aspopov1@inp. nsk. su	BINP	Novosibirsk	Russian
Prof. QIAO, CONGFENG	qiaocf@ucas. ac. cn	University of CAS	Beijing	China
Dr. REDMER, Christoph Florian	redmer@kph. uni-mainz. de	JGU Mainz	Mainz	Germany
Prof. ROBERTS, B. Lee	roberts@bu. edu	Boston University	Boston	United States
Dr. ROIG, Pablo	proig@fis. cinvestav. mx	Dpto. Fisica Cinvestav	Mexico DF	Mexico
Dr. RONGGANG, Ping	pingrg@ihep. ac. cn	IHEP	Beijing	China
Dr. SAVRIE', Mauro	savrie@fe. infn. it	University of Ferrara and INFN	Ferrara	Italy
Prof. SHEN, Chengping	shencp@ihep. ac. cn	Beihang University	Beijing	China
Prof. SHEN, Xiaoyan	shenxy@ihep. ac. cn	IHEP	Beijing	China
Prof. SHWARTZ, Boris	shwartz@inp. nsk. su	BINP / NSU	Novosibirsk	Russian
Dr. SUN, Yanjun	yjsun@mail. ustc. edu. cn	Northwest Normal University	Lanzhou	China
Mr. TAN, Yaxing	tanyx@mail. ustc. edu. cn	USTC	Hefei	China
Dr. TODYSHEV, Korneliy	todyshev@inp. nsk. su	BINP	Novosibirsk	Russian
Dr. WANG, Boqun	boqunwg@ucmail. uc. edu	U. Cincinnati	Cincinnati	United States
Dr. WANG, Dayong	dayong. wang@pku. edu. cn	Peking University	Beijing	China
Dr. WANG, Ping	wangp@IHEP. ac. cn	IHEP	Beijing	China
Prof. WANG, Qun	qunwang@ustc. edu. cn	USTC	Hefei	China
Mr. WANG, Weiping	cloud13@mail. ustc. edu. cn	USTC	Hefei	China
Prof. WANG, Xiaolian	wangxl@ustc. edu. cn	USTC	Hefei	China
Dr. WANG, Yadi	wangyd@ihep. ac. cn	HIM-GSI	Mainz	Germany
Mr. WANG, Yaqian	whyaqm@gmail. com	KPH	Mainz	Germany
Dr. WANG, Zhihong	wzh1988@mail. ustc. edu. cn	USTC	Hefei	China
Mr. WANG, Zhiyong	wangzy@ihep. ac. cn	IHEP	Beijing	China
Mr. WEI, Yifeng	weiyf@mail. ustc. edu. cn	USTC	Hefei	China
Ms. XUE, Mingxuan	xuemx@mail. ustc. edu. cn	USTC	Hefei	China
Mr. XUE, Sirun	xuesr@ihep. ac. cn	IHEP	Beijing	China
Mr. XU, Qingnian	xuqingnian10@mails. ucas. ac. cn	UCAS	Beijing	China
Dr. XU, Xinping	xuxp@ihep. ac. cn	Soocow Univ.	Suzhou	China
Prof. YAN, Wenbiao	wenbiao@ustc. edu. cn	USTC	Hefei	China
Prof. YUAN, Changzheng	yuancz@ihep. ac. cn	IHEP	Beijing	China
Mr. ZENG, Zhe	zengzhe@mail. ustc. edu. cn	USTC	Hefei	China
Mr. ZHANG, Bingxin	zhangbx@ihep. ac. cn	IHEP	Beijing	China
Dr. ZHANG, Jingzhi	jingzhi@ihep. ac. cn	IHEP	Beijing	China
Dr. ZHANG, Liming	liming_zhang@tsinghua. edu. cn	Tsinghua University	Beijing	China
Mr. ZHANG, Yateng	zyt1988@mail. ustc. edu. cn	USTC	Hefei	China
Dr. ZHANG, Zhenyu	zhangzhenyu@ihep. ac. cn	Wuhan University	Wuhan	China
Prof. ZHANG, Ziping	zpz@ustc. edu. cn	USTC	Hefei	China
Mr. ZHANG, Jielei	zhangjielei@ihep. ac. cn	IHEP	Beijing	China
Prof. ZHAO, Qiang	zhaoq@ihep. ac. cn	IHEP	Beijing	China
Prof. ZHAO, Zhengguo	zhaozg@ustc. edu. cn	USTC	Hefei	China
Dr. ZHEVLAKOV, Alexey	zhevlakov@phys. tsu. ru	Tomsk State University	Tomsk	Russian
Ms. ZHOU, Xiaorong	zxrong@ustc. edu. cn	USTC	Hefei	China
Mr. XIA, Lei	jessemcc@mail. ustc. edu. cn	USTC	Hefei	China
Dr. ZHENG, Bo	zhengb@ihep. ac. cn	University of South China	Hengyang	China